Development of mass spectrometric approaches to advance drug discovery

Rachel Emma Heap

A thesis submitted for the Degree of Doctor of Philosophy

Institute for Cell and Molecular Biosciences

Newcastle University

October 2019

Abstract

The work in this thesis concerns the development of advanced mass spectrometric techniques to study model systems for drug discovery and accelerate the process of high-throughput screening (HTS) in the field of inflammation. This has primarily been achieved using matrix-assisted laser desorption/ionisation time-of-flight mass spectrometry (MALDI-TOF-MS) to develop screening assays for anti-inflammatory compounds. MALDI-TOF-MS utilises a laser to ablate and consequently ionise biomolecules that are co-crystallised with a matrix. The absorbed laser energy enables the transfer of charge to the analyte molecule from the excited matrix molecules before acceleration into the TOF tube where analytes are then separated based on their mass to charge ratio (*m/z*) and detected to generate a mass spectrum. With the development of advanced mass spectrometers that have unmatched laser and digitiser speeds these instruments now rival established fluorescent based drug discovery assays.

The first study presented in this thesis is the development of a HTS assay to identify inhibitors of salt inducible kinases (SIKs) *in vitro*. These kinases are an attractive drug target as they mediate the production and secretion of the cytokine interleukin 10 (IL-10) in immune cells. When secreted, IL-10 dampens the pro-inflammatory response in surrounding macrophages and suppresses a further inflammatory response. Using a peptide-based assay, a proof of concept screen generated a positive correlation with an established fluorescent based assay, thus validating MALDI-TOF-MS as a viable alternative for HTS. Interestingly, several compounds were identified as kinase activators. Inhibitors of SIKs could be particularly beneficial for patients with autoimmune diseases who require immunosuppressive drugs as they may increase the production of IL-10, thus preventing excessive inflammation and subsequent onset of pathogenesis.

MALDI-TOF-MS was then applied to the development of cellular based assays to screen compounds against cell types that transition into different phenotypes. Rigorous development of a technically reproducible sample preparation technique enabled robust phenotyping of different cell lines. This method was then successfully applied to study mouse embryonic stem cells (mESCs), which transition between naïve and pluripotent phenotypes under pharmacologically controlled conditions. Moreover, a cellular assay to identify inhibitors of inflammation in the presence of a bacterial ligand lipopolysaccharide (LPS) in monocytes was developed. Here, the BCR-ABL inhibitor nilotinib was identified as having anti-inflammatory properties. Interestingly, its first-generation counterpart imatinib was not identified as having this effect, suggesting novel off-target effects for nilotinib. Its anti-inflammatory properties were then validated by cell biology techniques that demonstrated the reduction of the pro-inflammatory cytokine TNF-α in nilotinib-treated cells.

Finally, I utilised advanced high-resolution mass spectrometry to undertake secretomic analysis of L929 fibroblasts, which are commonly used to generate supplemented media that aids the differentiation of bone marrow-derived macrophages (BMDMs). These cells are promising drug targets and the understanding of their differentiation state is paramount to potential drug screening campaigns. A detailed proteomic profile of L929 supplemented media, as well an in-depth proteomic profile of BMDMs differentiated under various conditions were generated.

Taken together the work of this thesis contributes valuable knowledge in the field of how mass spectrometry can be utilised to advance HTS campaigns as well as provide valuable insight to the biology of promising drug models.

Declaration

(i) I declare that this thesis is my own work and that I have correctly acknowledged the work of others. This submission is in accordance with University and School guidance on good academic conduct.

(ii) I certify that no part of the material offered has been previously submitted by me for a degree or other qualification in this or any other University.

(iii) I confirm that the word length is within the prescribed range as advised by my school and faculty.

Rachel E Heap
Institute of Cell and Molecular Biosciences (ICaMB)
Medical School
Newcastle University
Newcastle upon Tyne

Acknowledgments

Firstly, I'd like to thank Matthias Trost for hiring me to do a PhD in his lab. I have learnt a lot and have undoubtedly become a much better scientist because of my time in the Trost Lab.

I would like to thank all of those who I started with in Dundee – Julien, Anetta, Orsi, Megan, Richard, Jean-Baptiste, Virginia, Ryan and Jenny as well as Bob, Joby and David of the mass spec facility in Dundee. Particular thanks to Anetta, who has urged me to think about think about the biological impact of my work, which was tough as a chemist but has truly transformed my outlook on science. I'd also like to thank my collaborators from Dundee: Anthony, Kathleen, David, Lesley, Greg and Anna.

In Newcastle, I'd like to thank all those I've thoroughly enjoyed working over the years: Sandra, Tiaan, Maria, Megan, Joe, José, Andrew, Nine, Frances, Fred, Alex, Abeer, Achim, Shin and especially Adam - my best lab pal whose resignation almost had me in tears. All of you guys have been one of the absolute highlights of my time in Newcastle – it's been awesome. A special thanks to Julien, who has been a thorn in my side from the get-go but my biggest cheerleader and supporter in life ever since. You drive me insane but you're the best. I'd also like to give a shout out to my mentor of 6 years, Jane Thomas-Oates, who has always given me the best advice when things get tough and who I look up to immensely. I know I wouldn't be here if it wasn't for you.

A big thanks to my international friends of Synergy and the Danish mafia. Blowing off steam and laughing with you guys kept me sane over the past 4 years. And finally, a huge thank-you to family and my friends at home who've always been on the other end of the phone when the going gets rough: Mum, Dad, Jess, Matt – I know you don't understand a word, but I appreciate all the effort!

List of Publications

Heap. R. E., Hope. A. G., Pearson. L. A., Reyskens K. M. S. E., McElroy. S. P., Hastie. C. J., Porter. D. W., Arthur J. S. C., Gray D. W., Trost M. Identifying Inhibitors of Inflammation: A Novel High-Throughput MALDI-TOF Screening Assay for Salt-Inducible Kinases (SIKs). *SLAS Discovery*. **22 (10)**, 1193-1202 (2017)

Heap. R. E., Gant. M. S., Lamoliatte. F., Peltier. J., Trost. M. Mass spectrometry techniques for studying the ubiquitin system. *Biochem. Soc. Trans.* **45 (5)**, 1137-1148 (2017)

Heap. R. E., Segarra-Fast. A., Blain. A. P., Findlay. G. M., Trost. M. *Analyst*. (2019)

Heap. R. E.,* Marín-Rubio. J. L.,* Inns. J., Heunis. T., Peltier. J., Saxty. B., Trost. M. A MALDI-TOF-MS cellular screening assay for identifying inhibitors of bacterial ligand triggered inflammation *(under preparation)*

Heap. R. E., Peltier. J., Heunis. T., Marín-Rubio. J. L., Moore. A., Trost. M. Proteomic profiling of the L929 secretome to understand the subtleties in BMDM differentiation. (*under preparation*)

Table of Contents

List of Figures

Abbreviations

a	atto
ACN	acetonitrile
ADP	adenosine diphosphate
AMI	acoustic mist ionisation
ATP	adenosine triphosphate
BCA	bicinchoninic acid assay
BET	bromide and extra-terminal motif proteins
BMDM	bone marrow-derived macrophage
cAMP	cyclic adenosine monophosphate
CHCA	α-cyano-4-hydroxycinnamic acid
CID	collision-induced dissociation
CREB	cAMP response element-binding protein
CRTC3	CREB Regulated Transcription Coactivator 3
C-terminus	carboxy terminus
Ctrl	control
Da	Dalton
DAMP	danger-associated molecular pattern
DDA	data-dependent acquisition
DDU	Dundee Drug Discovery Unit
DHAP	2',5'-dihydroxyacetophenone
DHB	2',5'-dihydroxybenzoic acid
DIA	data-independent acquisition
DMEM	Dulbecco's modified Eagle's medium
DMSO	dimethylsulfoxide
DNA	deoxyribonucleic acid
dsRNA	double stranded
DSTT	Division of Signal Transduction Therapy

DTT	dithiothreitol
EDTA	sodium ethylenediaminetetraacetic acid
ELISA	enzyme-linked immunosorbent assay
ESI	electrospray ionisation
EtOH	ethanol
f	femto
FA	formic acid
FACS	fluorescence-activated cell sorting
FBS	fetal bovine serum
FDA	food and drug administration
FDR	false discovery rate
FT	Fourier transform
FT-ICR	Fourier transform ion cyclotron resonance
g	gram
GAPDH	glyceraldehyde 3-phosphate dehydrogenase
GO	gene ontology
HEPES	4-(2-Hydroxyethyl)piperazine-1-ethanesulfonic acid
HPLC	high performance liquid chromatography
HPRP	high pH reverse phase
hr	hour
HRP	horseradish peroxidase
HTS	high-throughput screening
IBD	inflammatory bowel disease
ICaMB	Institute of Cellular and Molecular Biosciences
ID	identification
IFN	interferon
IFN-α	Interferon alpha
IFN-β	Interferon beta
IFN-γ	Interferon gamma

IL-10	Interleukin 10
IL-4	Interleukin 4
IL-6	Interleukin 6
IMDM	Iscove’s modified Dulbecco’s medium
k	kilo
KO	Knock out
L	litre
LC-MS/MS	liquid chromatography – tandem mass spectrometry
LFQ	label free quantification
L-glut	L-glutamine
LPS	lipopolysaccharide
M	Molar
m	milli
m/v	mass to volume
m/z	mass to charge ratio
MALDI	matrix-assisted laser desorption/ionisation
MALDI-TOF-MS	matrix-assisted laser desorption/ionisation – time of flight – mass spectrometry
MAPK	mitogen activated protein kinase
M-CSF	macrophage colony stimulating factor
MeOH	methanol
mESC	murine embryonic stem cell
MIF	macrophage migration inhibitory factor
min	minute
mol	mole
mRNA	messenger ribonucleic acid
MS	mass spectrometry
n	nano
NaCl	sodium chloride

NF-κB	nuclear factor κB
N-terminus	amino terminus
p	pico
PAGE	polyacrylamide gel electrophoresis
PAMP	pathogen associated molecular pattern
PBS	phosphate buffered solution
PCA	principle component analysis
PCR	polymerase chain reaction
PE	percentage effect
Pen/strep	penicillin/streptomycin
PFA	paraformaldehyde
PLK1	Polo-like kinase 1
PMF	peptide mass fingerprint
Poly(I:C)	polyinosinic:polycytidylic acid
PRR	pattern recognition receptor
qRT-PCR	real-time quantitative reverse transcription polymerase chain reaction
RFU	relative fluorescent units
rpm	revolutions per minute
RPMI	Roswell Park Memorial Institute medium
s	second
S/N	signal–to-noise
SA	sinapinic acid
SAM	self-assembled monolayer
SD	standard deviation
SDS	sodium dodecyl sulfate
SIK	salt inducible kinase
SPE	solid phase extraction
TAK1	transforming growth factor β-activated kinase 1

TBK1	TANK-binding kinase 1
TCEP	tris(2-carboxyethyl)phosphine
TEAB	tetramethylethylenediamine bicarbonate
TFA	trifluoroacetic acid
TLR	Toll-like receptor
TMT	tandem mass tag
TNF-α	Tumour necrosis factor alpha
TOF	time–of-flight
Tris	tris(hydroxymethyl)aminomethane
UT	untreated
WT	wild-type
xg	g-force
µ	micro

Chapter 1. Introduction

1.1 Fundamentals of Mass Spectrometry

1.1.1 Core mass spectrometry principles

Mass spectrometry is an analytical technique that measures the mass to charge ratio (*m/z*) of ions to generate a mass spectrum that can in turn yield chemically relevant information such as empirical mass or structure about a particular analyte. In its simplest form a mass spectrometer consists of an ionisation source coupled to a mass analyser and detector. Modern mass spectrometry techniques were first described by Dempster and Aston in 1918-19, respectively.[1] Since then, mass spectrometry technology has advanced exponentially with the development of a vast array of ionisation techniques, mass analysers and hybrid instruments. In addition, ion traps and soft ionisation techniques such as electrospray and laser desorption technologies have gained international recognition after being awarded the Nobel prizes in 1989[2] and 2002[3], respectively, thus highlighting the importance of this technology across all scientific fields. For successful MS experiments analytes must reach the gaseous phase as ions, therefore they must carry a positive or negative charge. The charge of the ions is then exploited to enable filtering, storage, fragmentation or detection using electric and magnetic fields. Once detected, the signal is deconvoluted and translated into information that can provide an ion's mass, abundance or chemical structure. The way in which analytes are now ionised, separated and detected have advanced significantly in the past century with respect to precision, resolution, mass accuracy and a more user-friendly interface. These advances have resulted in applications of mass spectrometry that are now wide ranging with use in

clinic, research and industrial settings. The diversity of mass spectrometry applications is vast and the work in this thesis will focus on two mass spectrometric techniques: MALDI-TOF-MS and LC-ESI-MS/MS and their application to the analysis of biomolecules.

1.1.2 Matrix-assisted laser desorption/ionisation (MALDI)

Matrix-assisted laser desorption/ionisation, or MALDI, is a soft ionisation method that was first described in 1985 by Karas *et al.* who used ultraviolet laser irradiation to ionise and analyse intact organic molecules.[4] This was particularly novel at the time as previously techniques such as electron bombardment were considered "hard" ionisation methods that utilised high energy electrons to generate ions. However, the process of electron bombardment or electron ionisation (EI) induced substantial fragmentation of the biomolecule, thus information regarding the intact analyte was lost. The soft ionisation success was taken further by the addition of a matrix to improve ionisation of large intact biomolecules, and in 1988 Tanaka *et al.* were able to detect analytes with an *m/z* of up to 100,000 Da by applying a thin layer of ultra-fine cobalt powder dissolved in an organic solvent as a matrix. [5,6] These two studies were the first of their kind to show the power of MALDI to ionise intact biomolecules. The basic principles of MALDI sample preparation and ionisation are described in Figure 1-1, where a sample is first mixed with an excess of matrix solution and allowed to co-crystallise onto a target to produce a dried spot (Figure 1-1.A). Ablation of the dried spot enables transfer of both matrix and analyte molecules into the gas phase. Matrix molecules readily absorb the laser irradiation and enter an excited state. This irradiation process enables transfer of protons between excited matrix ions and vaporised analyte molecules that generates analyte ions which are then accelerated by an electric field to enter the mass analyser.

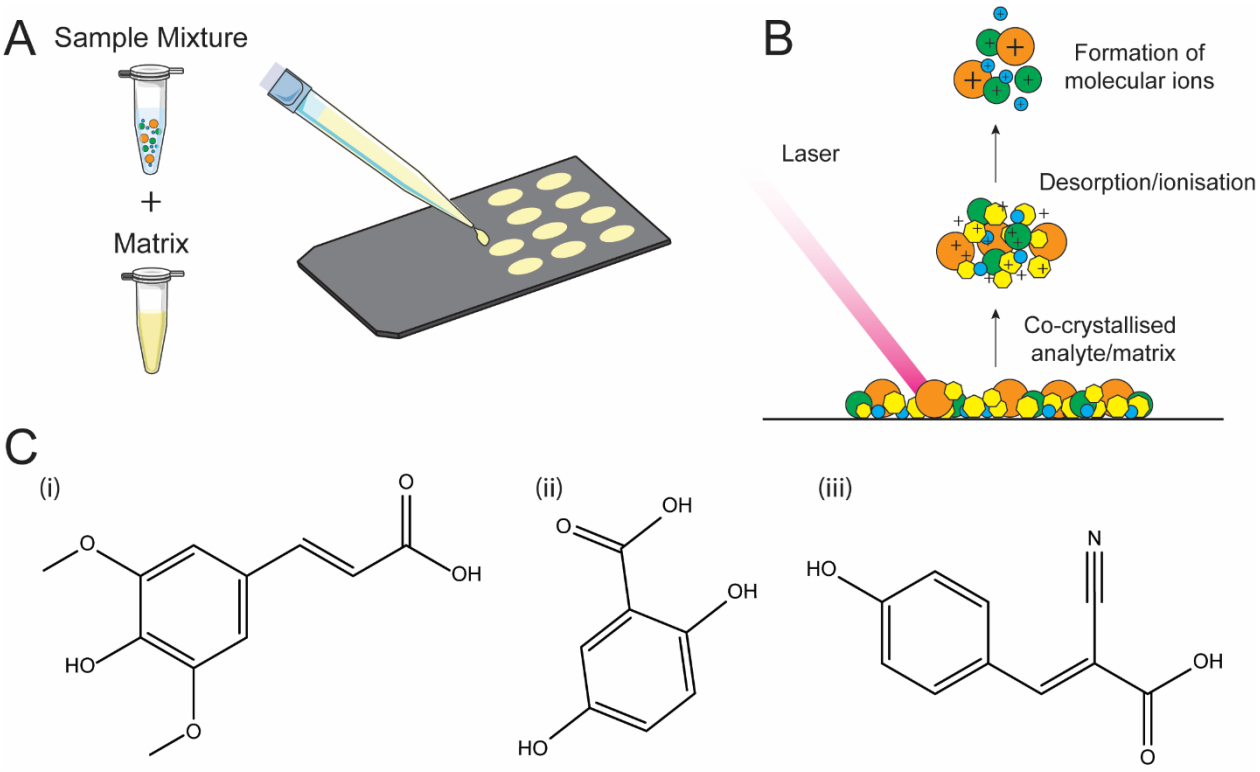

Figure 1-1. Principles of MALDI-TOF-MS analysis. *(A) Graphical representation of the mixing of matrix and sample mixture that is then deposited as spots onto a MALDI target. (B) The process of MALDI. Crystallised spots of matrix and analyte are ablated by a laser that first induces transfer into the gas phase followed by ionisation as charge is transferred between the matrix and the analyte to form ions. (C) The chemical structures of the three most common MALDI matrices: sinapinic acid (SA), 2-5-dihydroxybenzoic acid (DHB) and α-cyano-4-hydroxycinnamic acid (CHCA)*

Utilisation of a suitable matrix in MALDI analyses is imperative to ensure successful ionisation, however the transfer of charge between matrix and analyte is still theorised. There are several theories that postulate the MALDI process and how this soft ionisation method predominantly produces singly charged species as the dominant ion.[7–9] The most accepted of these models was presented by Karas *et al.*, a “lucky survivor” mechanism that describes the role of photoionisation and photochemical reactions that drive the ionisation process and the neutralisation that occurs within the gaseous plume.[10] This generates charged positive and negative species of analyte and matrix ions that then

collide to induce charge neutralisation. This neutralisation is most effective for highly charged cluster ions, which in turn leads to the preferable formation of singly charged ions that survive the ionisation process to enter the mass analyser. More recently, compelling evidence was published that validates the lucky survivor model with gas phase protonation as the driving mechanism behind this ionisation process.[11]

The matrix choice in most experimental designs is typically a low molecular weight aromatic organic acid with phenolic groups that has a strong optical absorption in the range of the laser wavelength used. In their original study, Karas *et al.* mixed samples with saturated nicotinic acid, which although effective for laser desorption of different peptide or protein samples, also produced unwanted adduct effects between analyte and matrix ions.[6,12] The matrix composition varies according to the analyte of interest and the type of laser used. This therefore led to the development of a plethora of different matrices to suit a wide range of different potential biomolecules. The most commonly used matrices for biomolecule analysis are α-cyano-4-hydroxycinnamic acid (CHCA), sinapinic acid (SA), 2,5-dihydroxyacetophenone (DHAP), and 2,5-dihydroxybenzoic acid (DHB), which have been shown to be effective for the analysis of peptides, glycopeptides, proteins, glycans, and lipids respectively (Figure 1-1.C).[12–14]

MALDI sources are now widely used in commercial instruments, as they are often user friendly and can be coupled to a variety of mass analysers such as orbitraps, fourier transform ion cyclotron resonance analysers (FT-ICR) and more recently, instruments that use ion mobility sectors. These allow a great variety of speeds and resolutions to be achieved, but the most common mass analyser coupled to a MALDI source is the time-of-flight (TOF) mass analyser.

1.1.3 MALDI-TOF-MS

Time-of-flight tubes or TOFs are one of the oldest mass analysers described along with magnetic sector separation technology that dates back to 1950's. This is due to their simple separation principle and the fact that the subsequent manufacturing of TOF instruments is relatively inexpensive when compared with other mass analysers. In brief, pulsed ions from a MALDI source are accelerated into a TOF tube that is under strong vacuum and are separated by their time of flight, which is dependent on their mass-to-charge ratio (*m/z*) and the energy that is used to accelerate the ions into the TOF.[5] The longer the flight path, the better the separation of ions as described by the equation below. The simplest mode of a TOF instrument is that extracted ions from a MALDI source enter the TOF tube and then pass through a field free zone along a linear flight path where the lighter ions travel fastest to a detector. This is described as linear geometry (Figure 1-2.A) and is particularly suitable for large molecules such as intact proteins above 20 kDa. As the flight path is relatively short, individual ion packets are not well separated leading to a lower resolution; however, as all ions are detected, this mode is highly sensitive.

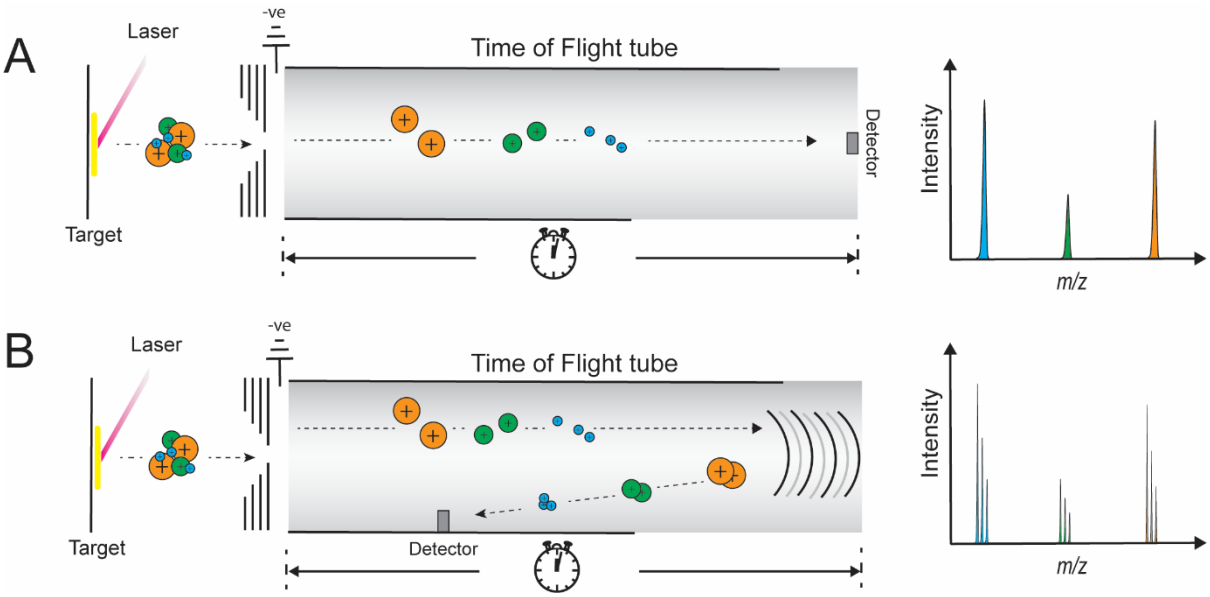

Figure 1-2. Principles of time of flight (TOF) mass spectrometry. *(A) Linear operation of a MALDI time-of-flight mass spectrometer where ions are separated by their m/z and detected at the end of the TOF tube. (B) Reflectron operation of a MALDI time-of-flight mass spectrometer where ions at the end of the TOF enter a reflectron that normalises their kinetic energy and reflects ions back down the TOF tube to a detector.*

Theory dictates that all ions enter the TOF tube with the same kinetic energy, however in practice this is often not the case as not all ions are vaporised evenly by the laser pulse. This generates a small kinetic energy distribution for each discrete *m/z*; therefore, ions do not arrive at the detector at the same time as they possess different initial potential energies. This in turn results in a broadening of the peaks and a poorer resolution when operated in linear mode geometry.[15] To correct for this, inclusion of a reflectron at the end of the field free region of the TOF tube was described by Mamyrin *et al.* to enhance MALDI-TOF-MS detection and resolution.[16] A reflectron consists of stacking metal plates to which a gradient electric current is applied, thus creating an ion mirror. Ions penetrate the electric field to different extents before they are repelled out of the field in the opposite direction towards a detector, therefore greatly increasing the ion path. Ions of the same *m/z* are refocussed to correct for differences in the initial potential energy and generate

much tighter “ion packets”. These ions then reach the detector at the same time, as they are more spatially grouped, which results in significantly superior resolution over linear mode.[17] Further to this, the reflectron is often displaced slightly to deflect ions back along the TOF tube (Figure 1-2.B), the flight path length can be almost doubled, thus enhancing instrument resolution and mass accuracy. This mode of operation is typically limited to smaller molecular weight biomolecules as larger molecular weight species experience decay and ion dissociation faster than smaller molecules as they take longer to travel through the drift free zone. Thus, application of a reflectron to correct for initial energy distributions of large molecular weight species leads to the loss of these ions. However, reflectron MALDI-TOF-MS is exceptionally powerful for analysis of peptides, lipids, carbohydrates and small organics as full isotopic resolution can be achieved up to approximately 15 kDa.

Commercially available MALDI-TOF-MS technologies are now utilised as analytical methods for a broad range of biological and chemical questions. Potentially the most well-known application is peptide mass fingerprinting (PMF), where proteolytic peptides can be analysed and sequenced to identify proteins.[18] This technique is widely used for proteomic studies with mammalian and plant species, but has also proven particularly powerful for archaeological studies and detection of ancient proteins.[19,20] As well as this, MALDI-TOF-MS is now widely applied as an imaging technique. Here, it has been possible to exploit the speed and sensitivity of MALDI-TOF-MS to rapidly profile the abundance of an analyte within a sample whilst also preserving the spatial information.[21] This technique is particularly versatile and can now be applied to assessing lipid, metabolite and drug distribution within a tissue. Finally, one of the most recent and rapidly growing uses for MALDI-TOF-MS is the clinical profiling and screening of micro-

organisms. Here, tissue or biofluid samples can be rapidly analysed by MALDI-TOF-MS to identify unique signatures of bacteria genera, thus enabling the identification of a bacterial infection as well as accurate species determination.[22] This approach enables sensitive whole cell analysis of micro-organisms and generates a unique protein mass fingerprint, mostly from bacterial ribosomal proteins. Consequently, this has led to robust phenotyping of bacteria taxonomy by spectral matching that allows classification of subtle differences in strains of infectious pathogens such as *Mycobacterium tuberculosis*.

This demonstrates the diversity of MALDI-TOF-MS for a wide range of applications and the work of this thesis will seek to develop and optimise novel methodologies using state-of-the-art MALDI-TOF-MS instruments

1.1.4 Electrospray ionisation

Similarly to MALDI, electrospray ionisation (ESI) is a soft ionisation technique that uses electrical energy to assist the transfer of ions from solution to the gas phase. The development of ESI first began in 1968 by Dole *et al.,* who successfully introduced a polystyrene polymer into the gas phase as a charged species through electrospraying.[23] However, studies showing ESI coupled to mass spectrometry for large biomolecules were first presented by Yamashita and Fenn *et al.,* who in 2002 were awarded the Nobel prize for their work.[24,25]. This technique works by flowing liquid phase analytes through a fine tipped metal capillary to which a high voltage (2-6 kV) is applied relative to the source-sampling entry cone of the mass spectrometer.[26] This generates a strong electric field that causes the dispersion of the sample aerosol into highly charged droplets in a process known as nebulisation.

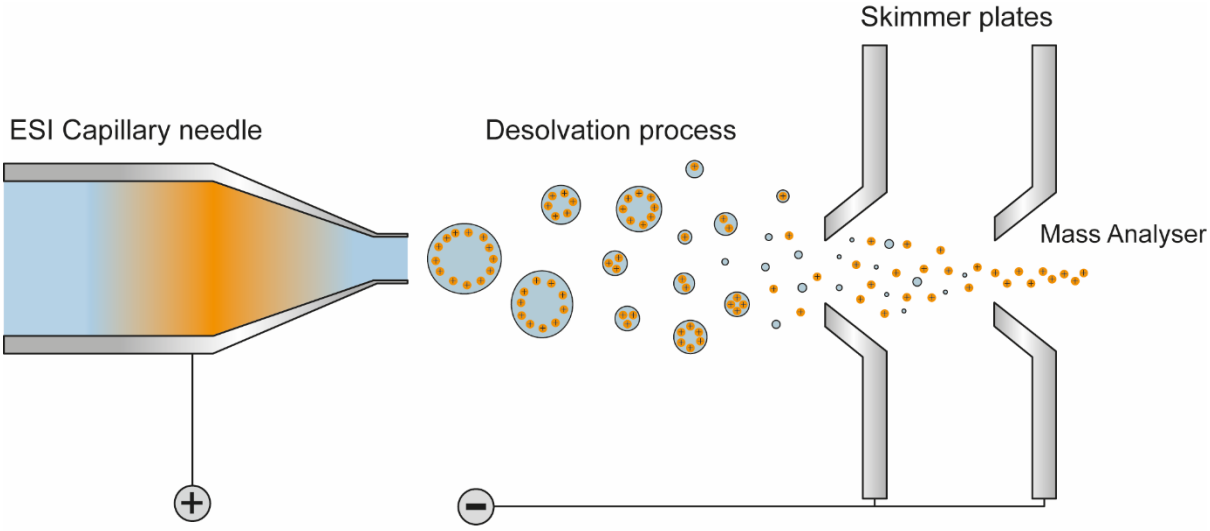

Figure 1-3. Principles of electrospray ionisation (ESI). *Graphical description of the electrospray ionisation process where liquid phase analytes are nebulised under high voltage to generate an aerosol. These aerosol droplets then undergo a desolvation process, typically with a drying gas, to produce highly charged ions that then enter a mass analyser.*

Formation of charged ions from the aerosol mists requires rapid desolvation, thus the droplets are often vaporised under the flow of nitrogen and ion-pairing agents such as organic acids can also be added to increase conductivity. Ions are eventually formed as the ever-decreasing droplet reaches its Rayleigh limit upon which it undergoes a coulombic explosion or fission where the Coulomb repulsion becomes too large for the droplet surface tension and ions are expelled.[27] During this process, there is a significant loss of mass and charge, but the surviving ions are now often multiply charged species and enter the mass analyser. The efficiency of ESI-MS is highly dependent on an analyte's structure and the solvent used but it has been shown to be particularly versatile with respect to biomolecule diversity such as intact proteins, peptides and metabolites.[28–30]

1.1.5 The Orbitrap and ion trap mass analysers

Ion trap mass analysers are trapping instruments that utilise both magnetic and electric fields to capture ions. Ion Traps are versatile mass analysers that can used to be as the primary mass analyser or integrated into hybrid instruments. The Orbitrap is an ion trap mass analyser that is based on an earlier ion storage device, the Kingdon trap.[31] The Orbitrap was first described by Makarov in 1995 and is a mass analyser that consists of an outer barrel-like electrode and a coaxial inner spindle-like electrode that traps ions in an orbital motion around the spindle.[32,33] The ions rotate around an electrode system with a harmonic oscillation path along the axis of rotation at a frequency characteristic of their *m/z* value. At close proximity, a current from the trapped ions is detected on receiver plates as a time-domain signal and deconvoluted to generate a mass spectrum using fourier transformation (FT) of the frequency signal.

FT-based mass spectrometers, such as the Orbitrap and FT-ICR, provide high mass resolution and mass accuracy that enables the separation of ions with the same nominal mass, as well as confident assignment of empirical formulas for small molecules and lipids. This is particularly beneficial in the low mass range (<1000 Da) where background features such as matrix peaks and endogenous species can interfere with signal identification and intensity when analysing specific compounds or metabolites. However, the acquisition times of these instruments are typically much longer than lower resolution instrumentations, such as TOF's and quadrupoles, therefore their use for studies that require throughput are limited. Many studies now utilise the high resolution Orbitrap instruments for analysis of small metabolites, lipids and drug compounds as well as large intact proteins and native mass spectrometry. However, to date the most successful

application of the Orbitrap has arguably been to the field of proteomics where these instruments are now at the forefront of mass spectrometry based proteome research.

1.1.6 Proteomics

The large-scale study of proteins and their function within an organism or system is termed proteomics and is complimentary to genomics and transcriptomic research. The proteome covers the entirety of proteins that are produced and/or modified by an organism or system that alters significantly in composition and function depending on cellular demands or perturbation by external stimuli. Proteomics itself is an interdisciplinary field that covers all research into protein function and behaviour, however, the large-scale study of complex cellular proteomes is typically achieved using mass spectrometry.[34,35] This can be achieved by either a top down or bottom up approach depending on the experimental design.

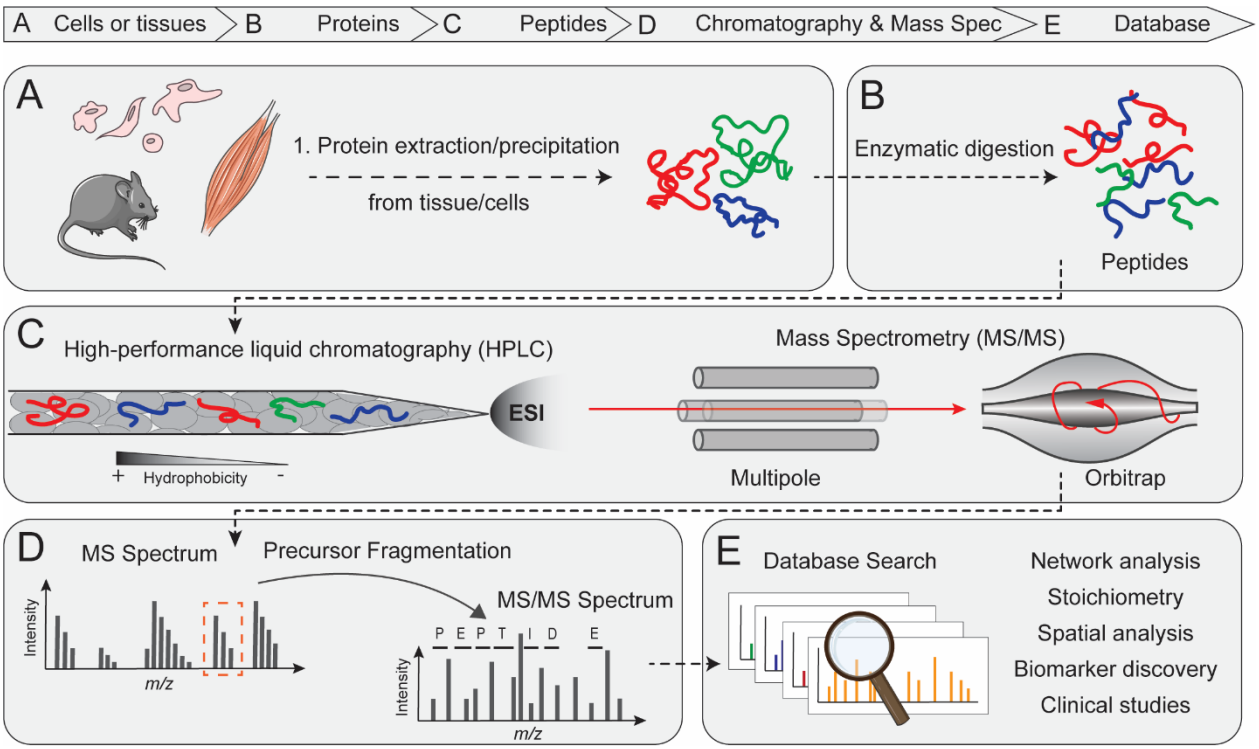

Figure 1-4. Overview of bottom up strategy of mass spectrometry based proteomic

workflow. *(A) Proteins are first isolated from tissues or cells before (B) enzymatic digestion into peptides that are analysed by HPLC-MS/MS (C & D). Spectra are entered into a search engine to yield a list of proteins and their associated information depending on experimental design.*

Bottom up strategies are most common, and here proteins are first extracted from tissues or samples before being digested enzymatically into their component peptides, typically by trypsin, which is a specific endopeptidase (Figure 1-4).[36] Peptides are then analysed by MS/MS, usually utilising online high-performance liquid chromatography (HPLC) separation to enhance peptide identification and deepen the proteome coverage. Combining fragmentation spectra, precursor *m/z* values and endopeptidase specificity allows specialist software to search protein databases obtained from genome sequencing. This software then utilises the amino acid sequencing of peptides to identify the digested protein, thus resulting in generation of a proteome. Currently, the most successful commercial instruments for proteomic studies use electrospray coupled orbitrap mass analysers. These instruments can perform fragmentation and MS scans with great resolution and can be coupled with ion traps and multipoles to generate hybrid instruments such as the Q Exactive or Fusion Lumos instruments that have multiple modes of action and are incredibly functional.

The generation of total proteomes can now regularly exceed 10,000 protein identifications for an experiment, thus yielding huge datasets and information regarding a system.[37] Optimisation of methods for the isolation and purification of organelles such as mitochondria, phagosomes and cell secretomes has enabled the separation of these discrete proteomes. When combined with MS proteomic analysis, these methods have led to deep characterisation of sub cellular and extra cellular protein composition and in turn lead to ground breaking research into their function. Standard proteomic methods

may now be coupled to quantification techniques using isobaric labelling such as iTRAQ, TMT, and SILAC[38], all of which enable the relative quantification of proteins within a system, thus generating more robust and accurate data sets. In more recent years, these technologies and methods have been exploited to perform more functional studies such as protein conformation changes, thermal cellular shift assays and subcellular spatial studies. Consequently, the combination of these strategies and advanced mass spectrometry instruments enables valuable insights into the composition and functional dynamics of a system's proteome.

1.1.7 Sample preparation methods and proteomic workflows

There are now many published methods that describe the digestion of proteins into peptides for proteomic analysis that range from traditional in-solution digestion[39] to in-gel digestion[40], magnetic bead digestion[41,42] and matrix trapping techniques.[43–46] It is paramount that efficient enzymatic digestion is achieved; thus, proteins must be in a denatured conformation to allow proteolytic enzymes such as trypsin to reach peptide regions that would otherwise be conserved by the natural conformation of the protein (Figure 1-5.A). This is typically achieved by resuspending samples in either a strong detergent such as sodium dodecyl sulfate (SDS) or highly concentrated urea, before the addition of a reducing agent such as DTT or TCEP to reduce the sulfur of disulfide bridges from cysteine residues, which are strong intra-protein interactions that influence protein conformation. As these bonds can re-form under oxidising conditions, it is standard practice to use an alkylation reagent such as iodoacetamide or 4-vinyl pyridine to alkylate the sulfur groups and prevent reformation.[47] From this step onwards, sample preparation protocols diverge depending on the method chosen. For in-solution digestion (Figure 1-

5.A), samples are simply diluted to a working concentration that allows stable digestion by the addition of an endoproteinase such as trypsin, Lys-C or Lys-N and incubated overnight. After digestion, samples typically require clean-up as detergents and high salt concentrations are incompatible with mass spectrometry analysis. Previously, C18 clean up columns have been used for this purpose. However, recently, there has been development of matrix trapping protein digestion methods that dramatically reduce sample preparation time and can enable significantly faster sample throughput by integration of plate formats.

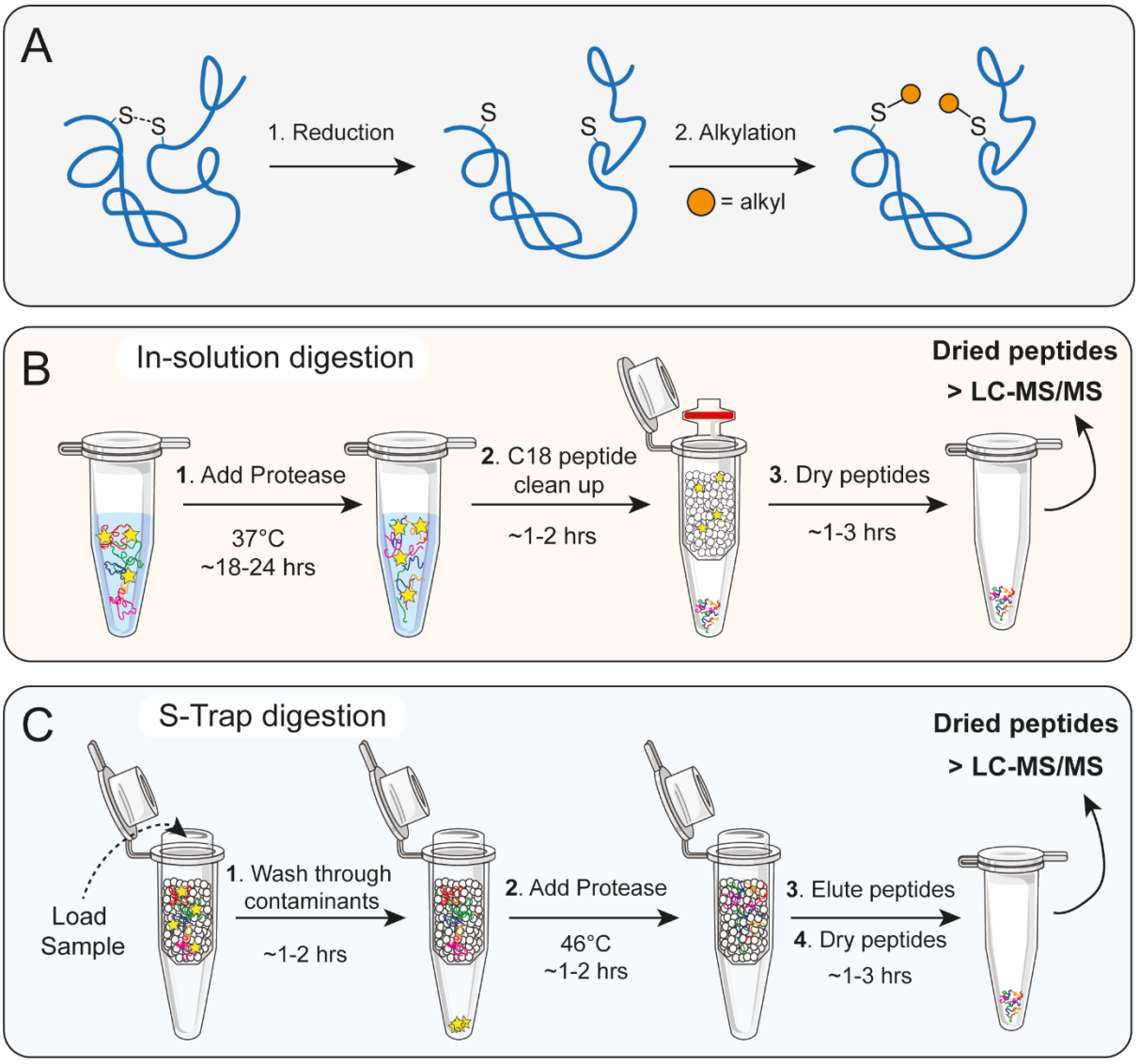

Figure 1-5. Workflows for proteomic sample preparation methods. *(A) Graphical*

representation of reduction/alkylation where cysteine disulfide bonds are first reduced and alkylated to denature proteins. (B) Workflow for in-solution digestion where proteins are digested and the resulting peptides are cleaned-up using C18 spin columns to remove contaminants prior to LC-MS/MS. (C) S-trap workflow where proteins are aggregated onto a solid phase and contaminants removed through washing. Proteins are digested on-phase before peptides are eluted and analysed by LC-MS/MS.

Here, denatured and alkylated protein samples are first acidified and then loaded onto a spin column that contains a solid phase that non-specifically immobilises proteins. The driving force behind this is the induction of protein aggregates that enables the capture of proteins onto solid matrices or microspheres leading to very little flow through of sample during subsequent washing steps.[48] Consequently, columns are then typically washed with buffers that contain high organic solvent concentrations to remove contaminants before a fast digestion for 2 hrs at an elevated temperature. Digested peptides can then be directly eluted, dried and resuspended for proteomic analysis.

This technology is fast being adopted for previously complicated sample analysis such as tissue embedded in formalin, for which previous techniques would have been unfavourable. Matrix trapping protocols dramatically improved the proteomic profiles of these tissue samples, as nearly all sample contaminants including melted formalin can be removed by washing. This opens up new avenues of research that had previously been unexplored, such as archaeology or precious clinical samples where sample volume is limited. Furthermore, this trapping technology is now being supported for clinical applications, where robust sample digestion can be coupled to automated liquid handling robots and there is no need for sample clean up that can lead to unnecessary sample loss.[49] From both these sample preparation methods, dried peptides can then be resuspended in a suitable buffer and injected into a mass spectrometer for analysis.

1.1.8 Protein identification and quantification

After mass spectrometric analysis, precursor (MS) and fragment scans (MS/MS) can be combined to identify the digested peptide amino acid sequence and consequently protein identification. Endopeptidase specificity is particularly important here as it simplifies downstream analysis. Typically, trypsin is used in most workflows as it is highly specific for cleavage after arginine or lysine residues with the exception of missed cleavages where a proline residue resides directly after or within close proximity.[50,51] Furthermore, this cleavage formation is particularly advantageous for mass spectrometry analysis as lysine or arginine side chains can be easily protonated by ESI or MALDI techniques to generate peptides that can be multiply charged. Other endopeptidases such as elastase or proteinase K are relatively unspecific in their cleavage sites and are more frequently used for specific experimental designs such as membrane proteomics.[52] Traditionally, proteomic analysis is conducted in data dependent acquisition (DDA), where the most abundant peptides are selected by the multipole as precursors for MS/MS analysis (Figure 1-6.A). This technique results in good coverage and protein identification but can be biased towards highly abundant peptides. Therefore, data independent acquisition (DIA) can be more suitable in some cases (Figure 1-6.A).[53] Here, rather than identifying specific precursors, narrow sequential *m/z* windows are scanned within the multipole and fragmented to result in fragmentation spectra of multiple species. This enables the unbiased identification of peptides and detection of low abundant proteins. However, this approach is more arduous as it relies on having a comprehensive spectral library for spectra matching as the fragmentation of several peptides results in complex MS/MS spectra. Therefore, this often necessitates prior DDA acquisition to generate sample specific libraries for optimal matching and protein identification.

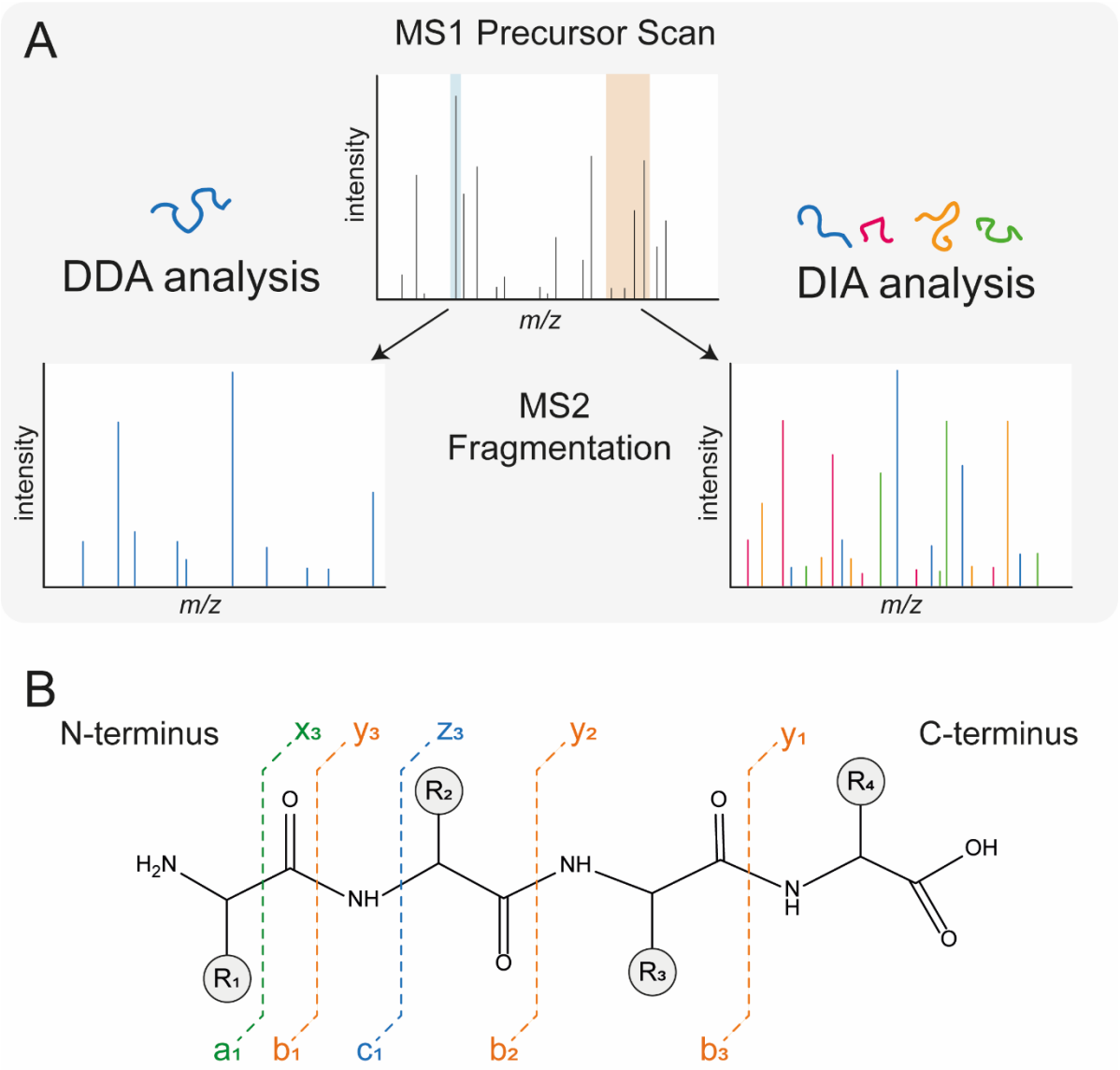

Figure 1-6. Principles of peptide fragmentation strategies. *(A) Comparison of DDA and DIA analysis showing peak selection and complexity of MS2 fragmentation spectra depending on acquisition mode. (B) Fragmentation of peptides to produce either b+y, a+x or c+z ion pairs.*

Once precursors are selected for MS/MS analysis, they are sent for fragmentation. The most common peptide fragmentation technique is collision induced dissociation (CID).[54] Here, an inert gas such as nitrogen or helium is used as a collision gas within a fragmentation cell and as the charged peptides collide with the inert atoms they are vibrationally activated, leading to the breakage of the weakest chemical bond. The

resulting product ions are characteristic for peptides as cleavage is favourable at the amide bond of the peptide back bone to generate b and y ions (Figure 1-6.B). The b and y ions are formed from the N- and C- terminus, respectively, and their sequencing allows for precursor peptide structures to be elucidated and in turn their parent proteins identified. Alternative fragmentation methods such as electron transfer dissociation (ETD) and photodissociation techniques induce the formation of a+z and c+x ions (Figure 1-6.B) that can be used for peptide structure identification and are particularly important for branched peptides and identification of post-translational modification sites.[55,56] Once acquired, raw spectral data files can be processed by using available search engines such as MaxQuant[57], Mascot[58] or PEAKS[59]. Using the specificities described previously, proteins can be identified by *de novo* peptide sequencing algorithms, which match fragment spectra and their parent ion mass to *in silico* protein digest. An *in silico* database is a computationally generated model of the biological experiment. For proteomic experiments, each desired protein sequence and the specific proteolytic method is used to predict the potential proteolytic peptides for each protein within the model. Using the theoretical mass, charge states and sequences the signals detected in the mass spectrum and their MS/MS data can then be matched to theoretical peptides and identified. Not only can proteins be identified, but also the relative abundance of each protein can be determined if combined with isobaric tagging techniques. More recently, these search techniques are moving towards live identifications, where Wichmann *et al.* showed that it was possible to target more than 25,000 peptides in real time during a single LC-MS run.[60]

Hybrid orbitrap mass spectrometers are still currently the most common instruments for proteomic analyses, however the development and optimisation of ion mobility (IM) mass analysers are showing promise in this field.[61] Here, IM is being conjugated to lower

resolution TOFs to dramatically increase acquisition speeds, resolution and sensitivity.[62] This technology has been demonstrated to be very powerful for clinical applications and low sample volumes and more recently is expanding into the DIA space for broader application in MS based proteomics.[63] However, despite this technology's enhanced speed it lacks the resolution of orbitrap and FT technologies, which is paramount when utilising isobaric labelling techniques such as TMT 10, 11 and 16 plex.[64] Overall, taken combined these advanced mass spectrometers enable the identification and quantification of diverse proteomes towards understanding biological function and are paramount for answering complex biological questions.

1.2 Drug discovery

1.2.1 The drug discovery pipeline

The drug discovery and development pipeline is an interdisciplinary process that engages multiple phases of research to facilitate the production of effective therapies (Figure 1-7). The timeline itself is typically divided into two groups: drug discovery and drug development. The discovery phase entails the development of diverse compound libraries, target validation and high-throughput screening campaigns to identify hit compounds. The development process occurs after, where lead compounds undergo further optimisation such as pharmacokinetic and *in vivo* validation studies before moving forward into pre-clinical and clinical trials. The result of these combined stages is a a long and arduous process to get FDA approval of compounds, often with high failure rates across all stages and taking up to a decade for successful therapies to reach the clinic.[65] Due to the time and capital investment needed during the development and clinical trial process, there is a growing need to develop more biologically relevant and diverse

screening assays to qualify hit compounds during the discovery phase. However, current assays are often biochemical, and although high-throughput, can result in false positive hits. Here, mass spectrometry and other more advanced technologies could aid the drug discovery process by identifying better quality lead compounds.

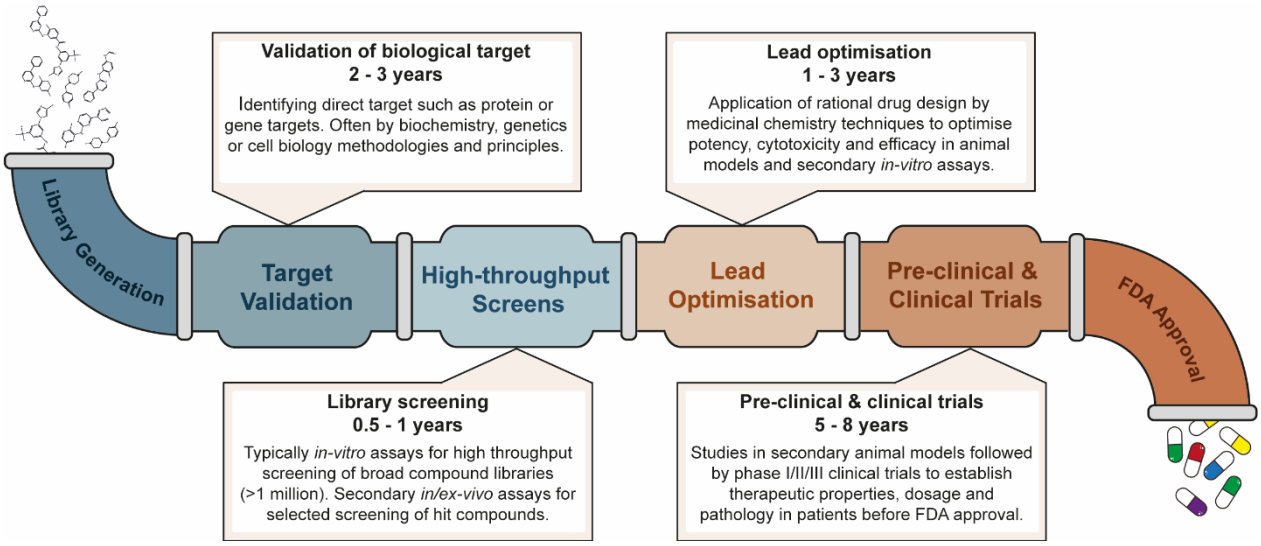

Figure 1-7. Drug discovery pipeline highlighting the time taken for each stage of drug development.

Knowledge of the molecular mechanisms underpinning diseases such as cancer, inflammation and neurodegenerative diseases has advanced significantly in the past decade and in turn has led to a demand for more personalised and precise medicine. Historically, small molecules have predominantly ruled the approved treatments for such diseases, but large biomolecules such as antibodies, liposomes and gene therapies have emerged as promising targeted treatments. However, design and validation of these therapies is significantly different to the development of small molecule inhibitors, therefore more specialised and advanced technologies must be integrated into the existing pipeline. Mass spectrometry is already well established as a sensitive and versatile technique in research for the analysis of large biomolecules and is a natural choice for the development of new therapies.

1.2.2 Use of mass spectrometry within drug development

Mass spectrometry techniques are already widely used throughout the drug development pipeline from target identification and screening to clinical studies and quality control of FDA approved compounds (Table 1-1). At the initial stage of drug discovery, MS based exploratory techniques such as proteomics, metabolomics and analysis of clinical tissue samples are an important part of lead compound discovery to identify and validate therapeutic targets.

Table 1-1. Mass spectrometric techniques and their associated application within the drug discovery and development pipeline.

MS Technique	Stage of drug discovery/ development	Application
MALDI-MS		
MALDI-TOF-MS	• HTS • Lead Optimisation	Peptide mass fingerprinting, bottom up shotgun proteomics, HTS, intact mass analysis
MALDI-Imaging	• Target validation • Lead optimisation	Either FT-ICR or TOF; high resolution or speed. Clinical validation of tissue disease state as well as drug efficacy and localisation.
MALDI-FT-ICR	• Target validation • Lead optimisation	High resolution for intact target characterisation studies. Sub-cellular organelle analysis.
LC-MS/MS		
Triple-TOF Triple-Quad	• Lead optimisation • Pre-clinical and clinical trials	Targeted assays for lead optimisation: SRM, MRM. Drug and antibody detection from biofluids in clinical studies.
Q-Trap / Ion trap	• Manufacturing QC • FDA QC • Library generation	Large fragmentation data enables maximum structural information that can characterise compound libraries.

Orbitrap/Q-TOF	• Target discovery and validation	High resolution, large complex data sets: Metabolomics, proteomics.

Despite mass spectrometry being a powerful tool within the drug development process, its application to the compound library screening has lagged behind, often due to a lack of throughput. However, advances and development of novel MS instruments and liquid handling system's have, in principle, enabled MS based screening methods that rival conventional biochemical assays, especially with respect to large biomolecule screening.

1.2.3 Mass spectrometry as a tool for high-throughput screening

For high-throughput screening, MS-based readouts have been largely dominated by instruments containing SPE and ESI-MS, such as the RapidFire™ system.[66] Here, as a conventional liquid chromatography module would not produce the sample processing speeds required for HTS, the LC-unit is replaced by a sample clean up cartridge that enables higher flow rates and faster sample processing within a 384 plate format.[67] Coupled with an automated microfluidic sample collection and purification system as well as high-speed robotics to directly aspirate fluidic samples directly from 96- or 384-well screening plates sample processing speeds of 4-8 seconds can be reached. This fully automated system can remove non-volatile assay components such as salts, buffers and detergents in an online fractionation step to deliver purified analytes to the mass spectrometer.[66] In addition, the RapidFire source can be coupled to either a triple quadrupole or TOF mass analysers, thus enabling various modes of action such as intact mass or fragmentation methods as well as selected reaction monitoring (SRM). Hence, there has since been a plethora of HTS assays developed for RapidFire MS for a variety of drug targets including acetyl-coenzyme A carboxylase,[66] stearoyl-CoA desaturase,[68]

sphingosine kinases,[69] histone lysine demethylase[10] and phosphatidylserine decarboxylase.[70] These assays demonstrate that ESI-MS is capable of achieving the robustness necessary for HTS, as well as the throughput of libraries >10,000 compounds. However, the speed of sample injection and analysis still does not yet rival conventional assays that can achieve a <1 second per sample throughput. To tackle this, Leveridge *et al.* proposed a simple multiplexing strategy using mass tagged substrates and JmjD2d as a model system to increase the throughput of RapidFire assays, thus making ESI-MS more viable as a HTS platform.[71] Here, four H3 peptides from separate JmjD2d demethylation reactions were pooled and simultaneously analysed by MRM, which in turn offered a four-fold increase in compound throughput over the standard RapidFire assay. This could be implemented to enable diverse screening where substrates differ in mass and transition, thus enabling screening of libraries against one or more drug target in parallel. More recently, RapidFire BLAZE-mode was developed that retains the same quality and robustness as previous operating systems, but modification of the switch valve connections and operational pumps enabled rapid cycling times of 2.5 seconds per sample.[72] This technology is the fastest commercially available ESI-MS instrument at this time and is very attractive for low-molecular mass or poor performance analytes that require more sensitive methods. However, it still does not reach the speeds of true ultra-HTS assays that process samples in under a second, therefore exploring into alternative liquid dispensing techniques such as acoustic mist MS or open-port probe MS is growing.[73–75]

Acoustic technology dispensing has been utilised widely within the drug discovery pipeline for preparation of screening microplate from compound stocks and dosing in cellular assays.[76,77] Therefore, recent research has explored the use of acoustic mist ionisation

(AMI) as a technique to introduce liquid samples into a mass spectrometer to solve the current sampling throughput bottleneck in HTS mass spectrometry.[78] Current advancements in the design of the AMI-MS instruments led to the development of technologies that can introduce samples at speeds of three samples a second that are robust throughout drug screening campaigns. Recently, AstraZeneca performed a 2 million compound library screen to identify inhibitors of a human histone deacetylase and measure their half-maximal inhibitory concentration in under 7 weeks, totalling 2.75 million wells screened on a single AMI-MS instrument.[79] However, although this technology shows great potential, it is currently limited by the high well-to-well variability as smaller mists are generally harder to control compared with nanolitre droplets and can lead to poorer assay quality and Z' values.[73] Further to this, AMI-MS is prone to matrix interference as it is more similar to direct injection ESI-MS where no clean up or separation can be performed, thus assays can lack sensitivity.[80,81]

1.2.4 Rise of MALDI-TOF-MS within high-throughput screening

The potential of MALDI-TOF-MS assay development for HTS is broad as the technology can be applied to potentially any reaction that involves a mass change or intensity shift.[82] These assays enable label-free quantitation, a gold standard for assays in the drug discovery field over conventional assays. This is particularly attractive to the pharmaceutical industry as the use of assays with fluorophore labelled substrates or secondary amplification assays can lead to false positive or negative hits with auto-fluorescent compounds. Utilising MALDI-TOF-MS assays, a compound's potency can be measured independently to any inherent luminescent properties, thus enable the screening of larger libraries. This has naturally led to the development of enzymatic

assays that measure the rate of post translational modification of either a protein or peptide substrate by a potential drug target enzyme. Many of these optimised assays match or exceed conventional assays in performance and speed, but assay development can be challenging. Direct translation of assay buffers to MALDI-TOF-MS assays has often been problematic, as mass spectrometry is sensitive to ion suppression from salts, glycerol and other common reagent buffers that are imperative for biologically relevant assays and to preserve protein function. This may in turn result in significantly different enzyme activity, conformation or compound interaction and it would be interesting to further understand whether these buffer substitutions influence compound hit profiles. To ease the process of assay development for non-experts in the field, Haslam *et al.* published a systematic study of buffers for small molecule analysis that are compatible with MALDI-TOF-MS.[83] Combined with novel, user friendly software and a fully automated, integrated liquid handling platform, MALDI-TOF-MS has become a promising novel tool for future drug screening campaigns.[84]

1.2.5 In vitro biochemical screening assays

Development of *in vitro* MALDI-TOF-MS assays that were able to evaluate the IC_{50} of drug compounds was presented by Greis *et al.*, who describe a kinase phosphorylation assay that probes inhibitor action.[85] However, sample analysis speeds here were still relatively slow for HTS speeds with a 10 second per spot analysis required to acquire good spectra. The development of the RapifleX mass spectrometer overcame this and enabled a 1 second sample analysis speed that rivalled the more conventional HTS assays and the field MALDI-TOF-MS assays expanded rapidly.

The first studies utilising the high speed of these new generation MALDI-TOF-MS instruments for drug discovery was the development of an assay to study deubiquitylases (DUBs) specificity and drugability by Ritorto *et al*.[86] Ubiquitylation is a post-translational modification that involves a discrete set of ligases and conjugating enzymes to modify target proteins by conjugation of ubiquitin, a small 8.5 kDa protein.[87] The cleavage of ubiquitin moieties from target proteins is catalysed by DUBs, whose primary role is to modulate the levels and types of ubiquitylation within a system. However, as ubiquitin itself can be conjugated to proteins through either of its seven lysine residues or n-terminus, the system becomes inherently more complex and there is formation of complex chain linkage architecture. Therefore, it is known that DUBs must have a certain degree of specificity for different chain types so as to modulate the vast landscape of ubiquitylation. Aberrant or accumulation of certain chain linkage types by dysregulated DUB activity has since been linked to diseases such as Parkinson's disease and cancer, therefore elucidating the DUB specificity and screening for potential inhibitors has become prominent in the drug discovery field.[88] Previously, profiling DUB specificity required the use of activity based probes,[89,90] or DUB activity to be profiled by conjugation of fluorogenic probes such as Rhodamine110.[91] Neither of these assay types provided conclusive specificity and activity of DUBs *in vitro*, used label-free substrates or were not suitable for use on a high-throughput platform, therefore the development of a MADLI-TOF-MS assay for screening DUB specificity and activity has revolutionised the field.[86] In brief, DUBs were incubated with synthetic ubiquitin dimers of different linkage type and the amount of mono-ubiquitin resulting from dimer cleavage was quantified using an isotopically labelled internal standard. This set up was fast, label-free and enabled the determination of DUB specificity for different linkage types as well as drug specificity. This

assay was unique to the field as it could be expanded to a HTS platform and this lead to the development of an assay to screen for E3 ligase inhibitors by De Cesare *et al*.[92] Here using the same technology and experimental set up, E2-E3 ligase pairs could be established by measuring conjugation of ubiquitin rather than cleavage of dimers, which also translated to screening of inhibitors of the auto-ubiquitylation process. Taken together, these two methods added significant value to the expanding tool box of mass spectrometric techniques for elucidating ubiquitylation signalling and has aided the discovery of several new DUB inhibitors.[93–95]

The targeting of enzymes that catalyse the addition or cleavage of PTMs for MALDI-TOF assay development has grown from ubiquitylation to phosphorylation[96,97],[98], acetylation and methylation (Figure 1-8.B)[99,100]. Here, several assays were compared with existing biochemical assays and report good correlation of compound hits and IC_{50} values, as well as identifying potentially new compounds that could have previously been missed with labelled substrates.

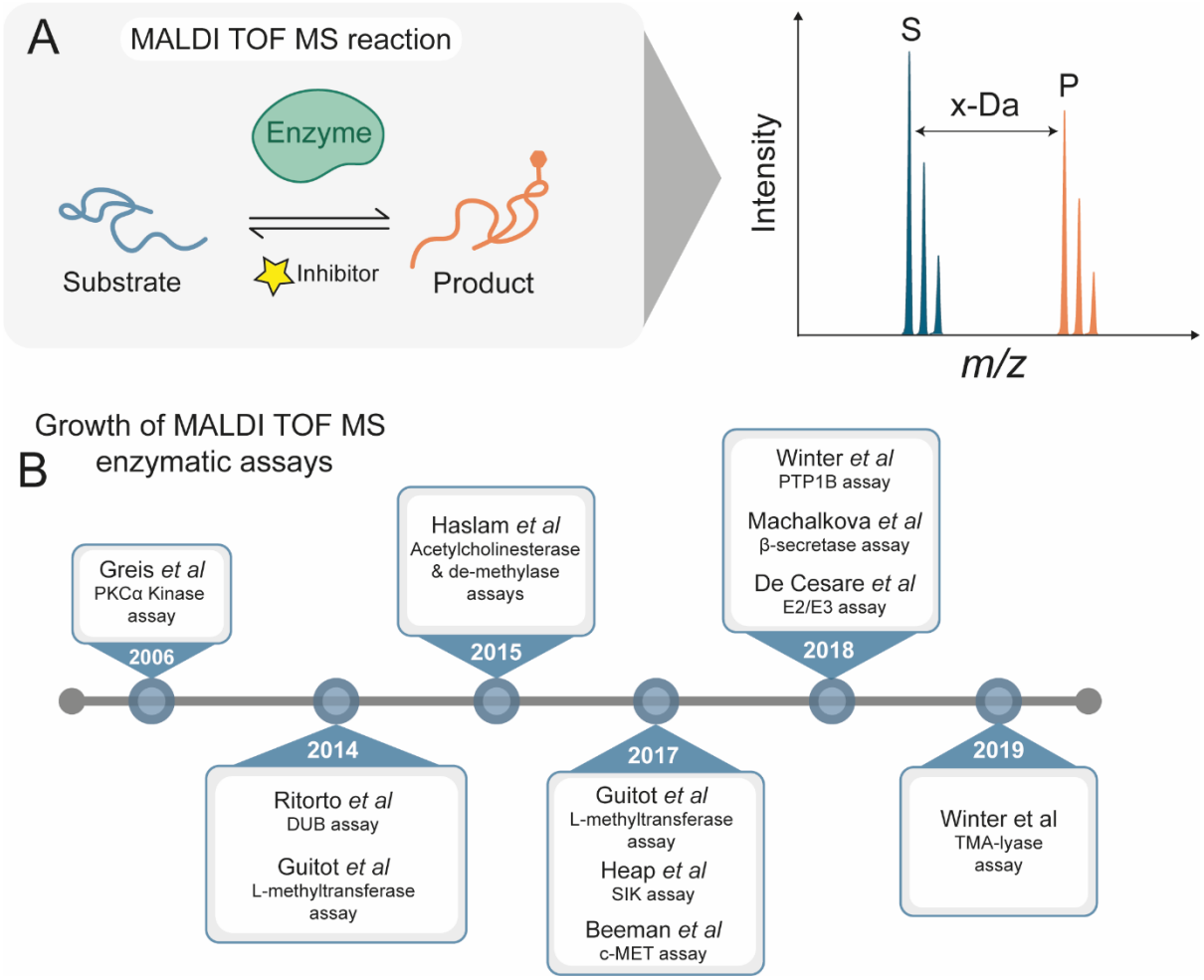

Figure 1-8. MALDI-TOF-MS as a tool for enzymatic activity assays*. (A) Graphical representation of enzymatic reaction that converts substrate to product has a mass change that can be measured by MALDI-TOF-MS. This reaction allows relative quantitation between substrate and product peaks and can be reversed with hit compounds that can be detected by MALDI-TOF-MS. (B) Timeline of the past 15 years showing the growth of published enzymatic MALDI-TOF-MS assays.*

Self-assembled monolayers (SAMs) can be coupled with MALDI to form another surface-based MS technique: SAMDI-TOF. A similar method coined surface enhanced laser desorption ionisation (SELDI) affinity technology was developed in 1993. however, the binding of substrates to the surface was unspecific and poorly distributed and could result in diminished sensitivity.[101,102] In the case of SAMDI, a single nano-scale monolayer, or SAM, is first formed on the surface that will capture substrates. The chemistry of the mono-

layer molecules are carefully selected for substrate capture suitability as well as their ability to self-assemble into a crystalline upon the surface.[103] These molecules have typically been alkanethiols as they form a strong disulphide bond with the surface and can be modified to have wide range of terminal functional groups for specific analyte capture.[104] In the case of biochemical assays, a peptidic substrate would typically be immobilised and then individually treated with enzyme with or without the presence of inhibitors. The targets can then be treated with a matrix, similar to a traditional MALDI experiment, and upon irradiation with a laser the monolayers and substrate are desorbed from the surface through cleavage of the substrate-target bond and ionised. This technology was pioneered by the Mrksich lab and is well-suited for measuring a broad range of enzyme activities as SAMs can be customized to use a variety of immobilisation chemistries. As SAMDI benefits from the same instrumentation as MALDI, it is also a promising strategy for a HTS targeted approach with a potential throughput of >100,000 compounds per day. A strength of this technology is that the bond between surface and bound molecule is strong enough to permit thorough washing to remove assay contaminants, yet weak enough to be analysed by MALDI-MS.[105]. To demonstrate drug discovery assay suitability, a study by Patel *et al.* utilised this technology and discovered a novel specific inhibitor of sirtuin 3 (SIRT3) from a label-free screen of 100,000 compounds library using SAMDI-TOF.[106] From this, SAMDI has also been used for *in vitro* screening of diverse enzyme classes such as phosphatases[107], glycosyltransferases[108], deacetylases[109]. More recently, VanderPorten *et al.* developed a new tool using SAMDI that allows screening and identification of non-covalent binding small molecules to target proteins.[110] In this study, a proof of concept workflow demonstrated a novel screening format of a pooled compound mixture using affinity capture and purification followed by

SAMDI-MS. Here, binders with affinities below the micro-molar range were identified in a robust and reproducible manner that correlated well with biochemical assay potencies.[110]

1.2.6 Cellular assays

Whole cell analysis or cellular assays for evaluating compound efficacy at moderating or reversing a cellular phenotype presents an interesting challenge for MALDI-TOF-MS analysis as the system becomes inherently more complex. A well-established application for whole cell MALDI-TOF-MS is the classification of micro-organisms, also known as biotyping, which was first presented by Claydon *et al.* in 1996.[111] Here, microbe classification is achieved by identifying protein biomarkers in a MALDI-TOF-MS spectrum to generate a signature spectral mass fingerprint. Typically, the *m/z* region selected is 2–20 kDa as this reflects the unique ribosomal protein profiles of a bacterial species, which are highly abundant and reproducible.[112,113] For classification, the specific spectral fingerprint is then either compared against a database of known bacteria genus spectra to identify an unknown species, or masses can be matched to a prokaryote proteome databases.[114,115] This genus and sub-species specificity can be achieved as the bacterial genome is relatively simple compared with eukaryote proteomes, thus proteins can be matched to identified *m/z* values confidently with the aim of generating a comprehensive database.[116–118] Throughout the past decade this has led to sensitive and robust phenotyping of micro-organisms in clinical microbiology for the diagnosis of infectious diseases as the technology is fast, inexpensive and can be automated.[119,120] More recently, MALDI-TOF-MS has also been used to accurately identify *Mycobacterium tuberculosis* (TB) sub species, which is particularly important with the rapid progression of TB infections worldwide. Therefore, this technology could be important for detecting

subtle changings in bacterial ribosomal proteome that may indicate a mutation or adaptation towards treatment or environmental exposure. This approach has already been applied in the field of antibiotic resistance, where MALDI-TOF-MS can be used to evaluate whether antibiotics are efficient or detect biomarkers of antimicrobial resistance.[121–123]

Application of whole cell MALDI-TOF-MS methodologies to mammalian cells has not yet reached the heights of microbial biotyping but is rising as a promising technology for phenotypic screening and the development of drug discovery assays. Similarly to bacterial biotyping, fingerprinting of mammalian cell protein biomarkers has been successfully applied to phenotype different cancer cell lines[124], classify immune cells[125] as well as monitor early stress or apoptosis signals in cell lines.[126] The classification of cell lines from primary tissues can be complicated by cell heterogeneity, but MALDI-TOF-MS has proven to be sensitive and robust at distinguishing tissue derived cell mixtures[127] as well as classifying differentiated cells from primary blood monocytes.[128] Typically, these strategies utilise multivariate analysis and detection of unique features for classification that, when combined with flow cytometry, microscopy or known biomarker analysis result in robust MALDI-TOF-MS methodologies. However, as mammalian cell PMFs can be complex and difficult to deconvolute, several strategies have been developed to quantify and identify sub-categories of cells. These include dual-biomarker approaches that uses a ratiometric quantification between common features of co-cultured cells[129], as well classifying cell secretion such as extracellular vesicles to sensitively identify chemoresistance in cancer cells.[130] This in turn could be a less invasive way of characterising a patient's response to cancer treatment.

Complimentary to cell proteomes, mammalian cells exhibit dynamic lipid profiles that are often indicative of cell phenotype or a diseased state such as liver or heart disease.[131–133] Imaging mass spectrometry has already demonstrated that MALDI-MS is well suited for lipid analysis of cells, and therefore research has expanded into cellular classification using lipid analysis.[134] Typically, this has been performed using high resolution MALDI-FT-ICR instruments, as lipids can be identified empirically from spectra, which is often needed as the generated data are more complex than protein marker data and many hundreds of lipids are identified. This in turn has led to single cell lipid profiling, which enabled the classification of astrocytes and neurons by Neumann *et al.*, who were also able to show that this was robust across 30,000 individual rodent cerebellar cells.[135,136] However, these methods are not as fast nor suitable for high-throughput drug discovery as MALDI-TOF-MS, therefore Weigt *et al.* combined the power of both MALDI-FT-ICR and MALDI-TOF-MS instruments to develop a cellular drug discovery assay.[137] In this study, a proof-of-concept assay demonstrated that inhibitors of fatty acid synthase (FASN), which are key for cancer proliferation can be identified by MALDI-MS. Using MALDI FT-ICR, lipids were first empirically identified before transferred to a MALDI-TOF-MS platform that rapidly profiled compounds and showed good IC_{50} correlation of hits with a biochemical assay.[137] Combined with automated liquid handling and sample preparation, this study demonstrates that lipid analysis of whole mammalian cells by MALDI-TOF-MS is suitable for the development of drug discovery assays to identify inhibitors of lipid metabolism.[138]

Taken together, these studies demonstrate the compatibility of cellular analysis with high-throughput MALDI-TOF-MS technology. Here, biomolecules such as proteins and lipids

can be identified from whole cells and used to classify cell types as well as evaluate a compound's activity in-cell.

1.3 Inflammation and the innate immune response

The innate immune system is a host's first line of defence against invading pathogens or injury. This response is evolutionarily conserved and tightly regulated by a host's immune cells such as monocytes, macrophages, neutrophils and other myeloid cells, whereas lymphoid cells like T-cells and B-cells propagate the adaptive immune response. Unlike the adaptive immune response, the innate mechanism is a rapid response that is initiated within hours of initial infection and involves the recruitment of immune cells to the site of infection and development of a physical barrier between pathogens and the host. Both these systems are important for host protection and resolving infection and are key targets for drug discovery as sustained inflammation is linked to a plethora of diseases.

1.3.1 Macrophages in the innate immune response

Macrophages play an important role in the innate immune response but are also highly plastic cells that can be polarised to a spectrum of activated states (Figure 1-9).

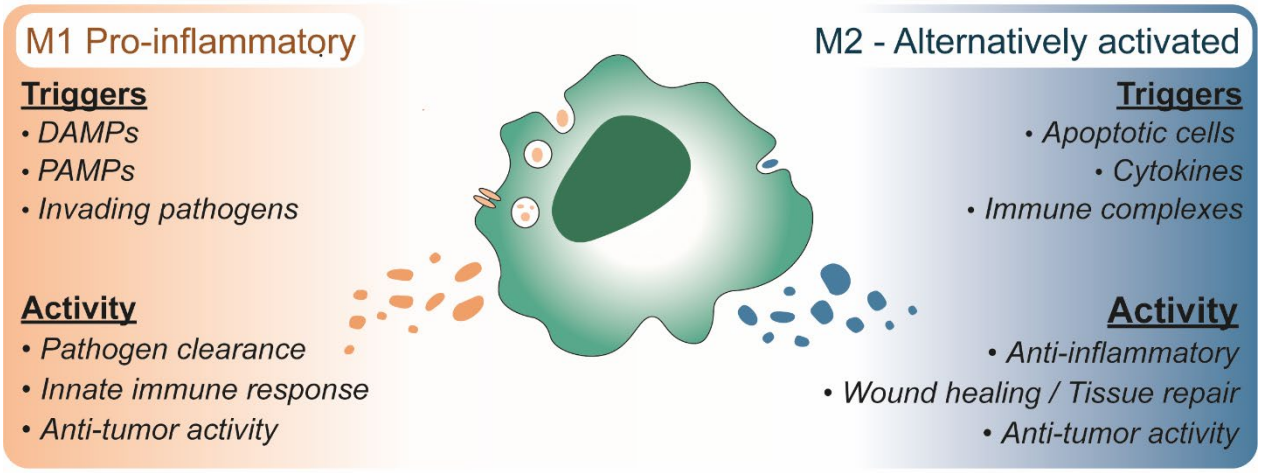

Figure 1-9. Polarisation of macrophages. *Activation states of M1 and M2 macrophages and their activity in response to specific triggers.*

A simplified model of macrophage activation describes two macrophage states that are coined classically activated (M1) or alternatively activated (M2). While M1 is a proinflammatory state import for infection and inflammation, M2 is important for maintaining homeostasis within an organism (Figure 1-9).[139,140] The M1 state is the better described macrophage phenotype, however, understanding the M2 phenotype is becoming more necessary as these macrophages can modulate M1 phenotype and help maintain homeostasis.[141] Alternatively activated M2 macrophages and their signalling cascades are poorly understood, but they have particularly important roles in tissue regeneration and wound healing.[142,143] In nature, these macrophages are often polarised by the presence of apoptotic cells or debris, presence of fungi or host secreted immune complexes but can also be polarised by cytokines such as IL4 and IL10.[141] Furthermore, M2 macrophages have a distinctly different chemokine profile to M1 macrophages. During anti-inflammatory polarisation, macrophages induce Th2 cytokine secretion including IL10, TGF-β and IL1-ra that can signal for tissue remodelling in surrounding cells.[144,145] Consequently, the functional study of these macrophages is paramount to understanding

the complexities of inflammation, wound healing and immune cell activation within an organism.

Unlike alternatively activated macrophages, M1 classically activated macrophages have a well described proinflammatory phenotype.[146]

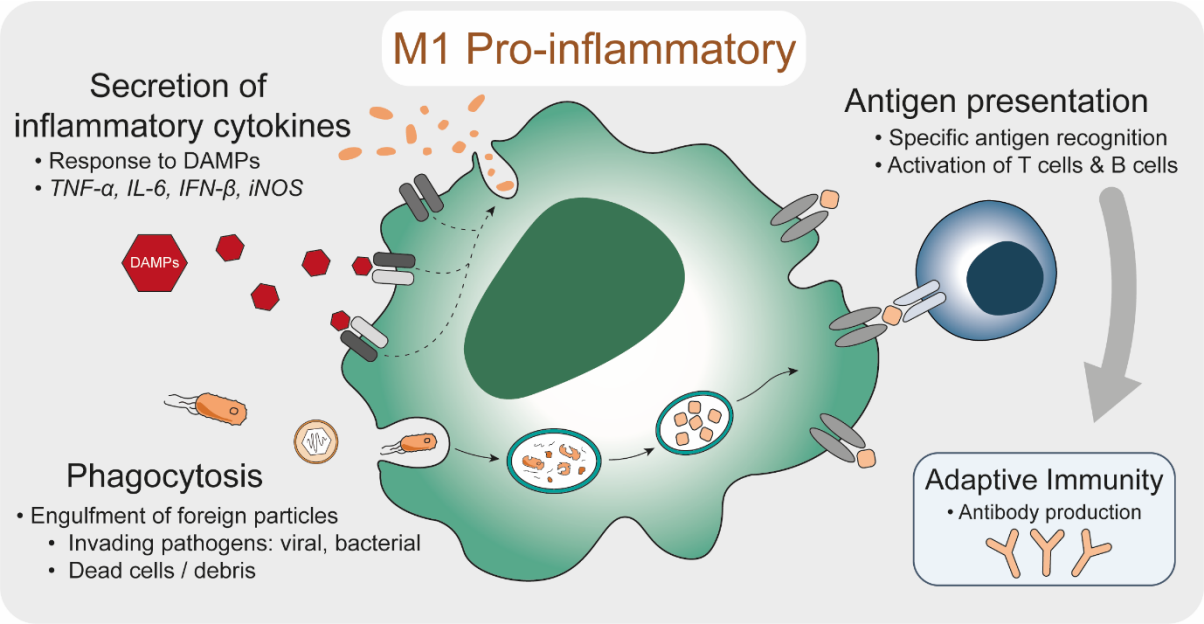

Figure 1-10. Classical activation of M1 macrophages. *Stimulation induces the secretion of pro-inflammatory cytokines, phagocytosis of invading pathogens and links the innate and adaptive immune response through antigen presentation.*

During pathogenic inflection, M1 macrophages are particularly important as they are often the first responders to danger. Here, they can perform a multitude of functions as shown in Figure 1-10 to eliminate pathogens and induce a protective inflammatory response. This primarily involves the engulfment of pathogens through phagocytosis, which results in the degradation and processing of the biological material and subsequent antigen presentation.[147] Unique markers or antigens of the pathogen are retained and presented on the surface of the M1 macrophages or dendritic cells to engage T cells. Consequently, this ties in the innate with the adaptive immune response and induces the production of T cells and antibodies specific for a particular bacterial or viral species to prevent

subsequent infection.[148] As well as this, biological markers such as pathogen-associated or danger associated molecular patterns (PAMPs & DAMPs) help propagate the innate immune response through a host cell's pattern recognition receptors (PRRs).[149] These PRRs include c-type lectin receptors (CLRs) or NOD-like receptors (NLRs), but perhaps the most common and well described receptors are Toll-like receptors (TLRs).[150] Typical PAMPs signal through TLRs and include exo- or endotoxins such as lipopeptides expressed by bacteria that when recognised induce a pathogenic infection immune response (Figure 1-10).[151,152] Conversely, DAMPs such as heat shock proteins or free DNA are released by host cells and perpetuate an inflammatory response independent of pathogenic infection.[153] Transmission of PAMPs or DAMPs signalling by receptors results in the production of pro-inflammatory cytokines such as TNF-α, IL-6 and IFN-β that can propagate the inflammatory response to other cells within the environment. At a tissue level, this results in swelling, pain and redness that is indicative of a localised immune response coordinated by immune cells to isolate the injury.

Inflammation can progress from acute to persistent to chronic inflammation if dysregulated and therefore the inflammatory response must be suppressed to prevent tissue pathogenesis.[154] Under normal conditions, resolution of inflammation is well managed by the production of mediators to prevent further recruitment of immune cells to site-specific inflammation as well as macrophage remodelling. Here, macrophages can undergo transformation from classically to alternatively activated cells that initiate wound healing and prevent the tissue infiltration of further immune cells such as neutrophils.[155] Chronic or severely acute inflammation occurs when anti-inflammatory mechanisms fail to resolve inflammatory signalling that can lead to tissue injury and in some cases to diseases, such as cardiovascular diseases, cancers and diabetes. Therefore, macrophages themselves

are key drug targets as their phenotype can be manipulated to prevent systemic inflammation and enable the discovery and development of targeted therapies.

1.3.2 Macrophages as drug targets for dysregulated inflammation

Macrophages themselves and consequently dysregulated inflammation are implicated in variety of diseases ranging from lifestyle disorders such as obesity and diabetes, to the some of the most common diseases including cancer, arthritis and heart disease.[156] Therefore, they are considered key drug targets and the focus of anti-inflammatory drug discovery. Macrophages are distributed throughout tissues in the human body and contribute to clearing pathogenic infection but also tissue homeostasis and repair. As all tissues and organs comprise of specialised cells depending on the function, specialised macrophages with variable functions are often found integrated into tissues. For murine studies, macrophages are distinguished within tissue by morphology or expression of surface proteins such as F4-80 or CD11b that can be detected by histology staining and flow cytometry, which in turn allows monitoring of macrophage progression within tissue over time or within a diseased state.[157,158]

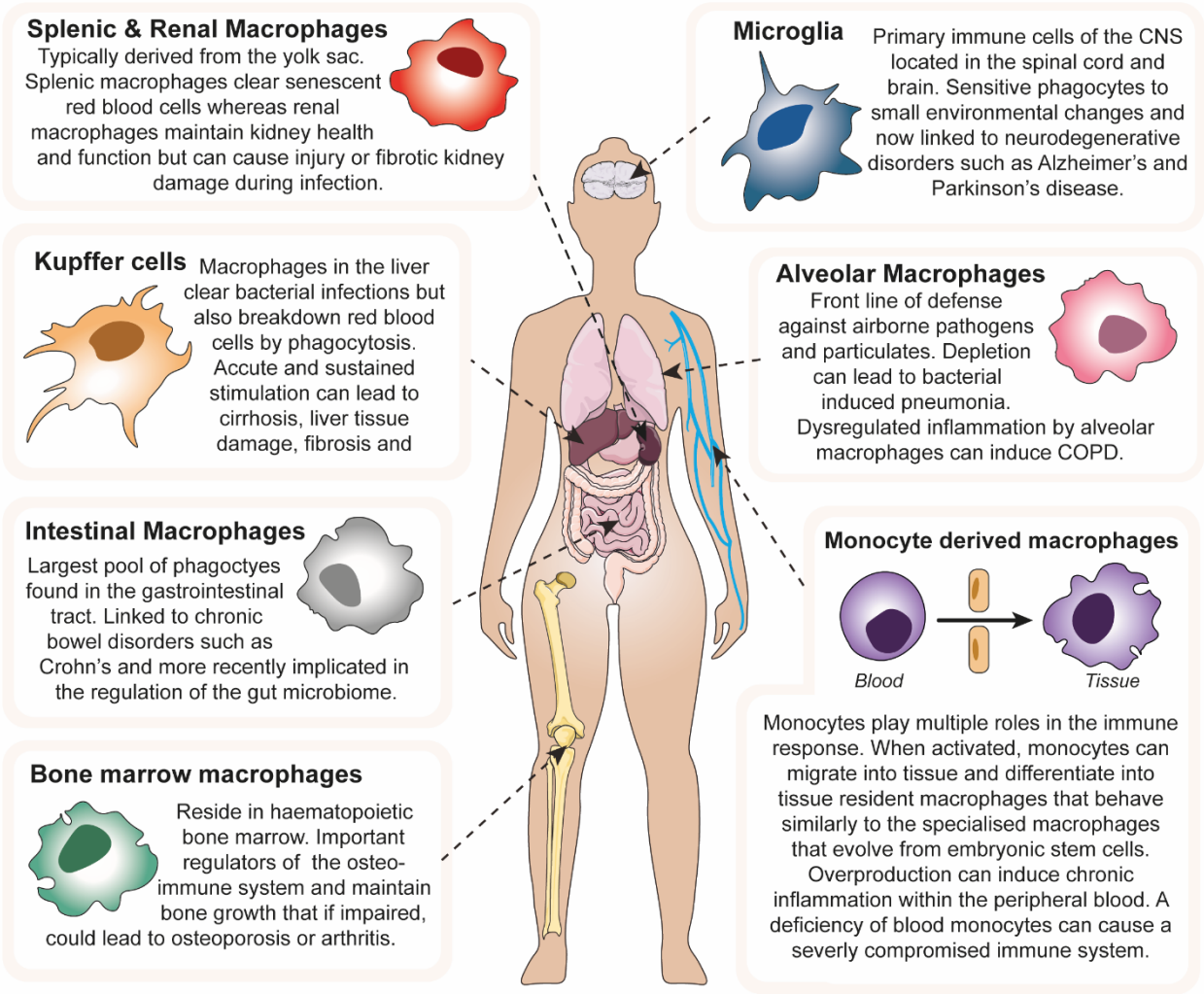

Figure 1-11. Graphical representation of the specialism of macrophages within the human body. *Specific roles of macrophages in maintaining tissue homeostasis alongside descriptions of the function of a particular macrophage specialism as well as their role in disease when inflammation is dysregulated.*

The diversity of these macrophage populations is highlighted by their functions described in Figure 1-11. For example, the resident macrophages within the gastrointestinal tract are localised to specific regions associated with digestion, nutrition and maintaining homeostatic balance in the gut. Interestingly, they can utilise their phagocytic abilities to modulate the microbial flora activity within the gut, thus developing a symbiotic relationship between bacteria and macrophage.[159,160] This process is essential for maintaining gut health and if dysregulated can result in inflammatory bowel disorders. On the other hand,

microglia are localised to the brain or spinal tissues and are extremely sensitive to subtle changes in tissue.[161] The speed at which these macrophages engage invading pathogens in brain tissue is unmatched when compared with other tissue resident macrophages as the damage incurred could potentially be fatal. Microglia are highly adept at killing bacteria unlike intestinal macrophages that sense and modulate bacteria populations. However, they are now linked to chronic neurodegenerative disorders such as Parkinson's and Alzheimer's and the knowledge surrounding the mechanism of these macrophages is limited.[162] Therefore, there is a strong drive to develop new therapies that can combine or replace existing treatments to increase efficacy and improve prognosis.[163]

One such area that has grown significantly in recent years is the relationship between inflammation and cancer, thus resulting in the targeting of tumour associated macrophages or TAMs for targeted therapies.[164] These macrophages are key drivers of tumour promoting inflammation and can dampen anti-tumour therapies by promoting an environment that is preferable for tumour growth in the presence of anti-cancer compounds.[165,166] This has resulted in the on-going clinical trials of over 30 compounds that target TAMs, with many of these manipulating the macrophage behaviour such as inhibiting recruitment or re-programming.[167] Some of the current therapies in clinical research include antibodies against CD47, a "don't eat me signal", inhibiting phagocytosis.[168,169] Some tumour cells exhibit high expression of CD47, that in turn prevents them from being efficiently phagocytosed and enable proliferation and metastasis.

Taken together, this vast biological landscape of inflammation highlights that a comprehensive knowledge of immune signalling is necessary for effective drug discovery. The complex signalling and mechanisms that surrounds the immune response presents

an interesting challenge for the field. The selection of the correct model for the specific disease is therefore critical. The model can vary significantly from *in vitro* models such as cellular or enzymatic assays to a myriad of *in vivo* models including zebrafish, mice, rats and primates.[170,171] These layers of complexity make the discovery of novel anti-inflammatory compounds difficult. Interestingly, there has recently been a drive to assess whether existing therapies could be repurposed for treating chronic inflammation which presents an interesting avenue of research for targeting diseases that present dysregulated inflammation.[172,173]

Chapter 2. Materials and Methods

2.1 Materials

2.1.1 Chemicals

All solvents were HPLC grade unless otherwise stated. Ethanol (EtOH), methanol (MeOH), dichloromethane (DCM), isopropanol, hexane, chloroform, acetonitrile (ACN), water (H_2O), dimethyl sulfoxide (DMSO) were purchased from Merck (Darmstadt, GER). Trifluoroacetic acid (TFA), phosphoric acid, formic acid (FA) ammonium hydroxide were purchased from Sigma Aldrich (St. Louis, MO, USA). Sinapinic acid (SA), 2-5-dihydroxybenzoic acid (DHB), 2-5-dihydroxacetophenone (DHAP), α-cyano-4-hydroxy-cinnamic acid (CHCA) were kindly provided by Bruker Daltonics (Bremen, GER). Peptide calibration standard (II), protein calibration standard (I), protein calibration standard (II) were provided by Bruker Daltonics used for calibration purposes (Tables 2-1, 2-2 and 2-3).

Table 2-1 Peptide calibration standard (II)

Peptide	$[M+H]^+$ Monoisotopic	$[M+H]^+$ Average
Bradykinin 1-7	757.3992	757.86
Angiotensin II	1046.5418	1047.19
Angiotensin I	1296.6848	1297.49
Substance P	1347.7354	1348.64
Bombesin	1619.8223	1620.86
ACTH clip 1-17	2093.0862	2094.43

ACTH clip 18-39	2465.1983	2466.68
Somatostatin 28	3147.4710	3149.57

Table 2-2 Protein calibration standard (I)

Protein	Charge state	Average *m/z*
Insulin	$[M+H]^+$	5734.51
Ubiquitin I	$[M+H]^+$	8565.76
Cytochrome C	$[M+H]^+$	12360.97
Myoglobin	$[M+H]^+$	16952.30
Cytochrome C	$[M+H]^{2+}$	6180.99
Myoglobin	$[M+H]^{2+}$	8476.65

Table 2-3 Protein calibration standard (II)

Protein	Charge state	Average *m/z*
Trypsinogen	$[M+H]^+$	23982
Protein A	$[M+H]^+$	44613
Albumin-bovine (BSA)	$[M+H]^+$	~ 66.5 kDa
Protein A	$[M+H]^{2+}$	22307

Albumin-bovine (BSA)	$[M+H]^{2+}$	~ 33.3 kDa

2.1.2 Toll-like receptor agonists and cytokines

Salmonella lipopolysaccharide (LPS) and phorbol 12-myristate 13-acetate (PMA) were supplied by Sigma Aldrich (St. Louis, MO, USA). PAM2CSK4, PAM3CSK4, Poly(I:C), Poly(A:U) were from Invitrogen. Macrophage inhibitory factor (MIF) and Macrophage colony stimulating factor (M-CSF) were purchased from Invitrogen (Carlsbad, CA, USA).

2.1.3 Inhibitors

Staurosporine, HG-9-91-01, MRT199665, MRT67307, KIN112, NG-25, BI2536 were provided by the Division of Signal Transduction Therapy (DSTT) Dundee, UK. The 2648 kinase inhibitor panel was kindly provided by Dundee Drug Discovery Unit (DDU), Dundee, UK. The 78 select macrophage compound panel, Nilotinib and Imatinib were kindly provided by LifeArc (Stevenage, UK).

2.1.4 Cells & cell culture reagents

L929, THP-1, MCF7, HEK293, U2OS and BMA cell lines were all purchased from the American Type Culture Collection (ATCC, Manassas, VA, USA). Bone marrow derived macrophages (BMDM's) were isolated from 3 month old WT female C57BL/6 mice femurs and tibiae that were kindly provided by the Institute for Aging, Newcastle University. Dulbecco´s modified eagle medium (DMEM), Roswell Park Memorial Institute medium (RPMI), Iscove's Modified Dulbecco's Medium (IMDM), Opti-MEM, phosphate buffered solution (PBS), fetal bovine serum (FBS) and β-mercaptoethanol (cell culture grade) and sterile DMSO were purchased from Gibco, Life Technologies (Darmstadt, Germany).L-glutamine, penicillin & streptomycin (Pen/strep) were purchased from Lonza (Basel,

Switzerland). Trypsin-EDTA solution and 37% paraformaldehyde solution (PFA) were purchased from Sigma Aldrich (St. Louis, MO, USA).

Table 2-4 Buffer compositions

Buffer	Composition
10-12% acrylamide resolving gels	375 mM Tris/HCl (pH 8.5), 0.1% SDS (w/v) and 8-12% (w/v) acrylamide. 0.1% (w/v) ammonium persulfate (APS) and 0.1% (v/v) TEMED were used to polymerise the gels.
6% Stacking gels	250 mM Tris/HCl (pH 6.6), 0.1% SDS (w/v) and 4% acrylamide (w/v). 0.1% (w/v) ammonium persulfate (APS) and 0.1% (v/v) TEMED were used to polymerise the gels.
Tris-glycine SDS/PAGE running buffer	25 mM Tris base, 192 mM glycine, 0.1% (w/v) SDS, pH 8.3
SIK Assay buffer	50 mM Tris/HCl, 10 mM magnesium acetate, 2 mM DTT, pH 7.5

2.2 Methods

2.2.1 Cell culture & treatments

Adherent cell lines U2OS, MCF7 and HEK293 were lifted from 10 cm culture plates by addition of trypsin-EDTA solution. All cell lines were incubated in a controlled atmosphere at 5% CO_2 and 37°C. Cells were harvested and centrifuged at 300 xg for 3 minutes before resuspension in PBS and counted using a haemocytometer. Cells were then aliquoted at

a concentration 1 × 10^6 into 1.5 mL microtubes and centrifuged at 1000 xg, 4 °C for 10 minutes.

2.2.1.1 Mammalian immortalized cell-line culture

All procedures were carried out under aseptic conditions meeting biological safety requirements.

2.2.1.2 Adherent cells lines.

BMA, HEK293, MCF7, L929 and U2OS cell lines were cultured in 10 or 15 cm cell culture treated dishes. HEK293, L929 and U2OS cells were maintained in Dulbecco´s modified eagle medium (DMEM), 10 % (v/v) foetal bovine serum (FBS), 1 mM L-Glutamine, 100 U/ml penicillin, 100 µg/ml streptomycin, whereas BMA and MCF7 cell lines maintained in Roswell Park Memorial Institute medium (RPMI-1640), 10 % (v/v) foetal bovine serum (FBS), 1 mM L-Glutamine, 100 U/ml penicillin, 100 µg/ml streptomycin. Cells were maintained in this media under 5% CO_2 at 37°C in a water-saturated incubator.

2.2.1.3 Suspension cell lines

THP-1 cells were cultured in tissue culture treated flasks (25 - 225cm^2 surface area) and maintained in Roswell Park Memorial Institute medium (RPMI-1640), 10 % (v/v) foetal bovine serum (FBS), 1 mM L-Glutamine, 100 U/ml penicillin, 100 µg/ml streptomycin and 55 µM β-mercaptoethanol. Cells were maintained in this media under 5% CO_2 at 37°C in a water-saturated incubator.

2.2.1.4 Harvesting of cell pellets

Adherent cell lines U2OS, HEK293 and MCF7 were lifted from 10 cm culture plates by addition of trypsin-EDTA solution. All cell lines were incubated in a controlled atmosphere at 5% CO_2 and 37°C. Cells were harvested and centrifuged at 300 xg for 3 minutes before

resuspension in PBS and counted using a haemocytometer. Cells were then aliquoted at a concentration 1 × 10^6 into 1.5 mL microtubes and centrifuged at 300 xg, 4 °C for 10 minutes.

2.2.1.5 *Mouse Embryonic Stem Cell (mESC) Culture.* (*Anna Segarra-Fas*)

CGR8 mESCs were cultured in 0.1% gelatine [w/v] coated plates in N2B27 medium (DMEM/F12-Neurobasal (1:1), 0.5% N2, 1% B27 (ThermoFisher Scientific, Waltham, MA, USA), 1% L-glutamine, 100 µM β-mercaptoethanol) containing "2i", 3 µM CHIR99021 (Axon Medchem, Groningen, Netherlands) and 1 µM PD0325901, in a controlled atmosphere at 5% CO_2 and 37°C. To induce multi-lineage differentiation, cells were plated at 4 × 10^4 cells/cm^2 in N2B27 medium without CHIR99021 and PD0325901 and incubated for 48h at 5% CO_2 and 37°C.

Total RNA extraction was performed by a column-based system (Omega Bio-tek, Norcross, GA, USA) and then subjected to reverse transcription using iScript reverse transcriptase (Bio-Rad) according to the manufacturer's guidelines. qPCR reactions were carried out using SYBR® Premix Ex Taq™ II Supermix (Takara Bio, Shiga, Japan) in a CFX384 real-time PCR system (Bio-Rad, Hercules, CA, USA). Samples were analysed for gene expression in 2i release conditions relative to 2i medium culture using the ΔΔCt method, and GAPDH expression was analysed as a loading control. Data from three independent biological replicates, with two technical replicates for each, were analysed in Excel software (Microsoft) and plotted in GraphPad Prism v.6.00 software (GraphPad). Primers used are listed in Table 2-5.

Table 2-5 List of primers for RT-qPCR analysis

Gene	Forward (5' to 3')	Reverse (5' to 3')
Nanog	CTCATCAATGCCTGCAGTTTTTCA	CTCCTCAGGGCCCTTGTCAGC
Klf4	ACACTTGTGACTATGCAGGCTGTG	TCCCAGTCACAGTGGTAAGGTTTC
Oct4	AGCTGCTGAAGCAGAAGAGG	AGATGGTGGTCTGGCTGAAC
Fgf5	GCTGTGTCTCAGGGGATTGT	CACTCTCGGCCTGTCTTTTC
Dnmt3b	CTGGCACCCTCTTCTTCATT	ATCCATAGTGCCTTGGGACC
Gapdh	CTCGTCCCGTAGACAAAA	TGAATTTGCCGTGAGTGG

2.2.1.6 Cell passaging

Adherent cell lines were grown to 80-90% confluency in a 10 or 15 cm cell culture dish. Cells were washed twice with warm PBS before addition of trypsin-EDTA (0.25%) solution and incubation at 37°C. After approximately 5-10 minutes cells were dissociated from the plate and the trypsin was quenched by addition of complete RPMI or DMEM media and the cells were centrifuged down at 1300 rpm for 3 minutes. Medium was aspirated and cells were resuspended in fresh media. Cell suspension of 1-2×10^6 were transferred to seed in new tissue culture dishes.

THP-1 monocytes were maintained at a confluency between 2.5x10^5 – 1.0x10^6 per millilitre of media. Every two days cells were centrifuged down at 1300 rpm for 3 minutes. Medium was aspirated and cells were resuspended in fresh media at the desired concentration.

2.2.1.7 Thawing of cells

For thawing, cryogenic vials were placed into 37°C water bath and then transferred into tube with pre-warmed media. Cells were pelleted and resuspended in pre-warmed growth media and transferred into a cell culture dish or flask.

2.2.1.8 Production of L929 supernatant

L929 cells were grown for three passages from cryogenic storage before seeding for secretion collection. Cells were seeded in 50 mL of complete DMEM at a density of ~6500 cells per cm^2 of available surface area. Media was carefully removed after seven days of culture and replaced with 50 mL of fresh DMEM media for a subsequent seven days. The two supernatant collections were then combined and sterile filtered before aliquoting into 50 mL falcon tubes and stored at -20°C.

2.2.1.9 Culture of bone marrow derived macrophages (BMDMs)

BMDMs were isolated from femurs and tibiae of WT C57BL/6 mice. The cells were treated with red blood cell lysis buffer (155 mM NH_4Cl, 12 mM $NaHCO_3$, 0.1 mM EDTA) and suspended in 2 mL of un-supplemented IMDM media. Here, BMDMs were transferred into one of three different culture conditions: L929, M-CSF or M-CSF + MIF. One mL of the suspension was added to tissue culture treated 10 cm dishes containing 9 mL of IMDM supplemented with 10% FBS, 1% L-glutamine, 1% pen/strep and either (1) 20% L929 conditioned supplement, (2) 10 ng/mL of M-CSF or (3) 10 ng/mL of M-CSF and 10 ng/mL of MIF. After 24 hours, cells in suspension were transferred to 10 cm petri dishes and seeded at 5.0 – 7.5×10^5 cells per dish. Differentiation occurred over 7 days with an additional 2 mL of media being added at 2, 4 and 6 days.

2.2.1.10 Collection of supernatant for proteomic analysis

L929 cells were seeded in a six well plate for secretomic analysis with cell density and media volume consistent with the protocol described in 1.3.1.8. For secretome collection, cells were first washed 2x with warm PBS and 1x with Opti-MEM 1 mM L-Glutamine, 100 U/ml penicillin, and 100 µg/ml streptomycin. One millilitre of Opti-MEM media was added to each well for a maximum of 3hrs before being carefully removed to avoid disturbing adherent cells. Supernatants were centrifuged at 2000xg, 4°C for 10 minutes to pellet cell debris. The supernatant was then carefully removed and stored in 1.5 mL lo-bind tubes at -80°C.

2.2.1.11 Pro-inflammatory stimulation of THP-1 monocytes

THP-1 cells were treated with one of six pro-inflammatory stimuli: LPS, Pam2CSK4, Pam3CSK4, IFN-γ, Poly(A:U) and Poly (I:C). Assay concentration was maintained at 1 µg/mL of each treatment, or 100 U/mL of IFN-γ for 24 hrs.

2.2.1.12 Treatment of cells with inhibitors

For all cellular treatments with inhibitors cells were incubated with compounds for 1hr prior to further stimulation. Compounds were stored in DMSO at 10 mM stocks, however DMSO concentration never exceeded 2% in-culture. For single point inhibition measurements, a concentration of 5 µM was used. For IC_{50} titrations compound concentrations ranged from 30 µM – 0.0001 µM.

2.2.2 Biochemistry Techniques

2.2.2.1 Cell microscopy and diameter measurements

The four cell lines were measured for number, viability and cell diameter by light microscopy using an Evos XL Core Cell Imaging System (Invitrogen). To assess

permeability, cell pellets were resuspended in PBS before mixing 1:1 with trypan blue. Trypan blue positive cells were then automatically counted using the same microscope to calculate cell viability. For mESC phenotype visualization, brightfield light microscopy was used in a Leica DM IL LED microscope at 10X magnification.

2.2.2.2 BCA protein quantitation

For whole cell MALDI-TOF-MS quantitation were titrated from 300,000 to 9,000 in a 96 well plate format. For proteomic and secretomic quantification samples were quantified at two different concentrations that were typically 1% SDS and 0.1% SDS. BCA reagent (Pierce, Thermo Fisher Scientific, Waltham, MA, USA) was then prepared to the manufacturer's instruction by mixing Reagent A and Reagent B at a ratio of 50:1, respectively. 20 µL of the mixed reagent was added to 180 µL of sample and incubated at 37°C for 30 minutes. The plate was then read on a plate reader measuring absorbance at 562 nm and protein concentration calculated from these values.

2.2.2.3 Protein precipitation

In 5 mL lobind tubes (Eppendorf) 960 µL of ice cold methanol was added to ~1 mL of protein supernatants and vortexed briefly before subsequent addition of 160 µL of ice cold chloroform and thorough mixing. 2.5 mL of ice cold water was then added to each tube, vortexed and centrifuged at 4000×g, 4°C for 30 minutes. A protein layer could then be observed at the interface of the organic and aqueous phases and the top layer was carefully removed to prevent disruption of the protein layer. A further 500 µL of ice cold methanol was then added and the solution vortexed thoroughly before transfer to a 1.5 mL lobind tube (Eppendorf) followed by centrifugation 20,000×g, 4 °C for 30 minutes. The supernatant was then carefully aspirated and the pellet ambient dried.

2.2.2.4 Separation of proteins by SDS-PAGE

Sodium dodecyl sulfate-polyacrylamide gel electrophoresis (SDS-PAGE) allows proteins to be separated according to their molecular weight. Protein samples are denatured and reduced by treatment with SDS, an anionic surfactant, and the reducing agent β-mercaptoethanol boiled before loading.

A resolving gel was first prepared according to the recipe described in Table 2-4. A stacking gel of different pH and acrylamide percentage (Table 2-4) was then layered on top, which acts to concentrate proteins into one tight band before entering the resolving gel, thus enhancing gel resolution. The gels were run in Tris-glycine SDS running buffer (Table 2-4) at 60 V initially through the stacking gel, and this was voltage was then increased to 120 V through the resolving gel. The voltage applied to the gel promotes migration of negatively charged proteins away from the cathode to the anode. Commercial pre-cast gels (4-12% Bis-Tris, NuPAGE) were used for precious samples. Commercial gels were run in MOPS buffer (NuPAGE) or MES (NuPAGE) buffer at a constant 120 V.

2.2.2.5 Protein staining of SDS/PAGE and PVDF membranes

After SDS/PAGE gels were washed in deionised water and incubated in 10 ml of InstantBlue (Expedeon, Cambridge, UK) on a rocking platform for 1-24h. Following this, the gel was washed repeatedly in deionised water to de-stain.

2.2.2.6 Measurement of cytokines by enzyme-linked immunosorbent assay (ELISA)

For experiments pertaining to BMDM differentiation, mouse TNF-α, IL-6, IFN-γ and IFN-β DuoKits were used (R&D Systems, Minneapolis, MN, USA). BMDMs cultured in either M-CSF, M-CSF + MIF or L929 supernatant were seeded in six well plates and treated with 100 ng/mL of LPS. The supernatant was collected at 6 hrs and centrifuged at 10,000 xg

for 10 minutes to remove cell debris. The supernatant was transferred to a new tube and ELISAs were performed according to the manufacturer's instructions.

For THP-1 experiments, a human TNF- α DuoKit was used (R&D Systems, Minneapolis, MN, USA). Cell supernatants were collected after 24 hr LPS stimulation centrifuged at 10,000 xg for 10 minutes to remove cell debris. The supernatant was transferred to a new tube and ELISAs were performed according to the manufacturer's instructions.

2.2.2.7 Antibody labelling for flow cytometry (FACS) analysis

BMDMs cultured in either M-CSF, M-CSF + MIF or L929 supernatant were collected at 1 × 10^6 cell per tube in 1.5 mL microtubes tubes (Corning Incorporated, New York, NY, USA). Cells were transferred to a 96 conical well plate and were washed twice in FACS buffer (1% FBS in PBS, pH 7.2) by centrifugation at 1,200 xg for 3 min and resuspended in 300 µl FACs buffer. Cells were then incubated with alexa fluor 488-conjugated antibodies against CD11c and F4/80 (Invitrogen) or allophycoyanin (APC)-conjugated CD11b (eBioscience, San Diego, CA, USA) antibody at 1:1000 dilution in FACS buffer for 20 min in the dark for 4°C. The reaction was quenched by addition of more FACS buffer. After washing for three times in PBS/FBS, cells were analysed by flow cytometry.

2.2.3 In vitro assays

2.2.3.1 Preparation of plates for SIK screening

For single-concentration screening, 15 nL (MALDI TOF assay) or 24 nL (ADP Hunter assay) of 10 mM compound solution in DMSO was transferred into 384-well HiBase, non-binding microtiter plates (Greiner, Stonehouse, UK), using an Echo 550 acoustic dispenser (Labcyte, USA), to give a final screening concentration of 30 µM. Staurosporine at 10 µM was used as a positive control in column 24, with column 23 containing only

DMSO as the negative control. The Dundee Drug Discovery Unit (DDU) small molecule kinase library contains 2648 commercially available ATP mimetics describing a diverse region of kinase pharmacophore space.

2.2.3.2 MALDI-TOF-MS SIK assay

In this assay the synthetic peptide CHKtide (KKKVSRSGLYRSPSMPENLNRPR) and NUAK peptide (ALNRTSSDSALHRRR) were used as a substrate for SIKs. Both CHKtide and the NUAK peptide are phosphorylated at the third serine residue (KKKVSRSGLYR**S**PSMPENLNRPR) and (ALNRTSSD**S**ALHRRR) to give phosphorylated products. Both these peptides and their products were measured by MALDI-TOF-MS at *m/z* 2700.47 (CHKtide), *m/z* and *m/z* 2780.37 (CHKtide + Phosphoryl) as a read out for SIK activity. Screening assays were performed with an XRD-384 Automated Reagent Dispenser (FluidX) by dispensing 3 µL of freshly prepared SIK assay buffer 1 µL of 15 nM SIK2 prepared in SIK assay buffer onto prepared compound plates followed by 30 minutes incubation at 30˚C. The reaction was then initiated by addition of 1 µL substrate solution containing a mixture of CHKtide and ATP, to a final concentration of 1 µM and 100 µM respectively. Plates were then returned to incubation at 30˚C for 30 minutes before being quenched by addition of 1.2 µL of 10% TFA to a final concentration of 2%.SIK ADP Hunter assay (*Anthony Hope & Lesley Pearson, Drug discovery unit, University of Dundee*)

The ADP Hunter technology (DiscoverX, UK) is a coupled enzyme assay that detects the production of the resorufin fluorophore as a downstream consequence of the conversion of ATP to ADP. It therefore provides a generic high throughput assay for the measurement of kinase enzyme activity. Screening of full length GST-tagged human SIK2 was performed using CHKtide as a substrate peptide. Compounds were stamped into 384-

well, low volume, black wall, assay plates (Greiner Bio-one, UK) as described above. The assay window was defined by addition of DMSO in the presence (no effect) or absence of enzyme (maximum effect), to defined control wells. Using a Wellmate liquid dispenser (Thermo Scientific, UK), 4 µL of a 2x enzyme solution (ADP Hunter Plus assay buffer, 1mM DTT, enzyme) was dispensed into all wells and pre-incubated for 20 minutes at room temperature. The assay enzyme reaction was initiated by the addition of a 4 µL of a 2x substrate solution (ADP Hunter Plus assay buffer, 100 µM CHKtide, 200 µM ATP Gold) such that the final assay concentration of SIK2 was 10 nM. Assay plates were incubated for 30 minutes at room temperature after which the reaction was stopped by the addition of 4 µL ADP Hunter Plus Reagent A and 8 µL ADP Hunter Plus Reagent B. Following a further incubation for 30 minutes at room temperature, resorufin elicited fluorescence was measured (ex 550 nm; em 595 nm) using a PHERAstar FS (BMG Labtech, UK).

2.2.3.3 Whole cell MALDI-TOF-MS assay for U2OS, HEK293, THP1, HEK293 cell lines and mESCs

After initial harvesting, cell pellets were processed in one of three ways:

(1) Direct analysis where cell pellets were washed twice with PBS and centrifuged at 1000×g, 4°C for 5 minutes. Cell pellets were then resuspended in 0.1% TFA before subsequent spotting.

(2) Cell pellets were snap frozen on dry ice and stored at -80°C until required. Thawed cell pellets were centrifuged at 1000 xg, 4°C for 10 minutes before either being washed 1x with PBS or fixed in 4% paraformaldehyde solution or methanol on ice. For the methanol fixing method, cells were allowed to fix for 10 minutes on ice. Cell suspensions

were then centrifuged at 1000×g, 4°C for 10 minutes before being resuspended in 0.1% TFA.

(3) Cell pellets were washed twice with PBS and centrifuged at 1000×g, 4°C for 10 minutes. Cell pellets were then either washed 1x with PBS or fixed in 4% paraformaldehyde solution or methanol on ice. For the methanol fixing method, cells were allowed to fix for 10 minutes on ice. Cell suspensions were then centrifuged at 1000×g, 4°C for 10 minutes before being resuspended in 0.1% TFA, snap frozen on dry ice and stored at -80°C until required.

Resuspended cell samples were mixed 1:1 with matrix and spotted either manually or using the Mosquito HTS in accordance with the dried droplet method.

2.2.3.4 MALDI-TOF-MS THP-1 cellular assay

THP-1 monocytes were seeded at 1×10^6 cells per mL in either a 6, 12 or 24 well plate at 1, 0.5, 0.2 mL respectively. For stimulus titrations, cells were treated with either LPS, PAM2CSK4, PAM3CSK4, Poly (IC) or IFN-γ from 100 pg – 10 µg/mL for 24 hours. For inhibitor studies, cells were incubated with either NG-25, BI2536, MRT67337, Nilotinib or Imatinib at 5 µM for one hour before addition of pro-inflammatory stimuli. IC_{50} curves were generated by incubating cells in a 24 well plates with compound concentrations ranging from 30 -0.0001 µM for one hour before addition of LPS for 24 hrs.

For the 78 compound screen, THP-1 monocytes were aliquoted at a density of 1×10^6 per mL into a 6 well plate and incubated with each compound at 5 µM for one hour in technical triplicate with a final concentration of DMSO at 0.5%. LPS was then added to a final concentration of 1 µg/mL for 24 hours. Compounds were staggered into 8 sets of 10 compounds, each with individual positive and negative controls to enable maximum

relative peak area calculations. This screening process was repeated three times with cells at different passage numbers.

Cells were harvested by manual scraping, pelleted at 1000 xg, frozen and stored at -80°C until required. Thawed cell pellets were washed with 200 µL Tris buffer (100 mM Tris, pH 7.5) and centrifuged at 1000 xg, 4 °C for 10 minutes. Cell pellets were then resuspended in Tris buffer at a concentration of 5000 cells/µL.

Cell suspensions were spotted with CHCA that was prepared in 50% ACN, 0.1% TFA at 10 mg/mL. For manual deposition cell suspensions were mixed at a 1:1 ratio with matrix solution and 1 µL spotted onto a ground steel MALDI target before ambient drying.

2.2.4 MALDI-TOF Mass spectrometry

2.2.4.1 Preparation of DHAP matrix solution

Ammonium citrate dibasic was resuspended in water (MS grade) to a final concentration of 12 mg/mL. 7.6 mg of 2,5-DHAP was resuspended in 375 µL of ethanol and vortexed briefly before addition of 125 µL of the ammonium citrate dibasic solution. The microtube was then sealed with parafilm and mixed vigorously for 1 hour. The resulting suspension was then centrifuged 5000 xg for 1 minute and the supernatant carefully removed into a separate tube for use.

2.2.4.2 Preparation of CHCA, DHB and SA matrix solutions

Sinapinic acid (SA), α-cyano-4-hydroxycinnamic acid (CHCA) and 2,5-dihydroxybenzoic acid (DHB) were all resuspended in acetonitrile/TFA buffers to various concentrations and ratios. Solutions were prepared ranging from 2.5 mg/mL to saturated concentration depending intended use. TFA concentration was varied from 0.1 – 5% and the acetonitrile

component from 30 – 70%. For all preparations, matrix suspensions were mixed vigorously for 30 mins and centrifuged 5000 xg for 1 minute prior to use.

2.2.4.3 Cleaning of MALDI targets

All target types were first sonicated in HPLC grade isopropanol for 5 minutes, followed by further sonication in 30% acetonitrile, 0.1% TFA for 5 minutes. AnchorChip targets (1536, 384) were then allowed to airdry.

Ground steel or polished steel targets (384 or no geometry, Bruker Daltonics) were often used for cellular analysis and required more rigorous cleaning. Targets were washed first with protocol described above but were then sonicated with 1% ammonium hydroxide, follow by HPLC grade methanol and any residual spots were wiped with a KIMTECH science wipe before a final rinse with methanol. Targets were then dried thoroughly under a stream of nitrogen gas.

2.2.4.4 MALDI-TOF-MS Spotting

Spotting of targets for MALDI-TOF-MS can be achieved through various techniques. Within this thesis, I have utilised two techniques: the dried droplet method or sandwich spot. Both these methods utilise liquid deposition of sample and matrix to spot sample arrays onto a MALDI target. For the dried droplet method, sample and matrix are mixed prior to deposition onto the target. The sandwich method deposits aliquots sample and matrix sequentially onto the target, with each layer drying before the next to produce MALDI spot arrays. This technique allows deposition of multiple layers of either matrix or sample. For all automated target spotting a Mosquito liquid handling robot (TTP Labech) was used for both dried droplet and sandwich spotting.

For the SIK in vitro screening assay spotting a dried droplet technique was used and all spotting was performed with the Mosquito. First 1200 nL of matrix solution was mixed with 1200 nL of sample before subsequent deposition of 200 nL of the matrix: sample mixture an AnchorChip MALDI. The target was allowed to ambient dry before MALDI-TOF-MS analysis.

Manual spotting of targets for cell based studies were performed using the dried droplet technique. Automated target spotting was achieved by the sandwich method. First, 200 nL of cell suspension was deposited onto a 1536 AnchorChip MALDI Target (Bruker Daltonics, Bremen, GER) and allowed to dry before subsequent deposition of 200 nL of the matrix solution. The target was allowed to ambient dry before MALDI-TOF-MS analysis.

2.2.4.5 MALDI-TOF-MS Parameters for SIK assay

A RapifleX MALDI-TOF/TOF mass spectrometer (Bruker Daltonics, Bremen, GER) equipped with a smartbeam^{TM} 3D laser was used in positive-ion mode with Compass 2.0 control for all data acquisition. Samples were run in automatic mode (AutoXecute, Bruker Daltonics) acquiring 5000 shots at 10 kHz frequency per spot in a random walk on spot laser ablation pattern and M5 smartbeam^{TM} parameter at a 25 µm x 25 µm scan range. Ionization was achieved using a fixed laser power of 70% (laser attenuator offset 7%, range 30%) and detected by the FlashDetector at a detector gain of ×2 in the *m/z* range of 2500 –2800. Samples were analyzed in Reflector mode with optimized voltages for reflector-1 (20.82 kV), reflector-2 (1.085 kV) and reflector-3 (8.8 kV), Ion sources, (Ion Source 1 20 kV, PIE 2.66 kV), Lens (11.3 kV) and a pulsed ion extraction of 200 ns. A novel 10-bit digitizer was used at a sampling rate of 5.00 GS/s.

Spectra were accumulated with FlexControl software (v4.0) and processed using FlexAnalysis software (v4.0) (Bruker Daltonics). Peaks were centroid detected with a signal-to-noise threshold of 6.00 with a Snap2 algorithm to detect only the intense peaks before being processed with a Savitzky-Golay smoothing algorithm (*m/z* width of 0.05, 1 cycle) and 'TopHat' baseline subtraction. External calibration was performed before each new target in Cubic Enhanced mode with Pepmix II calibrant (Bruker).

The laser parameters were set up as follows: Global Attenuator Offset 0%, Attenuator Offset 42%, Attenuator Range 30%, Focus Offset 0%, Focus Range 100%, Focus Position 19%, smartbeam^{TM} index 1.

2.2.4.6 MALDI-TOF-MS Parameters for whole cell analysis

A RapifleX PharmaPulse MALDI-TOF/TOF mass spectrometer (Bruker Daltonics) equipped with a smartbeam^{TM} 3D laser was used in positive ion mode with Compass 2.0 control for all data acquisition. Samples were acquired in automatic mode (AutoXecute; Bruker Daltonics), totalling 10,000 shots at a 10-kHz frequency per spot. A random walk pattern (complete sample) on spot laser ablation pattern was used with a M5 Smart beam Parameter at a 45-µm × 45-µm scan range. Spot diameter was limited to 2000 µm and a random walk pattern movement enabled at 1000 shots per raster position. Ionization was achieved using a variable laser power between 50-85% (laser attenuator offset 14%, range 30%) with a detector gain of ×6.8 in the *m/z* range of 2000 to 20,000 with a suppression up to *m/z* 1600. Samples were analysed in a linear geometry with optimized voltages for ion sources (ion source 1, 20 kV, PIE 1.3 kV), lens (8.6 kV), and a pulsed ion extraction of 180 ns. A novel 10-bit digitizer was used at a sampling rate of 1.25 GS/s. Raw data were processed first by a TopHat baseline subtraction followed by smoothing

with a Savitzky-Golay algorithm. Calibration of the instrument was performed prior to each experiment using protein calibrant I.

The laser parameters were set up as follows: Global Attenuator Offset 0%, Attenuator Offset 42%, Attenuator Range 30%, Focus Offset 0%, Focus Range 100%, Focus Position 19%, smartbeam^{TM} index 1.

MALDI TOF data processed by the FlexAnalysis 4.0 software where a peak picking threshold of 3 S/N with a centroid algorithm was set before being exported as a .csv file using FlexAnalysis Batch Process (Compass 2.0) and further processed in Microsoft Excel and/or Perseus.[174] Spectra based PCA plots were generated using ClinPro Tools (Bruker Daltonics). Data was then formatted using both GraphPad Prism 7.0 and Adobe Illustrator.

2.2.5 Proteomics

2.2.5.1 Protein extraction, reduction and alkylation

Biological replicates were lysed in either 8M Urea, 50 mM TEAB pH 8.5 (in solution) or 5% SDS, 50 mM TEAB pH 7.55 (S-Trap), sonicated and protein quantification was determined using the BCA Protein Assay Kit (Pierce Protein) as described in 1.3.2.2. Each sample was reduced by addition of TCEP to a final concentration of 10 mM for 30 min at room temperature followed by alkylation with 10 mM iodoacetamide for 30 min at room temperature in the dark.

2.2.5.2 In-solution protein digestion

Samples were diluted to 1M Urea and digested overnight at 37°C by adding porcine trypsin (1:50, w/w) (Pierce). Peptides were then acidified, desalted and concentrated

using C18 SPE Macro Spin Columns (Harvard Apparatus). Peptides were then dried under vacuum.

2.2.5.3 S-Trap protein digestion

Samples were acidified by addition of 2.5 µL of 12% phosphoric acid and diluted with 165 µL of S-trap binding buffer; 90% MeOH, 100 mM TEAB, pH 7.1. The acidified samples were then loaded onto the S-trap spin column (ProtiFi, USA) and centrifuged for 1 minute at 4000 xg. Columns were washed five times with S-trap binding buffer before addition of porcine trypsin (1:20) (Pierce) in 25 µL of 50 mM TEAB to the column. Samples were incubated at 47°C for 2 hours. Peptides were eluted by washing the column with firstly 50 mM TEAB, pH 8.0 (40 µL), followed by 0.2% FA (40 µL) and finally 0.2% FA, 50% ACN (40 µL). Peptides were then dried under vacuum.

2.2.5.4 TMT 10-plex labelling

Isobaric labelling of phosphorylated peptides was performed using the 10-plex tandem mass tag (TMT) reagents (Thermo Fisher). TMT reagents (0.8 mg) were resuspended in 41 µL of acetonitrile, and 10 µL added to the corresponding samples that were previously resuspended in 50 µL of 50 mM TEAB, pH 8.5. After 1 hour incubation at room temperature the reaction was quenched by addition of 4 µL of 5% hydroxylamine. Labelled peptides were then combined and acidified with 200 µL of 1% TFA (pH ~ 2) and concentrated using C18 SPE on Sep-Pak cartridges (Waters). Mixing ratios of each channel and labelling efficiency was tested by injection of a small pool of each channel on a Fusion Lumos Tribid mass spectrometer. Each TMT-labelled sample was quantified by a MaxQuant with a labelling efficiency >95%.

2.2.5.5 Offline high-pH reversed-phase (HPRP) liquid chromatography fractionation

The combined TMT-labelled peptides were fractioned by offline HPRP. Labelled peptides were solubilized in 20 mM ammonium formate (pH 8.0) and separated on a Gemini C18 column (250 × 3 mm, 3 µm C18 110 Å pore size; Phenomenex). Using a DGP-3600BM pump system equipped with a SRD-3600 degasser (Thermo Fisher), a 40 min gradient from 1 to 90% acetonitrile (flow rate of 0.25 ml/min) separated the peptide mixtures into a total of 40 fractions. The 40 fractions were merged into 10 samples, dried under vacuum centrifugation and resuspended in 0.1% (v/v) TFA for LC-MS/MS analysis.

2.2.5.6 Q-Exactive HF mass spectrometer parameters

2.2.5.6.1 L929 Secretome acquisition

Peptide samples were separated on an Ultimate 3000 RSLC system (Thermo Scientific) with a C18 PepMap, serving as a trapping column (2 cm x 100 µm ID, PepMap C18, 5 µm particles, 100 Å pore size) followed by a 50 cm EASY-Spray column (50 cm x 75 µm ID, PepMap C18, 2 µm particles, 100 Å pore size) (Thermo Scientific). Buffer A contained 0.1% FA and Buffer B 80% ACN, 0.1% FA. Peptides were separated with a linear gradient of 1-35% (Buffer B) over 120 minutes followed by a step from 35-90% ACN, 0.1% FA in 0.5 minutes at 300 nL/min and held at 90% for 4 minutes. The gradient was then decreased to 1% Buffer B in 0.5 minutes at 300 nL/min for 10 minutes. Mass spectrometric identification was performed on an Orbitrap QE HF mass spectrometer (Thermo Scientific) operated “Top Speed” data dependant mode in positive ion mode. FullScan spectra were acquired in an *m/z* range of 400 to 1500, at a resolution of 120 000 (at *m/z* 200), with an automated gain control (AGC) of 1,000,000 and a maximum injection time of 50 ms. Charge state screening is enabled to exclude precursors with a charge state of 1. For MS/MS fragmentation, the minimum AGC was set to 5000 and the most intense precursor

ions were isolated with a quadrupole mass filter width of *m/z* 1.6 and an offset of *m/z* 0.5. Precursors were subjected to CID fragmentation that was performed in one-step collision energy of 25%. MS/MS fragments ions were analysed in the Orbitrap mass analyser with a 15 000 resolution at *m/z* 200.

2.2.5.7 Fusion Lumos Tribrid mass spectrometer parameters

2.2.5.7.1 BMDM TMT total proteome acquisition

Peptide samples were separated on an Ultimate 3000 RSLC system (Thermo Scientific) with a C18 PepMap, serving as a trapping column (2 cm × 100 µm ID, PepMap C18, 5 µm particles, 100 Å pore size) followed by a 50 cm EASY-Spray column with a linear gradient consisting of (2.4–28% ACN, 0.1% FA) over 180 min at 300 nl min^{-1}. Mass spectrometric identification and quantification was performed on an Orbitrap Fusion LUMOS Tribrid mass spectrometer (Thermo-Fisher Scientific) operated in data dependent, positive ion mode. FullScan spectra were acquired in the *m/z* range of 400 - 1,500 with a resolution of 120,000, an automated gain control (AGC) of 300,000 ions and a maximum injection time of 50 ms. The 12 most intense precursor ions were isolated with a quadrupole mass filter width of *m/z* 1.6 and CID fragmentation was performed in one-step collision energy of 35% and 0.25 activation Q. Detection of MS/MS fragments was acquired in the linear ion trap in a rapid mode with an AGC target of 10,000 ions and a maximum injection time of 40 ms. Quantitative analysis of TMT-tagged peptides was performed using FTMS3 acquisition in the Orbitrap mass analyser operated at 60,000 resolution, with an AGC target of 100,000 ions and maximum injection time of 120 ms. Higher-energy C-trap dissociation (HCD fragmentation) on MS/MS fragments was performed in one-step collision energy of 55% to ensure maximal TMT reporter ion yield and synchronous-

precursor-selection (SPS) was enabled to include 10 MS/MS fragment ions in the FTMS3 scan.

2.2.5.7.2 THP-1 total proteomes

Peptide samples were separated on an Ultimate 3000 RSLC system (Thermo Scientific) with a C18 PepMap, serving as a trapping column (2 cm × 100 µm ID, PepMap C18, 5 µm particles, 100 Å pore size) followed by a 50 cm EASY-Spray column with a linear gradient consisting of (2.4–28% ACN, 0.1% FA) over 240 min at 250 $nLmin^{-1}$. Mass spectrometric identification and quantification was performed on an Orbitrap Fusion LUMOS Tribrid mass spectrometer (Thermo-Fisher Scientific) operated in data dependent, positive ion mode. FullScan spectra were acquired in the *m*/*z* range of 400 - 1500, at a resolution of 120,000, with an automated gain control (AGC) of 300,000 ions and a maximum injection time of 50 ms. The 12 most intense precursor ions were isolated with a quadrupole mass filter width of *m/z* 1.6 and CID fragmentation was performed in one-step collision energy of 35% and 0.25 activation Q. Detection of MS/MS fragments was acquired in the linear ion trap in a rapid mode with an AGC target of 10,000 ions and a maximum injection time of 40 ms.

2.2.6 Data analysis

2.2.6.1 *In vitro* SIK assay data analysis

For enzyme characterization, initial rates in both technologies were determined using time-course experiments under conditions of either excess ATP or CHKtide. The rates were plotted against variable substrate concentration and subjected to standard Michaelis-Menten analysis to derive Km and Vmax values. IC_{50} curves were fitted with GraphPad Prism (V7, USA) using a four parameter non-linear regression curve fitting algorithm to generate mid-point IC_{50} values for the inhibitors.

Values were normalised for volume and protein concentration across the two technologies for comparative purposes. SIK2 activity was measured by the percent phosphorylation (%P) of the CHKtide substrate by the following equation:

$$\left(\frac{(Peak\ area\ phosphorylated\ product)}{(Peak\ area\ phos\ product) + (Peak\ area\ substrate)}\right) \times 100$$

Peak areas were determined using a SNAP II algorithm incorporated into the FlexAnalysis post acquisition software (Bruker Daltonics, Bremen, GER).

Raw data from the ADP Hunter assay (relative fluorescence units [RFU]) were also exported as a comma delimited (.csv) file. All subsequent primary single-point screening data processing and analysis for both assays were conducted within Activity Base version 8.1.2.12 using Activity Base XE Runner version 8.1.1 (IDBS, Guilford, UK). Data were normalised and expressed as a percentage effect (PE) value for each test compound as follows:

MALDI-TOF-MS:

$$PE = \left(\frac{\%PE_{test} - \%PE_{high}}{\%PE_{low} - \%PE_{high}} \times 100\right)$$

ADP Hunter:

$$PE = \left(\frac{RFU_{test} - RFU_{high}}{RFU_{low} - RFU_{high}} \times 100\right)$$

Where PE or RFU test is the signal associated with the test compound, high is the median of the no-effect signal (reaction in presence of enzyme only), and low is the median of maximum effect control signal (reaction in absence of enzyme [biochemical] or presence of staurosporine [MALDI TOF]). The performance of the assay on each screening plate

was evaluated using internal controls to determine robust signal-to-background (s:b) and robust Z′ values, which were calculated as follows:

$$s{:}b = \frac{high}{low}$$

$$Z' = 1 - \left(\frac{\left(3 \times sMAD_{high}\right) + \left(3 \times sMAD_{low}\right)}{(high - low)}\right)$$

High refers to either RFU_{high} or $\%P_{high}$ and low corresponds to either RFU_{low} or $\%P_{low}$, as appropriate for each assay. $sMAD_{high}$ is 1.4826 × median absolute deviation of signal associated with the no-effect control, and $sMAD_{low}$ is the 1.4826 × median absolute deviation of signal calculated for the maximum effect control. All database querying for global data analysis and report creation was undertaken using the Dotmatics Browser (version 4.9.623.45008-s) and Vortex analysis software (version 2015.12.46651.25; Dotmatics, Bishop Stortford, UK).

2.2.6.2 MaxQuant parameters

Protein identification and label free quantification was performed using MaxQuant Version 1.5.8.3. Trypsin/P set as enzyme; stable modification carbamidomethyl (C); variable modifications Oxidation (M), Acetyl (Protein N-term), Deamidation (NQ), Gln & Glu to pyro-Glu; maximum 8 modifications per peptide, and 2 missed cleavage. Searches were conducted using either a murine (downloaded March 2019, 17008 entries) or human (downloaded March 2019, 20416 entries) database depending on proteomic experiment plus common contaminants. Identifications were filtered at a 1% FDR at the peptide level, accepting a minimum peptide length of 5 amino acids. Quantification was performed using razor and unique peptides and required a minimum count of 2. “Re-quantify” and “match

between runs" were enabled. Label free quantification (LFQ) intensities were extracted for each protein/condition and used for downstream analyses.

2.2.6.3 Statistical Analysis

Statistical analyses were performed in Perseus (v1.6.0.7 - v1.6.6.0). Contaminants and reverse removed from the data sets prior to analyses. T-test-based statistics were applied to the LFQ protein ratios to extract the significant regulated proteins. Hierarchical clustering was performed in Perseus with Euclidian distancing on either Log_2 fold changes or Z-score averages of ANOVA significant proteins.

Chapter 3. Identifying inhibitors of inflammation: a MALDI-TOF-MS screening assay for Salt Inducible Kinases (SIKs)

3.1 Introduction

The variety of cells and signalling pathways that are involved in the process inflammation are incredibly complex and constantly evolving. In recent years, systemic inflammation has been linked to almost all acute and chronic diseases such as cancer, diabetes[175], auto-immune diseases[176], obesity[177] and many more. This in turn has established a prolific platform for research to identify anti-inflammatory compounds, which is challenging but has revealed a wide range of potential new drug targets. These are often linked to key processes in macrophages, who are important players in the innate immune response and exhibit great plasticity in response to environmental stimuli. Macrophages that are polarised towards a pro-inflammatory state, or an M1 activation state, are important for sensing invading pathogens and responding to infection. However, prolonged activation can lead to sustained and systemic inflammation and, in severe cases such as Crohn's disease and rheumatoid arthritis, pathogenesis and tissue damage.[178] These effects can be countered by interleukin-10 (IL-10), a potent repressor of proinflammatory cytokine production, and key immunoregulator during infection and resolution of inflammation.[179] Treatment with recombinant IL-10 to reduce inflammation in patients with inflammatory bowel disease has been hypothesised and despite some success in mouse models clinical trials showed no clear therapeutic or clinical improvement.[180,181] Furthermore, as large biomolecule therapies with recombinant cytokines and antibodies are very expensive and become an increasing burden for health systems, small molecule inhibitors to treat inflammatory disease are urgently needed.[182] Therefore, innovative therapeutic

approaches to target these diseases could exploit this macrophage plasticity in an attempt to reduce the inflammatory response and alleviate patient symptoms.[183] Current work in this field has highlighted that one or potentially all three isoforms of salt-inducible kinases (SIKs) play a major regulatory role in macrophage phenotype switching to an M1 activation state by negatively regulating the production of the anti-inflammatory cytokine IL-10 (Figure 3-1).[184–186]

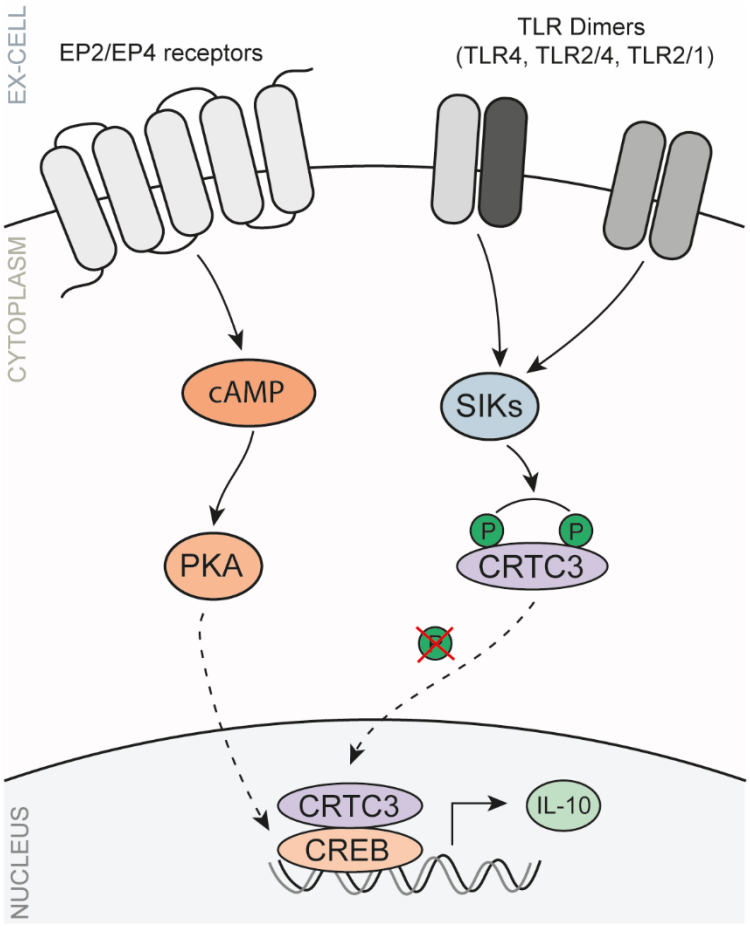

Figure 3-1. SIK signalling pathway from TLR stimulation and EP2/4 stimulation. *SIKs phosphorylate CRTC3 that then sequesters in the cytoplasm and is unable to initiate transcription of IL-10 with CREB, thus promoting the inflammatory phenotype. Inhibition of SIKs would lead to de-phosphorylated CRTC3 that can translocate to the nucleus and initiate transcription of IL-10.*

SIKs belong to the serine/threonine protein kinase family and have been implicated in a wide range of biological processes such as insulin signal transduction and metabolic regulation, but their importance in the inflammatory response is best established.[187,188] Previously, it was shown that prostaglandins activate protein kinase A (PKA), which prevents SIKs from phosphorylating its substrates in cells. This leads to dephosphorylation of the SIK target CREB-related transcriptional coactivator 3 (CRTC3) at Ser62, Ser162, Ser329, and Ser370 subsequently its nuclear translocation promoting CREB dependent gene transcription and increased IL-10 production.[186,189] Consequently, small-molecule inhibitors affecting SIKs have been shown to increase IL-10 production, thereby switching macrophages to an anti-inflammatory phenotype.[190,191] This suggests that SIKs are attractive drug targets to combat chronic inflammatory diseases.[192]

Kinases are a family of enzymes that catalyse the transfer of phosphate groups to specific substrates.[193] Modification of protein substrates by phosphorylation is the most common post-translational modification in cells and plays a role in almost all biological and cellular process.[193] Dysregulated phosphorylation of proteins disrupts complex intracellular signalling mechanisms and is now linked to a variety of different diseases such as Parkinson's[194], Alzheimer's[195] and systemic inflammation[196].[197] Consequently, kinases are considered excellent drug targets and development of small molecular inhibitors that are able to neutralise aberrant phosphorylation is at the forefront of drug discovery.[198,199] Methods for kinase profiling and screening are well established and have led to the discovery of kinase inhibitors involved in a variety of cellular processes,[200–202] but also yielded a much better understanding of kinase catalytic activity and inhibitor selectivity.[203] However, these *in vitro* methods of kinase profiling are often indirect, measuring fluorescence of labelled non-physiological peptides or adenosine diphosphate (ADP),

and/or inclusion of coupling enzymes, or, if direct, require the incorporation of ^{33}P through radio-labelled adenosine triphosphate (ATP). There is therefore a clear need to develop a complimentary screening assay that avoids the use of labelled reagents.

MALDI-TOF-MS has been shown to be particularly powerful for monitoring post translational modifications on both protein[86] and peptide substrates[100], however these assays have not been directly compared to traditional methods. The phosphorylation of a substrate results in a mass shift of 79.96 Da, thus is a suitable reaction for MALDI-TOF-MS assay development.

3.2 Aims

In this chapter I will describe the development of an *in vitro* MALDI-TOF-MS screening assay for the salt inducible kinases (SIKs). This body of work has been peer reviewed and published.

Heap, R. *et al*. Inhibitors of Inflammation: A Novel High-Throughput MALDI-TOF Screening Assay for Salt-Inducible Kinases (SIKs). *SLAS Discovery* **10**, 1192-1202 (2017)

3.2.1 Sub-chapters

1. Determining SIK isoform activity and substrate specificity for a MALDI-TOF-MS assay.
2. Characterising the enzyme reaction kinetics of the MALDI-TOF-MS assay compared with ADP Hunter fluorescent assay.
3. Determining IC_{50} values for known compounds and compare correlation between MALDI-TOF MS and ADP Hunter assay and cellular validation.

4. Proof of concept screen of 2648 compounds with both the MALDI-TOF-MS and ADP Hunter assays.

3.3 Results

3.3.1 Determining SIK isoform activity and substrate specificity for a MALDI-TOF-MS assay.

Salt-inducible kinases (SIKs) exist in the human genome as three isoforms: SIK1, 2 and 3, all of which are responsible for regulating a wide range of cellular and biological processes. The SIK family structures are all relatively similar and share common features such as a ubiquitin associated domain (UB), an RK-rich region and a highly conserved kinase domain with T-loop activation.[204]

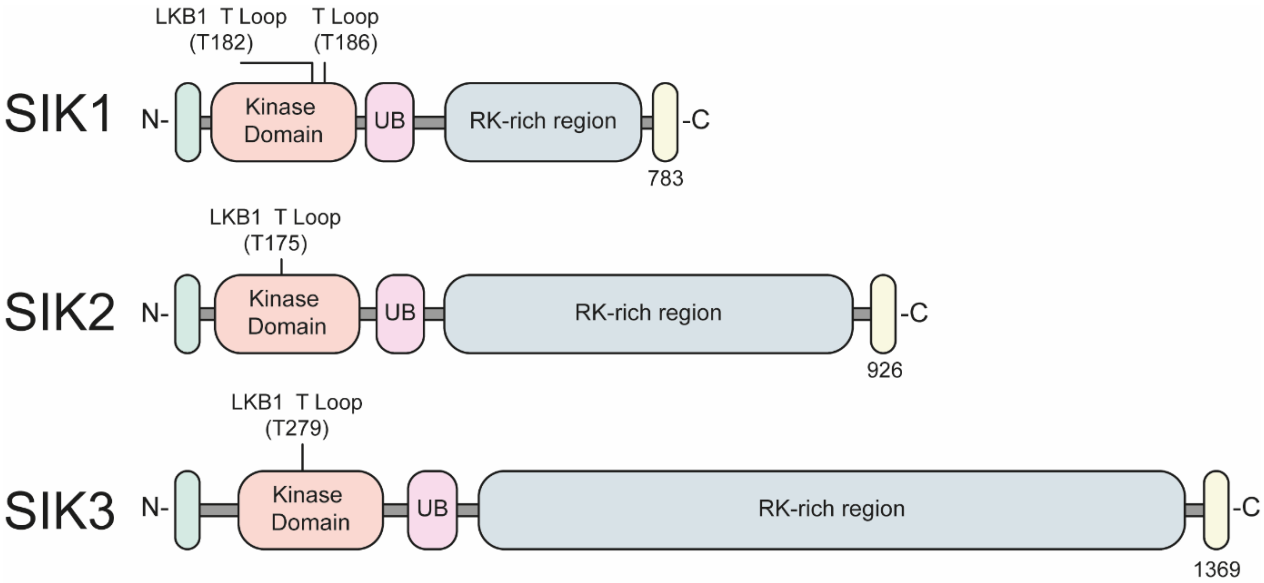

Figure 3-2 The domain structure of SIK isoforms. *Position of the LKB1 T loop phosphorylation sites of the three SIK isoforms. SIK1,2 and 3 all contain kinase domains (KD) a ubiquitin associated domain (UB) and an RK-rich region. Adapted from Taub.*[204]

SIKs are expressed ubiquitously throughout tissue, with SIK1 expression being closely linked to external stimulation such as high salt intake and metabolic signalling.[205] In contrast, SIK2/SIK3 are broadly expressed at all times in tissue, with SIK2 levels observed to be at their highest in adipose tissue and SIK3 in brain tissue.[206] Therefore, there was a distinct possibility that despite their structural similarities, these three isoforms could exhibit variable activity with different substrates. I therefore chose to evaluate the activities of the three SIK isoforms with two readily available synthetic peptides as substrates: (1) NUAK peptide, which is derived from NUAK2, a stress-activated kinase from the LKB1 signalling pathway, and (2) CHKtide, a peptide derived from the CHK1 protein kinase involved in the DNA repair pathway (Figure 3-3.A&B).[207] The matrix α-cyano-4-hydroxycinnamic acid was used for co-crystallisation as it is well known to be preferable for peptide analysis and crystallises homogenously. Both CHKtide and NUAK peptide ionised well by MALDI-TOF-MS and could be detected at 1 fmol when diluted with SIK assay buffer (50 mM Tris/HCl, 10 mM magnesium acetate, 2 mM DTT, pH 7.5) at *m/z* 2700.47 and 1739.52 respectively. However, CHKtide exhibited much better ionisation sensitivity over NUAK peptide (Figure 3-3.B) as it was detected at a significantly higher signal to noise (S/N) at the lower concentrations and could be detected at ~100 amol, 10-fold lower than NUAK peptide. This ionisation bias is likely due to differences gas-phase basicity between the peptides, which has been shown to dramatically effect ionisation efficiency.[208] Peptides rich in the basic residues arginine- or lysine- tend to exhibit greater ionisation efficiency as these residues contain very basic side chains. CHKtide contains seven arg- and lys- residues (**KKK**VS**R**SGLY**R**SPSMPENLN**R**P**R**), whereas NUAK peptide contains only four arginine residues (ALN**R**TSSDSALH**RRR**). Theoretically, CHKtide should transfer more efficiently into the gas phase with a positive charge

associated with the guanidino group of these residues or the n-terminus as under acidic conditions as CHKtide possesses three more sites for potential protonation. This could explain why I observe CHKtide to have a greater ionisation efficiency as it is more readily protonated at one of its proton-acceptor sites. Interestingly, I also observed more sodium salt adduct formation $[M+Na]^+$ with CHKtide peptide at *m/z* 2723.7, compared with NUAK peptide, which may be due to glutamic acid residue. However, this adduct formation never exceeded 5% of the total substrate peptide signal and did not interfere with subsequent quantitation.

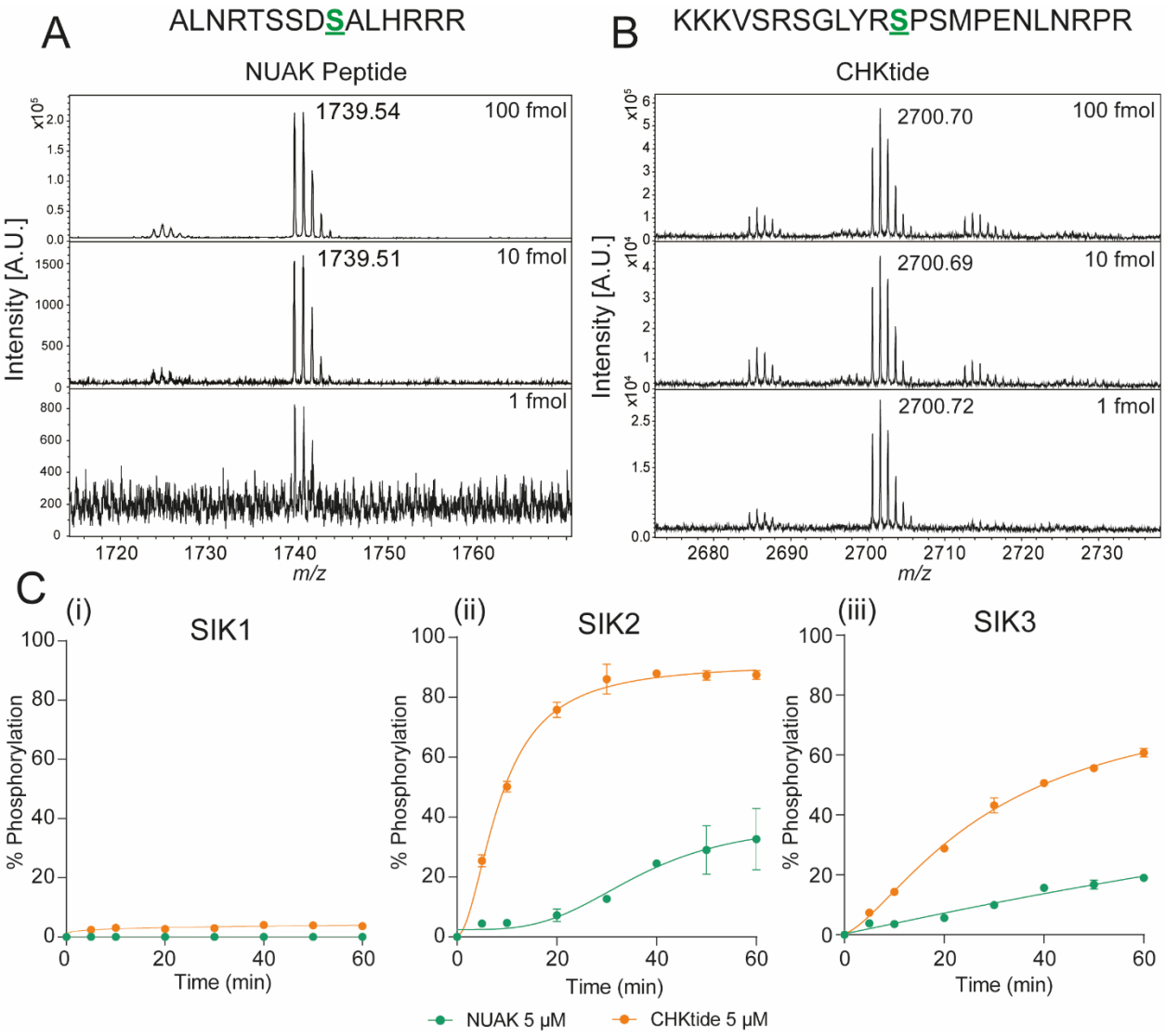

Figure 3-3. SIK assay activity and peptide sensitivity. *(A) & (B) Amino acid sequence*

of both NUAK peptide and CHKtide, respectively, with highlighted in green the phosphorylation site of a serine residue of both peptides. MALDI-TOF-MS spectra sensitivity of both peptides from 100 – 1 fmol showing that CHKtide can be detected at a lower limit of detection (LOD). (C) activity of SIK1, 2, 3 with both NUAK peptide and CHKtide at 5 μM concentration in-assay. All error bars are given as ± SD over three technical replicates.

To test enzyme activity all three SIKs were incubated at 5ng/μL final concentration with both NUAK peptide and CHKtide (5 μM) and the phosphorylated product was measured at *m/z* 1819.82 and 2779.48 respectively (Figure 3-4) and the reaction was quenched at regular intervals over one hour. The percentage phosphorylation was calculated by the following equation:

$$\%\ phosphorylation = \left(\frac{(peak\ area\ product)}{(peak\ area\ product + peak\ area\ substrate)}\right) \times 100$$

Overall, I observed significantly less activity of all the SIKs with NUAK peptide versus CHKtide (Figure 3-3.C) and therefore all further experiments and optimisation was performed with CHKtide as the substrate. Interestingly, for both the NUAK peptide and CHKtide I observed multiple other mass features in the phosphorylated spectra. For both peptides, the neutral loss of phosphate (*m/z* 94.97) from the phosphorylated peptide product is observed as a well resolved peak at either m/z 1723.85 or 2684.4 for NUAK peptide and CHKtide respectively. This can sometimes be observed for phosphorylated peptides where they experience post source decay that results in the neutral loss of the phosphate ion.[209] Interestingly, I also observe a broad, poorly resolved peak adjacent to the substrate peptide peak at a lower *m/z* value for both peptides. These peaks could also be due to the formation of metastable ions post-source as the breakdown of ions after acceleration and is sometimes referred to as meta-stable decay.[210] This would in turn lead

to the formation of ions that possess a shift in kinetic energy to the original ions and therefore a partitioning of their energies and different flight times. This could explain the mass difference that is observed in this case, as well as the poorer resolution as these ions may exhibit a broader range of kinetic energies compared with the parent ions.[210] In addition, for both phosphorylated and unphosphorylated CHKtide I observed a peak of +15.98 Da, which corresponds to single oxidation. Interestingly, this oxidation is not seen to the same extent with NUAK peptide. This could be due to CHKtide possessing a methionine residue within its sequence whereas NUAK peptide does not as methionine is known to be readily oxidised and its derivatives can be readily detected by MALDI-TOF-MS.[211]

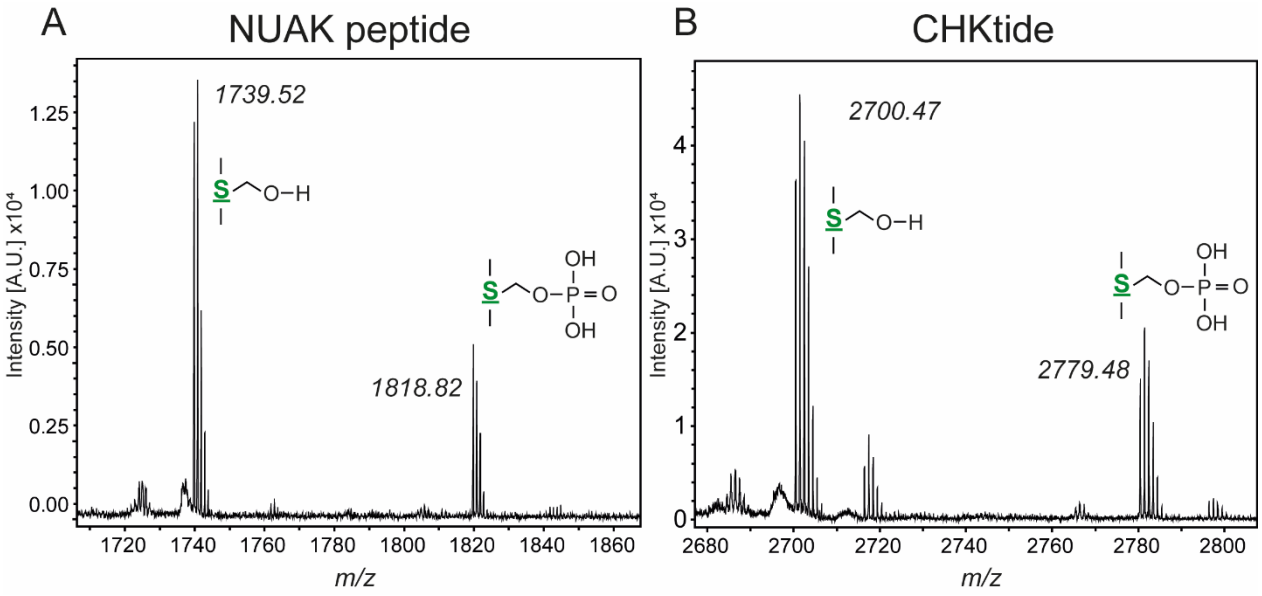

Figure 3-4. Representative spectra of SIK mediated phosphorylation of peptide substrates. *The serine phosphorylation reaction with (A) NUAK peptide and (B) CHKtide by SIKs.*

The CHKtide substrate could be efficiently phosphorylated by SIK2 and SIK3 with SIK2 proving to be the more active enzyme. However, there was little to no activity observed with SIK1 only obtaining a maximal % phosphorylation of ~6% with CHKtide (Figure 3-

3.C). More concentrated reactions of SIK1 were tested up to 50 ng/µL, however enzyme activity did not improve and salt / glycerol concentrations from the SIK enzyme storage buffer become MALDI intolerable, therefore I proceeded with SIK2 and SIK3 for further assay development.

3.3.2 Characterisation of enzyme reaction kinetics of the MALDI-TOF-MS assay

To truly compare the MALDI-TOF-MS assay with the fluorescent ADP Hunter assay we performed experiments that would characterise the kinetics of the reaction with both assay types. All experiments that used the ADP Hunter assay method were performed by Lesley-Anne Pearson, a biologist of the University of Dundee drug discovery unit. The ADP Hunter technology (DiscoverX, UK) is an enzyme coupled assay that detects the abundance of the resorufin fluorophore at ex 550 nm; em 595 nm as a downstream consequence of the conversion of ATP to ADP. This readout method is generic for a high-throughput biochemical assay that measures kinase activity. The SIK ADP Hunter assay was performed using the same CHKtide as a substrate peptide but used ADP as a measure of SIK activity rather than the direct phosphorylation of CHKtide that is measured with the MALDI-TOF-MS assay.[212] As the ADP Hunter assay buffer contains high levels of salt that would be incompatible with MALDI-TOF-MS, we utilised a comparable buffer containing the same concentrations of magnesium chloride and a tolerable Tris/HCl concentration for both assays to maintain as much similarity as possible. We chose to use Michaelis-Menten kinetics to describe the rate of the enzymatic reaction in both assays with the following equation:[213]

$$v = \frac{Vmax[S]}{K_M + [S]}$$

Here, v is equal to reaction rate and [S] equates to substrate concentration. The two quantities of interest V_{max} and K_M can be calculated for the substrates based on the hyperbolic relationship between reaction rate and the substrate concentration. In the case of the SIK reaction, these entities would be the CHKtide peptide and ATP. The V_{max} for a given reaction is the maximum rate of reaction under enzyme-substrate saturated conditions whereas K_M is the Michaelis constant equates to half V_{max}. This parameter represents the dissociation constant for the ES complex in this case was the most important parameter for assessing the differences between the ADP Hunter and MALDI-TOF-MS assay for both ATP and CHKtide consumption. This in turn enabled us to determine whether the rate of formation of the product was affected by the availability of substrate, which for kinases is particularly important to determine for ATP. A high K_M value indicates that the reaction is significantly dependent on the availability of a substrate, whereas a low K_M indicates independence. Therefore, it was important to determine K_M for both assays as it enabled us to determine whether both assays were performing under similar physiological conditions.

For this, substrates were titrated from very high concentrations to very low to determine dependence of the reaction rate on the substrate availability. For determining ATP K_M this was relatively straight forward (Figure 3-5.C), where values of 23.0 and 40.0 for MALDI-TOF-MS and ADP Hunter were calculated respectively (Table 3-1.) This indicates that the rate of consumption of ATP under physiological conditions is very similar, and therefore enzyme activity is not impaired with the MALDI-TOF-MS buffers.

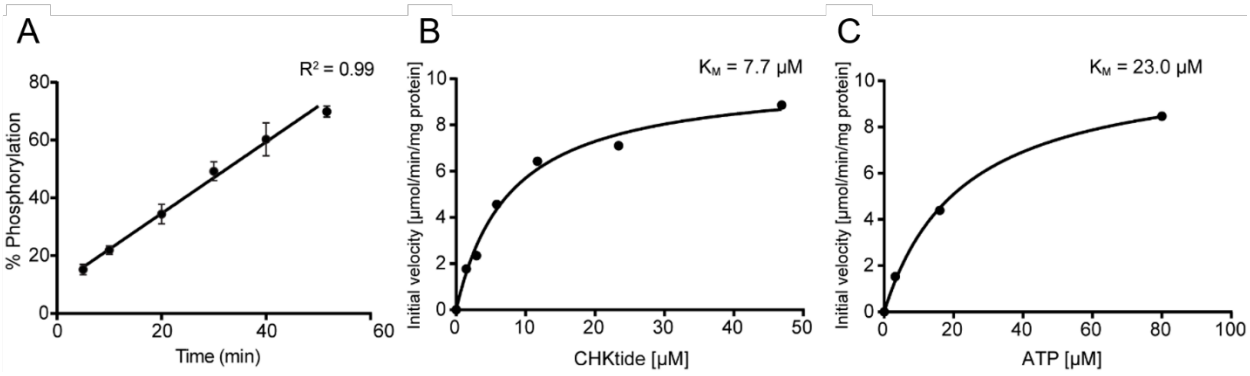

Figure 3-5. Michaelis-Menten kinetics of the SIK2 reaction. *(A) Reaction rate SIK2 phosphorylation of CHKtide over one hour showing linear correlation up to 75% phosphorylation with error bars representing the ± SD from the mean average of three technical replicates. (B) CHKtide concentration versus reaction velocity curve for determining Km for CHKtide in the MALDI-TOF-MS assay. (C) ATP concentration versus reaction velocity curve for determining K_M for ATP in the MALDI-TOF-MS assay.*

However, for CHKtide, the calculation of K_M was more difficult with the MALDI-TOF-MS assay as calculation of the rate of reaction is dependent on the substrate concentration. At very high concentrations the rate of reaction was no longer well represented by the relative peak areas of the substrate and product as the peak area of CHKtide substrate suppresses the phosphorylated product in the spectrum. This in turn resulted in highly underrepresented reactions rates where the reaction rate appeared to decline with increasing CHKtide concentration. Therefore, there was a limited window for determining CHKtide K_M (Figure 3-5.B) where the reaction rate was accurate, which may account for the discrepancies in K_M between the MALDI-TOF-MS and ADP Hunter assays. Here, the K_M value for MALDI-TOF-MS was significantly lower than the ADP Hunter assay, which may imply there are some subtle differences in enzyme activity. However, it is more likely that the inability to perform the kinetic experiment at high concentrations causes an underestimation of K_M and the reaction rate is similar for both reactions.

Table 3-1. KM values for ATP and CHKtide with the MALDI-TOF-MS and ADP Hunter assays.

K_M ATP [µM]	*MALDI-TOF-MS*	*ADP Hunter*
SIK2	22.0 ± 1.3	40 ± 6
K_M CHKtide [µM]	*MALDI-TOF-MS*	*ADP Hunter*
SIK2	7.7 ± 0.5	93 ± 10

The problem with calculating K_M for the direct substrate by MALDI-TOF-MS is likely to only occur when there is relative quantitation between the substrate and product peak areas. This in turn could be solved utilising a method that does not consider substrate concentration to calculate reaction rate such as using an internal standard.

3.3.3 Determining IC_{50} values for known compounds and compare correlation between MALDI-TOF MS and ADP Hunter assay and validation in cells

The final step of validating the MALDI-TOF-MS assay for screening was to test the potency of known SIK inhibitors by calculating IC_{50} values and to compare with the ADP Hunter assay. Five kinase inhibitors with reported activity in SIKs were chosen for this study: staurosporine, HG-9-91-01, MRT199665, MRT67307 and KIN112 (Figure 3-6).[184,214] Staurosporine is a potent and broad kinase inhibitor, where as KIN112 and the more potent analogue HG-9-91-01 target the ATP binding site of kinases. MRT199665 inhibits the vast majority of AMPK-related kinases, but unlike MRT67307 it does not inhibit IKK-related kinases.

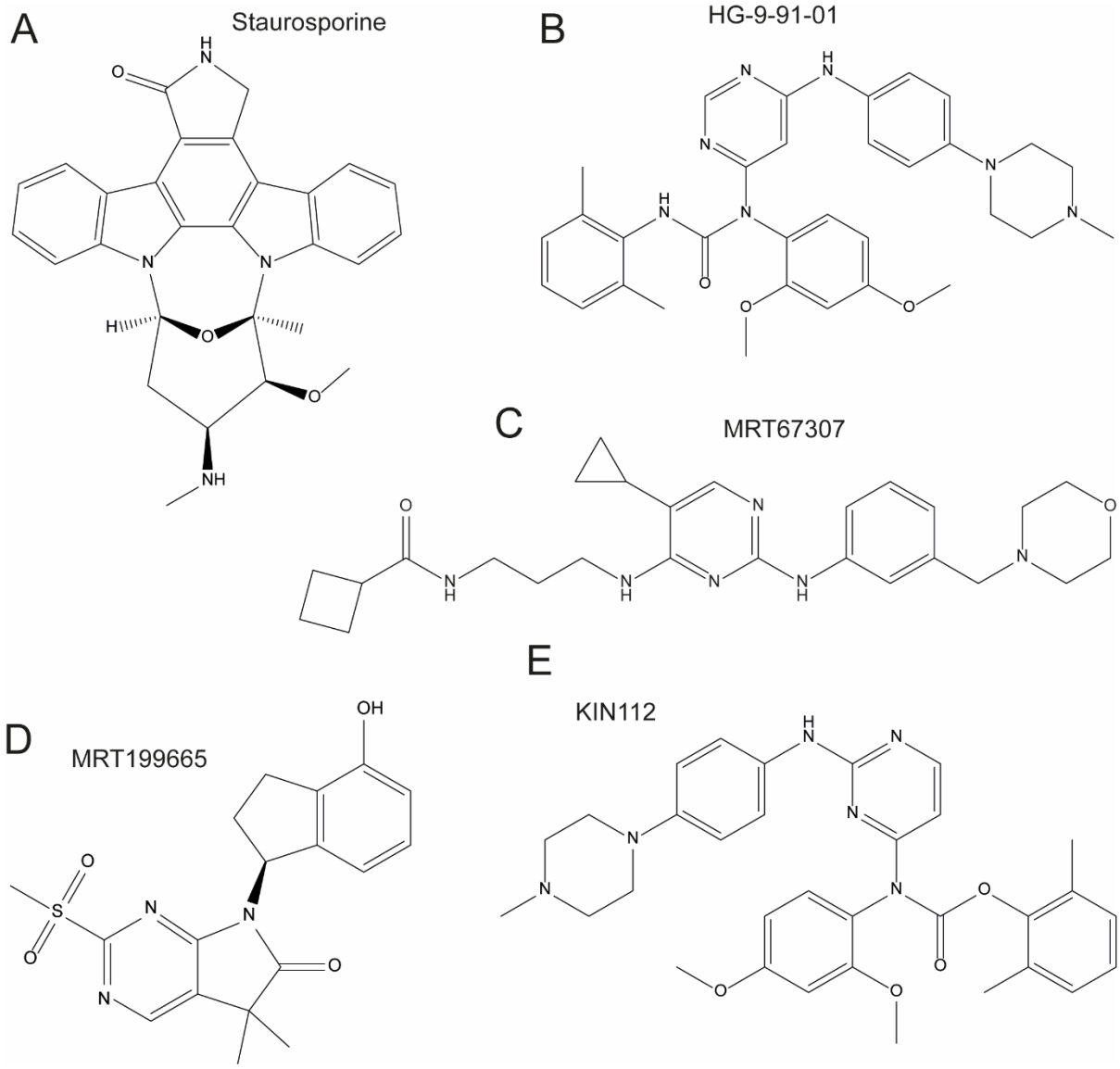

Figure 3-6. Chemical structures of the five inhibitors of SIKs. *(A) Staurosporine, (B) HG-9-91-01, (C) MRT67307, (D) MRT199665, (E) KIN112.*

IC_{50} curves spanning 1000 – 0.03 nM were generated for each compound against SIK2 (Figure 3-7.A). I was able to fit good R^2 values >0.95 for all compounds using a four-parameter variable slope algorithm, thus validating MALDI-TOF-MS as a readout for potential hit compound titrations. Staurosporine was the most potent inhibitor for both assays exhibiting an IC_{50} below 1 nM (Figure 3-7) and also had the poorest slope fit. This poor fitting could suggest that other factors such as tight-binding could be causing

uncertainty in the potency of staurosporine.[215] Tight binding results in an IC_{50} value being near or below the SIK2 concentration in the assay as there is depletion of the free inhibitor by binding to the target enzyme, which in turn would underrepresent the true potency of the inhibitor. The other four compounds behaved similarly for both assays, with HG-9-91-01 also exhibiting ~1 nM inhibitory concentration for both SIKs. MRT199665, MRT67307 and KIN112 MALDI-TOF-MS IC_{50} values were more potent than those previously described by Clark *et al.*, but do follow the same trend where all compounds were stated as being more specific for SIK2 rather than SIK3.[184] Comparing the data against the fluorescent ADP Hunter assay for SIK2 generated a correlation plot with a good R^2 of 0.81, however there was a five-fold difference between KIN112 IC_{50}s generated by MALDI-TOF-MS and ADP Hunter assay. Moreover, the low measured IC50 of <1 nM for staurosporine suggests that either the concentration of active SIK2 enzyme, which was provided by the Drug Discovery Unit, was likely substantially lower than 15 nM, or the provided inhibitor stocks had concentrations substantially higher than requested.

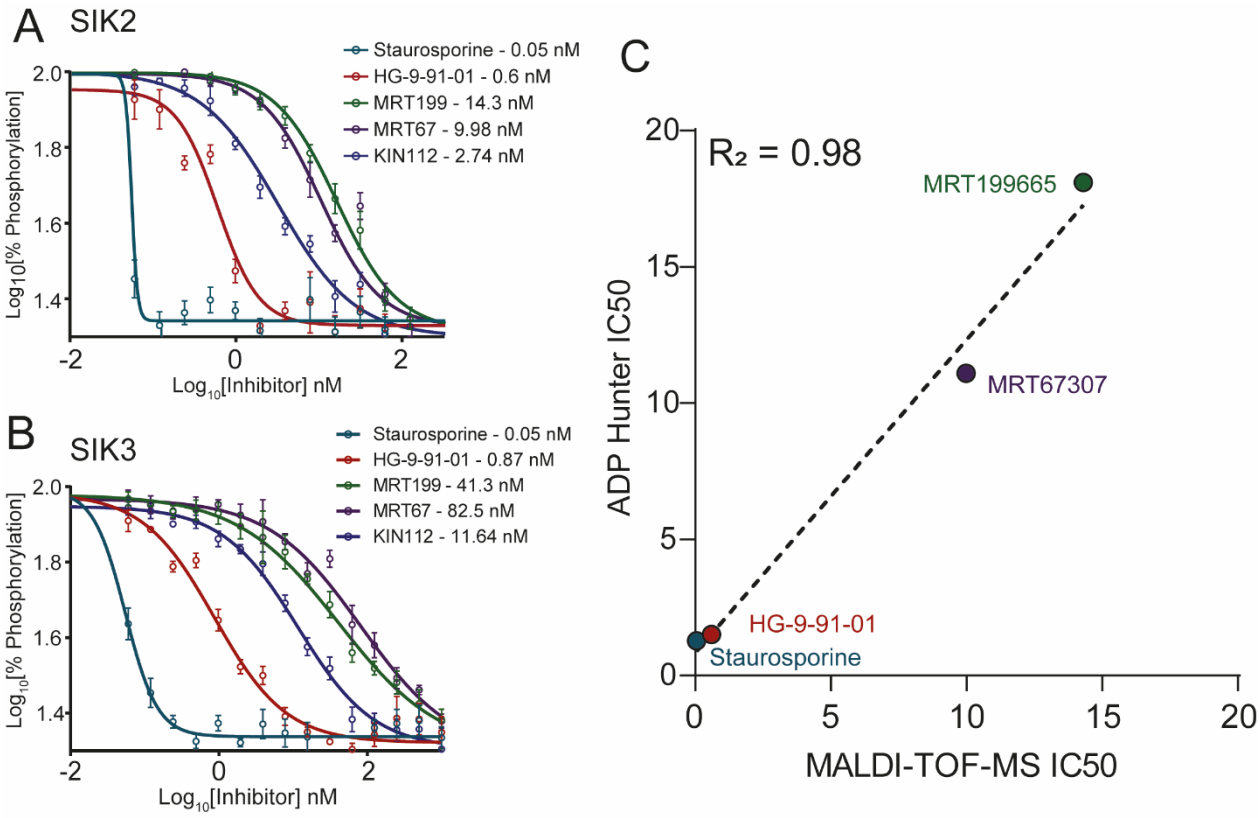

Figure 3-7. Evaluation of known SIK inhibitors by MALDI-TOF-MS. *(A) & (B) MALDI-TOF-MS IC_{50} curves for Staurosporine, HG-9-91-01, MRT199665, MRT67307 and KIN112 for SIK2. Compounds were titrated from 1000 – 0.06 nM (SIK3) and 125 - 0.06 nM (SIK2) in a twofold dilution curve. (C) Correlation plot of MALDI-TOF-MS and ADP Hunter assay IC_{50} values for the 5 compounds generating an R^2 value of 0.81. All error bars are given as ± SD from the mean average of three individual well replicates.*

Finally, Katherine Reyskens (Postdoctoral researcher, Division of Cell Signalling and Immunology, University of Dundee 2017) validated all five compounds by a fluorescent-based assay that was built on the fact that CRTC3 translocates into the nucleus when SIK kinases are inactivated. This is driven by dephosphorylation of four serine residues that are targeted by SIKs. This nuclear translocation is essential for activating the transcriptional program for IL-10 production and polarization toward regulatory-like, anti-inflammatory macrophages.[205]

Human U2OS cells were treated for 1 hr with inhibitors, cells were fixed, and nuclear CRTC3 translocation was analysed by fluorescence-labelled antibody staining on a high-throughput fluorescence imaging platform (PerkinElmer Operetta). The cellular assay showed that nuclear translocation of CRTC3 is enhanced by SIK inhibition. Comparable with our *in vitro* data, CRTC3 translocation correlated with the potency of the inhibitors. Staurosporine and HG 9-91-01 were the most potent of the inhibitors compared to DMSO, showing a very dense nuclear localization of CRTC3. Kin112 was not as potent, and although MRT67307 does induce localization, this was with much greater variation versus the other compounds. MRT199665 was the least potent of all the inhibitors tested. These data show that this is a useful platform to differentiate screening hits efficacy for SIK inhibitors at the cellular level.

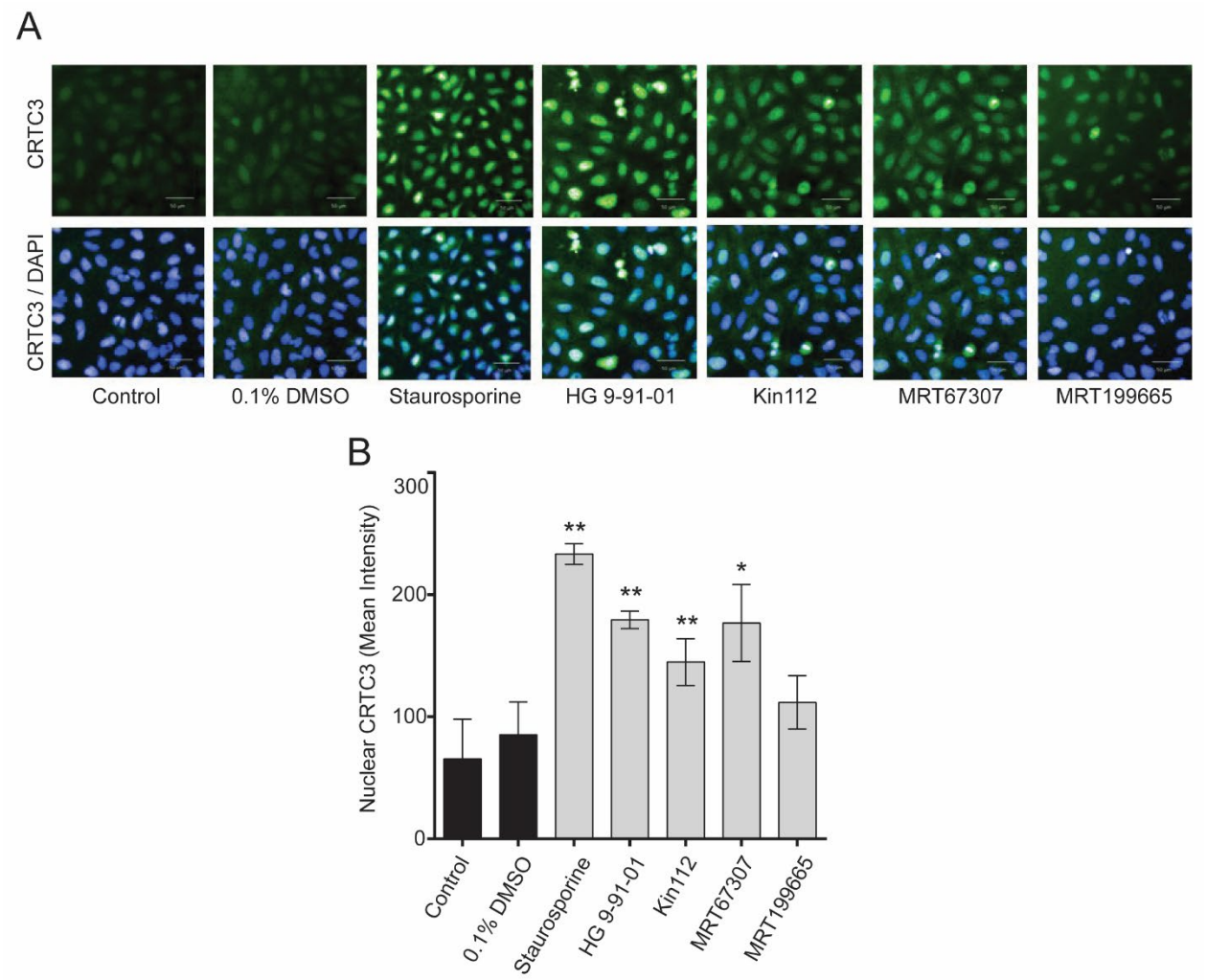

Figure 3-8. Performed by <u>Katherine Reyskens.</u> Nuclear localization of CRTC3 with small-molecule salt-inducible kinase (SIK) inhibitors. *U2OS cells were treated for 1 h with 0.1% DMSO or small-molecule inhibitors serially diluted. (**A**) Representative microscopic images at 20x magnification from the high-throughput system at 10 μM inhibitor with CRTC3 (Alexa 488, green) and nucleus (DAPI, blue) shown. Scale bar = 50 μm. (**B**) Inhibition of SIK kinases induces strong nuclear translocation of CRTC3. Mean fluorescent intensity of nuclear CRTC3 calculated with data represented as mean ± SD. The* p *values versus 0.1% DMSO are as follows: staurosporine,* p = 1.31×10^{-19}*; HG 9-91-01,* p = 4.45×10^{-14}*; Kin112,* p = 2.95×10^{-6}*; MRT67307,* p = *0.0061; MRT199665,* p = *0.533.* *p < *0.01,* **p < *0.001 vs 0.1% DMSO.*

Overall, the IC_{50} values were all in the low nanomolar range and about 0.5 to 1 order of magnitude higher potency than published biochemical assays, suggesting a specific trend

in the MS-based assay. However, this is not unexpected as previous IC_{50} values were determined by less direct measurements, such as IL-10 messenger RNA (mRNA) induction or cell-based methods. In cells, a higher ATP concentration and the presence of other potential targets such as AMPKs and a number of protein tyrosine kinases, cellular penetration of the compound, and inclusion of high concentrations of proteins that may bind to compound could contribute to differences seen for the inhibitor potencies.

3.3.4 High-throughput screen of an ATP mimic library set of 2648 compounds with both the MALDI-TOF-MS and ADP Hunter assays.

To test the potential of the SIK2 MALDI-TOF-MS assay for compound screening, I performed a single-concentration screen of 2648 commercially available ATP mimetics that describe a diverse region of kinase pharmacophore space and compared the data with the ADP Hunter assay. Lesley Pearson (Biologist, Drug discovery unit (DDU), University of Dundee 2017) performed the corresponding ADP Hunter assay with the same set of compounds. In brief, the final MALDI-TOF-MS assay conditions were as follows. Compounds were transferred into 384 HiBase non-binding assay plates using an Echo 550 acoustic dispenser to give a final concentration of 30 μM in-assay with staurosporine included as a positive control at 10μM. Assay buffer (3 μL) and SIK enzyme master mix (1 μL) were added and the reaction was incubated for 30 minutes at 30°C prior to addition of substrate master mix (1 μL) that initiated the reaction. Plates were then incubated for 30 minutes at 30°C before subsequent addition of TFA to final concentration of 2% to quench the reaction and plates were taken straight for spotting.

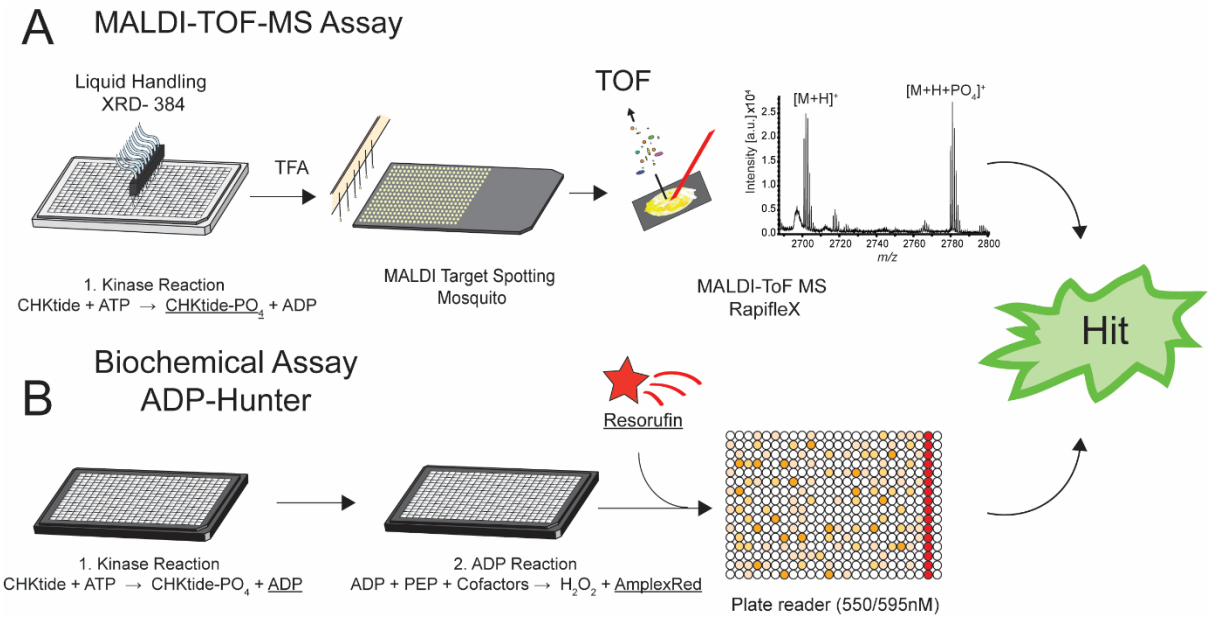

Figure 3-9. Graphical representation of the compound library screening workflow. *Description of how both the (A) MALDI-TOF-MS Assay and (B) ADP Hunter assay identify hits in a high throughput screening set up.*

The output of both screens for SIK2, expressed as percentage effect for the MALDI-TOF-MS and ADP Hunter assays exhibited a normal distribution (Figure 3-10.A), which gives confidence in the data set quality and hit identification. I calculated mean percentage effects of 2.3 (MALDI-TOF-MS) and 7.6 (ADP Hunter) for SIK2 and standard deviations of the whole screening data set were comparable with 20.6% and 14.6% for MALDI-TOF-MS and ADP Hunter respectively. To further evaluate assay quality, I performed Z' analysis on both data sets and measured the statistical effect size. This is calculated by the following equation where *(μ)*, *(σ)*, *(p)* and *(n)* equate to the mean and standard deviations of the positive and negative controls respectively.[216]

$$Z' = 1 - \left(\frac{3(\sigma p + \sigma n)}{|\mu p - \mu n|}\right)$$

A good Z' of >0.5 was generated for both assays (Table 3-2), which was also observed for robust Z' analysis. Robust Z' substitutes the outlier-insensitive median and median

absolute deviation (MAD) for the mean and standard deviation respectively in the Z' equation.[217] This Z' calculation is less sensitive to extreme outliers and both assays were demonstrated to be robust methods for screening (Table 3-2).

Table 3-2. Robustness of SIK2 screening assays

SIK2 Assay	Z'	Robust Z'
MALDI-TOF-MS	0.53	0.50
ADP Hunter	0.95	0.90

To identify hit compounds for both screens a statistically significant effect was defined as a percentage effect (PE) of greater than or equal to mean effect ± 3 SD of the whole screening data set. In addition, the number of compounds producing percentage effect greater than 40% was also determined for each assay and the number of hits for each definition is shown in Table 3-3 for both assays.

Table 3-3. Number of hit compounds for both assays

SIK2 Assay	PE ≥ Mean ± 3 SD	PE ≥ 40%	Unique hits: PE ≥ Mean ± 3 SD	Unique hits: PE ≥ 40%
MALDI-TOF-MS	45	107	14	45
ADP Hunter	59	79	26	16

As expected for single-shot, single concentration screens, the number of hits for both of the assays was not identical for the two screens, but they did correlate (R^2 = 0.44)

between the percentage effects measured for compounds producing greater than 40% effect in the two assays (Figure 3-10.D). With further replicates and I would expect a tighter correlation between the hits of the two assays.

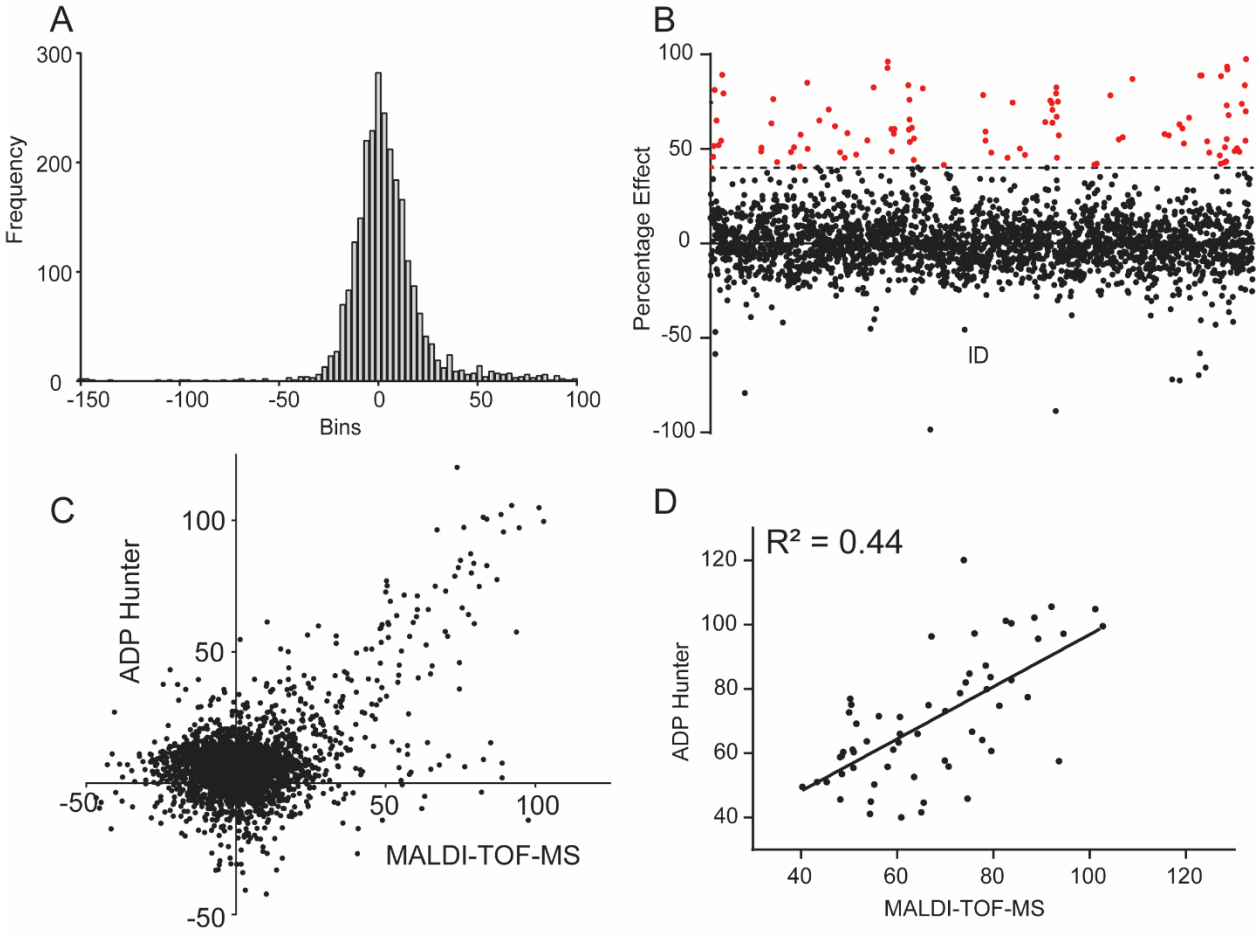

Figure 3-10. Comparison between biochemical and matrix-assisted laser desorption/ionization time-of-flight (MALDI-TOF-MS) salt-inducible kinase 2 (SIK2) assay. *(A) Data distribution of the MALDI-TOF-MS SIK2 kinase assay shows a normal distribution. (B) Blot showing significant hits (>40% inhibition, in red) of the MALDI-TOF-MS assay. Data also show some apparent activators (<–50% effect). (C) Comparison of percentage inhibition for all compounds tested between the biochemical ADP Hunter assay and the MALDI-TOF-MS assay. (D) Comparison of "hits" (>40% inhibition) from both biochemical ADP Hunter assay and MALDI-TOF-MS SIK2 assay showing high correlation between the two assays.*

Eighty percent of the ADP Hunter assay hits (PE >40%; 59 compounds) were identified in both screens (28 with PE >3 SD). There were also 16 hits that were only identified in the ADP Hunter assay and a significant number of hits (45) that were only present in the MALDI-TOF-MS assay suggesting that direct analysis of the peptide product might produce additional hits compared to the indirect ADP assay. Interestingly, when looking at the total correlation plot of hits between the MALDI-TOF-MS assay and the ADP Hunter assay, nine compounds appeared to increase the kinase reaction rate that were not identified in the ADP Hunter assay (Figure 3-11.A). When looking at the spectra, which were spotted in technical duplicate, these hits appeared to be genuinely increasing the product formation when compared with a no compound control on the same assay plate. To validate these findings, I took two of the hit compounds (DDD00853763 & DDD01510849) and two of the activating compounds (DDD00041312 & DDD01010801) and repeated the screening assay conditions. Both the hit compounds significantly inhibited SIK2 activity, whereas DDD01010801 exhibited significant activating potential with a 40% increased percentage effect observed (Figure 3-11.B&C).

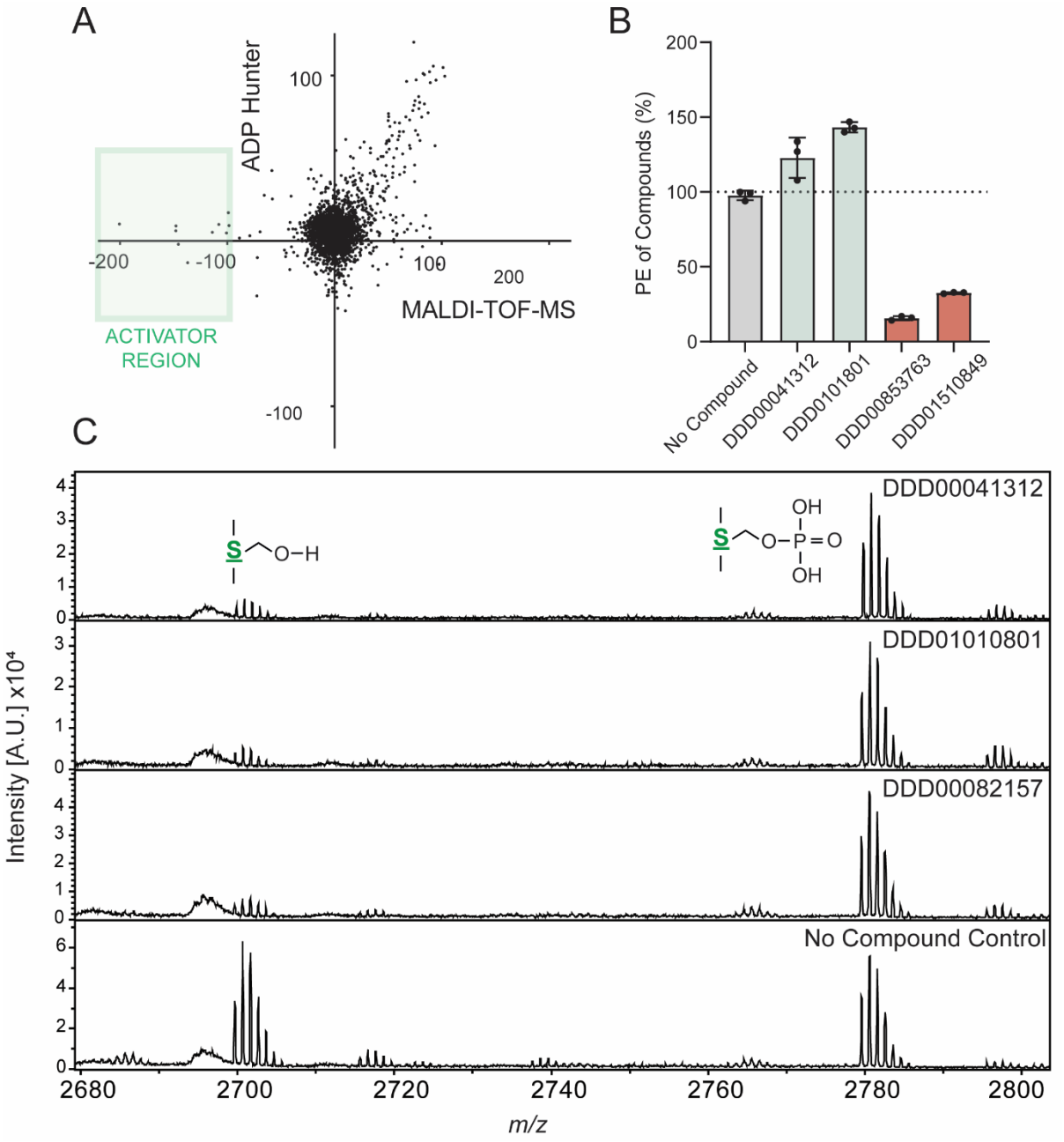

Figure 3-11. Identification of SIK activating compounds by MALDI-TOF-MS. *(A) Full scale axis correlation plot of ADP Hunter vs MALDI-TOF-MS assay showing the potential activating compounds. (B) Validation of two of the activating compounds (DDD0101801 & DDD000041312) and hit compounds (DDD00853763 & DDD01510849) by repetition of the screening conditions. Error bars represent ± standard deviation from the mean. (C) MALDI-TOF-MS spectra for three activating compounds and no compound control showing the acceleration of CHKtide phosphorylation.*

3.4 Discussion

Mass spectrometry-based assays are on the rise in the drug discovery field, with MALDI-TOF-MS proving particularly successful for the high-throughput screening of compounds. Salt inducible kinases regulate the production of the anti-inflammatory cytokine IL-10 by phosphorylating the cofactor CRTC3. This phosphorylation sequesters CRTC3 to the cytoplasm and prevents transcription of IL-10. SIKs can often become activated after the initiation of an inflammatory response as they enable to propagation and systemic spread of inflammation by dampening any IL-10 production that would reverse the response. Under normal circumstances, cytokine production is well balanced by homeostasis and enables efficient clearance of invading pathogens and protection of the host, but when dysregulated this systemic and severe inflammation can cause significant pathogenesis. This is particularly prevalent in auto-immune diseases such as Crohn's and rheumatoid arthritis. By inhibiting SIK activity during acute inflammation, IL-10 production should rise and dampen the inflammatory response, thus there should be an improvement in patient health. Current assays for screening against SIKs are often biochemical assays like the ADP Hunter assay, a secondary assay that measures ADP production by incorporation of the fluorophore resorufin. Although fast and relatively simple, these biochemical based assays are not label free, do not directly measure substrate phosphorylation and can be prone to false positives/negatives arising from auto-fluorescent interactions of test compounds. Therefore, in this chapter I aimed to develop and characterise a robust MADLI-TOF-MS assay for monitoring SIK phosphorylation activity and compare it with the already established biochemical ADP Hunter assay.

3.4.1 MALDI-TOF-MS is a viable readout for phosphorylation activity of SIK2 and SIK3

I first demonstrated the differences in SIK isoform activity by performing an *in vitro* reaction of each enzyme with two substrate candidates: NUAK peptide and CHKtide derived from NUAK2 and CRTC3, respectively. It became clear that our recombinant SIK1 was inactive with both these substrates as there was negligible phosphorylated substrate detected. This was not necessarily unexpected, as SIK1 expression is reported to be more regulated by external stimulus compared with SIK2/3 that are more ubiquitously expressed in tissues at a given time.[218] However, both SIK2/3 had measurable activity with both substrates, with CRTC3 derived CHKtide proving to be more preferable. This combined with its higher MALDI-TOF-MS ionisation efficiency made it the peptide substrate of choice for further assay development.

Characterisation of assay kinetics is key to developing a robust assay and subsequent compound screening. We were able to demonstrate how the MALDI-TOF-MS assay behaved linearly for the SIK2 assay over one hour at an enzyme concentration of 30 nM. By using the Michaelis-Menten model I could show how the cofactor ATP exhibits similar K_M values of 23 μM and 40 μM for MALDI-TOF-MS and ADP Hunter respectively. This calculation for the CHKtide substrate was significantly more challenging with the MALDI-TOF-MS assay as the rate of product formation is calculated from the substrate and product peak areas. At saturated concentrations of CHKtide, this caused significant under-representation of the reaction rate as the substrate peptide was suppressing the phosphorylated product peak and in turn a reduced reaction rate. Therefore, it was not possible to exceed concentrations of 50 μM of CHKtide. Using these modified conditions,

I was able to determine a K_M of 7.7 μM of CHKtide, which was significantly lower than 93 μM determined for the ADP Hunter assay. However, it is likely that the physiological constraints of calculating the reaction rates with relative MALDI-TOF-MS quantitation led to this underestimation, and it may be important in future work to include an internal standard to avoid this problem.

A compound's potency is often measured by determining the half maximal inhibitory concentration over a compound titration, thus giving an IC_{50} value. Four compounds that have been shown previously to have activity against SIKs as well as the non-specific kinase inhibitor staurosporine were chosen to validate the MALDI-TOF-MS assay and compare with the ADP Hunter assay.[184] Generation of IC_{50} curves showed very good fits for both SIK2 and SIK3. However, for staurosporine it is likely that its potency may be underestimated due to tight-binding kinetics. This is due to the IC_{50} value being dependent on enzyme concentration, and therefore tight-binding kinetics occurs with inhibitors when the inhibitor constant Ki approaches the enzyme concentration or tight-binding limit. Correlation of the determined IC_{50} values between the MALDI-TOF-MS and ADP Hunter assays showed good correlation, thus suggesting that the reaction kinetics and behaviour of both assays is similar. Interestingly, in both assays the compounds were significantly more potent than previously reported by Clark *et al*. We hypothesised that this was due to our assays being a single enzyme/substrate reaction, whereas previous studies measured mRNA transcription as a readout in cells where multiple other kinases are present. As many of these compounds are ATP mimetics, it is likely that SIK inhibition potency would be underestimated under cellular conditions due to off-target competition. We did, however, validate all five inhibitors in cells with CRTC3 translocation to the nucleus with a fluorescent cellular assay.

3.4.2 A 2648 compound screen demonstrates assay compatibility and highlights potential novel findings in MALDI-TOF-MS assay

A selected library of 2648 ATP mimetics was screened with both the MALDI-TOF-MS and ADP Hunter assays. Both assays were determined to be very robust with Z' and robust Z' values exceeding >0.5. We were able to identify 80% of the ADP Hunter assay hits with the MALDI-TOF-MS assay that generated a percentage effect correlation of 0.44. These data suggest that for the majority of hit identification both assays are comparable. We were able to identify unique hits from the library for both assays, with the MALDI-TOF-MS assay identifying significantly more. This suggests that by directly measuring the peptide phosphorylation rather than ADP formation we were able to identify hits that may be false negatives in a biochemical assay. It is also important to note that there were 16 unique hits to the ADP Hunter assay, and it would be interesting in future work if these could be determined as genuine hits or false negatives using other assay types such as the cellular fluorescent assay. Finally, we noted that with the MALDI-TOF-MS assay that 9 compounds appeared to accelerate the phosphorylation reaction rather than inhibit it, an observation that was missed with the biochemical assay. This is due to the larger dynamic range of the MALDI-TOF-MS assay which allows measurements of percentage effect to exceed 100%. These results were validated by spectral interrogation and further repetition of the assay conditions with two of the compounds that showed genuine reaction enhancing potential.

Collectively, these data confirm that the developed label-free MALDI-TOF-MS peptide substrate assay correlates with current biochemical approaches for screening inhibitors against SIKs. Moreover, we could show that both techniques generate comparable

IC_{50} data for known inhibitors of SIK kinases and reported significantly more potent findings than previously shown. We took these inhibitors further into a fluorescence-based cellular assay using the SIK activity-dependent translocation of CRTC3 into the nucleus, thereby providing a complete assay pipeline for the identification of SIK kinase inhibitors *in vitro* and in cells. Our data demonstrate that MALDI-TOF mass spectrometry is fully applicable to high-throughput kinase screening by way of a 2648 compound screen that when compared with the biochemical assay show considerable similarities in hit identification. These data also highlight interesting and novel aspects of a MALDI-TOF-MS assay, such as hits that may be falsely identified in biochemical assays, as well as potential SIK activators. The biological activity of these compounds would be of a significant interest and further work in this area would be required. Ultimately, this work confirms that MALDI-TOF-MS is robust for kinase screening and now ready to be scaled up within a pharmaceutical setting for high-throughput screening.

Chapter 4. Optimising a sample preparation method for phenotyping of whole mammalian cells by MALDI-TOF-MS

4.1 Introduction

Ascertaining a mammalian cell's state or phenotype prior to functional studies is key for understanding their biological processes and is often deduced through biochemical assays. This is particularly important for primary cells, as these cultures are typically isolated from animals or living tissues and they often exist as a heterogeneous population of different cell types. Biochemical assays and measurement of cellular biomarkers are two common techniques for cellular phenotyping and utilise flow cytometry[219,220], qPCR[221] or cell biology techniques such as western blotting. However, all these methods typically require long sample preparation methods and incorporate the use of a fluorescently labelled antibody or primer to quantify expression and identify cell phenotypes. Flow cytometry and cell sorting is currently the gold standard in the field for characterising, quantifying and separating heterogeneous cell preparations by analysing both physical and fluorescent properties. This technology has been shown to be particularly powerful for discriminating different immune cells and those undergoing phenotypic shifts.[222,223] However, this method is costly in time and reagents and involves complex data analysis. Moreover, some biomarkers of certain cell states are cytoplasmic, thus requiring cells to be lysed and stained prior to analysis, which can be detrimental for further functional assays.

There is a growing need for label-free and rapid techniques for whole mammalian cell analysis and phenotyping that are less costly compared with conventional methodologies.

Mechanical approaches show promise here as they take advantage of cell deformability and morphology to discriminate positive and negative single cells.[224–226] By utilising a micro-fluidic device, Gossett *et al.* described how a cell can be hydrodynamically stretched and manipulated in a high-throughput manner. The resulting data can then be used to assess changes in cytoskeleton and nuclear structure, thus giving rise to various different cellular phenotypes.[227]

In contrast, mammalian whole cell phenotyping by mass spectrometry approaches are often lower throughput, with mass cytometry[228,229] or MALDI imaging[230,231] being commonly used to classify cell or tissue types. A well-established application of cellular MALDI-TOF-MS is the phenotypic profiling and characterisation of micro-organisms, also known as biotyping.[22,232] Profiling of protein biomarkers specific to a bacterial taxonomy by MALDI-TOF-MS was first performed by Claydon *et al.* and enabled reproducible and robust identification of gram-positive and gram-negative species.[111] Since then, bacterial genera have been identified through various approaches from spectral mass fingerprinting, to more complex approaches that involve matching peaks identified in MALDI spectra to predictive masses from proteomic and genomic data sets.[114,233] This in turn enabled the generation of reference protein databases that list biomarkers specific to different bacterial species.[116] Combined with automated spectral acquisition and novel algorithms to tackle data analysis, biotyping has become a powerful, high-throughput tool for rapidly profiling bacterial genera in both academic and clinical settings.[117] However, inter-lab studies revealed surprising discrepancies in *E. coli* fingerprints as experimental variables such as sample preparation and instrument parameters can affect spectral quality and reproducibility.[234,235] Several studies have therefore scrutinised sample preparation methods for bacterial biotyping, looking at solvent extraction or direct analysis,

sample handling and also matrix choice affects spectra quality with the aim of developing a standardised method to enable universal identification of micro-organisms.[236–238]

Whilst bacterial biotyping has been very successful and has become a standard tool in the clinic, profiling of mammalian cells by MALDI-TOF-MS has not yet reached this level. Characterising the protein and peptide signatures of mammalian cells by MALDI-MS is less common when compared with lipid analysis, however it has been used successfully for phenotypic screening of human cancer cell lines[124], identification of cells within a co-culture[7] or tissues[231] and detection of transient changes within a specific cell type, such as immune cells[240]. However, many of these studies list dramatically different experimental procedures with several being adapted from existing biotyping protocols. This huge range of experimental parameters could therefore be problematic for translation of published assays into the pharmaceutical industry or further research. Therefore, it would be of interest to develop a universal sample preparation workflow that can be utilised for multiple cellular analyses and is ultimately compatible with a high-throughput screening platform.

4.2 Aims

The aim of this chapter was to address the variation in experimental workflows for preparing mammalian cells for whole cell MALDI-TOF-MS analysis (Figure 4-1). Therefore, I systematically tested different conditions at key steps in the preparation and have validated a robust and sensitive sample preparation workflow suitable for high-throughput phenotyping of mammalian cells. This body of work has been peer reviewed and published.

Heap, R. *et al*. Profiling embryonic stem cell differentiation by MALDI TOF mass spectrometry: development of a reproducible and robust sample preparation workflow. *Analyst*, (2019)[241]

4.2.1 Sub-chapters

1. Optimising of on-target concentration for protein and peptide mass fingerprinting.

2. Systematic characterisation and evaluation of the efficacy of different sample preparation techniques.

3. Identifying matrix suitability for whole mammalian cell analysis and liquid handling compatibility

4. Profiling stages of embryonic stem cell differentiation by MALDI-TOF-MS

4.3 Results

My workflow for optimising a whole cell MALDI-TOF-MS preparation is depicted in Figure 4-1, where I will explore different preparation steps in order to gain maximum cellular information and speed as well robust technical analysis. From previous studies, methods describing protein signatures in the *m/z* range 2000 – 20,000 have utilised several different parameters to discriminate cell phenotypes. These typically include common masses, features that differ in intensity, unique features or a shift between two peaks that are not baseline resolved that could indicate post-translational modification.[126,127,129,242] The developed method must be able to identify these types of distinguishing features clearly and I will use multivariate and statistical analyses to determine the features that describe clustering and to test robustness.

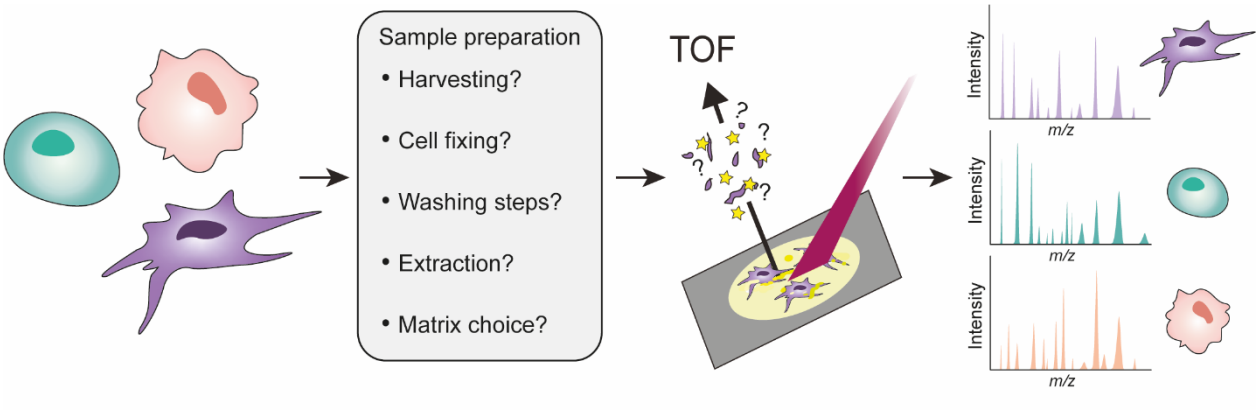

Figure 4-1. Concept of a mammalian whole cell analysis workflow by MALDI-TOF-MS highlighting missing information under sample preparation.

4.3.1. Optimising of on-target concentration for protein and peptide mass fingerprinting.

In order to optimise the sample preparation for whole cell MALDI-TOF-MS, I chose to work initially with four different human cell lines (U2OS, MCF7, THP1 and HEK293) (Figure 4-2.A). These were chosen as they vary in morphology and biological function, but are all derived from human tissues, thus I hypothesised that there would be no species clustering bias. As a starting point, I initially followed the protocol described by Munteanu *et al.*, who alongside other published studies report PBS washing to remove culture medium contaminants such as high levels of FBS and salts from the culture medium that could affect MALDI-TOF-MS ionization.[240] The number of PBS washes used has varied from one to three depending on the authors' experimental design, but my data indicated that a single initial PBS wash was sufficient to remove contaminants. This also significantly reduced sample preparation time. As the cell lines all vary significantly in size (Table 4-1), I sought to determine an optimal cell concentration, therefore a titration of 25 to 20,000

cells for each line was spotted on target. Unsurprisingly, the ionisation efficiency varied between the cell lines (Figure 4-2.B), and by taking the total spectral intensity, it was possible to identify an optimal on-target concentration from each cell line (Figure 4-2.B, C) (Table 4-1). This data shows that good signal and spectral intensity can be obtained from each cell line at a significantly lower number of cells than previously reported. We did also observe a narrow window where good spectra could be acquired, with large numbers of cells on-target proving to be detrimental to ionization.

Table 4-1. Mean cell diameter measurements and optimal on-target cell number for MALDI-TOF-MS for each of the four cell lines with ± standard deviation.

Cell line	**U2OS**	**MCF7**	**THP1**	**HEK293**
Cell diameter (µm)	21.6 ± 1.4	18.1 ± 0.75	8.0 ± 0.25	16.9 ± 0.63
Optimal cell number	250	500	1000	500

To further understand the relationship between cell lines and their individual optimal concentration the total protein concentration was determined by a standard BCA assay. The relationship between number of cells and total protein concentration correlated well, validating our previous observation with cell number (Figure 4.2.D). Therefore, I determined the in-solution diameter of all four cells lines by bright-field light microscopy and when plotted against the optimal cell number these generated a linear relationship with a very good correlation of $R^2 = 0.99$ (Figure 4.2.C). Taken together, these data show that to obtain optimal and reproducible spectra from mammalian cells by MALDI-TOF-MS, cell numbers on target need to be optimised and that this number is dependent on cell size / total protein concentration. This concentration can now easily be obtained by initially

measuring a cell populations diameter and calculating the on-target concentration with the equation described in Figure 4-2.C.

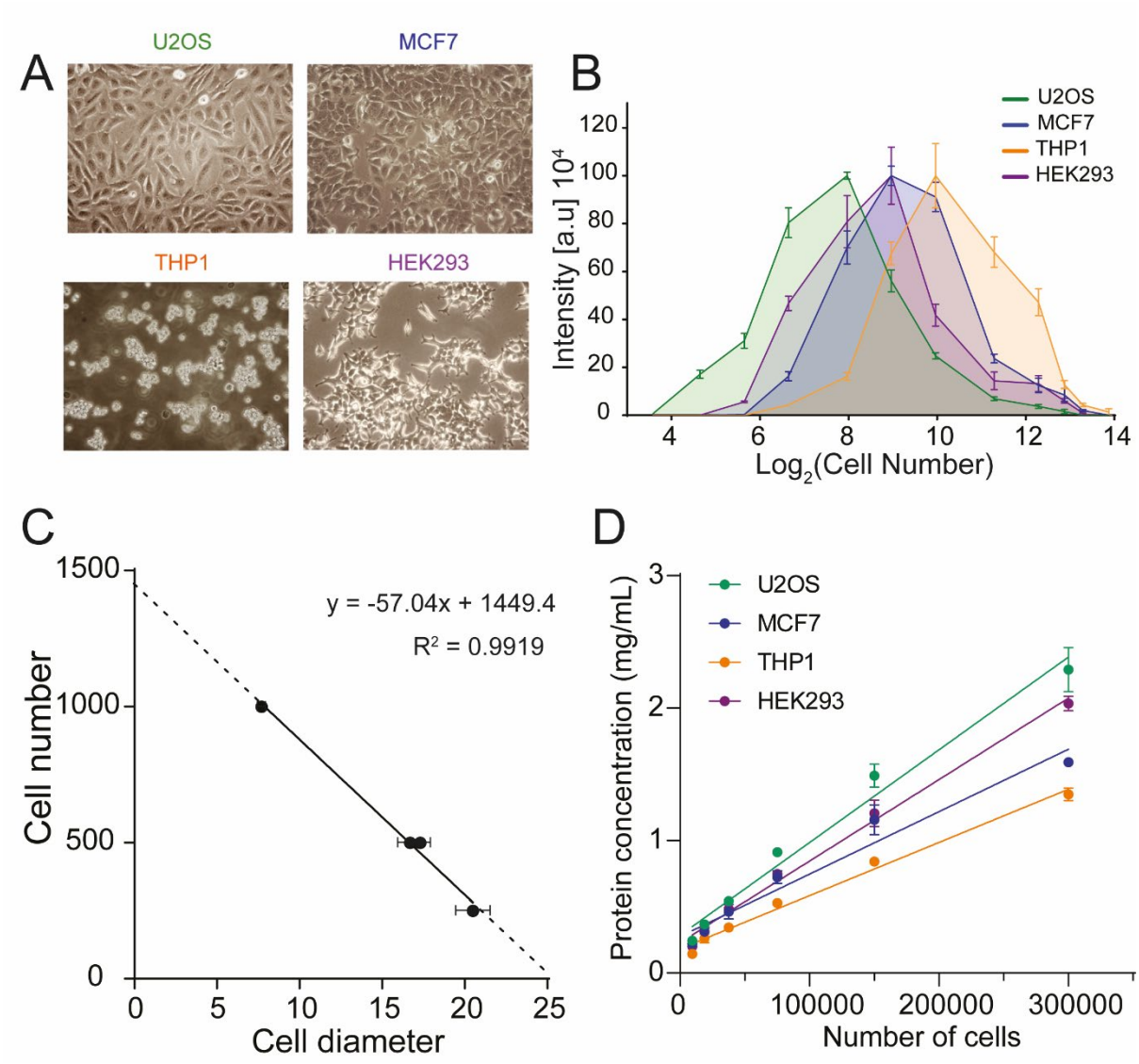

Figure 4-2. Differences in MALDI-TOF-MS ionisation efficiency for each of the four cell lines. *(A) Bright-field microscopy images of the four cell lines U2OS, MCF7, THP1 and HEK293. (B) Ionisation profiles of the four cell numbers generated from spectral intensity at 25 – 20,000 cells on target. (C) Correlation plot of optimal cell number on-target derived from (B) and each cell line's in-solution diameter measurement where error bars represent ± standard deviation from the mean. (D) Correlation plot of total protein concentration against cell number and error bars represent ± standard deviation from the mean.*

4.3.2. Systematic characterisation and evaluation of the efficacy of different sample preparation techniques.

I next determined whether lysis of cells enhanced the occurrence of unique mass features over intact cells. Employing harsh acidic lysing conditions resulted in spectra that were less distinguishable, which has also been observed by lysing with increasing acidity.[242] As well as this, strong lysing conditions such as mechanical disruption often resulted in a viscous solutions from the cellular DNA that was difficult to handle and would not be compatible with liquid handling robots. It was previously shown for bacterial culture analysis that mild lysis by freeze-thawing of cell pellets prior to MALDI-TOF-MS analysis was beneficial with respect to the number of features identified and overall spectral intensity.[235,238] I therefore decided to test whether a freeze/thaw cycle improved MALDI-TOF-MS analysis of mammalian cell lines and whether freezing before or after the initial PBS wash affected sensitivity and spectral quality compared with direct analysis (Figure 4-3.A).

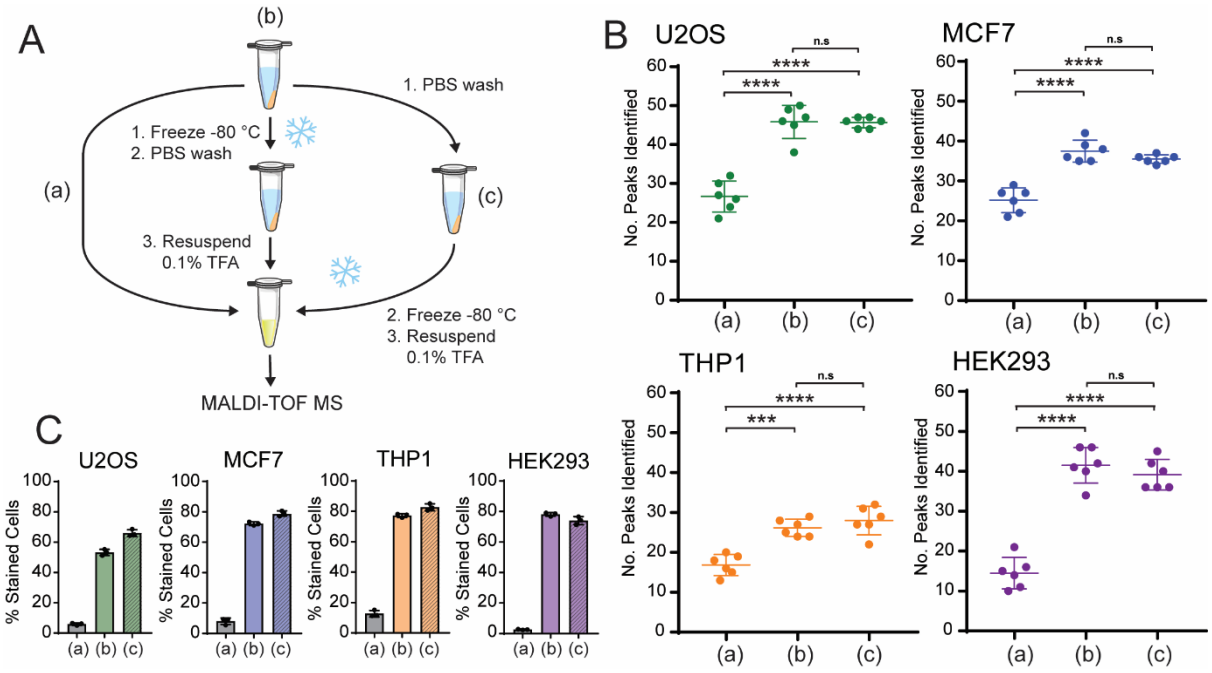

Figure 4-3. Comparison of three freeze/thaw techniques for MALDI-TOF-MS analysis of mammalian cells. *(A) Graphical representation of the three freeze/thaw strategies employed to test efficacy of this sample preparation method. (B) Number of features identified for each cell line with each strategy described in (A) and a S/N >4. (C) Trypan blue staining with each strategy described in (A) to determine the percentage cell membrane permeability for each cell in. In all cases error bars represent ± standard deviation from the mean over six technical replicates.*

Both strategies of freeze/thawing permeated the cell membrane of about 50-80% of the cells (Figure 4-3.C). This led to a significant increase in the number of peaks detected compared to "intact" cell samples within the *m/z* range of 2 – 20 kDa (Figure 4-3.B). As well as this, software analysis did not result in a significant difference between cells frozen before or after further treatment and manual inspection of spectra resulted in the same conclusion. Therefore, it was concluded to include a freeze/thaw cycle within the sample preparation method. However, the specific order in which this step was performed, did not affect the final readout.

Many protocols for both bacterial and mammalian cell analysis by MALDI-TOF-MS utilise specific solvents to extract and analyse biomolecules of interest.[243,244] This work has been particularly successful for lipid analysis, where solvent extraction can efficiently isolate lipids from cells.[245] However, for our particular study, where I aimed to look at peptide and protein features, these methods were unsuitable. I therefore I applied two cell and tissue fixing techniques and evaluated their efficacy for preparation of mammalian cells for MALDI-TOF-MS analysis. Initially, I employed formaldehyde and methanol fixing methods, as they have been used previously in MALDI imaging workflows.[246,247] In brief, cells pellets were thawed and resuspended in ice cold methanol or 4% PFA at 4°C for fixation before subsequent preparation steps. The resulting mass spectra revealed that samples treated with 4% PFA generated spectra were 5 – 10x less intense than other

methods and was therefore excluded from further work. Consequently, I systematically evaluated how both methanol fixing and PBS washing performed with respect to the number of identified peaks, quality of the acquired spectra, as well as technical reproducibility when analysed by MALDI-TOF-MS (Figure 4-4).

Each of the four cell lines could be distinguished by both manual spectra interrogation and principle component analysis (PCA) of mass spectra intensities after methanol and PBS washing steps (Figure 4-4. A-F). Each method was able to generate a unique set of peaks for each of the four cell lines, thus allowing classification of the different populations. Phenotype distinguishing peaks were often not the most intense or abundant peaks and were identified with a lower S/N and intensity than the base peak, thus were less likely to be quantified accurately. Therefore, I plotted the relative intensity distribution of the top 10 most intense peaks for each cell line (Figure 4-4. G&H). Both PBS washing and methanol fixation showed a generally even intensity distribution for each cell line. Finally, and arguably most importantly, I tested how reproducible peak detection was over six technical replicates (Figures 4-4. I&J). Methanol was the most consistent, with the majority of all peaks being detected in all six spectra, whereas PBS was slightly more variable. Taken together, this data suggests that methanol fixation is comparable to PBS washing for whole mammalian cell analysis and could be suitable for classification of subtle phenotypes.

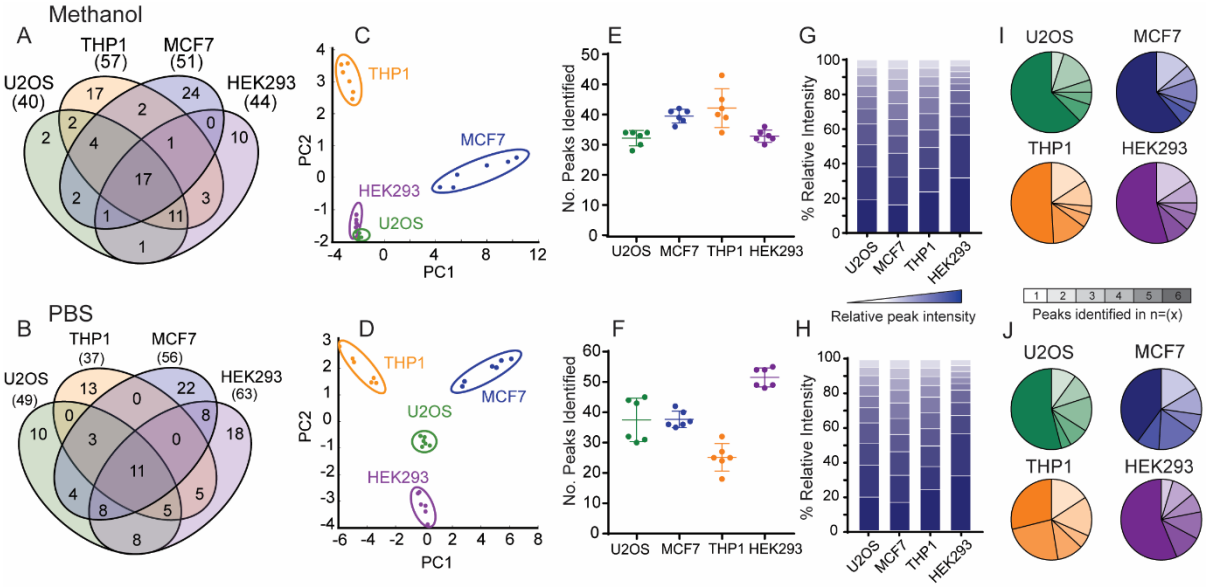

Figure 4-4. Technical reproducibility of MALDI-TOF-MS sample preparation methods. *(A & B) Number of detected unique features for any of the four cells after methanol fixation (A) and PBS washes (B). (C & D) PCA plots showing how multivariate analysis can distinguish each of the four cell lines after methanol fixation (C) and PBS washes (D). (E & F) Number of peaks detected for each cell line over six technical replicates where error bars represent ± standard deviation from the mean. (G & H) Relative intensity distribution of the top 10 peaks detected over six technical replicates for each cell line. (I & J) Pie charts displaying the % of peaks detected within each of the six replicates per cell line.*

4.3.3. Identifying matrix suitability for whole mammalian cell analysis and liquid handling compatibility

Next, I evaluated which type of matrix allows for the best MALDI-TOF-MS analysis of mammalian cells. Each cell line sample was prepared with one of the three most common peptide and protein matrices: saturated sinapinic acid (SA), α-cyano-4-hydroxycinnamic acid (CHCA) or 2-5-dihydroxybenzoic acid (DHB) in 50% acetonitrile, 0.1% TFA.

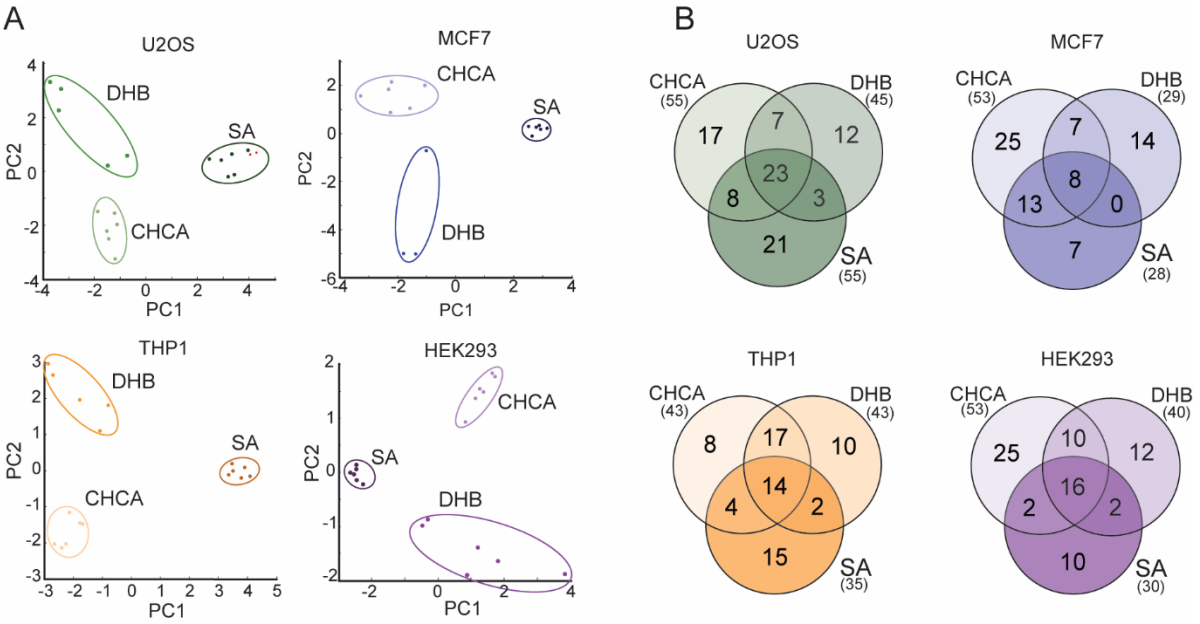

Figure 4-5. Classification of mammalian cell lines by MALDI-TOF-MS multivariate analysis. *(A) PCA plots showing unique groupings for each of the matrix conditions and (B) Venn diagrams showing unique and common peaks detected for each of the four cell lines (U2OS, MCF7, THP1, HEK293) over six technical replicates.*

Significantly different mass profiles of the same cell line were observed. Using DHB matrix resulted in more variable spectra over technical replicates, with the PCA analysis showing wider distances (Figure 4-5. A). Moreover, unique peaks could be assigned to each of the matrices, which indicates that different biomolecules are being ionised and mammalian cell profiles are matrix dependent (Figure 4-5. B).

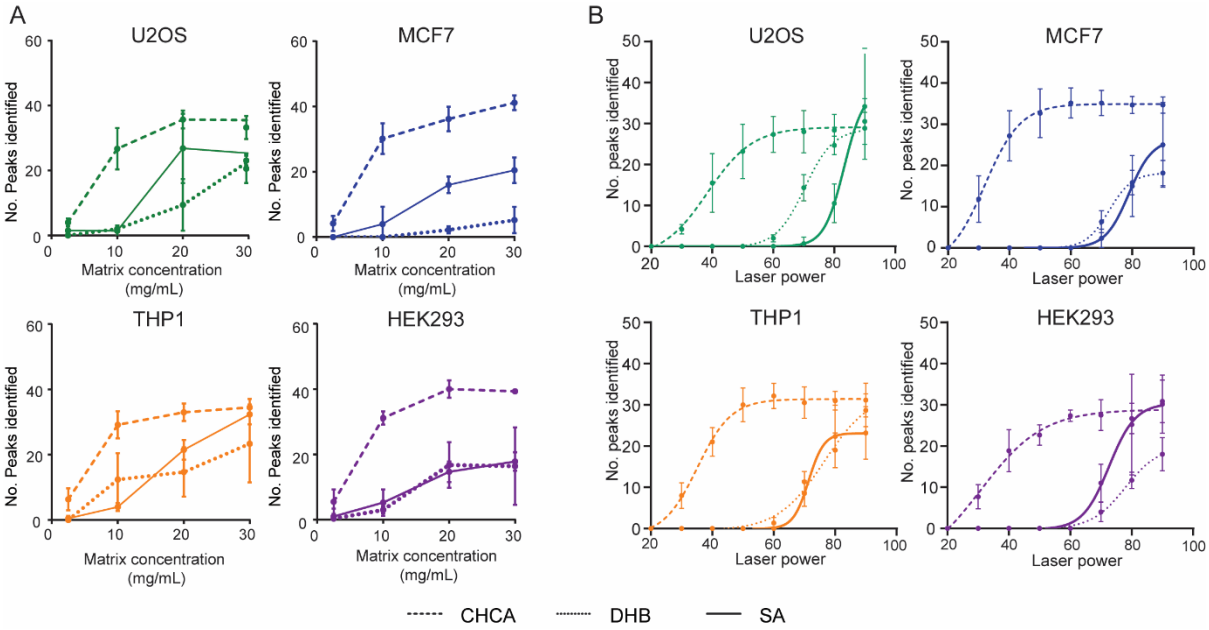

Figure 4-6. Impact of matrix choice on MALDI-TOF-MS ionisation of whole mammalian cells. *(A) Dependence of matrix concentration from 2.5 – 30 mg/mL (saturated) on number of peaks detected for each of the four human cell lines and three matrices. (B) Laser power dependence of each of the three matrices for each of the four cell lines. Non-linear regressions were fitted with a sigmoidal, 4PL curve with good fits of* R^2 *>0.85 – 0.99. All error bars are given as ± SD over six technical replicates.*

I then evaluated how each matrix performs with respect to concentration and increasing laser power. In all four cell lines, CHCA performed significantly better with respect to both parameters (Figure 4-6). Following this, I observed that CHCA matrix was also able to ionise cellular biomolecules at much a lower laser power than DHB and SA. I was able to fit non-linear curves to these data, thereby identifying optimal minimal laser power and approximate saturation points of each matrix (Figure 4-6. A). From these values, the fold change in laser power necessary to achieve an optimal sample acquisition could be determined between each matrix. A laser power of 60% corresponded to a laser energy fold change of 1.74x and 2.30x for 80% (DHB) and 90% (SA), respectively when compared to CHCA.

I pursued this study further to understand the dynamics of matrix behaviour with fixed cells in a mock screen MALDI plate and evaluate performance across a 1536 target. THP-1 cells were then mixed with each matrix using a Mosquito HTS and spotted in 200 nL aliquots. Each target was then analysed at the approximate saturation points described previously. From manual inspection as well as a positive MALDI response in which peaks could be detected at a S/N >3. A spotting accuracy of >96% could be achieved for each target and matrix using the Mosquito HTS spotting robot (Figure 4-7. A). This infers that methanol-fixed whole-cell samples are compatible with current liquid handling technologies, as well as MALDI TOF-MS.

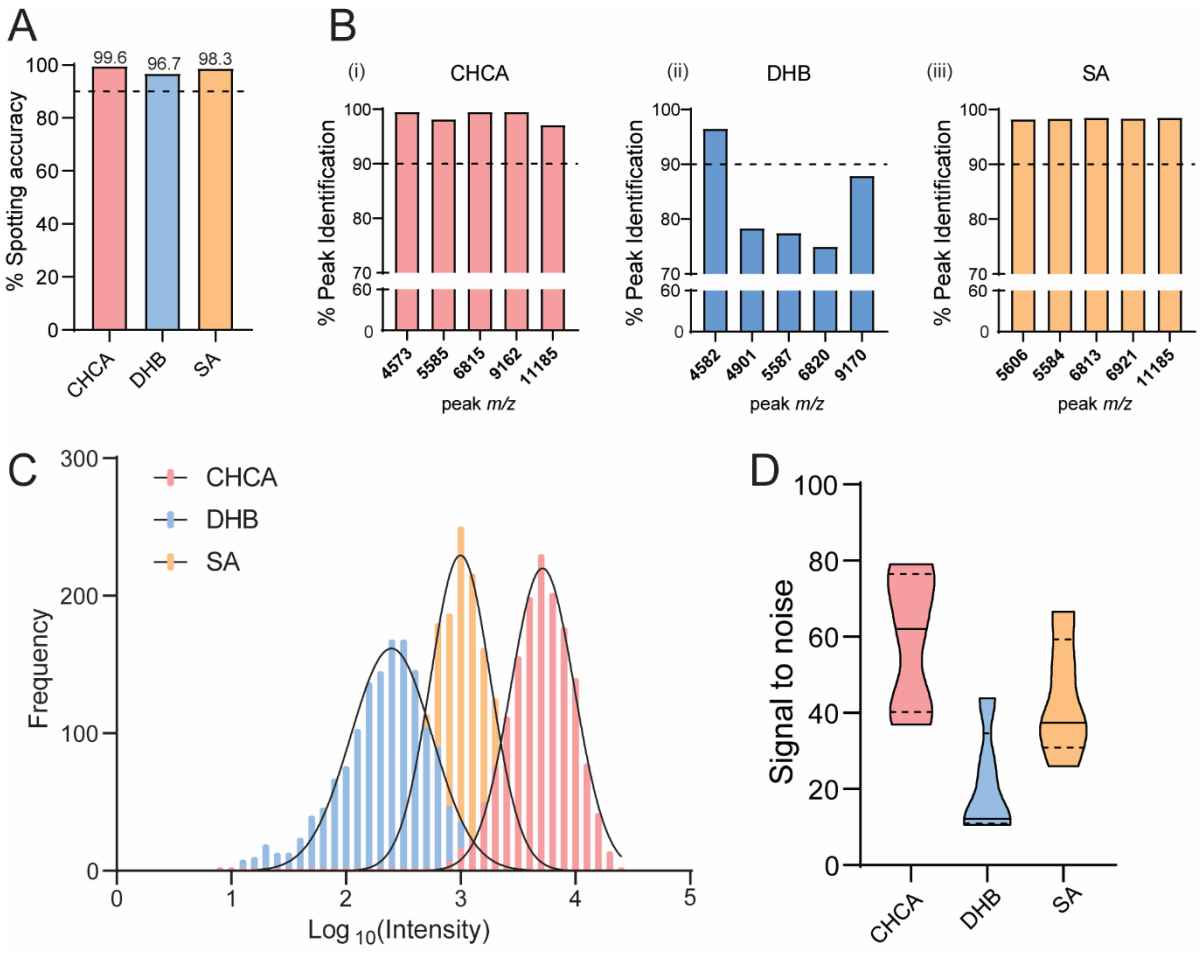

Figure 4-7. Mock screening plate demonstrates that CHCA is the preferable choice for MALDI-TOF-MS analysis of mammalian cells. *(A) Mosquito spotting accuracy*

determined by achieving a spectra where peaks could be detected with a S/N >3 in addition to manual inspection for each of the matrices. Percentage of 1536 spots. (B) Percentage peak detection of the top 5 most intense peaks over a 1536 target for each of the three matrices. (C) Frequency distribution of the top 5 most intense peak intensities of a 1536 target for each of the three matrices bin width = 0.1. (D) Violin plots showing distribution of the signal-to-noise of the top 5 most intense peaks over a 1536 target for each of the three matrices. Solid lines indicate median values and dotted lines the upper and lower quartiles.

Using the top five most intense features for each matrix preparation I was able to show that these were detected in >98% of spots for CHCA and SA, thus showing robustness for screening. Samples spotted with DHB matrix were much more variable and therefore had poorer repeat peak detection (Figure 4-7. B). Overall spectral intensity based on the top five peaks as well as signal to noise varied significantly between the three matrix conditions (Figure 4-7. C&D). Samples spotted with CHCA exhibited much greater spectral intensity compared to SA, and an almost 10-fold increase when compared with DHB (Figure 4-7. C), as well as significantly better S/N for these top 5 features (Figure 4-7. D). Interestingly, we observed different lens contamination patterns for each of the three matrices after accumulation of 3072 individual spectra with each matrix, although this did not negatively impact analysis. From this data, I concluded that CHCA would be the matrix of choice for whole cell analysis at a small and large scale due to its superiority across the parameters discussed above. Together, these results show how phenotyping cells by MALDI-TOF MS using the final optimised method (Figure 4-8) can be scaled up to a high-throughput platform and still enable robust identification of cell line specific features.

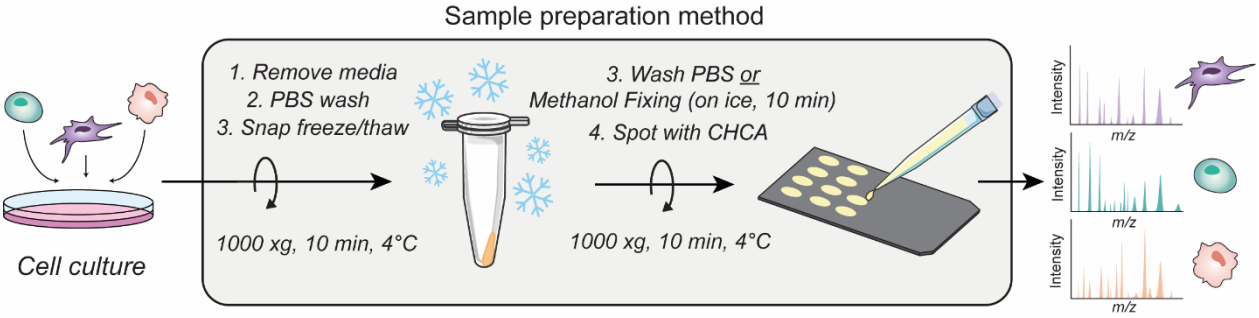

Figure 4-8. Final optimised workflow for mammalian whole cell analysis by MALDI-TOF-MS. *In brief, cells in culture are first harvested, washed once with PBS and snap frozen. Pellets are then thawed and either fixed with methanol or washed 1x with PBS. Cells are then resuspended in 0.1% TFA to the desired concentration and spotted with CHCA matrix either manually or with liquid handling instruments. Described fully in 2.2.3.4.*

4.3.4 Profiling stages of embryonic stem cell differentiation by MALDI-TOF-MS

To validate the complete workflow the sample preparation method was applied to profile cells in a physiologically relevant system that is employed in drug screening and toxicity testing and that has been used as a drug discovery model.[248,249] Murine embryonic stem cells (mESC) were utilised as they can be maintained in a naïve ground state pluripotency using the 2i kinase inhibitor system (PD0325901 and CHIR99021), which inhibit the kinases ERK1/2 and GSK3, respectively (Figure 4-9. A).[250,251] Efficient exit from this naïve ground state pluripotency towards differentiation upon 2i release is achieved by removal of the kinase inhibitors from culture resulting in distinct morphology differences (Figure 4-9.C). This results in two populations derived from a single mouse. These cells were prepared by Anna Segarra-Fas (University of Dundee) who also confirmed the 2i release state by supressed mRNA expression of naïve and pluripotency factors (Figure 4-9.B).

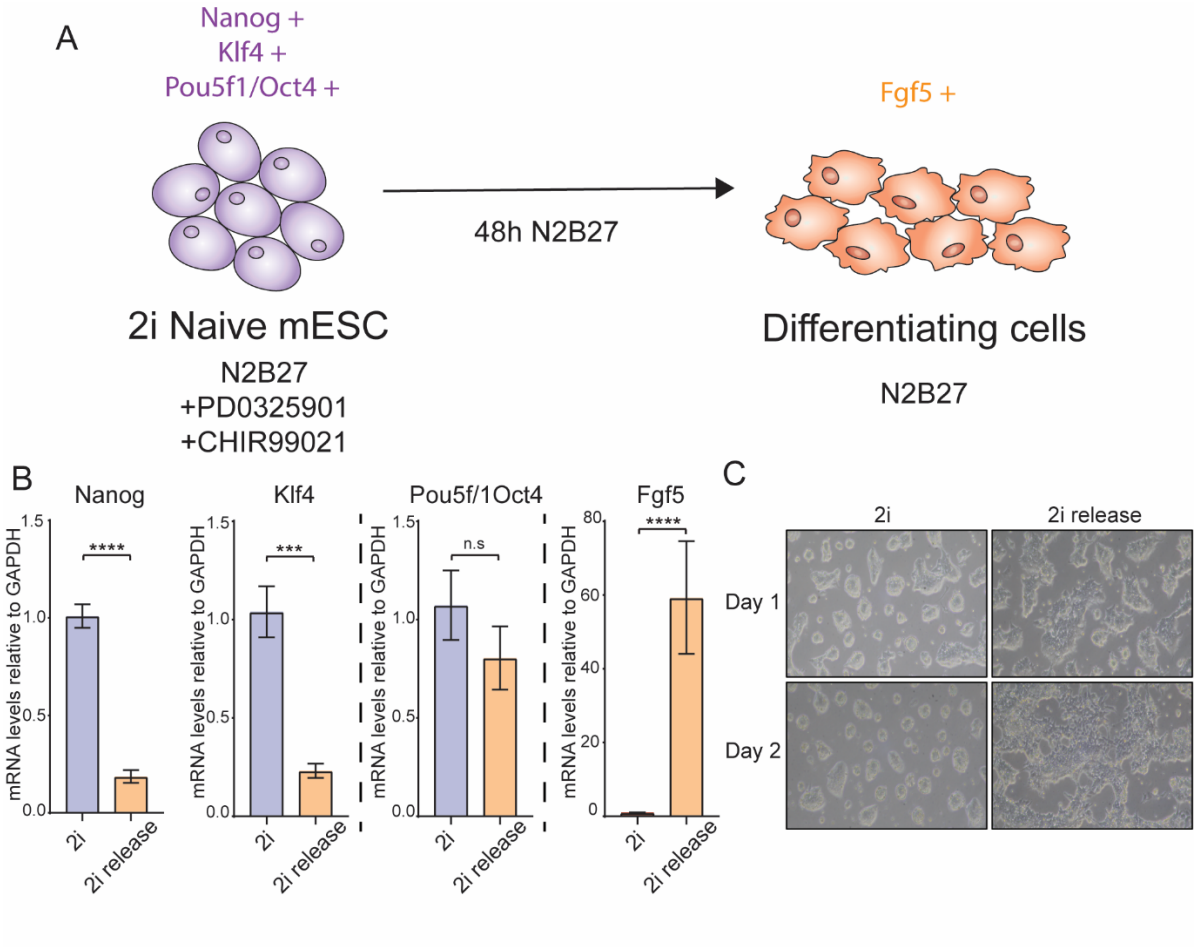

Figure 4-9. Performed by <u>Anna Segarra-Fas</u> Classification of mESC populations. *(A) Schematic showing the differentiation of naïve mESCs upon removal of the two kinase inhibitors (2i). (B) qPCR data showing changes in key mESC pluripotency and differentiation genes. (C) Light microscopy image showing the morphological change in naïve mESCs upon 2i release after 1 and 2 days. Error bars represent standard deviation of 2 technical replicates from 3 biological replicates. *** and **** represent p<0.001 and p<0.0001, respectively, student's t-test.*

Using MALDI-TOF-MS, I could robustly identify unique features to each population, as well as quantify changes in common peaks. For all spectra, the base peak was identified at *m/z* 4875, which made subsequent analysis simpler, as the raw spectral intensity can vary significantly from spot-to-spot (Figure 4-10).

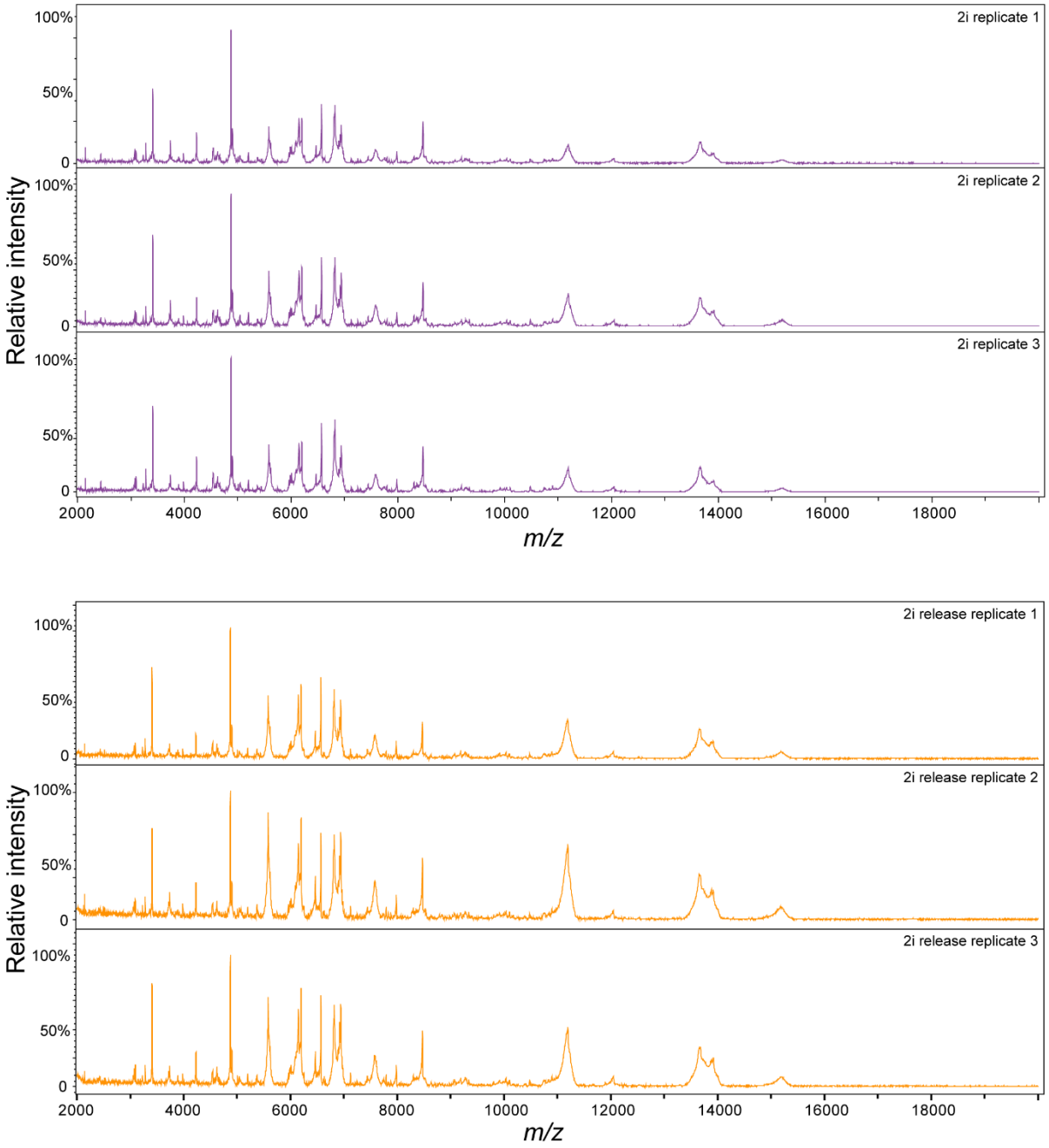

Figure 4-10. Representative MALDI TOF spectra of each of the three individual biological replicates for 2i and 2i release cell populations.

It was possible to use the relative intensity of each peak in the spectra as the base peak was identical in all spectra at *m/z* 4875*,* which I used for normalisation. A heatmap was generated using Z-score averaging (Figure 4-11A) where the averaging was performed by row and involved the mean value of each row being subtracted from the individual value. This value is then divided by the standard deviation of each row to generate a normalised expression matrix and a normal distribution for the population. Each Z-score value represents how many standard deviations a given value is away from the mean relative intensity for that particular *m/z* value. This enabled us to look at more subtle changes within the total data set and identify features that differentiate masses of the two phenotypes, whose relative intensity exhibits 3 or more standard deviations apart from each other.

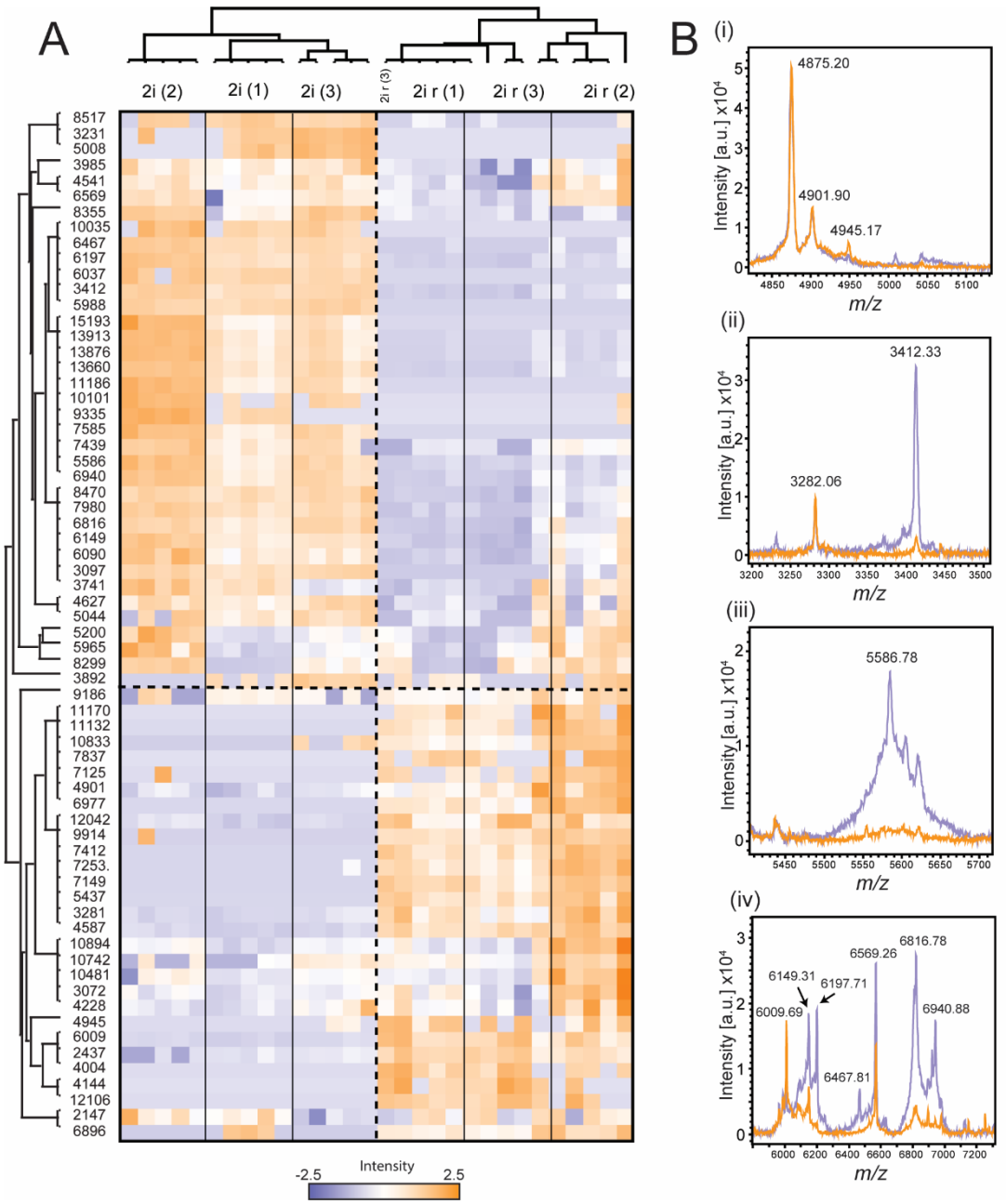

Figure 4-11. MALDI-TOF-MS analysis of naïve and pluripotent mESC populations. *(A) Z-score heat map showing how each normalised peak intensity changes with respect to 2i and 2i release condition over three biological and five technical replicates. (B) Selected examples of mass spectral regions that showed changes between mESCs cultured in 2i and 2i release conditions where the base peak (m/z 4875) is of identical intensity, thus allowing relative intensity comparison.*

For robustness, data were first filtered to include features that were identified in at least 30% of all technical replicates. The hierarchical clustering approach allowed us to look at the unique and common features combined across all independent

biological and technical replicates. The three biological replicates clustered well together and 2i and 2i release conditions were separated efficiently and two discrete row clusters emerged – peaks that were up-regulated and those that were down-regulated upon release from PD0325901 and CHIR99021 inhibitors. This was determined to be significant by a hierarchical dendrogram using bootstrapping (performed by Alasdair Blain, Newcastle University). This generated scores >95 for the two conditions, thus considered significant separation.

Finally, using multivariate analysis, 2i and 2i release conditions could be well differentiated as two populations by PCA (Figure 4-12.A & B) and we observed good grouping of biological replicates. A similar distribution was identified when using a jackknife method performed by Alasdair Blaine which is a resampling technique that estimates variance and bias within a dataset (Figure 4-12.C).

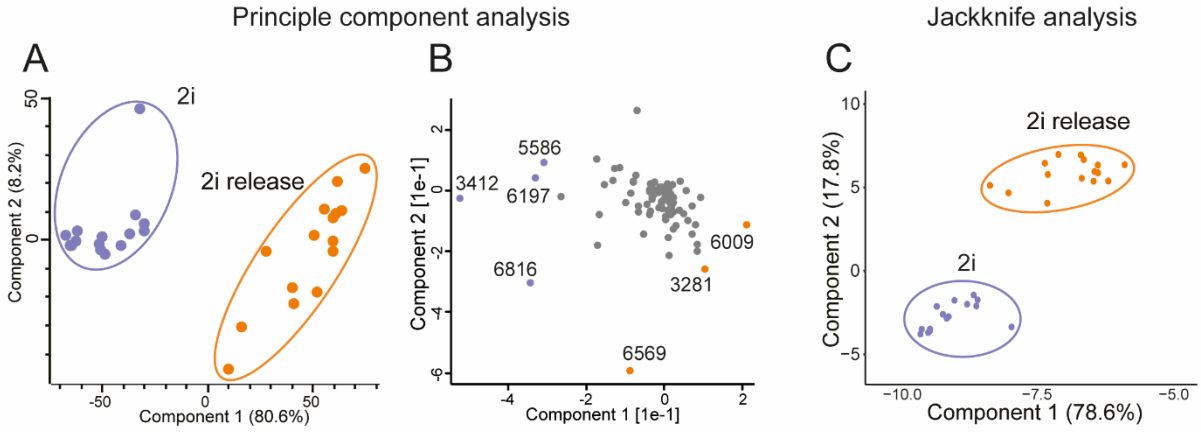

Figure 4-12. Multivariate analysis of mESCs analysed by MALDI-TOF-MS*. (A) PCA plot of the biological and technical replicates of 2i vs 2i release filtered MALDI-TOF-MS data showing separation of the two phenotypes. (B) loadings plot corresponding to (A) showing the m/z values that contribute most to the separation of the two cellular phenotypes. (C) Performed by Alasdair Blair: Jackknife statistical analysis of the MALDI-TOF-MS enables distinct clustering of the two phenotypes similar to that shown in (A).*

Analysing the loading plot of the PCA clustering identified the same features shown in Figure 4-11.B. to be driving the majority of the separation.

Taken together, in this data set several peaks were identified that changed significantly in intensity between the conditions by manual inspection, Z-score averaging and PCA analysis. These mass features can now be used as features of phenotypic screening of mESC differentiation. The analysis workflow was validated by Alasdair Blain, who performed independent statistical analysis to recreate the heatmap and PCA showing very similar data. Consequently, this confirms that the optimised MALDI-TOF-MS sample preparation method described in this chapter is suitable for phenotypic screening of different cell types.

4.4 Discussion

Due to its speed and relative simplicity, MALDI-TOF-MS has become increasingly popular for bacterial biotyping in clinic. Classification of cellular phenotypes by protein and peptide fingerprinting using MALDI-TOF-MS has been well described for discriminating prokaryote genera, however these methods have never truly been translated into mammalian cell phenotyping. Several applications for discriminating mammalian cell cultures by analysing their protein and peptide mass fingerprints have been reported such as discriminating cancer cell lines[124], profiling of immune cells[240] and identifying cells in a co-culture.[127] However, the methods presented are significantly different with some using protein extraction over direct analysis, and all utilising very different matrix compositions and preparations. Furthermore, some of the methods described would not be suitable for more automated analysis and therefore more throughput screening applications would not be possible. Consequently, there is a need for a universal method for sample preparation of whole mammalian cell samples for MALDI-TOF-MS analysis that enables robust, sensitive

and reproducible classification of cell phenotypes. In this study, I have used four human cell lines to systematically test various sample preparation techniques, thereby determining which ones are most technically robust and yield maximum information. Further to this, I validated the final optimised method with established liquid handling techniques to ensure compatibility for screening and finally applied the method to profile mESC differentiation.

4.4.1. Optimisation of a robust and sensitive MALDI-TOF-MS sample preparation method for whole mammalian cell analysis

By utilising the four human cell lines U2OS, MCF7, THP1 and HEK293, I was able to test several different sample preparation strategies to assess grouping of cell phenotype without species bias. Firstly, by titrating the cells from a very high number to a low number of cells, I could identify that each of the four cell lines had an optimal number of cells on target for MALD-TOF-MS analysis as well as their individual limits of detection. This was determined over six technical replicates utilising total spectral intensity and, unexpectedly, there was a significant drop in signal intensity at high cell numbers. This could be explained by the matrix: cell ratio resulting in inefficient ionisation, poor spot crystallisation or the total intracellular salt content of the cells.

A good linear relationship between total protein content and overall spectral intensity was observed and indicates that protein concentration could be used to calculate an optimal on-target cell concentration of an unknown cell population. However, as this approach is indirect and requires a significant number of cells it adds time and extra sample loss to the workflow which isn't favourable for screening assay development. Therefore, I aimed to develop a simple and fast method to determine this important parameter and evaluated cell diameter as an alternative measurement that can be performed without sample loss. Plotting the in-solution diameter against optimal

concentration a linear correlation was generated with very good R^2 >0.99, thus the equation derived from the linear regression could be used to estimate on-target MALDI-TOF-MS cell concentration based on the cellular diameter.

I then established that the use of a mild lysis method by freeze/thawing of cell pellets significantly increased the number of features detected by MALDI-TOF-MS for all cell lines. This is likely due to the permeabilization of the cell membrane enabling intra-cellular biomolecules to be more available for ionisation. I found that this lysing method was preferable to harsher lysing conditions such as sonication or use of detergents and salt buffers, as this often leads to viscous sample solutions due to release of nuclear DNA. It has also been reported that high concentrations of acids such as TFA results in spectra that are indistinguishable and an individual cell populations phenotype is lost.[242] These harsh lysis conditions likely result in the exposure of cellular components that are very abundant in most cell types, such as actin or histones, which in turn dominate the spectra and supress signals that may discriminate phenotypes. A freeze/thaw step was evaluated as a mild lysis step at two stages of the sample preparation workflow and there was no significant difference in ionisation or number of features identified. This was important to establish as it could be possible that distinguishing features of cell phenotype may be lost by washing of permeabilised cells. However, these data show that there is no loss of characteristic biomolecules and can therefore be used interchangeably depending on the specific application. For example, it is particularly important to preserve cell populations where transient and subtle phenotypes may be lost during sample preparation. Therefore, in some cases snap freezing immediately may be important to preserve a particularly dynamic phenotype.

Inclusion of an extraction step or solvent wash has been described for bacterial biotyping as well as analysis of lipids isolated from mammalian cells. However, for acquisition in the protein/peptide region for our analyses extraction was not suitable. For example, chloroform-methanol precipitation from cellular samples resulted in a large protein pellet, but subsequent mass spectrometry analysis resulted in little to no information in the mass region of interest. Therefore, I took inspiration from cellular fixing techniques to test whether this would preserve a cellular phenotype and extract some metabolites and/or lipids to reduce the complexity of the sample and improve MALDI-TOF-MS signal. Fixing with PFA resulted in significantly lower signal intensity compared to PBS washes, which is not necessarily surprising as there is some controversy about its use in MALDI imaging studies.[252] However, evaluation of cellular phenotype and technical reproducibility showed that methanol fixation was a comparable sample preparation alternative to PBS washing if not superior in some respects.

Finally, I evaluated the three most common matrices for protein and peptide analysis for whole mammalian cell analysis as the origin of the biomolecules being ionised is often unknown. As hypothesised, the choice of matrix had a significant influence on the resulting mass spectrum. Each matrix generated a different spectral fingerprint with unique peaks for each of the four cell lines that could be separated by distinct PCA clustering. Samples spotted with DHB showed the most heterogeneity, where in some cases such as MCF7 multivariate analysis distances between technical replicates were too wide to enable efficient grouping. This is somewhat expected as DHB crystallises into long, needle-like structures that produce a heterogeneous surface that causes significant spot to spot variation. As well as this, there was a matrix dependent effect with respect to increasing laser power and concentration. Each matrix performed optimally at a saturated concentration, however CHCA was

able to yield much more informative spectra and identified more features at a third of the concentration of DHB and SA. This was also the case with increasing laser power, where a two-fold lower minimum laser input was required to reach the same number of features with versus DHB. This observation was somewhat expected for detecting ions by UV MALDI-TOF-MS as it has been shown by the performance of a matrix is dependent on its optical absorbance coefficient (α).[253] Allwood *et al.* demonstrated that CHCA has a particularly high α in the UV wavelength region of 300-400 nm compared to DHB and SA.[253] These results have since been elaborated where a quantitative solid state study of matrices including CHCA and DHB further highlight the discrepancies in the optical absorption and optical cross section of different matrices with respect to variable laser fluences and wavelength.[254] Here, CHCA was also shown to have a significantly greater optical absorbance and cross section compared with DHB in their chosen UV absorbance range (200-500 nm). As the RapifleX employs an Nd:YAG laser that operates at a 355 nm wavelength, the matrix optical properties likely explain the discrepancies I observed with the minimum laser energy requirements of CHCA, DHB and SA. Taken together, this indicates that the features observed in the mass spectra are likely to be peptidic or small proteins, as they ionise more efficiently with either CHCA or SA. However, it is important that for masses greater than >10,000 Da, peak resolution is significantly improved by using SA and therefore may have a role to play in studies that identify significant features in this mass range.

Compatibility of the workflow for screening was validated with current liquid handling robots and performance of a mock-assay MALDI target with all three matrices. This data confirmed the previous observations that CHCA is most suitable for screening as it enabled acquisition of robust and intense mass spectra that were highly reproducible.

4.4.2 Differentiating embryonic stem cell phenotypes by MALDI-TOF-MS

This method has shown to be successful for phenotypic profiling of diverse cell lines, however it was necessary to assess its potential for distinguishing subtle phenotypes. Therefore, the optimised sample preparation was used to phenotype the naïve and pluripotent stages of differentiation of mESCs. The transition from naïve to differentiated is tightly controlled by removal of kinase inhibitors from the naïve culture and Anna Segarra-Fas provided validation data for the two cellular phenotypes with a standard qPCR approach. Using MALDI-TOF-MS, over 100 features were identified for both cell states and after filtering for reproducibility 66 were utilised for phenotyping. Interestingly, from multivariate analysis the loading plot indicates that most of the loading values lie closer to the 2i release grouping, thus indicating a noticeable shift from the naïve state to the pluripotent. Furthermore, a number of features were identified that significantly influence the separation of these two stem cell populations that was then validated by independent statistical analysis. Consequently, this demonstrates the suitability of MALDI-TOF-MS for studying subtle phenotypes that is highly consistent with genomic analysis.

Ultimately the work presented in this chapter describes a systematic study that explores initial sample handling, matrix choice and suitability of methanol fixing with whole cell MALDI-TOF-MS analysis. All three steps were found to have a profound impact on the resulting mass spectra and were evaluated by not only spectral quality and observable changes but also technical performance over replicate spots. This has resulted in a technically robust and reproducible workflow that is suitable for liquid handling with commercially available automated systems. This is due to the inclusion of mild lysis and extraction or fixing steps that ensures a non-viscous sample solution which is suitable for pipetting small volumes and is compatible with multiple matrices.

For application to high throughput screening assay, the assay could be miniaturised as automated centrifuges and cell culture systems could be used as only a small number of cells are required. However, the inclusion of the freeze/thaw step could prove problematic for automated studies as this is not routinely employed in a high throughput workflow and would require specialised input.

This method has multiple potential applications for biological studies and determining cell phenotype. For example, qualifying cell line validity is incredibly important as it has been shown previously that there has been use of misidentified or cross contaminated cell lines across multiple institutes that could compromise biological studies.[255] Typically, this analysis is performed by genome sequencing and is time consuming and expensive, therefore MALDI-TOF-MS analysis could be a viable alternative for qualifying cell phenotype against a validated spectral fingerprint. Furthermore, as this method is sensitive to transient phenotypic shifts there could be application to monitoring cell viability over multiple passages to ensure that studies are performed with cells of the same phenotype. As well as this, the basic premise of this method could prove versatile for future applications to lipids or metabolites for a specific cellular phenotype which could then be extended to MALDI imaging studies to identify cells in tissue. Taken as a whole, this novel sample preparation method is more sensitive to cell number than previously described methods and that enables robust, reproducible and rapid profiling of mammalian cells and is suitable for a wide range of biological applications.

Chapter 5. A cell-based MALDI-TOF-MS assay for identifying inhibitors of inflammation

5.1 Introduction

Cell-based assays make up one of the corner stones of drug discovery and have long been used throughout the development pipeline to characterise compounds.[256,257] Cellular assays have been shown to be more reliable at predicting *in-vivo* effects of compounds over biochemical assays at early stage drug discovery as the small molecule inhibitors often exhibit different activity in a cellular context.[258] Further to this, recent studies have been able to distinguish small molecule target interaction and differentiate between agonists, antagonists and allosteric inhibitors.[259–261] This information was previously limited to biochemical reactions that can deduce a compound's regulatory action through kinetic measurement of protein-compound interactions. A strength of cellular assays is that they provide more biologically relevant information on a cell's overall physiology and state. The most common readouts are compound toxicity, cell morphology, cell surface marker expression, proliferation and gene transcription. One of the appealing qualities of these types of assays for pharmaceutical industries is that more than one of these readouts can be acquired in a single cellular screen, such as cell viability and protein activity.[262] This simultaneous acquisition of information is known as multiplexing and is desirable in cellular assays as it significantly increases the efficiency of compound library screening.

Most cellular assays utilise either second messenger, reporter genes or proliferation/cytotoxicity assays as readouts for cell state and characterising drug characteristics.[258] However, there are significant pitfalls with these approaches as

frequently assay readouts are based on downstream effects of initial signal-transduction and the target protein. This is as often the case with reporter gene expression, as mRNA levels do not always correlate linearly with protein expression levels, and vice versa.[263] Methods for quantifying cellular activity are numerous, with the majority either exploiting mechanical and physical properties of cells, quantifying bioluminescence or integrating a fluorescent probe at a region of interest. For example, luciferase activity and subsequent bioluminescence is a common biosensor readout for secondary messenger assays,[264] whereas incorporation of fluorescent probes like GFP are popular for cellular FRET assays that assess protein-protein interactions.[265] Despite success in the HTS field, these reporter-based assays can be prone to formation of artefacts, non-native protein interactions and activity due to genetic engineering, which in turn compromises cell physiology.[256] Consequently, there is a growing desire for label-free cellular assays. However, despite these approaches showing potential they yet lack specificity and require further exploration before being implemented in drug discovery workflows.[266]

Inflammation is a core host response that is typically triggered by invading pathogens or endogenous host signals arising from cell damage or pathology that activates the innate immune response. This has led various new avenues of drug research, such as combined therapies targeting both unregulated host inflammation and tumour growth[267] and potent suppressors of dysregulated inflammation in sepsis.[268]. Cellular assays for identifying inhibitors of inflammation have been reported[269–271], but are yet to rise to the forefront of drug discovery. This could be due to the complexity of the specific signalling pathways and mechanisms that drive a pro-inflammatory phenotype. New connections and molecular cross talk between inflammation and existing diseases such as cancer, diabetes and autoimmune diseases are on the rise, thus making assay design complicated for even conventional cellular assays. Despite

the complexity of inflammatory signalling, the overall pro-inflammatory phenotype of macrophages is well described and could be used to assay the anti-inflammatory potential of compound collections. This concept would allow the development of a label-free cellular based assay that does not measure a specific drug-target engagement, but rather measures a cellular phenotype. This could be performed in response to drugs and various pro-inflammatory stimuli and could be complimentary to well established biochemical assays.[178]

Monocytes and macrophages are key players in the innate immune response and often form the first line of defence against invading pathogens. These myeloid cells are highly plastic and their function is closely related to their tissue localisation and surroundings that can induce an active pro-inflammatory phenotype and are therefore very attractive candidates for cellular assays.[167,272] Pathogen-associated molecular patterns (PAMPs) such as bacterial ligands and viral DNA can be sensed by membrane receptors such as Toll-like Receptors (TLRs) and initiate the production of pro-inflammatory cytokines such as TNF-α, IL-6, IL-1, IL-12 and type one interferons.[151] Tumour necrosis factor alpha (TNF-α) is a particularly potent cytokine primarily secreted during acute phase inflammation and is considered a central player in pro-inflammatory signalling.[273] Its primary role is to regulate immune cells through TNFR1 and TNFR2 signalling that induces a variety of cell responses ranging from proliferation, differentiation, pro-inflammatory activation and apoptosis or necrosis [274]. Despite being key for maintaining normal homeostatic mechanisms in the face of pathogenic invasion, acute or sustained overexpression of TNF-α can lead to significant dysregulation of the host immune response.[275] Acute TNF-α secretion has now been closely linked to fatal septic shock, as well as one of the principal causes of the pathogenesis observed in autoimmune diseases such as Crohn's disease, inflammatory bowel disease (IBD) and rheumatoid arthritis.[276–278] Several successful

treatments have been developed such as antibody based therapies[279,280], however the discovery and design of new small molecule compounds for inhibiting cellular TNF-α secretion or an inflammatory phenotype are typically limited by the high throughput methods currently available. Therefore, there is a growing need in the field of suppressing dangerous levels of inflammation to develop assays that can be high throughput and accelerate the discovery of inhibitors that tackle acute TNF-a secretion and pathogenesis.[281,282]

5.2 Aims

In this thesis thus far, I have demonstrated how MALDI-TOF-MS can be utilised for screening for anti-inflammatory compounds and cellular phenotypes. Therefore, in this study I combined these two concepts to develop a MALDI-TOF-MS assay that can quantify a pro-inflammatory phenotype and is capable of screening for anti-inflammatory compounds. Finally, I validated this assay by ELISA quantification of TNF-α secretion where the data showed striking similarities and correlation to the MALDI-TOF-MS assay.

5.2.1 Sub-chapters

1. Quantifying and determining specificity of a pro-inflammatory THP-1 phenotype by MALDI-TOF-MS.

2. Reversing the pro-inflammatory phenotype with known inhibitors.

3. Identifying inhibitors of inflammation with a 78 compound screen against LPS treated THP-1 monocytes.

5.3 Results

5.3.1 Quantifying and determining specificity of a pro-inflammatory phenotype by MALDI-TOF-MS.

My first aim of this study was to determine whether it was possible to distinguish a pro-inflammatory phenotype in THP-1 monocytes by whole cell MALDI-TOF-MS. For the initial assay, I proceeded by stimulation of THP-1 monocytes with lipopolysaccharide (LPS) derived from Salmonella. After 24 hrs of incubation with 1 µg/mL of LPS, cells were then processed in following with an adapted method from Chapter 4 (2.2.3.4) that is described in detail in Chapter 2: 2.2.3.5. (Figure 5-1).

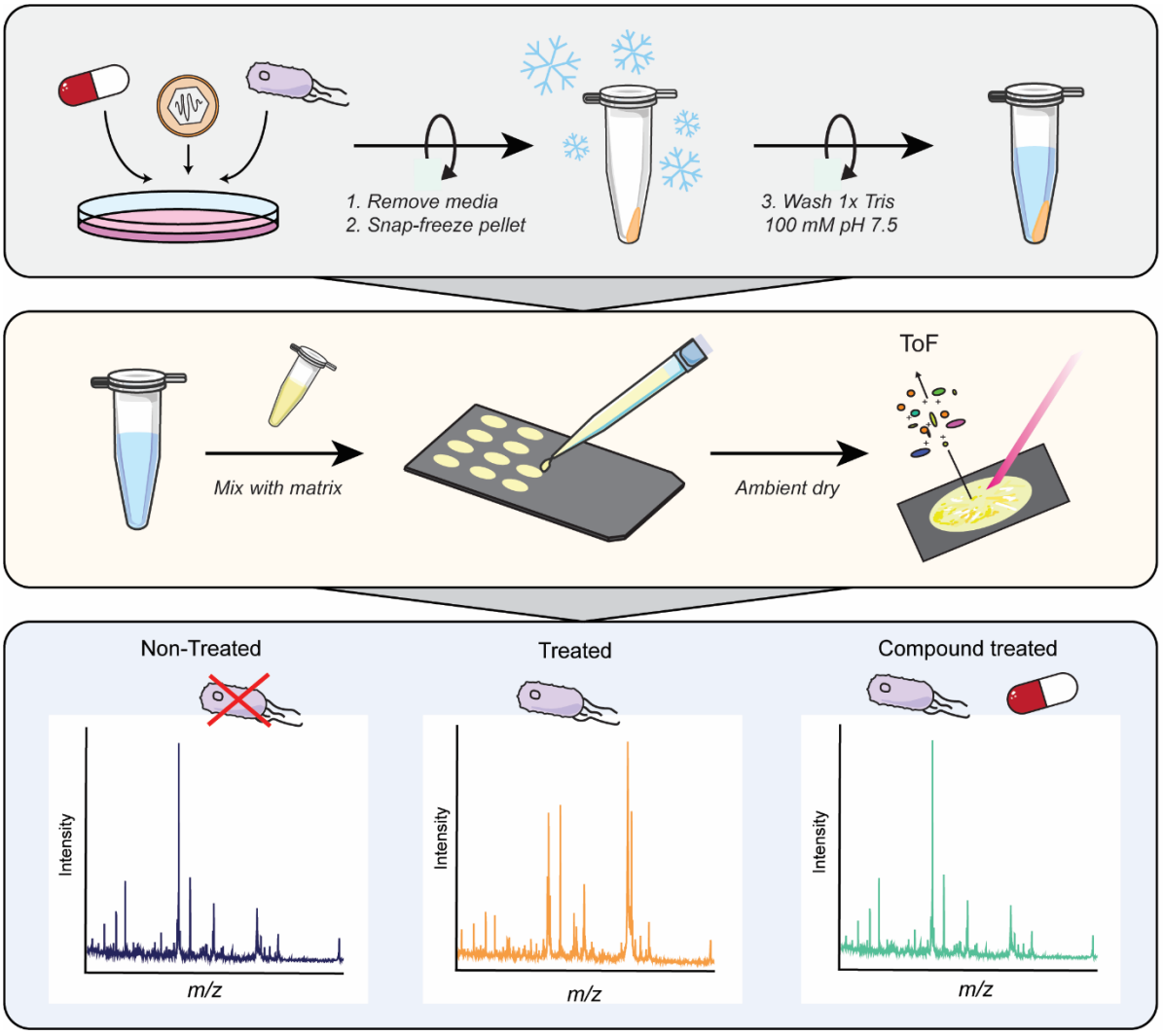

Figure 5-1. Workflow of whole cell MALDI-TOF-MS sample preparation of THP-1 monocytes. *Distinguishing a pro-inflammatory phenotype from resting or inhibitor treated cells (2.2.3.5).*

In brief, LPS-treated or untreated THP1 cells were harvested by scraping, pelleted and then snap frozen to perturbate the cell membrane and stored at -80°C until required for analysis. Thawed pellets were then washed once in an aqueous Tris buffer at 4°C to remove residual contaminants and background signals before resuspension in Tris buffer at a final concentration of 5000 cells/µL. 2500 cells were spotted on target with α-cyano-4-hydroxycinnamic acid (CHCA) matrix in either sandwich or dried droplet method onto a 384 or 1536 AnchorChip target depending on manual or automated analysis respectively. This workflow (Figure 5-1) enabled disruption of the cellular membrane and release of intracellular biomolecules for greater feature detection without full cell lysis that can result in release of DNA and a viscous sample solution that is problematic when handling small sample volumes. Spots were then analysed by MALDI-TOF-MS in positive ion linear mode in the *m/z* range 2000 – 20000 and data was acquired at approximately 2 seconds per spot and acquiring 10,000 laser shots per spot with typical spectra for untreated and LPS treated monocytes shown in Figure 5-2.A. From initial inspection of individual spectra, I observed differences in peak intensity between the two conditions and when the biological and technical replicates were combined in a relative peak intensity heatmap, it was possible to visualise and distinguish intensity-based differences between the two phenotypes. Both the untreated and LPS treated conditions separated into two distinct populations across three biological replicates. There was some difference from LPS1 to 2 and 3, but the trends in protein intensity remained similar. Furthermore, the reproducibility between technical replicates was very good, thus demonstrating that the sample preparation method is robust and reproducible.

From this data set I identified three features at *m/z* 4632, 4964 and 6891 that altered significantly in their abundance between untreated and LPS treated (Figure 5-2.C).

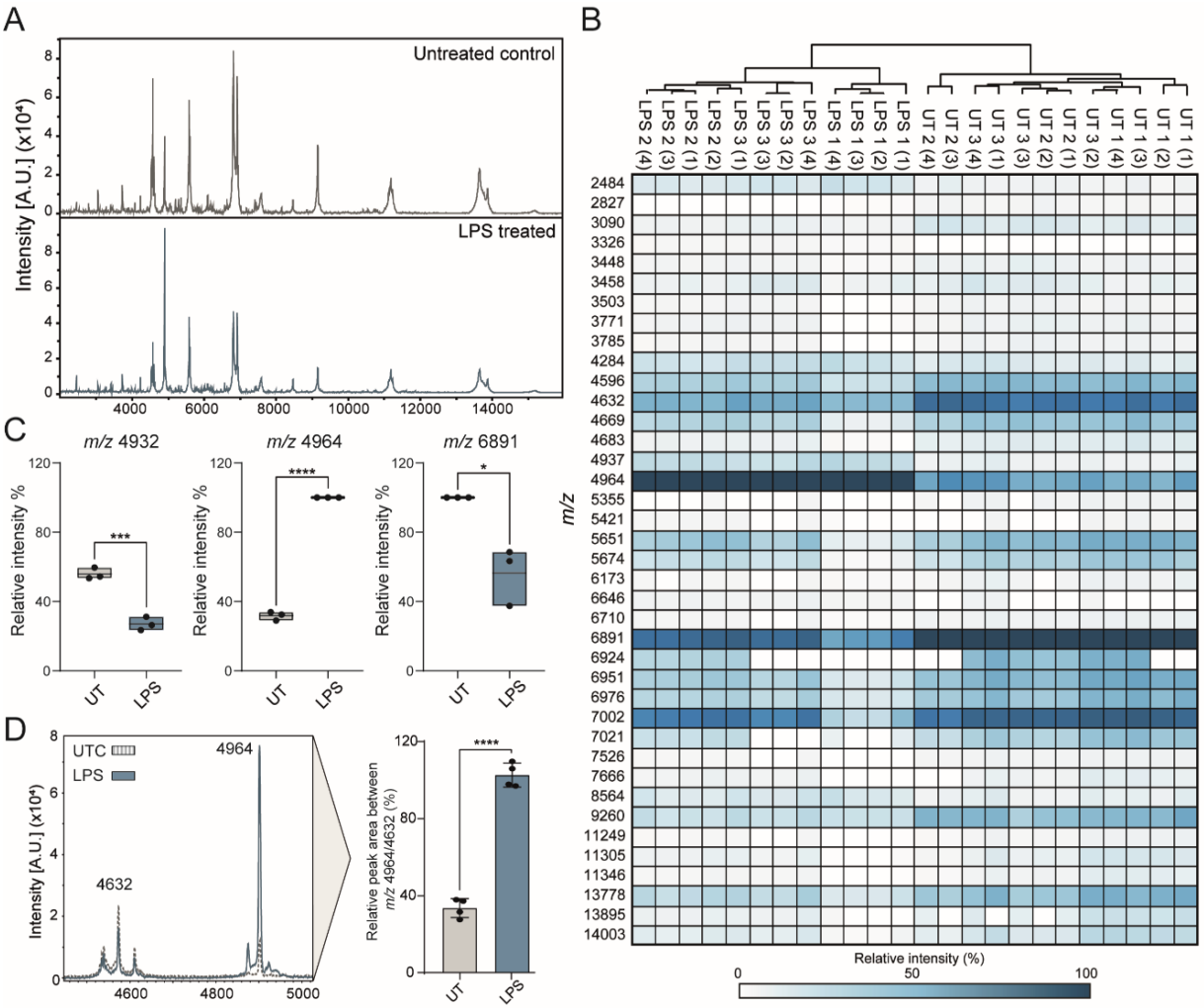

Figure 5-2. Analysis of pro-inflammatory stimulated and resting THP-1 monocytes by MALDI-TOF-MS. *(A) Representative spectra of untreated controls (UT) and LPS treated THP-1 monocytes. (B) Relative intensity heat map of three biological and four technical replicates of untreated and LPS treated monocytes showing significant separation of the two phenotypes. (C) Box plots of significantly changing intensities between untreated and LPS-treated monocytes identified at m/z 4632, 4964 and 6891. (D) Representative spectra of untreated and LPS-treated monocytes in the m/z range 4500 - 5000 and relative quantitation between the two features normalised to LPS treated conditions. Error bars represent standard deviation of 3 biological replicates that were each mean averaged from three technical replicates. *, *** and **** represent p<0.05, p<0.001 and p<0.0001, respectively, student's t-test.*

The relative intensity of these features alone was enough to distinguish resting and pro-inflammatory monocytes, but I aimed to develop an intra-spectral method to quantitatively measure the pro-inflammatory response to avoid any spot-to-spot or shot-to shot variation. I therefore sought to combine the intensity change in the two significant features at *m/z* 4964 and 4632 as biomarkers of the two phenotypes. Both these features were identified in all spectra, and their signal-to-noise and resolution was above the 75% percentile, thus they were robust features for classifying the two phenotypes. I chose to develop a ratiometric quantification approach using the two peak areas that was then normalised to the positive control as a read out as described in the equation below (Figure 5-2.D). Using this method, the phenotypic shift could be measured robustly when applied to LPS and untreated cells and it was possible to quantify a phenotypic shift in the assay with a significant p-value <0.0001. This method of intra-spectra quantification was robust over ten cell passages, where I was able to quantify the pro-inflammatory MALDI-TOF-MS response with a Z' >0.5 and a p-value <0.001.

$$Relative\ peak\ area\ \% = \left(\left(\frac{Peak\ area\ m/z\ 4964}{Peak\ area\ m/z\ 4632}\right) \Big/ \left(LPS\ \frac{(Peak\ area\ m/z\ 4964)}{(Peak\ area\ m/z\ 4632)}\right)\right) \times 100$$

To determine assay specificity and further understand the biology underpinning the pro-inflammatory response I tested a variety of different pro-inflammatory stimuli that cover a broad range of pro-inflammatory signalling receptors such as TLRs and interferon receptors (Figure 5-3). Each of these stimuli are derived from either pathogens or are host secreted cytokines that induce a pro-inflammatory response.

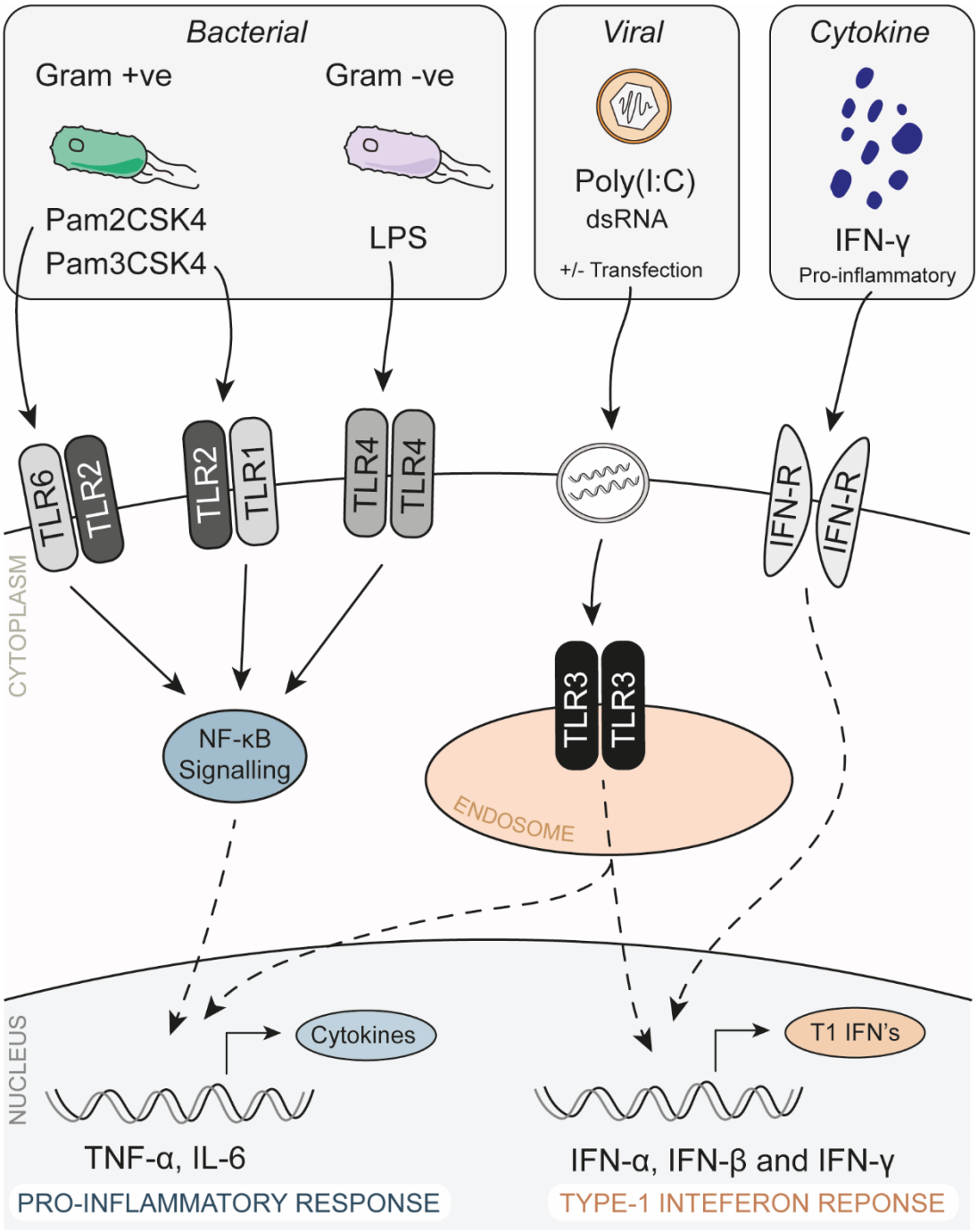

Figure 5-3. Determining MALDI-TOF-MS assay stimuli specificity. *The five stimuli used to treat THP-1 monocytes and their relative receptor proteins that initiate either the pro-inflammatory or type-1 interferon response.*

THP-1 monocytes were therefore incubated with the stimuli to yield six different experimental conditions: Pam2CSK4, Pam3CSK4, LPS, interferon gamma (IFN-γ) and the viral ligand Poly(I:C) with and without prior incubation of the dsRNA with the transfection reagent Fugene to form artificial liposomes that can cross the plasma

membrane (Figure 5-3). From initial spectral analysis Pam2CSK4 and Pam3CSK4 were more similar in peak intensity distribution to LPS treated monocytes over the untreated condition (Figure 5-4.A). Conversely, IFN-γ treatment resulted in spectra that more closely resembled untreated monocytes (Figure 5-4.A). Surprisingly, Poly(I:C) did not result in a pro-inflammatory phenotype by MALDI-TOF-MS with or without transfection, which was unexpected as it is reported to initiate both signalling pathways once it has crossed the plasma membrane (Figure 5-3). Visualisation of the data by a relative intensity heat map (Figure 5-4.B) and Euclidian clustering enabled clear separation of the bacterial ligand treated samples and the IFN-γ and untreated conditions within the column dendrogram over three biological repeats. Taken together, this data infers that the measured MALDI-TOF-MS response is due to specific engagement and activation of plasma membrane TLRs, which in this case was achieved by using different bacterial ligands.

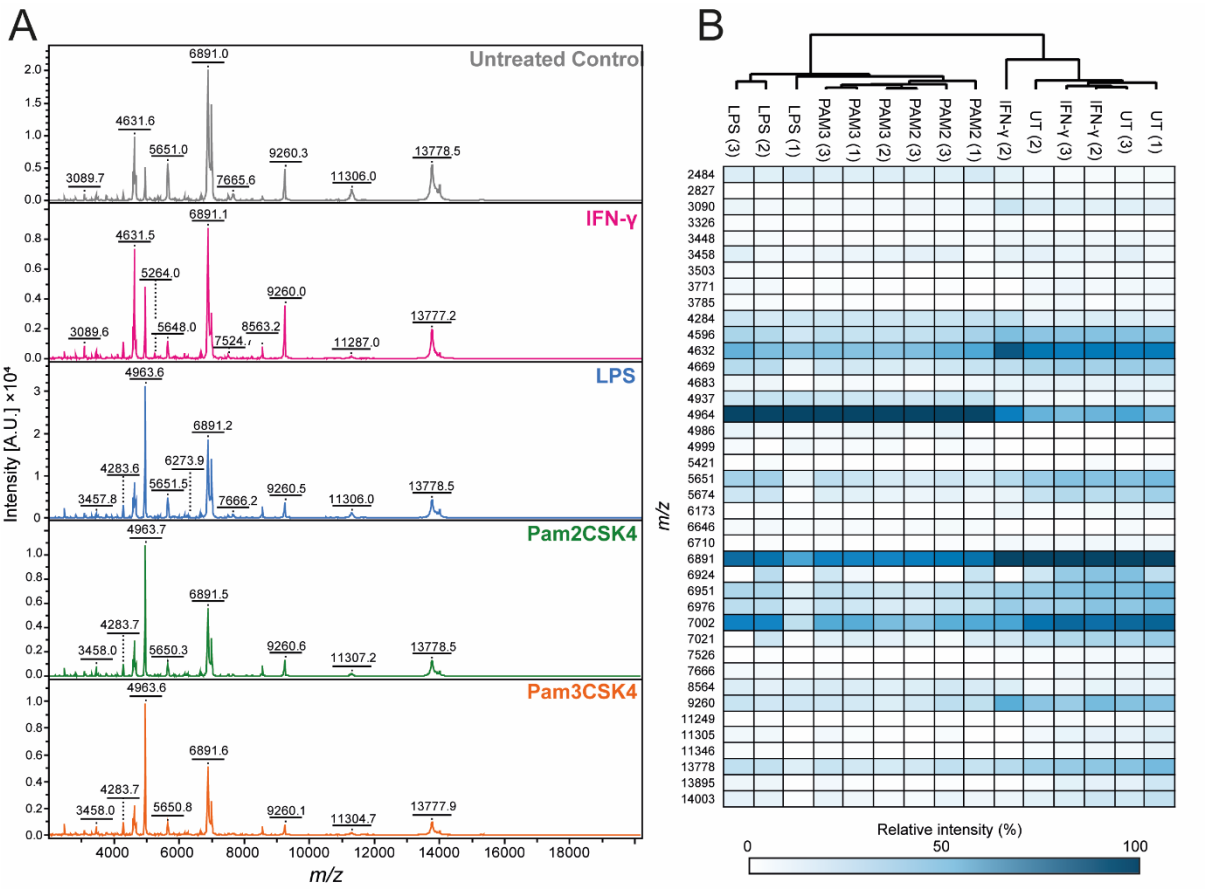

Figure 5-4. MALDI-TOF-MS assay phenotype is induced by bacterial ligand stimulation. *(A) Representative MALDI-TOF-MS spectra of untreated (UT) and IFN-γ, LPS, Pam2CSK4, Pam3CSK4 treated THP-1 monocytes. (B) Relative intensity heatmap of three biological replicates of LPS, IFN-γ, Pam2CSK4 and Pam3CSK4 treated THP-1 monocytes showing significant separation of bacterial ligand treated monocytes compared to IFN-γ and untreated monocytes. Each biological replicate is a mean averaged value of three technical replicates.*

Using the equation described previously, the relative peak area of *m/z* 4632/4964 enabled quantitation of the pro-inflammatory response for each stimulus condition. Here, LPS appears to be a more potent instigator of the pro-inflammatory response over Pam2CSK4 and Pam3CSK4, who generated a readout of 75% and 80% respectively compared with 100% for LPS. Both IFN-γ and Poly(I:C) conditions were not significant, apart from prior incubation of dsRNA with Fugene that resulted in a

lower quantification than the untreated control. These trends were reflected in a dose-dependent manner for the bacterial ligands and IFN-γ (Figure 5-5.D) with a concentration of 1 µg/mL being optimal.

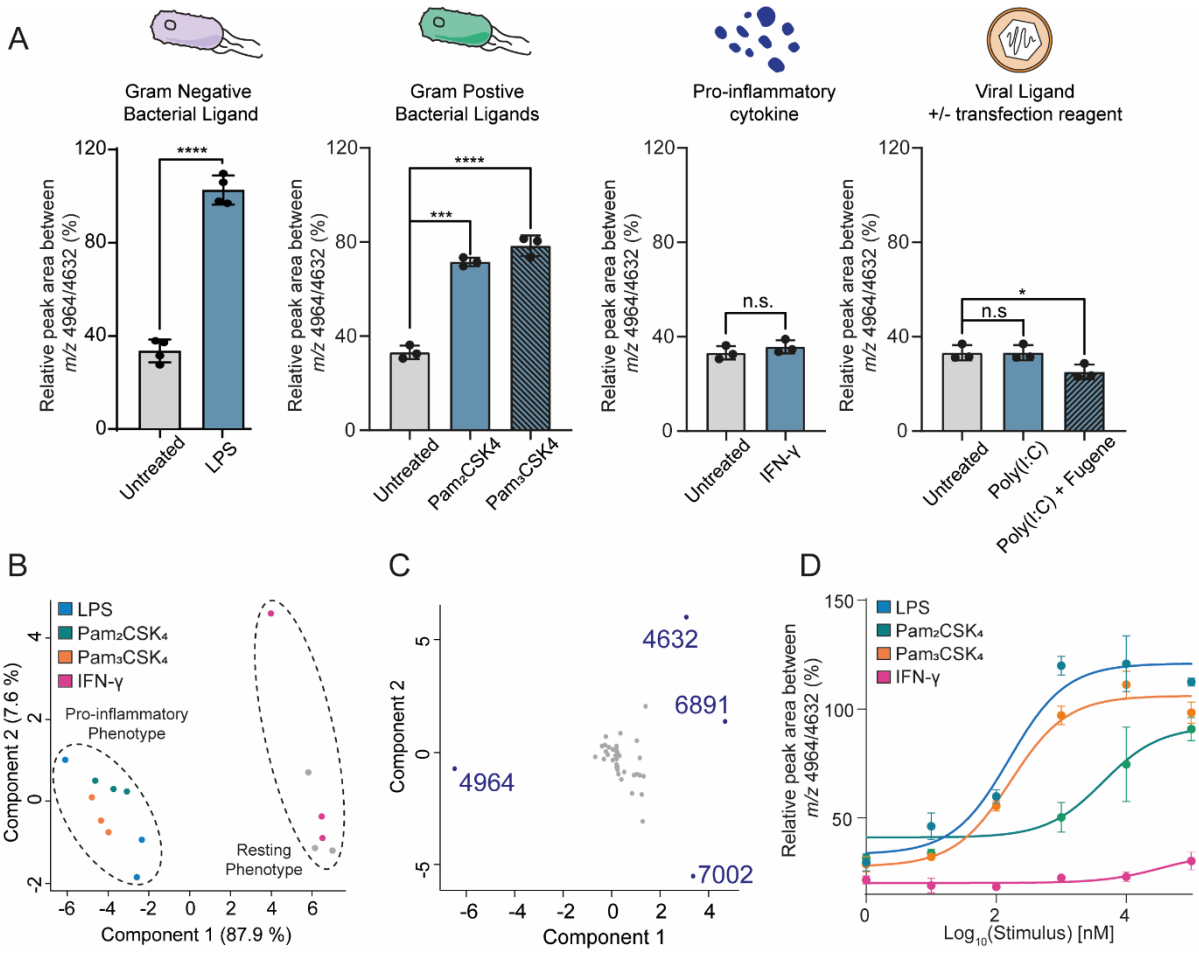

Figure 5-5. Quantifying the pro-inflammatory phenotype by MALDI-TOF-MS in response to the five stimuli. *(A) Relative quantitation of peak areas (4964/4632) of LPS, Pam2CSK3, Pam2CSK4, IFN-γ and Poly(I:C) ± Fugene treated macrophages compared to untreated THP-1 monocytes normalised to LPS positive control. (B) PCA plot of LPS, Pam2CSK4, Pam3CSK4 and IFN-γ treated THP-1 monocytes showing distinctly grouping of bacterial ligand-treated cells and resting/IFN-γ treated monocytes. (C) Loadings plot derived from PCA plot (B) showing that m/z 4964, 4632, 6891 and 7002 contribute the most to the separation of the two clusters in PC1 and PC2. (D) Titration of LPS, Pam2CSK4, Pam3CSK4 and IFN-γ treated monocytes from 10 µg – 100 pg/mL of stimulus. Error bars represent standard deviation of 3 biological replicates that were each mean averaged from three technical replicates. n.s, *, ****

*and **** represent non-significant, p<0.05, p<0.001 and p<0.0001, respectively, student's t-test.*

Multivariate analysis generated a 2D PCA plot with two distinct clusters (Figure 5-5.B). This grouped together all of the bacterial ligand data, which in turn localised separately from no treatment and IFN-γ stimulation. Furthermore, the corresponding loadings plot generated in Figure 5-5.C shows that features identified as *m/z* 4964, 4632 6891 and 7002 contribute most to the PCA clustering in both component 1 and component 2.

5.3.2 Reversing the pro-inflammatory phenotype with known inhibitors.

With the established analytical workflow and phenotype specificity I then aimed to use known inhibitors of pro-inflammatory signalling pathways to evaluate the potential of the assay to discriminate positive and negative hits. Initially, I chose three compounds; NG-25[283], BI2536[284] and MRT67303[184], which inhibited the pro-inflammatory response at different stages of inflammatory signalling pathways (Figure 5-6). These compounds cover a broad range of anti-inflammatory targets and inhibit the conventional pro-inflammatory signalling via NF-κB pathway and results in production of tumour necrosis factor alpha (TNF-α), as well as the interferon signalling pathway and secretion of type 1 interferons.

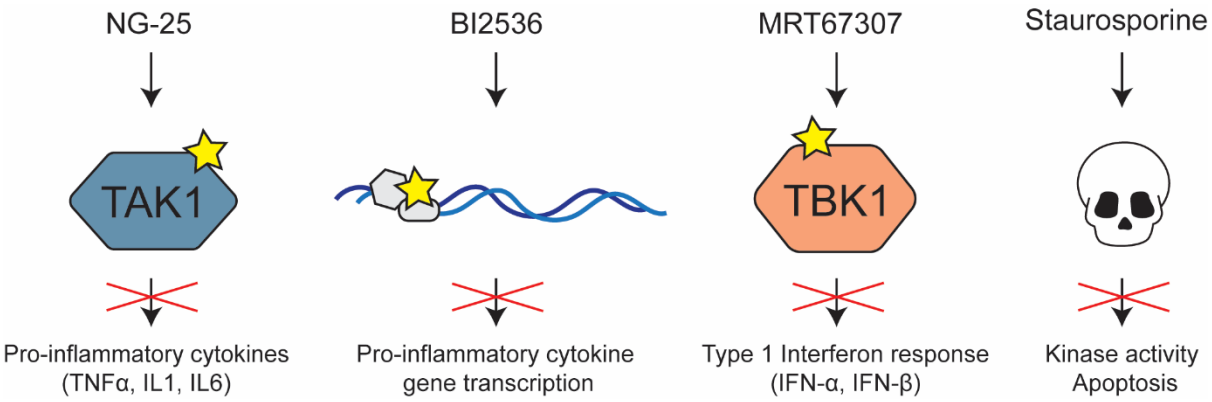

Figure 5-6. Inhibiting the pro-inflammatory phenotype by use of known inhibitors. *Targets of NG-25, BI2536, MRT67307 and staurosporine compounds that inhibit the NF-κB pro-inflammatory signalling pathway, pro-inflammatory gene transcription, type-1 interferon signalling and induce cell death, respectively.*

Compounds were incubated with THP-1 monocytes at 5 μM for one hour to allow equilibration in culture before subsequent addition of LPS for 24 hours. Interestingly, from manual inspection of the spectra (Figure 5-7) it was clear that NG-25 and BI2536 were able to reverse the pro-inflammatory phenotype with spectra resembling that of the untreated control. However, MRT67307 treatment did not reverse the phenotype.

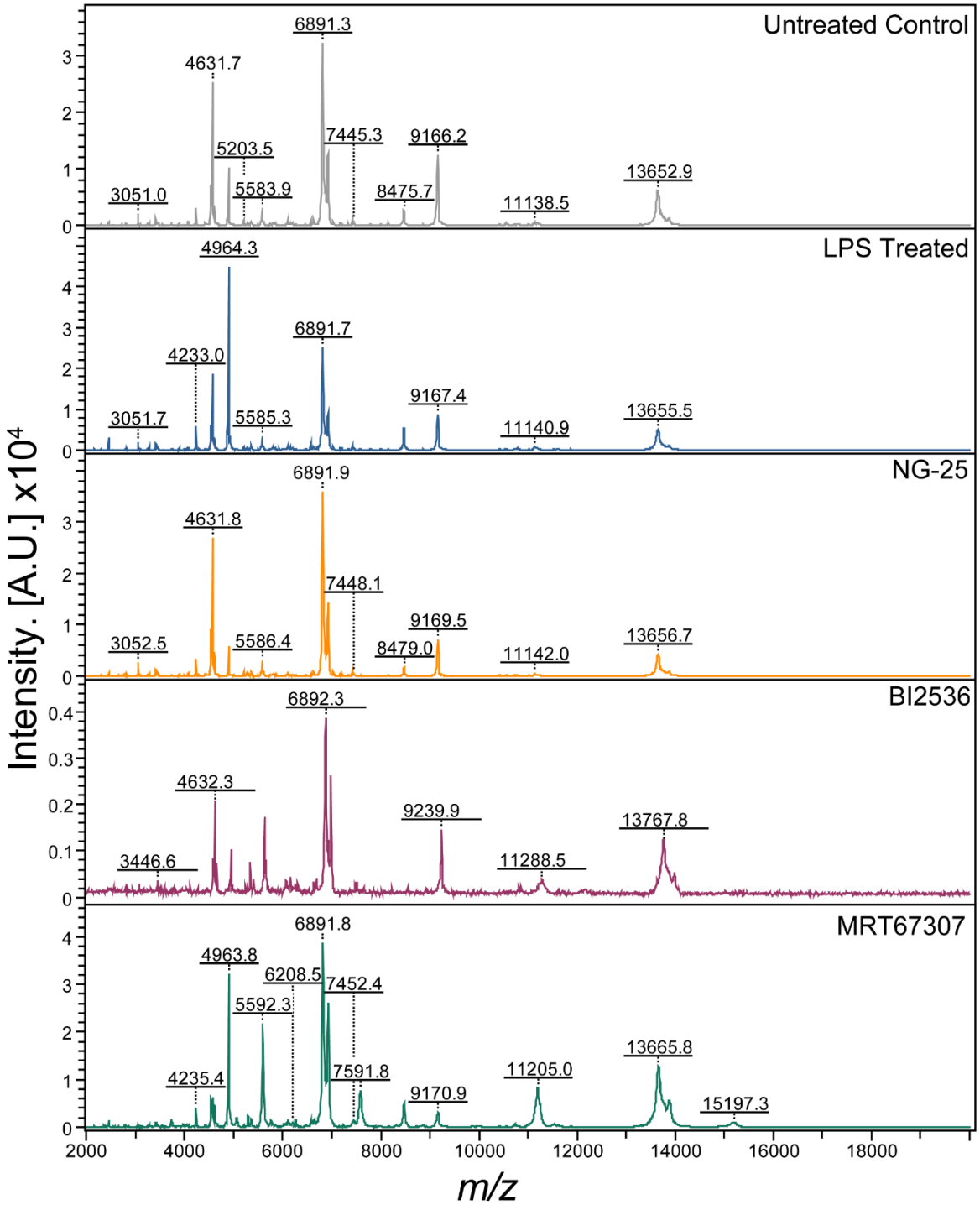

Figure 5-7. MALDI-TOF-MS spectra of positive and negative controls as well as THP-1 monocytes treated with NG-25, BI2536 and MRT67307 prior to LPS treatment.

The specific position of each compound's target proteins within their respective signalling cascades let me identify upstream and downstream inhibitors of the pro-

inflammatory response that were able to reverse the MALDI-TOF-MS phenotype, whereas inhibition of early type 1 interferon signalling had showed no effect (Figure 5-8. A). The inhibitor action was validated by qPCR kindly performed by Joseph Innes (PhD student, Prof. Trost Lab, 2019) and Dr. Anetta Härtlova (Post-doctoral assistant, Prof. Trost Lab, 2018), where all IFN-β transcription was down-regulated with the three inhibitors, but only NG-25 and BI2536 were able to suppress transcription of TNF-α mRNA. The secretion of TNF-α was quantified by ELISA (Figure 5-8.E), which showed statistically significant differences between the compound treatments and control samples that mirrored the MALDI-TOF-MS data (Figure 5-8.D).

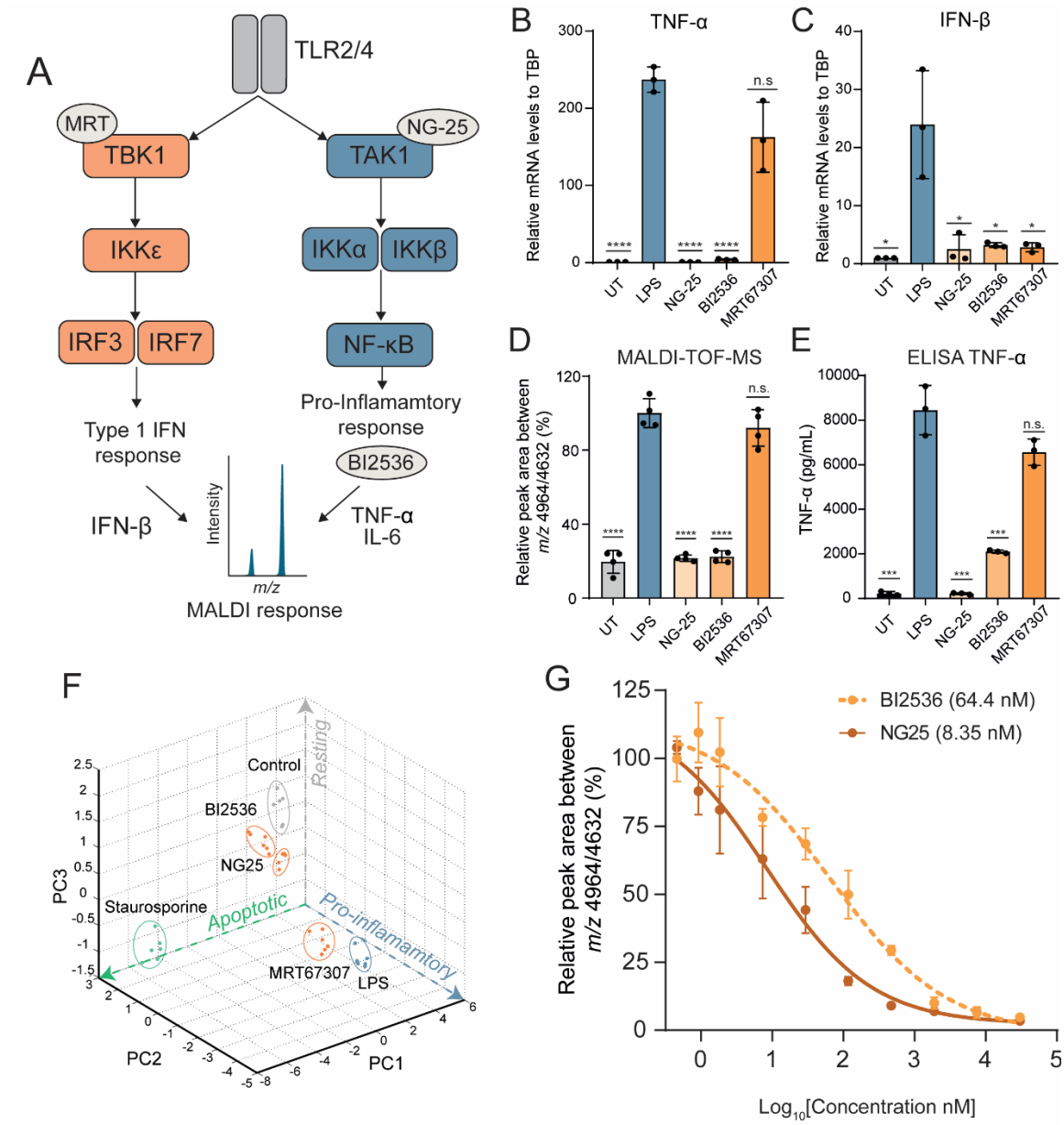

Figure 5-8. Induction of the classical pro-inflammatory signalling a pathway induces the MALDI-TOF-MS pro-inflammatory phenotype. *(A) Signalling pathways inhibited by MRT6307, NG-25 and BI2536. (B) qPCR analysis of known compounds measuring transcription levels of TNF-α mRNA and (C) IFN-β mRNA levels relative to TBP performed by Joseph Innes (PhD student, Prof. Trost Lab, 2019) & Dr. Anetta Härtlova (Post-doctoral assistant, Prof. Trost Lab, 2018). (D) Relative quantitation of untreated, LPS and inhibitor treated THP-1 monocytes derived from MALDI-TOF-MS whole cell spectra. (E) Measurement of TNF-α secretion by ELISA of untreated, LPS and inhibitor treated THP-1 monocytes. (F) 3D PCA plot of untreated, LPS, staurosporine and inhibitor treated monocytes showing separation of resting, apoptotic and pro-inflammatory treated monocytes along the PC1, PC2 and*

*PC3 axis. (G) MALDI-TOF-MS IC_{50} curves of BI2536 and NG-25 treated monocytes. Error bars represent standard deviation of 3 biological replicates that were each mean averaged from three technical replicates. n.s, *, *** and **** represent non-significant, p<0.05, p<0.001 and p<0.0001, respectively, student's t-test.*

Some anti-inflammatory compounds are known to induce mild to severe apoptosis as a side effect[285,286], therefore I sought to discriminate pro-inflammatory and apoptotic monocytes. THP-1 monocytes were incubated with 1 µM staurosporine, a broad kinase inhibitor (Figure 5-6), which induces cell death. Quantification of the MALDI-TOF-MS spectra did not result in a pro-inflammatory phenotype, but instead resembled a false positive hit using the dual biomarker quantification. However, when analysed by 3D PCA apoptotic cells clustered separately to both pro-inflammatory and resting phenotypes (Figure 5-8.F). As well as this, when inhibitor treated conditions were added these also clustered closer to either the positive or negative controls (LPS/untreated) depending on their efficacy, thus validating the previous MALDI-TOF-MS quantification. This 3D PCA plot now effectively allows evaluation of three distinct cell phenotypes; resting, apoptotic and pro-inflammatory along each of the component axes.

Finally, I evaluated the MALDI-TOF-MS method for generating IC_{50} data for both NG-25 and BI2536. Compounds were titrated from 30 – 0.001 µM over 11 concentration points and achieved an excellent four parameter sigmoidal fit of >0.98 for both BI2536 and NG25 (Figure 5-8.G). For BI2536 and NG-25, I obtained IC_{50} values of 64.4 and 8.35 nM, respectively, thus demonstrating the sensitivity of the assay and highlighting the difference in potency of the two inhibitors.

5.3.3 Identifying inhibitors of inflammation with a blind 78 compound screen against LPS treated THP-1 monocytes.

As a proof of concept, a set of 78 potential anti-inflammatory compounds provided by LifeArc were screened blindly with the MALDI-TOF-MS assay. I also included MRT63707 and NG-25 as control compounds. The experiment was performed in technical triplicates over three independent weeks. Compounds were staggered into 8 subsets of 10 compounds, each with positive and negative controls to enable manual handling of the assay. Across the three biological replicates a good Z' score was obtained for all assays (Figure 5-9.A) with an average of 0.8 ± 0.1 across all three screens.

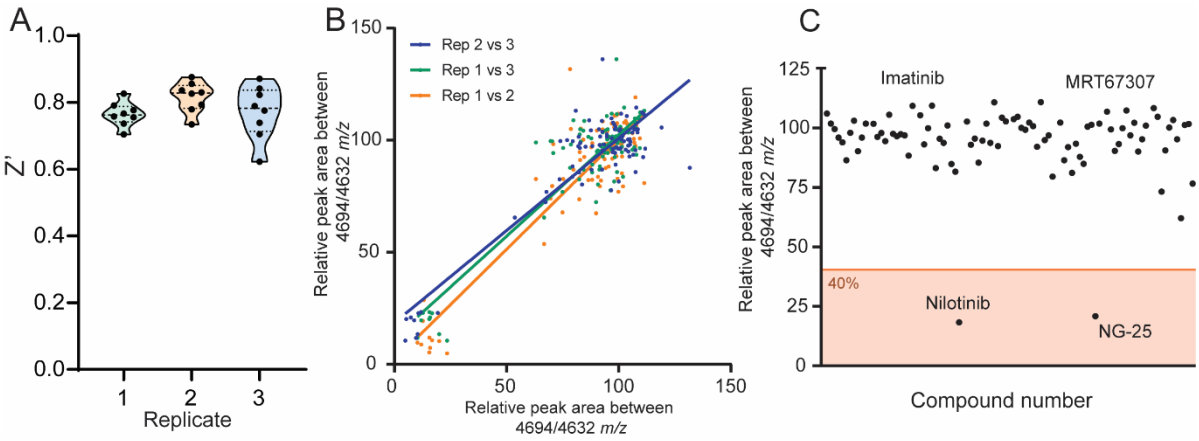

Figure 5-9. Proof of concept 78 compound screen. *(A) Z' scores of biological replicates 1, 2 and 3 from the 78 compound screen across the 8 staggered sets. Violin plot dashed and dotted lines represent the mean average and interquartile ranges respectively. (B) Correlation plots of biological replicates 1, 2 and 3 showing good correlation R^2 > 0.80. (C) Compound hit map of the averaged 3 biological replicates with 40% effectiveness cut off showing Nilotinib and NG-25 as positive hits.*

Good linear correlation between the three technical replicates was obtained for each screen (Figure 5-10) as well as between the biological triplicates with an R^2 >0.8 in all cases (Figure 5-9.B), thus confirming that the assay is robust and conforms to current screening standards to assess assay quality (Z' >0.5).

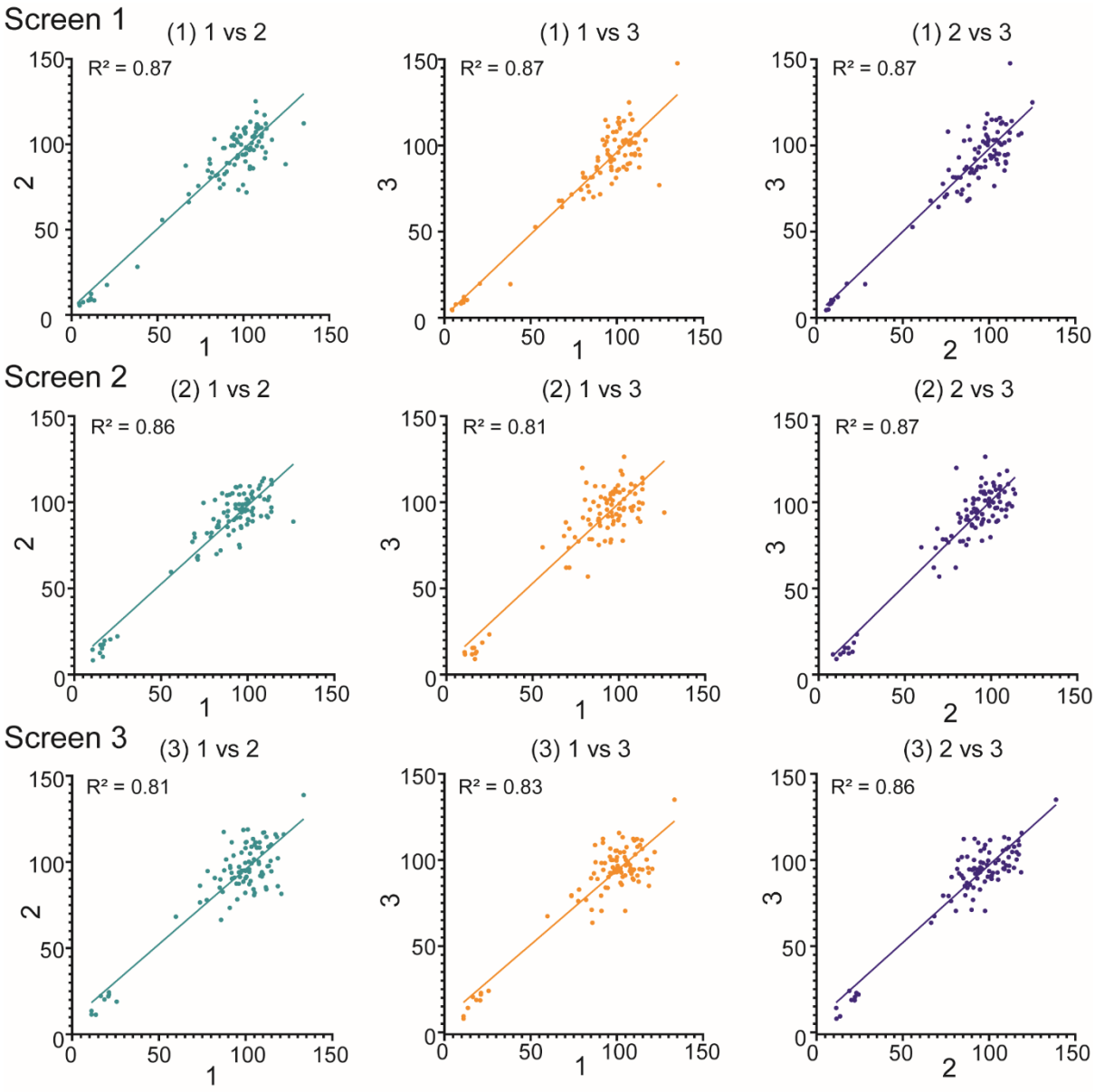

Figure 5-10. Technical reproducibility correlation plots between the three technical replicates from each biological replicate screen showing good correlation of R^2 >0.8

From the mean averaged data of the three screens I applied a percentage effect cut off of 40%, meaning that compounds must reduce the MALDI-TOF-MS quantification by 60% to be considered. From this, the control compound NG-25 was identified as a positive hit, as well as nilotinib, a second generation BCR-ABL inhibitor used in the treatment of chronic myeloid leukaemia (CML) (Figure 5-9.C) [287]. Interestingly, the first generation BCR-ABL inhibitor imatinib was also included in the assay panel, but was not identified as a positive hit. The spectra from each of the three biological

repeats of the screening were very similar (Figure 5-11), thus demonstrating the robustness of the sample preparation method as well as the behaviour of both compounds is reproducible.

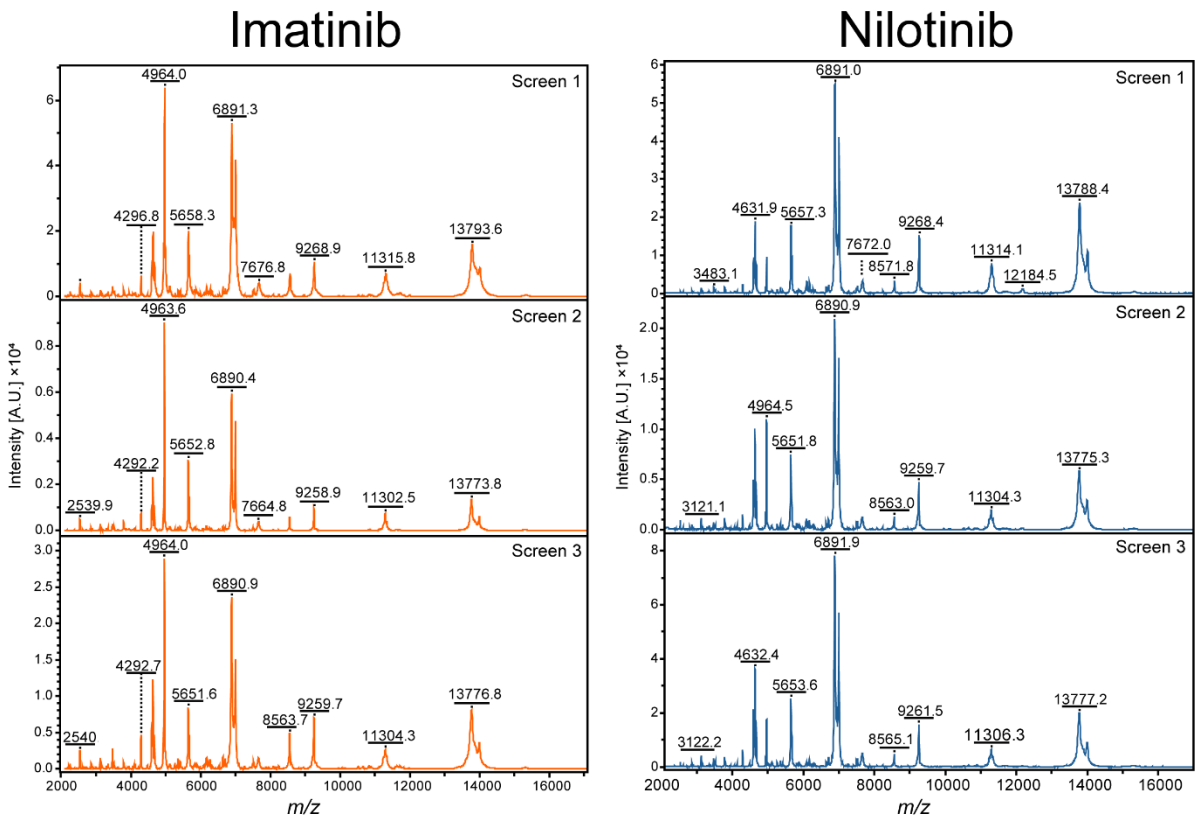

Figure 5-11. A representative spectrum of imatinib and nilotinib treated monocytes from each of biological replicates of the 78 compound screen.

Both compounds share a similar backbone structure (Figure 5-12) and, therefore, I further investigated the pro-inflammatory effect of these two compounds by MALDI-TOF-MS, secretion of the cytokine TNF-α as well as total proteome analysis.

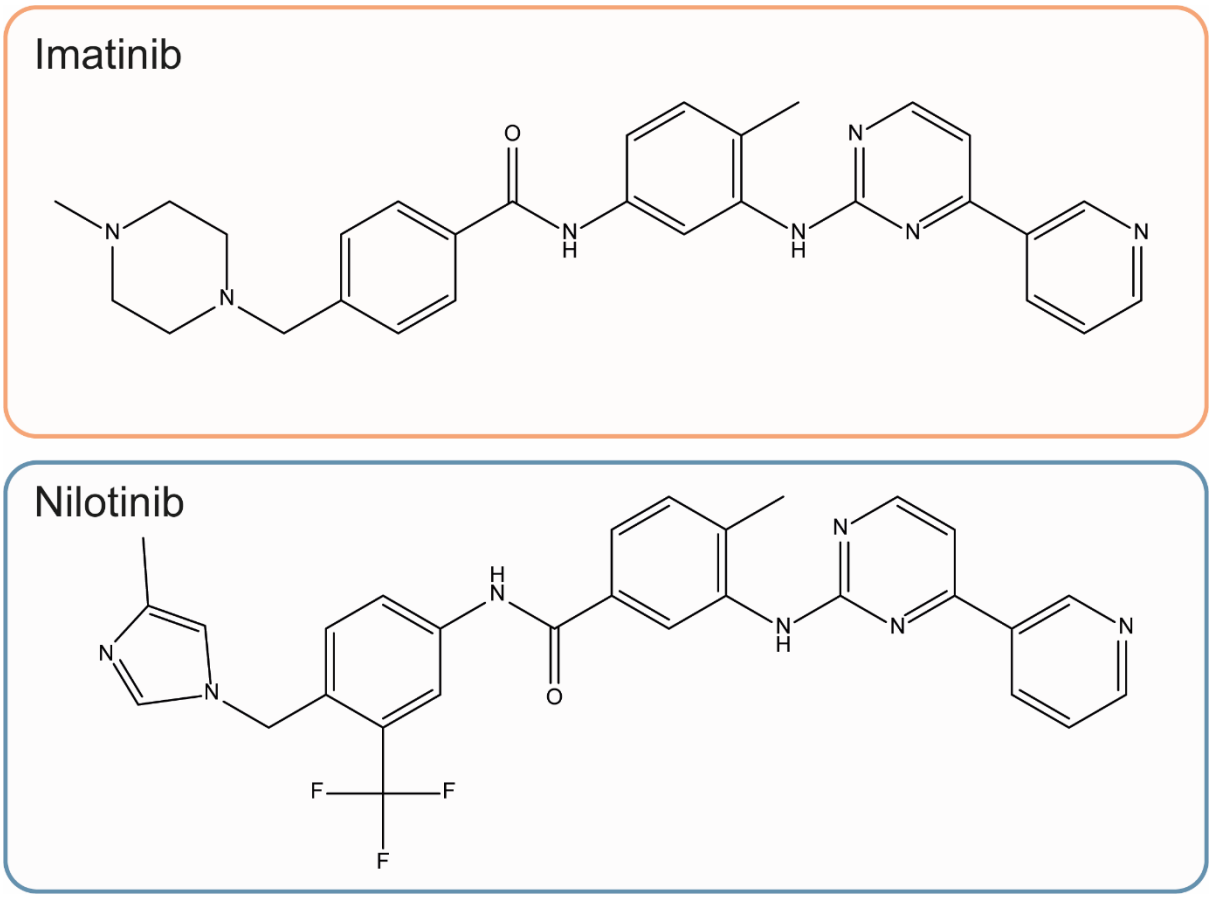

Figure 5-12. Chemical structures of imatinib (orange) and nilotinib (blue).

5.3.4 Validating Nilotinib as an anti-inflammatory compound and exploring its off-target effect

Firstly, qPCR analysis was performed by Joseph Innes and José Luis Marin Rubio to investigate the activity of nilotinib and imatinib on the transcription levels of TNF-α and IFN-β. Similarly to hit compounds NG25 and BI2536, Nilotinib was able to supress the transcription of both cytokines, whereas imatinib did not prevent transcription of TNF- α. Using the ratiometric pro-inflammatory quantitation by MALDI-TOF-MS the activity of nilotinib and imatinib was validated over three biological replicates (Figure 5-13.C) and when compared with the amount of secreted TNF-α the trends were almost identical (Figure 5-13.D). As well as this, IC_{50} curves could be generated for nilotinib using both readouts and a good R^2 of >0.95 was achieved as well as an IC_{50} value of 205.3 and 208.7 nM for MALDI-TOF-MS and TNF-α secretion, respectively. These data demonstrate that both readouts yield almost identical information and that

a nilotinib is a genuine inhibitor of the pro-inflammatory signalling pathway that induces TNF-α secretion with good potency.

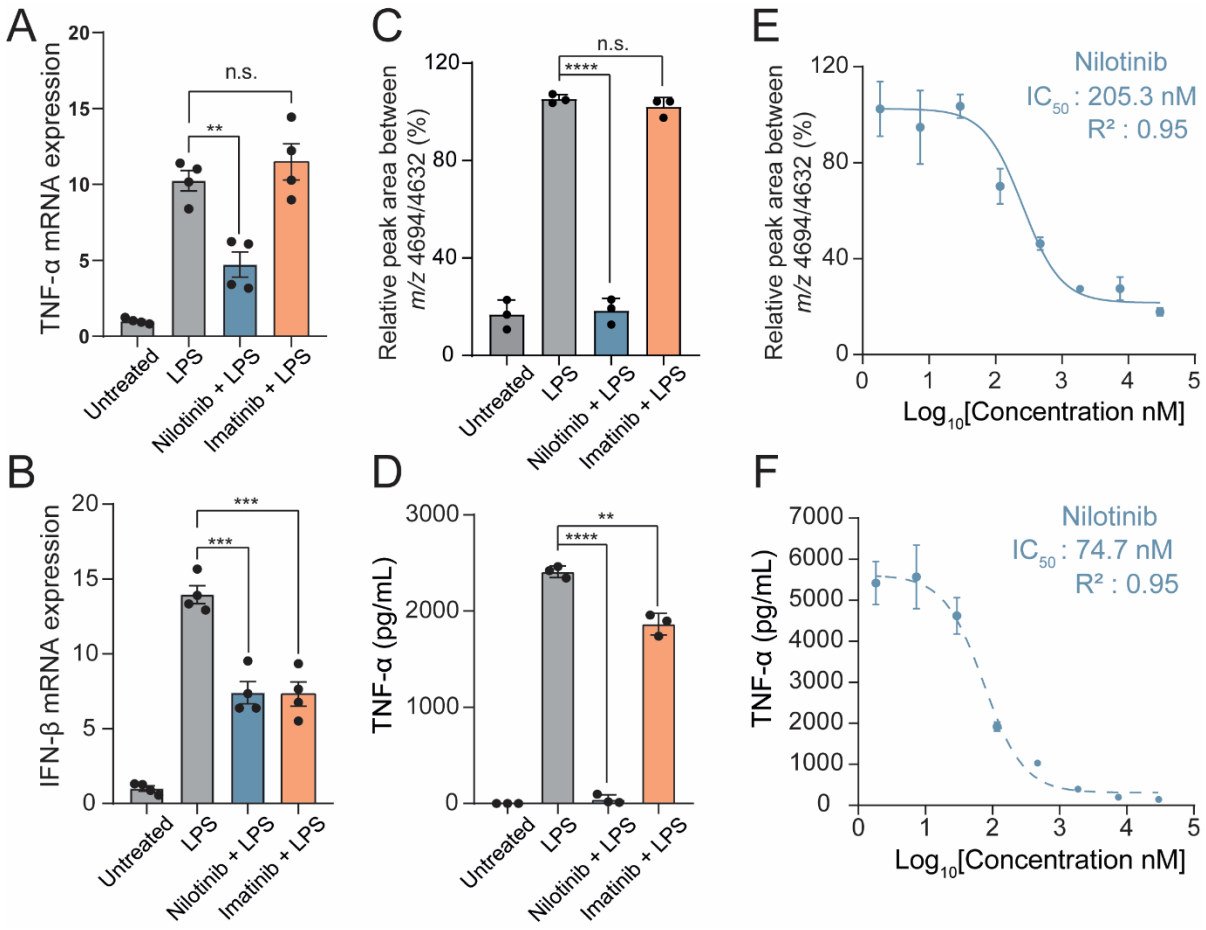

Figure 5-13. Validating the anti-inflammatory properties of nilotinib. *qPCR analysis of TNF-α (A) and IFN-β (B) mRNA expression relative to TBP performed by Joseph Innes (PhD Student, Prof. Trost Lab, 2019) & Dr. José Luis Marin Rubio (Post-doctoral researcher, Prof. Trost Lab, 2019). (C) Relative quantitation of untreated, LPS, Nilotinib and Imatinib THP-1 monocytes derived from MALDI-TOF-MS whole cell spectra from the 78 compound screen over three biological replicates. (D) Measurement of TNF-α secretion by ELISA of untreated, LPS Nilotinib and Imatinib treated THP-1 monocytes. (E) MALDI-TOF-MS IC_{50} curve of hit compound Nilotinib (F) ELISA TNF-α IC_{50} curve of hit compound Nilotinib. Each value represents a biological replicate averaged from three technical wells or MALDI spots. Error bars represent standard. n.s, *, **, *** and **** represent non-significant, p<0.05, p<0.01, p<0.001 and p<0.0001, respectively, student's t-test.*

Finally, to assess how both nilotinib and imatinib affected cells, global changes in cell proteomes were analysed. Over 7000 proteins were identified across all conditions with 5790 proteins quantified with >2 unique razor peptides. Multivariate analysis of the four conditions showed that imatinib treated monocytes clustered closely with the pro-inflammatory phenotype, whereas nilotinib localised between untreated and LPS treated, thus validating that nilotinib displays anti-inflammatory properties, but does not revert cellular physiology completely back to a resting state (Figure 5-14.B).

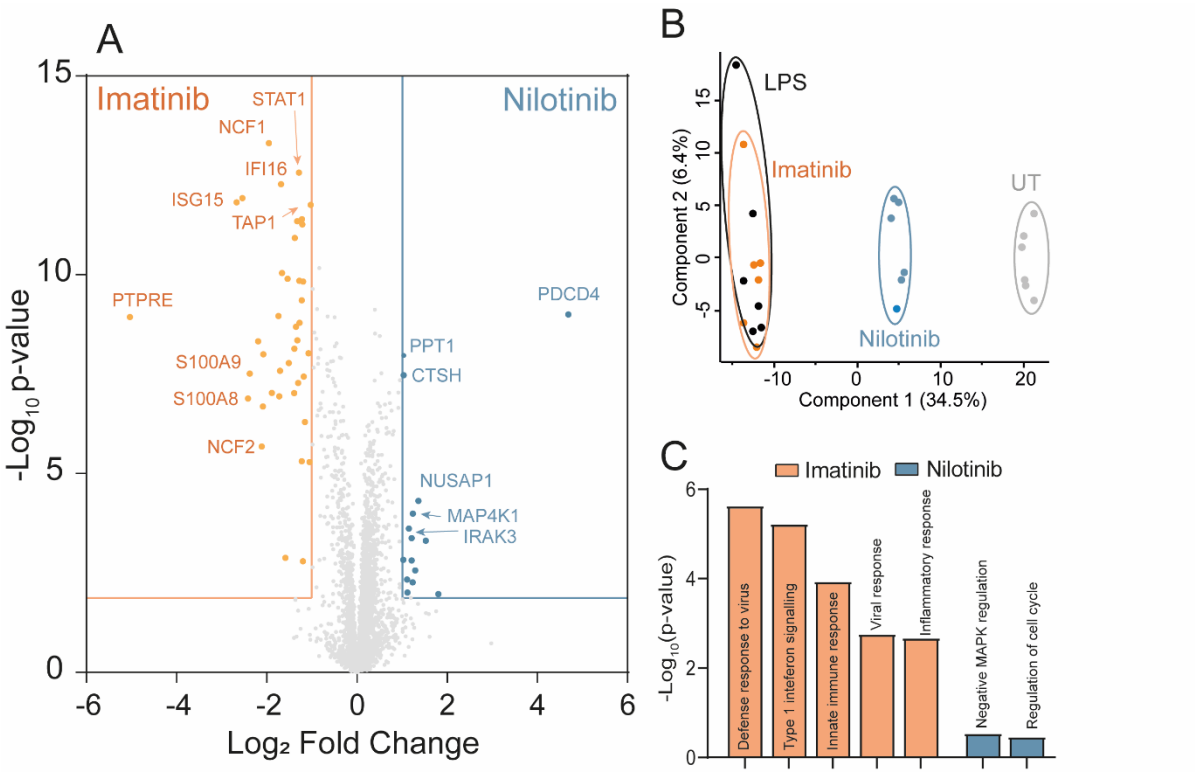

Figure 5-14. Proteomic profiling of nilotinib and imatinib treatment in THP-1 monocytes. *(A) Volcano plot of t-test data of nilotinib vs imatinib with statistical cut off at >1.5 fold change and >1.3 -Log$_{10}$(p-value) and annotated significantly differential proteins. (B) PCA plot of the four conditions showing Imatinib clustering with LPS, thus not affecting cellular inflammatory responses. (C) GO term analysis of biological processes upregulated by imatinib or nilotinib treatment.*

Data were filtered to leave only proteins that were identified in 3/6 replicates for each group. T-test statistical analyses with FDR correction between nilotinib and imatinib treated samples identified 29 upregulated proteins by nilotinib compared to 65 that

were upregulated by imatinib with a fold-change >1.5 and p-value <0.05. This generated a volcano plot shown in Figure 5-14.A, where proteins in the inflammatory signalling pathway were significantly upregulated in imatinib treatment over nilotinib, thus indicating more inflammatory signalling occurs with imatinib treatment. Further to this, 75 and 67 unique proteins were identified to nilotinib and imatinib treatment, respectively. GO term biological process analysis was performed with these proteins combined (Figure 5-14.C)

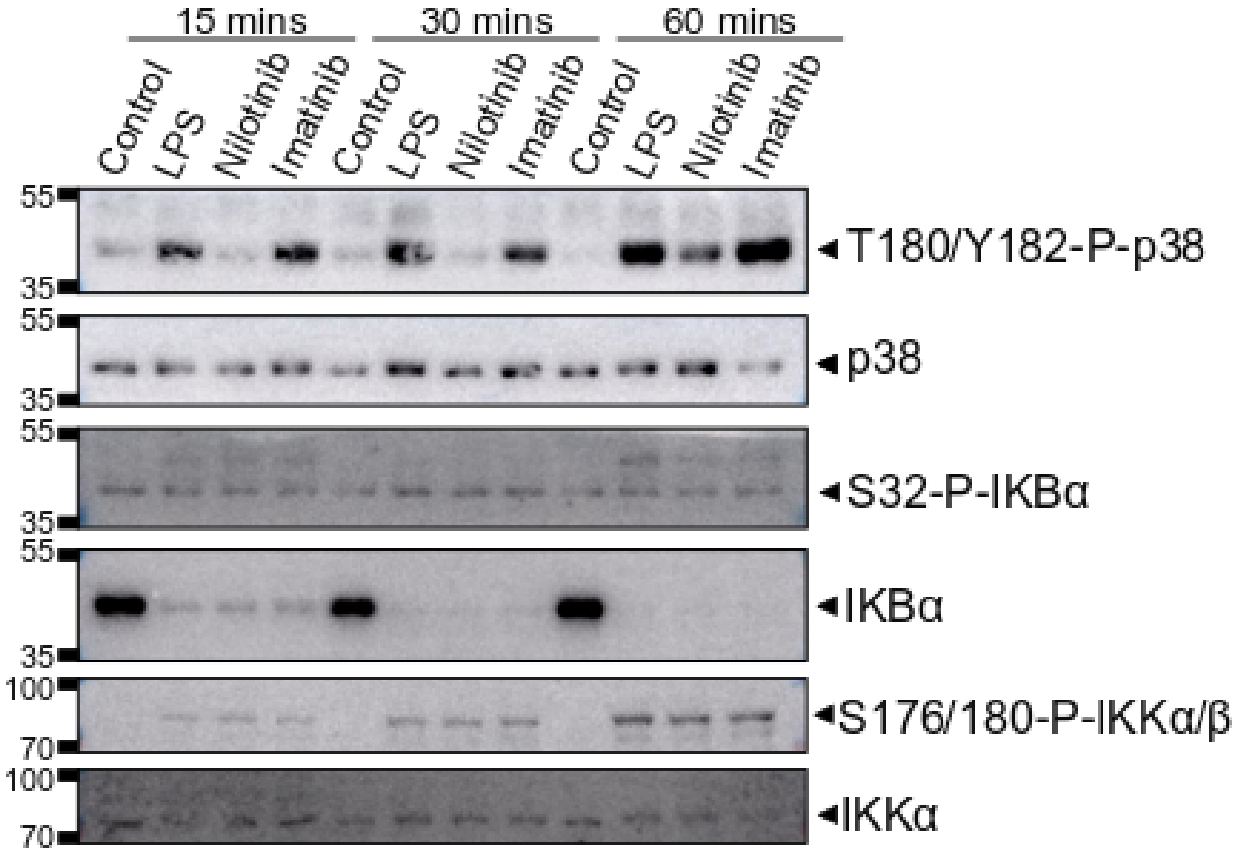

Figure 5-15. Autophosphorylation of p38 (MKK3) is inhibited by nilotinib*. Performed by* ***José L Marín-Rubio*** *(Post-doctoral researcher, Prof. Trost Lab, 2019). Immunoblot analysis (IB) showing the inhibition of p38 (MKK3) activation loop phosphorylation by nilotinib over 1 hour, while imatinib does not lead to p38 inhibition. p38 protein abundance is unchanged. Also shows that nilotinib has no impact on IKBα and IKKα phosphorylation or degradation*

Further to this, José Marín-Rubio performed immunoblot analysis to identify off-target effects of nilotinib in the NF-κB pathway (Figure 5-15). Here, these data show

specificity of nilotinib inhibiting the activation loop phosphorylation of the MAP kinase p38 (MKK3) over imatinib, which may explain why there is a reduction in TNF-α secretion and nilotinib was identified as a positive hit. More work is being undertaken to evaluate nilotinib influence on the NF-κB signalling pathway.

Taken together, this data validates that nilotinib unlike imatinib has anti-inflammatory properties. Preliminary data indicates that nilotinib inhibits to phosphorylation of p38 mitogen-activated protein kinase MKK3, which in turn could result in a dampened pro-inflammatory response. However, further work is required to characterise the off-target effect of nilotinib that reverses a pro-inflammatory phenotype.

5.4 Discussion

5.4.1 MALDI-TOF-MS is a viable label-free readout for phenotypic screening of anti-inflammatory compounds

Inflammation is fundamental biological response to injury or infection that coordinates multiple immune cell types and complex signalling pathways to protect the host and eliminate invading pathogens. Under normal homeostatic conditions, the levels of inflammation at any one time are tightly regulated, however, perturbation of this system can result in chronic or acute inflammation that can in turn lead to pathogenesis and tissue damage. In recent years, dysregulated inflammation is more and more frequently associated with debilitating conditions such as cancer, neurodegeneration and autoimmune diseases, therefore there has been a surge to study how these disorders interlink and often lead to a worse prognosis. Quantifying levels of inflammation is typically achieved by measuring the secretion pro-inflammatory cytokines by immune cells such as TNF-α, IL6 and IL-1b. Tumour necrosis factor alpha is a particularly potent cytokine and a well-established hallmark

of dangerous levels of acute inflammation in diseases such as sepsis and IBD, thus its secretion *in vitro* would be a valuable readout for compound screening. However, current methods for measuring TNF-α are expensive, often utilise labelled antibodies and lack throughput. Mass spectrometric techniques have been on the rise in the drug discovery and characterisation process, however despite being used to decipher the subtleties of TNF-α signalling, they have yet to be extended to screening for compounds that inhibit TNF-α secretion.[288] In this chapter, I have described the development of a MALDI-TOF-MS assay that quantifies the pro-inflammatory state of THP-1 monocytes in response to bacterial ligands and can be used to identify inhibitors of inflammation. Furthermore, I have shown that the MALDI-TOF-MS assay readout correlates very closely to TNF-α secretion with respect to differentiating nilotinib and imatinib as well as IC_{50} values, thus this assay is a viable alternative to ELISA-based screening.

As a model, the THP-1 cell line was chosen for assay development. This human leukaemia monocytic cell line has been used widely to study the role of inflammatory cytokine signalling in monocytes as well differentiated macrophages by phorbol ester.[289,290] As well as this, previous studies have used THP-1 monocytes to develop screening assays for measuring TNF-α in response to bacterial ligands.[291,292] Both methanol fixing and aqueous washing techniques described in Chapter 4 were tested to optimise a sample preparation method suitable for detecting a phenotypic shift in THP-1 cells, and in this case aqueous washing was more robust. It was also observed that washing and resuspension in a neutral pH buffer was beneficial for this study, with acidic buffers being less consistent when discriminating between pro-inflammatory and untreated THP-1 cells. This observation is similar to that reported by *Munteanu et al.* and discussed in Chapter 4 of this thesis, therefore I proceeded with a mild Tris buffer to maintain cellular integrity, as water alone sometimes caused

a strong osmotic effect and inconsistent sample prepartion.[242] THP-1 cells were first stimulated with LPS, the major cell wall component of Gram-negative bacteria, which consists of three different moieties, a core oligosaccharide, lipid A and the O-antigen that is particularly endotoxic for macrophages and monocytes and promotes secretion of pro-inflammatory cytokines. No unique features were robustly detected for either LPS or untreated monocytes, but there were significant shifts in common peak intensity that lead to significant separation of the two phenotypes, as well as formation of two defined clusters by PCA multivariate analysis. By taking the two features that induced the strongest polarisation for a pro-inflammatory and resting phenotype, *m/z* 4964 and 4632*,* respectively, I could generate a method that enabled ratiometric quantification of the pro-inflammatory response. A similar approach of intra-cellular dual-biomarker quantification approach has previously been described to successfully identify cell lines in a co-culture.[129] Interestingly, the feature detected at *m/z* 4964 has been described previously in several studies that have used MALDI-TOF-MS to study macrophages.[230,293] This feature has been identified as thymosin beta 4 (Tb4), a small molecular weight protein involved in binding and promoting actin polymerisation. Thymosin beta 4 itself is a highly abundant protein in cells and has also been described as having potential anti-inflammatory properties.[294,295] Using the dual biomarker approach provided a robust and reproducible analysis over biological and technical repeats with a consistently significant t-test difference $p<0.001$ and $Z' >0.5$, thus meeting the necessary assay screening qualities.

A significant pro-inflammatory MALDI-TOF-MS phenotype was quantifiable with three bacterial ligands that engage TLRs anchored in the cell membrane and induce pro-inflammatory signalling via the NF-κB pathway. Interestingly, other stimuli such as viral dsRNA and pro-inflammatory cytokines were ineffective in this assay. This suggests that the MALDI-TOF-MS phenotype is induced by the pro-inflammatory

signalling pathway and not the type I interferon pathway as IFN-γ treated THP1 cells separated with the untreated population. Further to this, it was surprising that induction of endosomal TLR3 signalling by poly(I:C) did not present a pro-inflammatory phenotype, as it has previously been shown to activate the NF-kB pathway.[296] However, the mechanism by which this occurs is different to membrane expressed TLRs (1,2,4,6) that require the adapter protein Myd88 to induce NF-kB, whereas TLR3 does not and directly recruits the TRAF6/TAK1/TAB1/TAB2 complex.[297] This alternate signalling could be an explanation for why there is no observable MALDI-TOF-MS pro-inflammatory phenotype with poly(I:C), but much more study would be required to conclude this confidently.

Having established the specificity of the MALDI-TOF-MS assay for bacterial ligand stimulation of TLRs and robust quantitation, I then proceeded to determine whether this LPS induced phenotype could be reversed with known inhibitors of pro-inflammatory and interferon signalling. Firstly, NG-25 was chosen as an upstream regulator as it is a widely unspecific TAK1 inhibitor that primarily inhibits pro-inflammatory cytokine signalling via NF-kB but also the type one interferon response.[283,298] The BET inhibitor BI25636 is a potent inhibitor of Plk1, 2 and 3, and has been implicated in the downregulation of pro-inflammatory cytokine transcription, thus down stream of NG-25.[299,300] Finally, the compound MRT67307 was previously been shown to be potent inhibitor in the SIK *in-vitro* assay but is also reported to be a specific inhibitor of TBK1. This compound was therefore a useful control TBK1 for discriminating the inflammatory pathways as TBK1 initiates upstream interferon signalling but does not inhibit NF-κB signalling transduction. Both NG-25 and BI2536 were able to inhibit the pro-inflammatory response, with MALDI-TOF-MS quantification similar to that of resting conditions, whereas treatment with MRT67307 still exhibited a pro-inflammatory phenotype. Compound efficacy validation by TNF-α

ELISA, where the results were almost identical. Interestingly, secretion of TNF-α was quantifiable in BI2536 treated conditions, which implies that there is activation of the NF-κB pathway and release of the cellular TNF-α reservoir, but further transcription of the pro-inflammatory cytokines is blocked. This could be a useful indicator of whether an unknown compounds mode of action is up- or downstream of initial NF-κB activation. Taken together, these three compounds were able to probe the specific signalling pathways involved in the pro-inflammatory response and reinforce previous conclusion the MALDI-TOF-MS phenotype is induced by activation of the pro-inflammatory signalling pathways. Furthermore, NG-25 and MRT67307 could now be utilised as positive and negative compound controls.

5.4.2 Characterising the anti-inflammatory properties of hit compound Nilotinib

Induction of apoptosis by staurosporine demonstrated that the MALDI-TOF-MS assay was capable of multiplexing readouts, a desirable outcome for cellular screening assays. By way of a 3D PCA plot, the three distinct cellular phenotypes apoptotic, resting and pro-inflammatory could be defined along one of the axes and therefore compound cytotoxicity could be characterised as well as their anti-inflammatory properties. This combined with determination of low nanomolar IC_{50} values for NG-25 and BI2536 confirmed assay suitability for screening, therefore I proceeded with a blind 78 compound screen, which generated excellent Z' scores and good reproducibility between biological repeats. Here, nilotinib, a second generation leukaemia drug, was reproducibly identified as hit compound that reduced the pro-inflammatory response back to resting levels. Surprisingly, imatinib, the first generation counterpart, was also included in the screen and did not show any anti-inflammatory effects. Both nilotinib and imatinib are structurally similar and potent inhibitors of BCR-ABL tyrosine kinase that are used as first line treatments for CML.[301]

Interestingly, both compounds have been previously suggested to have potential anti-inflammatory effects, particularly in autoimmune diseases such as rheumatoid arthritis.[302] These findings also extend to another second generation BCR-ABL tyrosine kinase dastanib, which was not included in this particular screen, but has been shown to reduce TNF-α secretion.[303] Despite nilotinib being structurally related to imatinib, the integration of a 3-methylimidazole group and trifluoromethyl groups enables it to make unique interactions within the Abl kinase domain.[304] This in turn means that once bound, the shape and conformation of nilotinib is very different to imatinib, which may account for differences in off-target protein effects. Interestingly, BI2536 has been shown to synergise with imatinib to prevent CML proliferation.[305] By inhibiting Plk1 an anti-inflammatory phenotype is induced that enables better imatinib efficacy, which may in turn account for why nilotinib is a more effective therapy.

Quantification of TNF-α secretion validated the MALDI-TOF-MS screening data as nilotinib was able to dramatically reduce TNF-α secretion compared with imatinib that only mildly reduced TNF-α levels. Further to this, using both TNF-α secretion and MALDI-TOF-MS as a readout IC_{50} curves for nilotinib generated with almost identical IC_{50} values of ~200 nM, thus validating the MALDI-TOF-MS assay as an alternative strategy to conventional ELISA assays for screening of anti-inflammatory compounds.

Finally, total proteome analysis of nilotinib and imatinib treatments enabled the significant changes in protein expression that are associated with inflammatory signalling. These included CD14 that is involved in the sensing of LPS alongside TLR4, as well as IRF7, TRAF1, and RelA/C, all of which are involved in the interferon or NF-κB signalling induced by activation of plasma membrane TLRs. Multivariate analysis indicates that nilotinib does prevent complete activation of inflammatory signalling as it does not cluster directly with untreated samples. This may explain why

certain proteins such as IRAK3, IRAK4 and TRAF2, were found to be upregulated in with nilotinib treatment. These proteins are associated with inflammatory signalling, with IRAK4 transducing a positive TLR response immune and TRAF2, which regulates activation of the NF-κB and JNK response and modulates cell survival.[306,307] Interestingly, IRAK3 is associated with negative regulation of TLR signalling by inhibiting dissociation of IRAK1 and IRAK4 from TLRs by preventing their phosphorylation.[308] Overall, this data infers that nilotinib has an off-target effect within the inflammatory signalling cascades that, although does not prevent signal-transduction, does disrupt the production of the cytokine TNF-α. Further work will be needed to identify the off-target involved with inflammatory signalling such as identifying phosphosites that are unoccupied with nilotinib treatment, as well as characterising the phosphorylation states of key proteins in the NF-κB signalling pathway.

Chapter 6. The L929 secretome – a study to understand the subtleties in bone marrow-derived macrophage differentiation

6.1 Introduction

Mouse models are key for studying inflammation and the innate immune response *in vivo* to decipher the complex signalling pathways that result in tissue pathogenesis and disease. These models have been important for the study of various diseases such as rheumatoid arthritis and inflammatory bowel disease, where research in mice has enhanced knowledge about how these diseases progress in humans.[309] Further to this, genetic engineering has advanced significantly in recent years to establish knock-out, knock-in or transgenic mice to further explore how specific genetic modifications influence physiological responses.[310] This has been particularly successful for the development of histone deacetylase inhibitors to target inflammatory diseases with dysregulated cytokine production.[311] However, these *in vivo* experiments do not always yield specific information about the behaviour of specific cells during infection or treatment, thus it is often necessary to perform *in vitro* experiments to understand specific cellular responses. There are numerous immortalised cell lines available as models for murine macrophages that have been used widely to study effects of stressors on the innate immune response and decipher signalling pathways. Combined with the development of advanced genetic engineering technologies such as CRISPR-Cas9 these lines have become a powerful tool for studying signalling cascades as it is relatively simple and fast to genetically engineer immortalised cell lines compared with mice.[312] These studies have advanced our knowledge of how macrophages interact specifically with bacterial

infections, their phagocytic behaviour and also their ability to switch between an M1 and M2 phenotype.[313] However, despite their advantages, there are studies that have highlighted the differences between these cell lines in response to infection or stressors.[314] It has been shown that the stability of some RAW264.7 macrophages can become compromised after 30 passages, as well as the fact that J774 macrophages exhibit a different response to *Mycobacterium tuberculosis* infection compared with primary cells. Consequently, the utmost care must be taken when selecting a model for a particular experiment as it is likely to affect the biological outcome.[315,316]

Primary macrophages are the ideal source of cells for *in vitro* experiments as they provide more biologically relevant models. These cells cannot be passaged but can be isolated from a variety of organs such as liver, spleen, peritoneum and bone marrow.[317,318] Importantly, any genetic modification incurred at the mouse genome level is translated into *in vitro* experiments and therefore results can be verified in the original *in vivo* model. The most common source of primary murine macrophages are derived from bone marrow, where stem cells are first isolated and then they undergo differentiation *in vitro* in the presence of macrophage colony stimulating factor 1; M-CSF or CSF-1 as described in Figure 6-1. This method was first described by Tushinski *et al.* and Guilbert *et al.* in 1982 and 1986, respectively, and generates a pool of bone marrow-derived macrophages (BMDMs).[319,320] Both these studies highlight the importance of M-CSF in the production of a highly homogenous population of mononuclear phagocytes. M-CSF is a secreted cytokine and growth factor that induces differentiation of hematopoietic stem cells into macrophages and stimulates phagocytic behaviour. It is closely related to granulocyte-macrophage colony stimulating factor (GM-CSF), a glycoprotein that has numerous

immunomodulatory functions *in vivo*, but can induce dendritic cell differentiation from stem cells.[321,322]

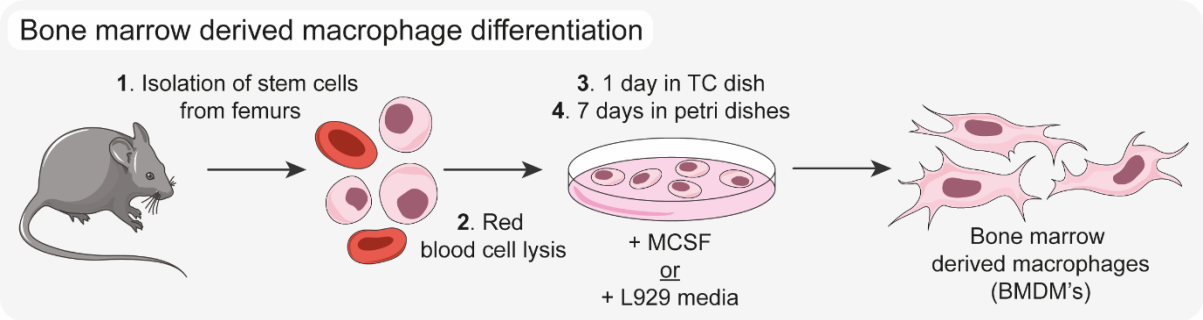

Figure 6-1. Differentiation culture method of bone marrow-derived macrophages from stem cells under the influence of either M-CSF or L929 supplemented media.

It has since been described how GM-CSF and M-CSF are highly expressed and secreted by the L929 murine cell line, an immortalised fibroblast cell line derived from connective tissue.[323,324] Consequently, this has led to the development of protocols that prefer to use L929 conditioned medium for BMDM differentiation over the addition of recombinant M-CSF as it is cheaper and simple to produce in house.[325] Moreover, substantially more BMDMs can be obtained from bone marrow differentiated in L929 supernatant compared to recombinant M-CSF. However, there remains scepticism in the field over BMDM production utilising L929 supplemented media. This is partially driven by the utilisation of different protocols, with L929 supplementation of media ranging from 10-30% and secretion collection from L929 cultures described from as early as 7 days up to 14 days with different seeding densities.[326–328] These different experimental procedures will likely influence resultant BMDM properties, as it has already been shown that cellular density during differentiation can alter the resulting macrophage phenotype.[329] Furthermore, early studies described how L929 medium could induce an interferon stimulated phenotype in BMDMs, which may then affect results due to the macrophage polarisation.[330,331] Despite this heterogeneity in culture

conditions, BMDMs differentiated under L929 conditioned media have been utilised widely for the study of macrophage behaviour such as regulation of antigen presentation by treatment with IL-4, as well as deciphering cell signalling pathways in response LPS treatment.[332–334]

The classification and phenotype of M-CSF derived macrophages has been well described in detail with respect to their adhesion and cell surface marker expression, however, this has not been compared with alternative differentiation methodologies.[318,335] Therefore, there is a need to characterise BMDM phenotypes under the different culture conditions to determine whether there are significant differences in biological function. Furthermore, despite the characterisation of M-CSF as a significant component of L929 secretion, the identification of total protein content has not yet been described. Consequently, there is a need to define the secretion profile of L929 to identify any factors that my influence resultant BMDM phenotype.

6.2 Aims

In this thesis thus far, I have explored different models that can be utilised for drug discovery from *in vitro* enzymatic reactions to immortalised cell lines. A well-established source of primary macrophage are BMDMs that have been used as models for drug discovery. However, their differentiation protocol is controversial, therefore, within this study I undertook proteomic profiling of the L929 secretome protein content. This identified M-CSF as a major component of the secretion along with macrophage inhibitory factor (MIF). Finally, I characterised the differences between BMDMs differentiated under three different culture conditions by total proteome analysis, flow cytometry and their cytokine secretion profiles in response to LPS.

6.2.1 Sub-chapters

1. Proteomic profiling of the kinetic L929 secretome over a two-week time course

2. Characterising BMDM differentiation under different culture conditions

6.3 Results

6.3.1 Proteomic profiling of the kinetic L929 secretome over a two-week time course

The collection of L929 supernatant is typically performed at 7 or 14 days, with some protocols combining both time points to generate potent differentiation media. This is because L929 supernatant collection follows a unique protocol where cells are initially seeded and not passaged from then on. Therefore, my first aim was to design a study that characterised the secretion profile of L929 fibroblasts over the two week time period by sampling at 3, 7, 10 and 14 days. For secretomic studies standard cell culture medium is incompatible due to the very high concentrations of fetal bovine serum (FBS) that skews the dynamic range for mass spectrometry analysis. Therefore, a reduced sera medium, named Opti-MEM, has been developed that enables biologically similar culture conditions without that addition of FBS, thus suitable for proteomic experiments. L929 fibroblasts were seeded in six well plates and grown in accordance with standard L929 supernatant collection (Figure 6-2.A). From this analysis, bright field light microscopy visualised the progression of cell confluency at days 3, 7, 10 and 14 (Figure 6-2.B), showing increasing confluency and morphology changes over time. Cells were well adhered with long protrusions at day 3, however cell size reduced significantly as confluency grew. At day 14, it was possible to visualise multiple layers of small, round cells that are dramatically different

in morphology compared with day 3. For the secretome, cells were washed prior to addition of Opti-MEM media for 3 hours to accumulate secreted proteins. Consequently, this approach measures the rate of protein secretion without compromising cellular biology throughout the growth period. Incubation with sera free media was limited to three hours as the absence of nutrients from FBS could impact cellular biology and may in turn induce stress and apoptosis. From a previous study, I was able to verify that under basal conditions in sera free media it was possible to collect cellular secretion for up to three hours without inducing PARP1 cleavage, which is indicative of cellular apoptosis.

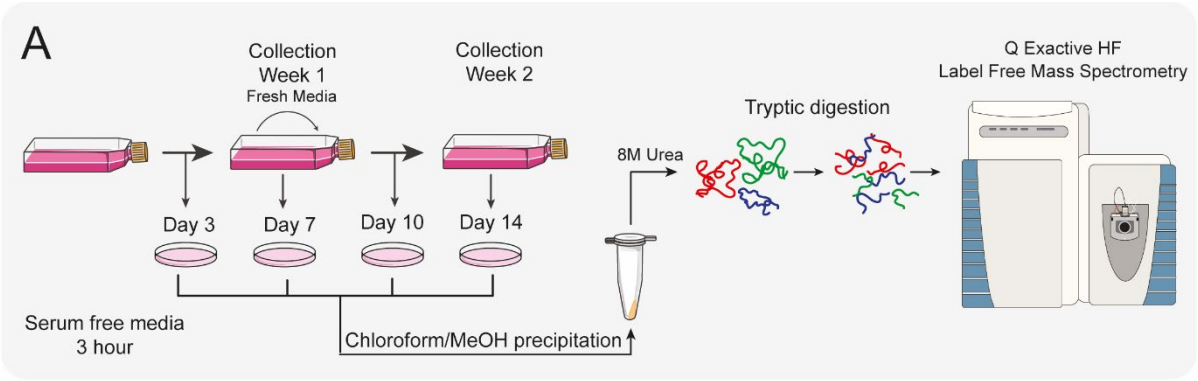

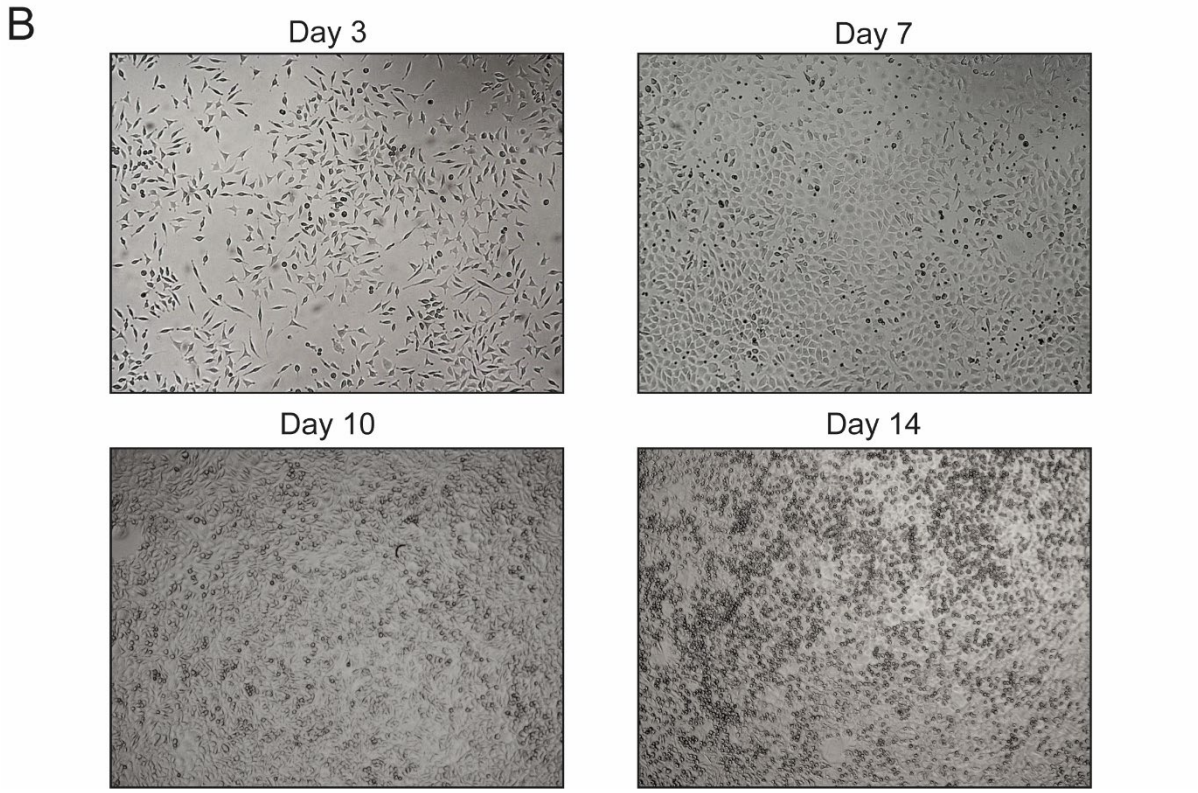

Figure 6-2. Proteomic profiling of the L929 secretome. *(A) Graphical representation of the collection of L929 supernatant over 14 days and the corresponding secretome collections for proteomic analysis. (B) Brightfield light microscopy images of L929 fibroblasts at the secretome time points showing significant changes in morphology with increasing confluency.*

This study identified 2877 proteins to define the L929 secretome, with 2198 being robustly identified with 2 or more razor + unique peptides. The top three proteins identified from the secretome based on overall intensity comprised of fibronectin, actin and collagen alpha-type-2, which is unsurprising for fibroblast cells as they are known to secrete high levels of these extracellular matrix proteins.[336,337] Using iBAQ ranking, a top twenty list of proteins that could influence subsequent BMDM phenotype was generated (Table 6.1). The iBAQ ranking enables quantitation of a protein's abundance relative to its molecular weight. Here, the sum of intensities for all the identified tryptic peptides for a given protein is divided by the number of theoretically observable peptides for that protein to yield an IBAQ intensity. This is particularly important when looking at smaller molecular weight proteins as there are much fewer potential tryptic peptide, thus they will often yield a lower intensity than larger proteins without IBAQ correction.[338]

Table 6-1. Twenty selected proteins identified in L929 secretome with iBAQ ranking

Rank	Uniprot Accession	Gene names	Protein names
1	P60710	Actb	Actin 1 (Beta-actin)
2	P11276	Fn1	Fibronectin
3	P21460	Cst3	Cystatin-C
4	P16045	Lgals1	Galectin-1
5	Q9DD06	Rarres2	Retinoic acid receptor responder protein 2
6	P01887	B2m	Beta-2-microglobulin
7	P34884	Mif	Macrophage migration inhibitory factor (MIF)
8	P47879	Igfbp4	Insulin-like growth factor-binding protein 4
9	P07091	S100a4	Protein S100-A4 (Metastasin)
10	P10923	Spp1	Osteopontin
11	Q61398	Pcolce	Procollagen C-endopeptidase enhancer 1
14	P06151	Ldha	L-lactate dehydrogenase A chain

16	P05064	Aldoa	Fructose-bisphosphate aldolase A
27	O09164	Sod3	Extracellular superoxide dismutase
39	P35700	Prdx1	Peroxiredoxin-1 Macrophage 23 kDa stress protein)
41	P14069	S100a6	Protein S100-A6 (Calcyclin)
49	Q03366	Ccl7	C-C motif chemokine 7
50	P50543	S100a11	Protein S100-A11 (Calgizzarin)
60	P07141	Csf1	Macrophage colony-stimulating factor 1
64	P10148	Ccl2	C-C motif chemokine 2

Taking the data set as a whole, gene ontology (GO) enrichment was performed for the cellular component subset. I observed significant enrichment of extracellular exosomal proteins with-$\log_{10(}$p-value) of 300 using a Benjamini-Hochberg FDR correction as well as enrichment in cytosolic protein groups (Figure 6-3.A). Using iBAQ ranking and cumulative protein intensity that ranks proteins in terms of their percentage contribution to the overall intensity, I was able to identify M-CSF and MIF as significant components of the L929 secretome (Figure 6-3.B&C). Both of these proteins are secreted cytokines that have reported function in the modulation of macrophage differentiation and function.[339,340] Taking the normalised Log_2 intensity of the proteins their expression rates were plotted against the day of secretion for both MIF and M-CSF (Figure 6-3.D). This data showed that the rate of M-CSF secretion is generally consistent throughout the two week L929 secretion time period. Conversely, the rate of MIF expression correlated with depletion of nutrients within the media, as rates decreased two fold after addition of fresh media. This could imply that MIF is secreted with a shift in metabolism when less nutrients are available.

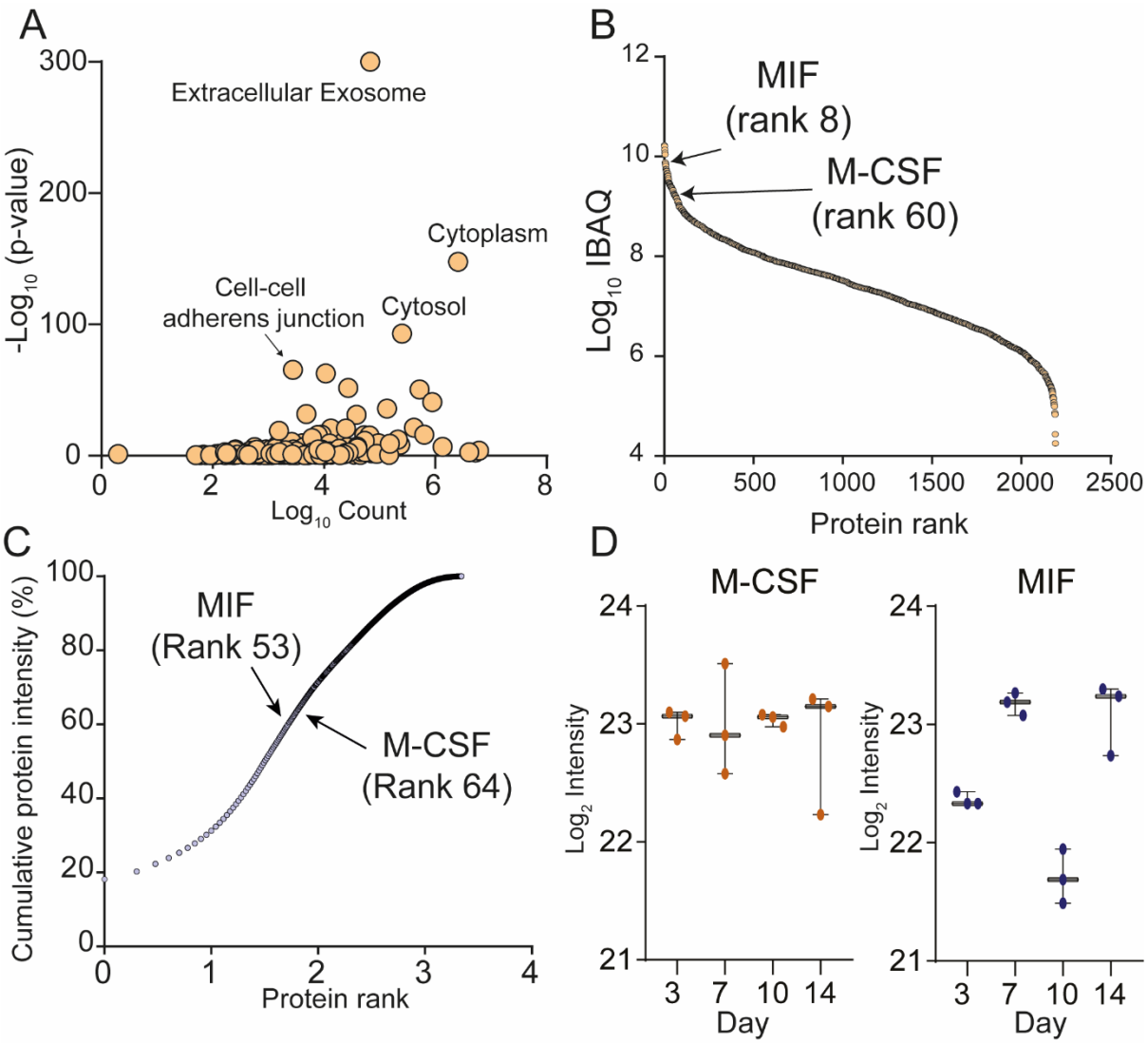

Figure 6-3. Proteomic profiling of L929 secretome identifies M-CSF and MIF as significant components. *(A) GO enrichment of L929 secretome cellular component showing enrichment of extracellular exosome. (B) Log10 iBAQ ranking of proteins from the L929 secretome showing positions of MIF and M-CSF. (C) Cumulative protein intensity ranking, i.e. not normalised, showing positions of MIF and M-CSF. (D) Log2 intensities of M-CSF and MIF showing expression rates over the two week time course. Error bars represent the mean average ± SD over three biological replicates.*

Prior to further analysis, the data set was filtered for protein groups that had values in two out of three biological replicates for each sampling day. To analyse for variance over multiple groups, I applied Benjamini-Hochberg FDR corrected ANOVA that identified 1128 significant protein groups. Using Z' score averaging and Euclidean

clustering, a group averaged heat map was drawn as shown in Figure 6-4 that exhibited distinct patterns in protein secretion rates over time.

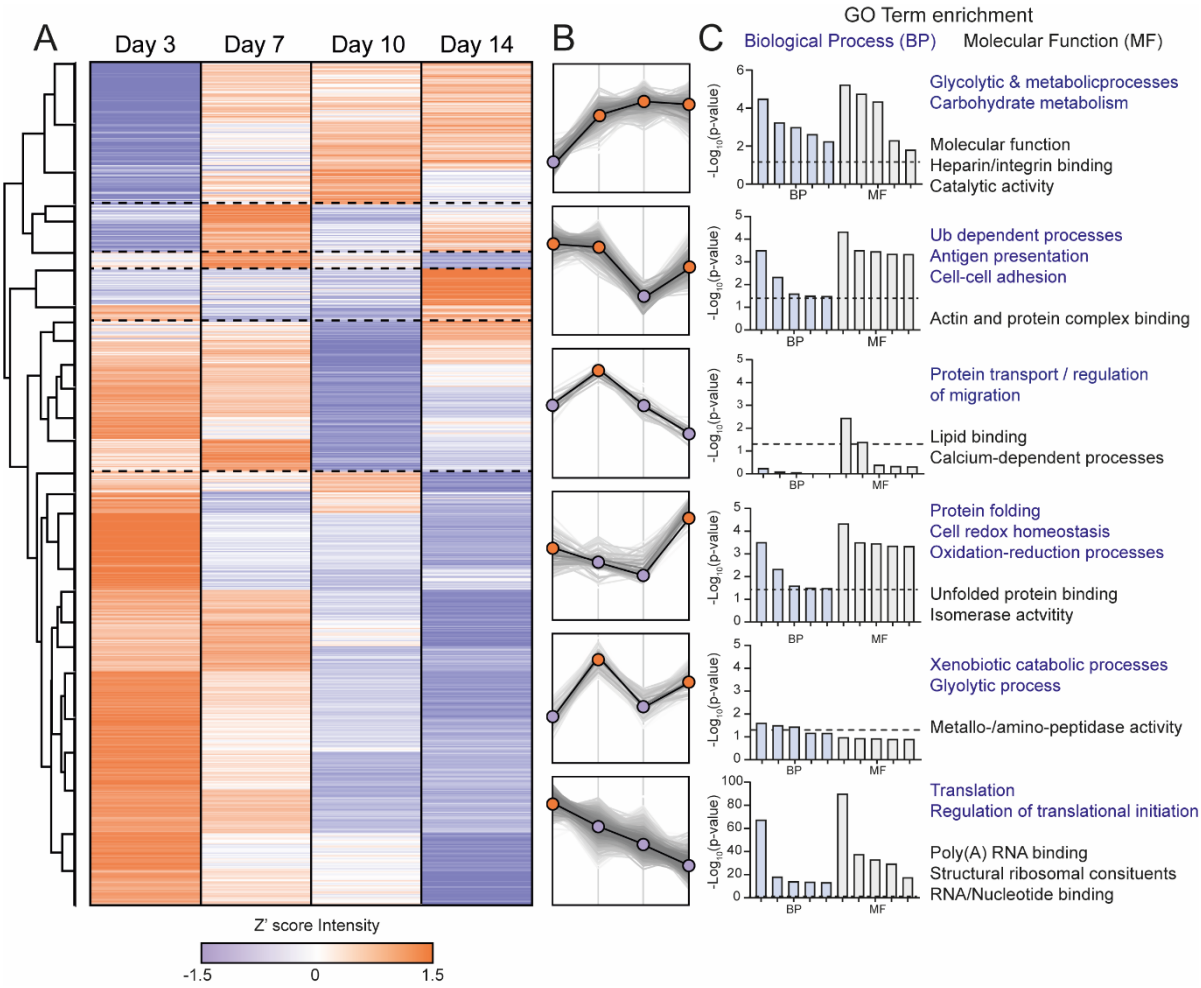

Figure 6-4. Global analysis of the L929 secretome kinetic. *(A) Z' heat map of ANOVA significant proteins across the sampling days. (B) Six distinct cluster profiles that show different secretion patterns over time with purple dots indicating down and orange dots up regulation. (C) Associated molecular function and biological process GO terms for the six cluster profiles.*

From this, six distinct clusters could be defined (Figure 6-4.B) that exhibited different rates of protein secretion over time. Interestingly, it appears that for the majority of proteins secretion rate decreases over time, which is inconsistent with an increase in cell confluency over the two week period. Analysis of the normalised Log_2 intensity histograms for each secretome sample showed an even distribution for all sampling days, thus this trend is not due to variation in injection volume or sample quantity. As

well as this, there are notable changes in protein secretion that may be induced by the presence or absence of nutrients over the time period. The associated GO enrichment plots for each cluster describe the enrichment in both the biological process and molecular function of each cluster subset, thus allowing insight into cell state at the different time points (Figure 6-4.C)

Taken together, these data provide a comprehensive list of proteins that are secreted by L929 fibroblasts over a two week time period. Within this data set, M-CSF was expectedly identified as being highly secreted, however, MIF was also identified as a highly expressed protein and may influence subsequent differentiation.

6.3.2. Characterising BMDM differentiation under different culture conditions

The original aim of this study was to identify the major protein components of L929 supernatant and subsequently characterise BMDM differentiation under either M-CSF or L929 supplemented media. However, as MIF was identified as a highly secreted protein by L929 fibroblasts and is known to play a role in regulating macrophage function it was deemed necessary to explore whether MIF impacts BMDM differentiation. Therefore, three culture conditions were defined: 10 ng/mL of M-CSF, 10 ng/mL of MIF + 10 ng/mL of M-CSF and 20% L929 supplemented media (Figure 6-5.A). The concentration of 10 ng/mL was chosen for M-CSF as this is the most widely reported differentiation concentration.[341,342] Furthermore, the L929 secretome data indicated that MIF (12 kDa) was about 5 times more abundant than M-CSF (60 kDa), thus indicating similar total amounts of both proteins in the L929 supplement. For L929 supplemented media the secretion collection was performed in tandem to the secretome proteomic analysis, thus the protein composition described is an accurate representation of the differentiation media.

Three female wild type C57BL/6 mice of the same age were taken for this experiment. After red blood cell lysis, the haemopoietic stem cells from each mouse were pooled into culture media excluding any differentiation agents to prevent cross contamination of different culture conditions. One millilitre of the mixture was added to three tissue culture plates containing the individual culture conditions 1, 2 and 3 to allow adhesion of contaminant cells such as leukocytes and osteoblasts before transfer into petri dishes for differentiation over seven days (Figure 6-5.A).

For proteomic analysis, the three biological replicates of each culture condition were first digested and then labelled with 9 out of 10 of the labels of a TMT10 plex reagent kit. This enabled pooling of all samples and offline-HPLC HPRP peptide separation to enable deeper proteome analysis as peptides are orthogonally separated. TMT labels consist of four parts: a reporter ion, mass normaliser, a reactive amine group and a cleavable linker. Samples are incubated with a specific tag that initiates a reaction between the ester-activated-amine group of a TMT tag and N-terminus of peptides, thus allowing conjugation. However, it is also possible for TMT tags to react with the amine group of lysine residues in a TMT label: peptide ratio dependent manner.[343] The mass normaliser balances the isotopic mass difference induced in the mass reporter. In turn, this allows peptides in the MS1 scan to be identified at the same *m/z*, but in the MS2 scan when selected peptides are fragmented the cleavable linker is broken and the reporter ion released that enables quantification (Figure 6-5.C).[64] As TMT labelled samples were processed on an on Orbitrap Fusion Lumos Tribrid mass spectrometer quantification can be performed at either the MS2 and MS3 level. Here, the relative quantification is either performed at the first fragmentation step of the peptides (MS2), or there is a further fragmentation step (MS3) that enables complete cleavage of the reporter ion by using higher energy CID known as HCD fragmentation.[344,345] This step is performed on the isolated precursor peptides

independently of the MS2 scan and results in almost complete fragmentation of the reporter ion, thus more accurate quantification. The introduction of MS3 fragmentation was particularly important for studies that required highly accurate and precise quantification, as it has been described previously for isobaric labelling strategies that there is often contamination from near-isobaric ions that are fragmented with the same precursor ion.[346–348] Consequently, this can lead to over- or under- estimation of peptide and protein intensities in the different channels and in extreme cases lead to identification of knock-out proteins in knock-out channels. This has led to the development of strategies to diagnose ion interference such as a two-proteome model for TMT-6plex labelling systems, and a triple knockout standard for TMT-10plex systems.[345,349] For this particular study, MS2 quantification was chosen as it enables a greater number of IDs. This was important to enable generation of the deepest possible proteomes of the different BMDM populations.

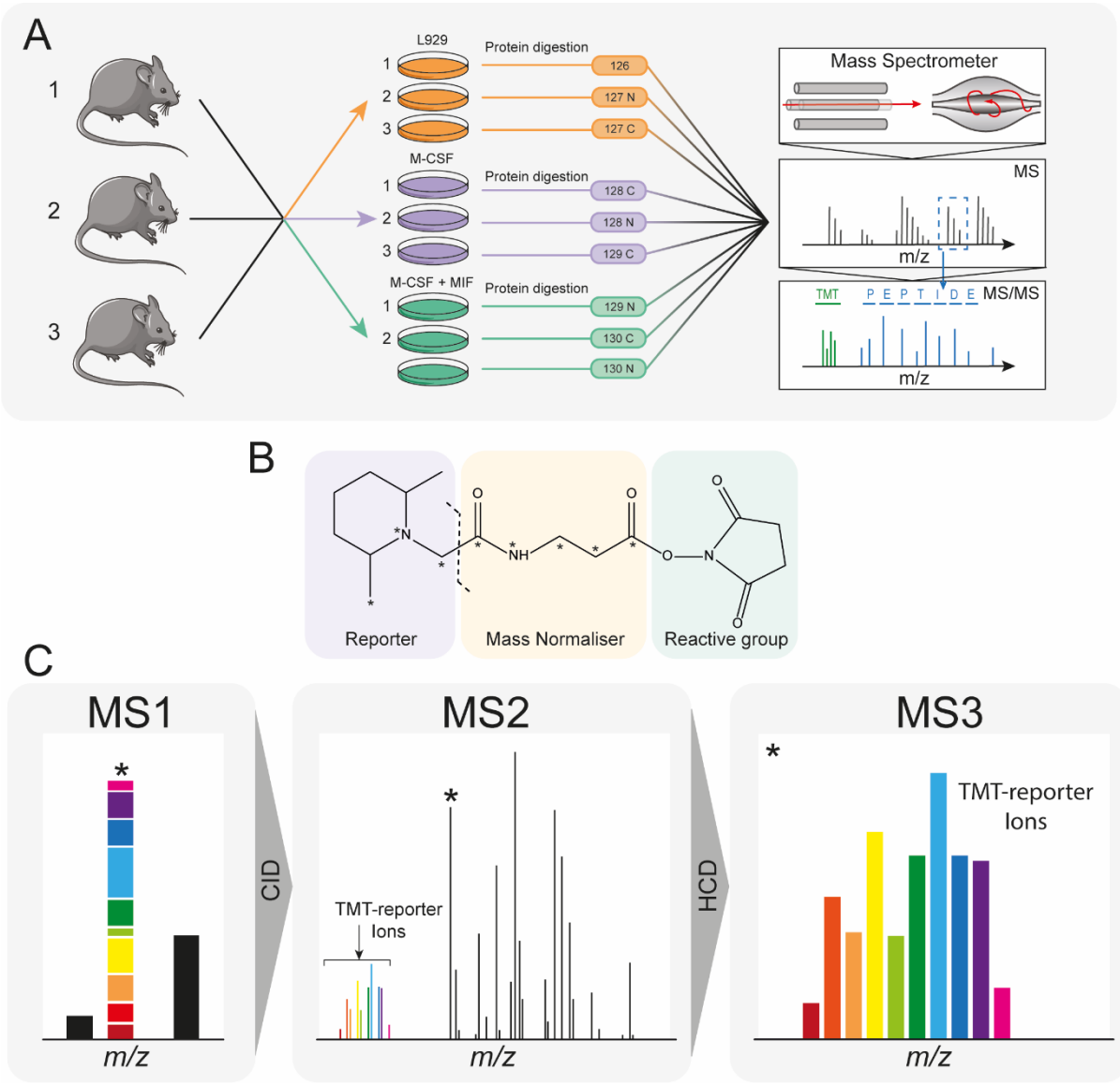

Figure 6-5. Proteomic profiling of the three BMDM populations by TMT quantitation. *(A) Experimental design of the three BMDM differentiation conditions coupled with TMT labelling and LC-MS/MS analysis. (B) Structure of the TMT label with reporter, mass normaliser, reactive group and cleavage point. (C) Schematic of LC-MS/MS fragmentation strategies for TMT quantification.*

Labelling efficiency was first determined prior to quenching of the reaction with a small pool that reported >98% labelling of peptides, thus the experiment was progressed to HPRP fractionation into 12 fractions and analysed by LC-MS/MS. Here, 6724 protein groups were identified with 5607 quantified with 2 razor + unique peptides. The LFQ data set was subjected to T-test statistics with Benjamini-Hochberg FDR correction between the three BMDM populations that generated the volcano plots shown in

Figure 6-6.A. Interestingly, there were no significant differences in protein expression between BMDMs cultured with M-CSF +/- MIF, thus implying that there is little impact of MIF on M-CSF induced differentiation. Conversely, over 100 differential proteins were identified between L929 differentiated BMDMs and the two other culture conditions (Figure 6-6.A).

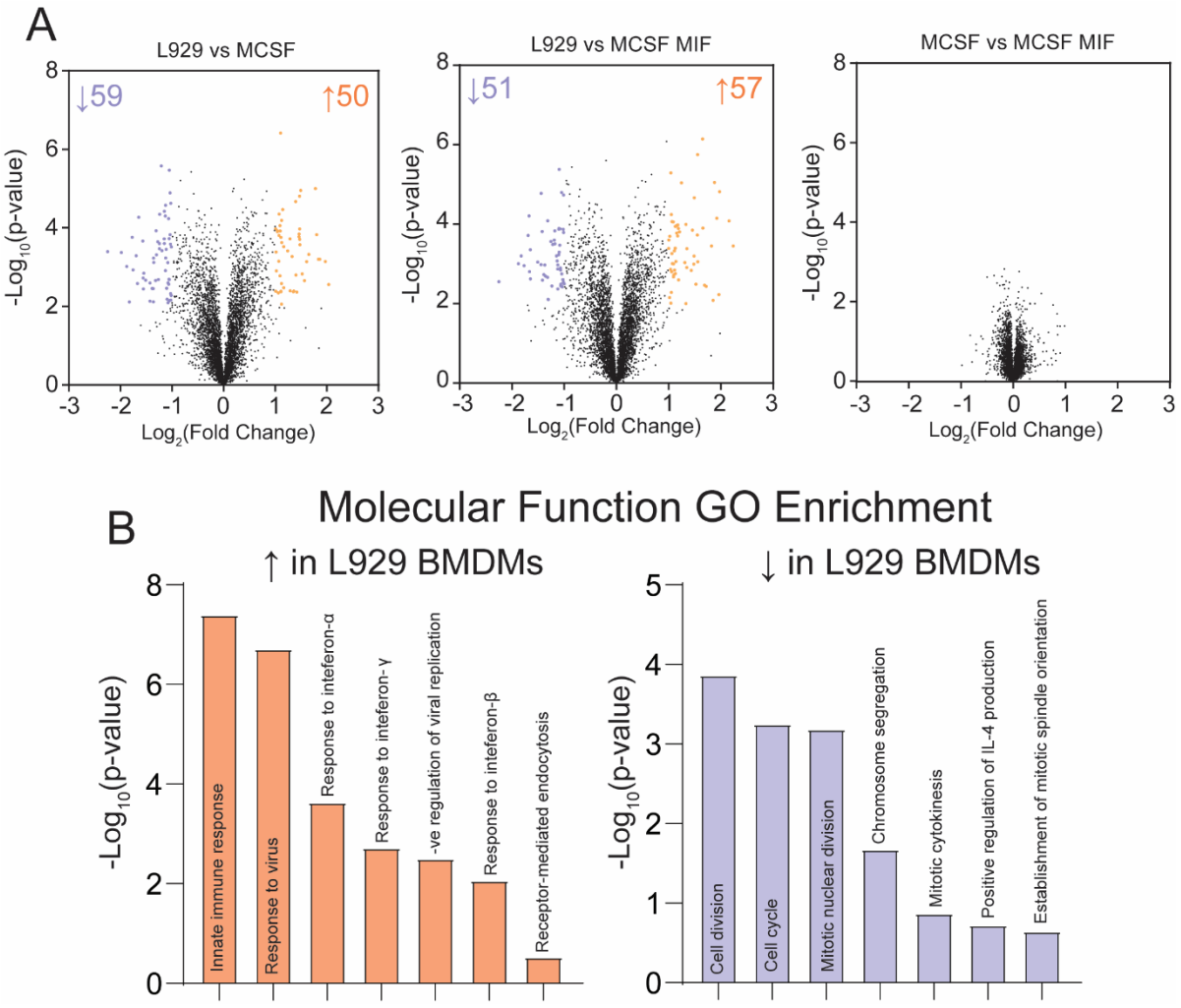

Figure 6-6. BMDM's differentiated with L929 supplementation exhibit significantly different proteomes over M-CSF/MIF differentiation. *(A) Volcano plots of the three culture conditions compared showing differential proteins with respect to BMDM populations. (B) Molecular function GO enrichment of proteins that up or down regulated in BMDMs with respect to M-CSF and MIF.*

Taking these differential protein lists GO terms showed significant enrichment with respect to molecular function (Figure 6-6.B). Interestingly, these data indicate that

BMDMs grown in L929 supplemented media have a heightened interferon and innate immune response compared with M-CSF/MIF cultured BMDMs. Conversely, BMDMs grown in L929 supernatant show down-regulation of cell division and mitotic machinery. These differential proteins were plotted using Log_2 fold change of the protein LFQ intensities and Euclidean clustering between L929 and M-CSF + MIF culture conditions showing good clustering of up and down-regulated proteins that were highly consistent over three biological replicates. These data also show the protein Dcaf11/DDB1, which was the only protein that was identified as up-regulated by inclusion of MIF showing similar protein expression levels to L929 cultured BMDMs. This could indicate that MIF may induce the up-regulation of Dcaf11/DDB1.

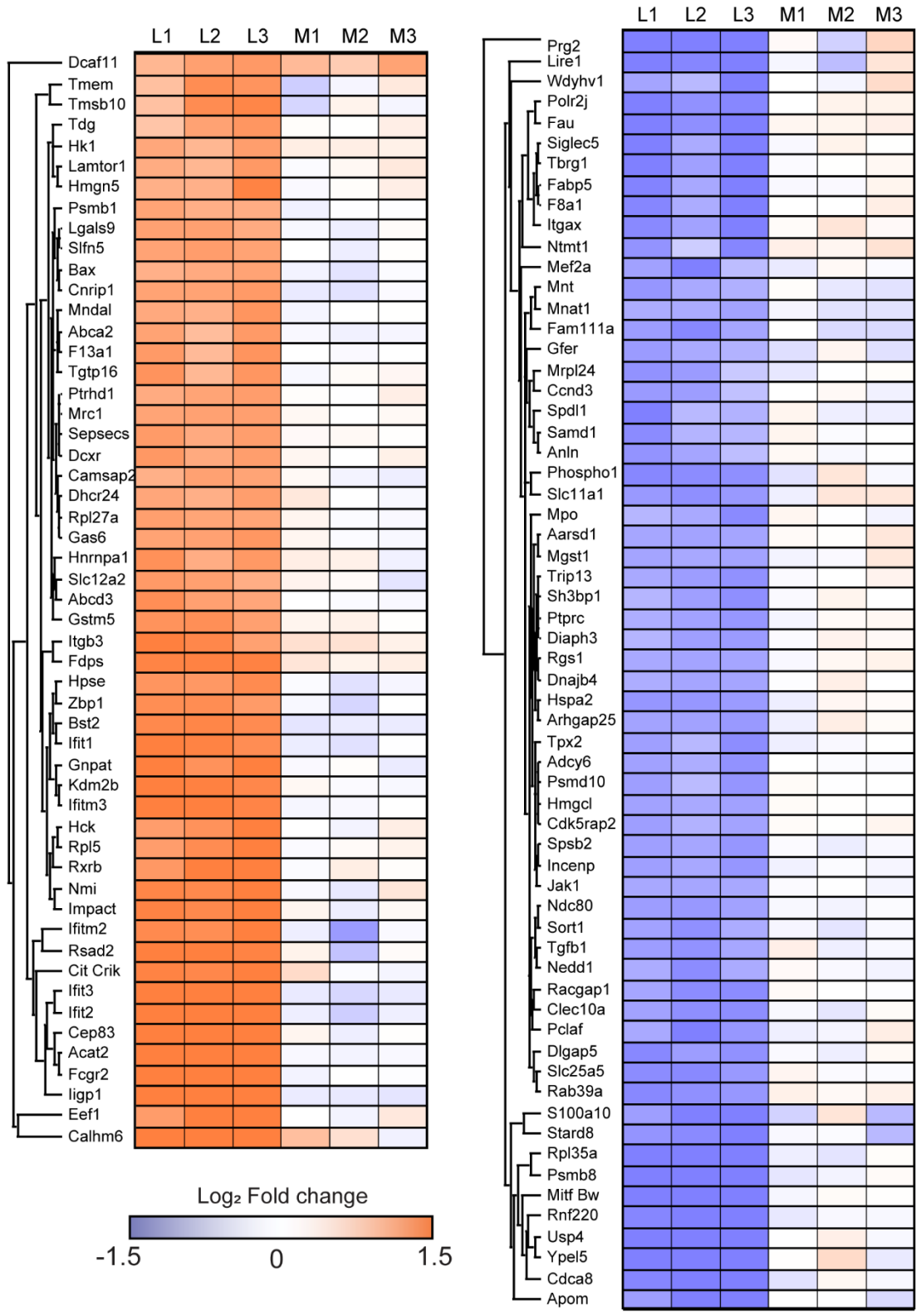

Figure 6-7. Significantly regulated proteins with respect to L929 supernatant BMDM differentiation. *Log₂ fold change heatmap of differential proteins identified by a significant t-test between L929 and MCSF+MIF BMDM differentiated populations.*

To validate biological function the three BMDM populations were subjugated to further characterisation using cell biology techniques. Firstly, cell surface protein biomarker expression was evaluated using flow cytometry. Three markers were chosen: F4/80, a widely used murine marker of macrophage populations, CD11b that recognises the antigen ITGAM that is highly expressed by macrophages and CD11c, a marker that is used to differentiate macrophage and dendritic cell populations.[158,350,351] Interestingly, there were significant differences between L929 cultured BMDMs and the M-CSF and MIF conditions.

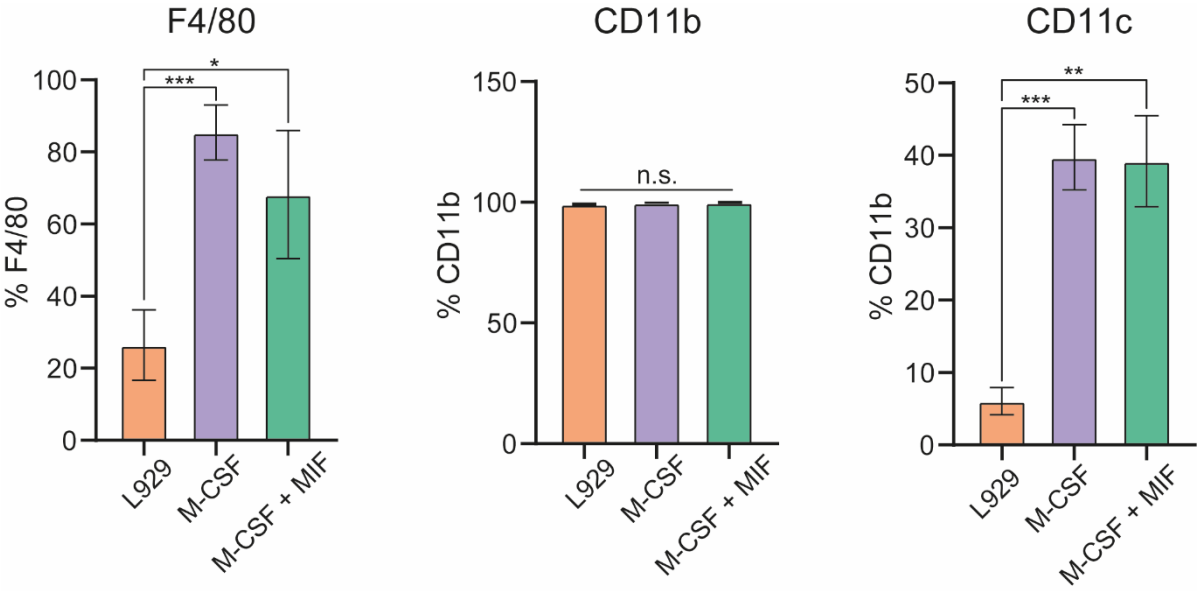

Figure 6-8. Flow-cytometry analysis of the three BMDM populations. *Percentage expression of cell surface markers F4/80, CD11b and CD11c measured by flow cytometry for the three BMDM populations. Error bars represent ± SD from the mean average of three biological replicates. n.s, *, **, *** represent non-significant, p<0.05, p<0.01 and p<0.001 respectively, student's t-test.*

It was surprising to observe that L929 cells did not express F4/80 ubiquitously, as this suggests that they lack macrophage-like functions. However, it has been shown that F4/80 is not required for the development and distribution of murine tissue macrophages.[352] CD11b was expressed by all detected cells in the three BMDM

conditions, which indicates a highly homogenous population of macrophages. However, measurement of CD11c showed that there was a four-fold higher expression on cells cultured with M-CSF with or without MIF. This in turn suggests that M-CSF induces a more dendritic like than BMDMs grown in L929 supernatant.

As the proteomic data showed a difference in innate immune response and interferon phenotype, I sought to assess the differences in pro-inflammatory cytokine secretion with and without pro-inflammatory stimulation by LPS. Here, I measured the secretion of TNF-α, IL-6 and IFN-β. Without stimulation, all three populations displayed either non-detectable levels of the pro-inflammatory cytokines TNF-α and IL6 or non-significant levels of the type one interferon IFN-β.

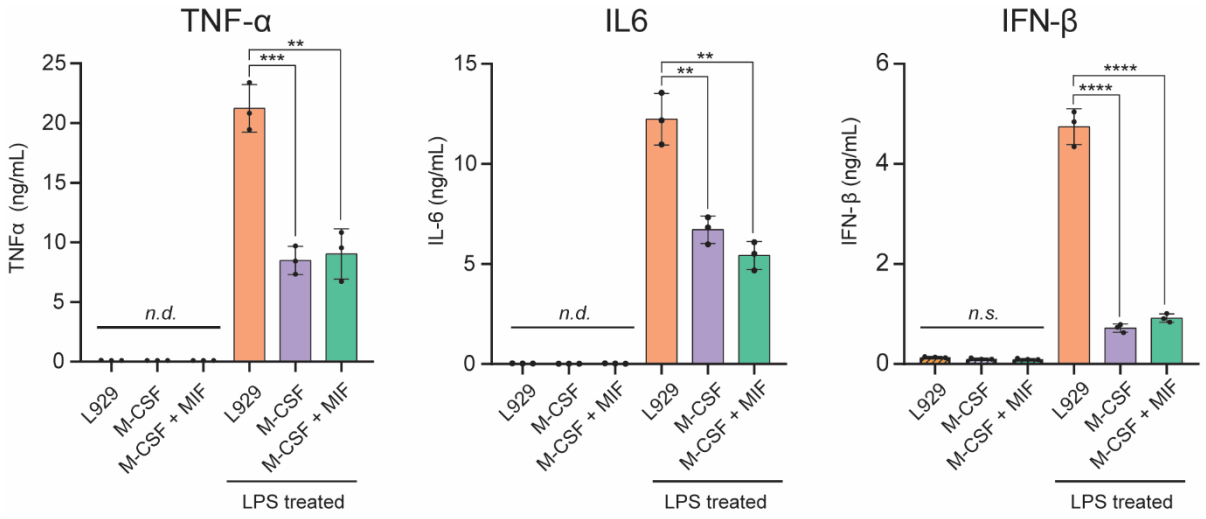

Figure 6-9. ELISA quantification of secreted cytokines TNF-α, IL6 and IFN-β under basal conditions and treatment with 100 ng/mL of LPS.

Upon treatment with 100 ng/mL of LPS for six hours BMDMs cultured with L929 supplement presented a much stronger pro-inflammatory and interferon response over M-CSF ± MIF differentiated conditions, thus correlating with the total proteome data presented in Figures 6-6 & 6-7. Error bars represent ± SD from the mean average of three biological replicates. n.d, n.s, **, *** and **** represent not detected, non-significant, $p<0.01$, $p<0.001$ and $p<0.0001$, respectively, student's t-test.

Taken together, these data show that different BMDM phenotypes result from the differentiating agent used with respect to total proteome and biological function. Therefore, it is important to consider the biological ramifications that result from the different BMDM differentiation strategies and resultant *in vitro* biological outcome.

6.4 Discussion

6.4.1 The L929 secretome protein composition is highly diverse

Bone marrow-derived macrophages are primary cells derived from the isolation of haemopoietic stem cells from mammalian femurs and tibia and differentiated *in vitro*. These macrophages are particularly important for the understanding of biological function and complex signalling cascades involved in the immune response as they provide the best models for *in vitro* experiments. Consequently, this had led to the development of high content screening assays against primary macrophages with the aim of reducing subsequent drug failures and generating more predictive *in vivo* results. This has been particularly successful in the development of anti-leishmanial drugs, where interaction with the entire parasite is necessary for effective *ex vivo* drug screening.[353,354] This can sometimes be compromised with the use of immortalised cell lines that do not necessarily exhibit native macrophage behaviour.

Initially, macrophage colony stimulating factor (M-CSF) was identified as the main driver of primary macrophage differentiation and was introduced *in vitro* as an active differentiation agent. However, in more recent years the supplementation of differentiation media with the secretion of L929 fibroblasts has become more favourable as it cheaper and relatively simple to produce in-house. L929 fibroblasts were isolated from connective tissue have been shown to produce and secrete large volumes of M-CSF. This may be physiologically relevant to the cell type, as fibroblasts

are a major component of connective tissue and play a critical role in wound healing and recruitment macrophages.[355] Further to this, fibroblasts secrete cytokines and chemokines to modulate macrophage behaviour and the inflammatory response, therefore the production of M-CSF is necessary for the initial recruitment of macrophages to site of injury.[356] However, the secretion of fibroblasts is much more complex than purely M-CSF, but this has never been truly characterised with respect to BMDM differentiation. Therefore, the primary aim of this study was to describe the protein composition of the L929 supernatant across the collection time period. Here, 2198 proteins were robustly identified over the two week time course with different expression rates. Interestingly, the top 100 proteins ranked by iBAQ contributed towards more than 60% of the total protein content with M-CSF and MIF being highly expressed. With respect to cumulative protein intensity, both M-CSF and MIF exist in similar proportions within the L929 secretion. However, I observe MIF to be ranked higher than M-CSF with respect to the IBAQ ranking as MIF is approximately five times smaller in size than M-CSF. This therefore suggests that MIF is produced and secreted in greater amounts by L929 fibroblasts with respect to protein count. In addition to MIF, many other cytokines were also identified alongside stress proteins such as peroxiredoxin-1 and two chemokines Ccl7 and Ccl2. This may indicate that the L929 supernatant may induce a pro-inflammatory activation state during the differentiation on BMDMs. However, secretion of both IFN-γ and IFN-β were measured by ELISA for all four sampling conditions and neither of the two interferons were detectable, thus disputing previous studies that reports the production of type 1 interferons by L929 fibroblasts during the supernatant collection period.[330] As well as this, three members of the S100 protein family were identified and multifunctional low molecular weight calcium binding proteins.[357] They are known to exist extracellularly

and modulate the immune response, however the two known members S100-8 and S100-9 that act as pro-inflammatory cytokines were not detected.[358]

Looking at the secretome as a whole, it was possible to identify protein expression rates that appeared to be regulated by nutrients and cell cycle. Initiation of translation and cell-cell adhesion was most highly upregulated immediately after initial seeding at three days, which supports rapid proliferation into available surface area. Conversely, as cell number increases, there is a significant increase in secretion of glycolytic and metabolic proteins. Interestingly, there is an increase in catabolic processes at day 7 and 14, which suggests that anabolic metabolism is occurring versus aerobic, which is likely due to depletion of nutrients within the media. At day 14, where cell confluency is at its highest, there is significant increase in protein folding, oxidative processes that are indicative of stress responses. This is important to note, as the secretion of stress proteins or induction of apoptosis due to confluency or lack of nutrients could impact the resultant BMDM phenotype. Therefore, it could be beneficial to collect L929 supernatant at earlier time points and test the potency in BMDM differentiation.

Overall, more than 2000 proteins were identified in the L929 secretome as well as high levels of M-CSF, the driving component of haemopoietic stem cell differentiation into bone marrow-derived macrophages. Unexpectedly, in this data set macrophage inhibitory factor MIF was highly abundant has been indicated in regulation of macrophage function. The protein composition of the L929 secretome provides a valuable resource to the community as it is a comprehensive list of protein secretion rates across a two week time period. This list is particularly beneficial for those who perform *in vitro* differentiation of BMDMs with knock-out or point mutation mice, as the endogenous protein may re-introduced into the system. Consequently, this could

compromise studies that aim to understand particular protein functions. In these cases, it would be more advantageous to use M-CSF as a differentiating agent so as to prevent contamination.

6.4.2 Culture conditions influence the resultant BMDM population phenotype

Utilising cell biology techniques and total proteome analysis I was able to assess the phenotypic differences between the three BMDM populations. Isolated stem cells were incubated with three different differentiation media compositions: M-CSF and MIF, pure M-CSF and L929 supplemented media. Relative quantification of protein expression was enabled by using TMT labelling. Here, MS2 quantification allowed the robust quantification of 5607 proteins across the three biological replicates. There was no significant difference in total protein expression between BMDMs cultured with or without the presence of MIF, which was interesting as it has previously been described as a mediator of host defence. This implies that MIF cannot solely influence macrophage phenotype and is likely to act in tandem with other cytokines that are released during injury or infection to coordinate a pro-inflammatory response. The only protein that appeared to be up-regulated in response to MIF was Dcaf11 as shown in the fold changes in Figure 6-7. This is somewhat ambiguous, as Dcaf11, or DDB1, is poorly described in the literature but has been implicated as a substrate receptor for the CUL4-DDB1 E3 ligase complex that modifies proteins by addition of ubiquitin. One substrate of this complex is thought to be involved in the control of cell cycle progression[359], however more exploration would be necessary to identify whether there is an interaction between MIF and DDB1.

The total proteome of BMDMs differentiated under L929 supplementation had a clearly distinct phenotype compared with pure M-CSF or M-CSF with MIF. Here, there were 109 differential proteins that GO term enrichment classified as either involved in

cell cycle/mitosis or the innate immune response. These cells showed much higher expression of proteins involved in the interferon and immune response such as interferon induced proteins IFIT1, IFIT3, IFITM2, IFITM3 and ISG15. As well as this, L929 differentiated BMDMs show decreased protein expression of cell division and cell cycle proteins such as cyclin-A2, spindle and centromere proteins SPDLY and INCE compared to pure M-CSF differentiation. Consequently, this implies that using M-CSF and MIF for differentiation does not halt the progression of cell cycle, whereas factors in the L929 supplement may cause cell cycle arrest, perhaps through faster differentiation. Several cell division control proteins were identified in the L929 secretome such as CARP-1 as well as multiple cyclin-dependent kinases (1, 2, 4 and 6), but neither of these have been implicated in cell cycle arrest. Therefore, this implies that differentiation with L929 supplement generates a population of macrophages that are more mature than those differentiated purely with M-CSF.

Following this, flow cytometry analysis of surface expressed markers correlated with proteomic data. Here, marker CD11c was highly enriched on macrophages differentiated with either M-CSF or MIF over L929 supernatant. This indicates that these macrophages are more dendritic-like, which may in turn justify why these BMDMs are less mature. Due to its close relationship with GM-CSF, the dendritic cell differentiating agent, it is unsurprising that these cells are more dendritic like, however inclusion of MIF does not reduce the expression of CD11c, thus it is unlikely to play an important role in the differentiation process. However, it was surprising to observe that the murine macrophage marker F4/80 was less expressed on the surface of macrophages differentiated with L929 supernatant over pure M-CSF/MIF. This implies that these cells are less macrophage-like, however previous data has suggested that F4/80 is not necessarily important for development of murine tissue macrophages.[352] Therefore, it would be important in further studies to evaluate

macrophage functions such as phagocytosis and both the M1 and M2 phenotype to fully characterise L929 differentiated BMDM phenotypes.

To assess the pro-inflammatory response of the three BMDM populations the secretion of pro-inflammatory cytokines was measured after stimulation with LPS. It was necessary to use LPS over IFN-γ stimulation so as to prevent bias with the interferon response as it was previously indicated that BMDMs under L929 culture may be interferon stimulated.[330] Three cytokines were measured in response to LPS: TNF-α, IL-6 and IFN-β, which cover the classical NF-κB pro-inflammatory and type one interferon response. At basal levels, with no treatment, there were undetectable levels of TNF-α and IL6, thus implying that all BMDM populations are not pro-inflammatory stimulated throughout the differentiation. There were detectable, but very low levels of IFN-β secretion under basal conditions. However, these were not significant between the three populations. This in turn shows that despite the variety of proteins present in the L929 supernatant, including MIF, they do not induce a pro-inflammatory activation state in BMDMs. Upon stimulation, BMDMs that were differentiated by L929 supplemented media showed significantly increased pro-inflammatory response across the three cytokines. This was particularly pronounced with IFN-β, where levels were elevated five-fold in response to LPS. These data correlate with the previously described proteomic data where GO enrichment showed an enhanced innate immune response and response to type one interferons (Figure 6-6.B).

Inclusion of MIF as a differentiation agent resulted in a negligible difference in cellular phenotype with respect to total proteome, cytokine secretion and protein marker expression. Overall, the combined cellular biology and proteomic data shows that differentiation with L929 supplemented media generates a population of cells that are

more macrophage-like than M-CSF or MIF alone. From a biological perspective this makes sense, as *in vivo* induction of macrophage differentiation would likely be initiated by cellular secretion of multiple factors in response to injury or pathogenic infection. Fibroblasts play a significant role in the recruitment of macrophages and their migration towards the site of infection. Therefore, differentiation under L929 fibroblast supernatant supplementation results in a macrophage population that is more relevant *in vitro*. Taken together, it is possible to conclude that M-CSF is a driving component of BMDM differentiation, but other factors secreted by L929 fibroblasts influences the resulting cellular phenotype. Further exploration of these factors would be necessary to understand the subtleties in BMDM differentiation and what induces a more macrophage-like phenotype.

Chapter 7. Perspective

Within this thesis I have explored how mass spectrometry techniques can be utilised to enhance the drug discovery process as well as develop better models of innate immunity for compound screening purposes. Here, my efforts have focussed on applying MALDI-TOF-MS as a screening tool for inhibitors of inflammation that can compete with current existing assays. This work demonstrated the potential of a MALDI-TOF-MS kinase peptide based assay for SIKs that avoids the use of a stable isotopically labelled (SIL) internal standard for compound screening. For the first time, we compared the developed MALDI-TOF-MS peptide based assay with an established fluorescent biochemical assay by performing an ATP mimetic compound screen. From this, we demonstrated a good correlation of hit compounds between both assay types, and also identified a subset of unique hits with the MALDI-TOF-MS assay. Furthermore, it was surprising yet promising to observe that the larger dynamic range of the MALDI-TOF-MS assay allowed activating compounds to be identified. The potential of a MALDI-TOF-MS assay to identify both activators and inhibitors within a single screen could be particularly interesting for future assay development. In addition, an assay that can ascertain whether a compound acts as an activator rather than a negative hit could help broaden the understanding of a particular chemotype as well as target engagement.

However, despite the advantages highlighted within this thesis, MALDI-TOF-MS for drug discovery does lack some of the benefits of traditional biochemical assays. For example, it would be difficult to fully resolve most full-length proteins and their post translationally modified product by MALDI-TOF-MS. Therefore, assays would realistically rely on truncated substrates, such as peptides, so that the shift in

molecular weight could be resolved and measured accurately. This may in turn not truly reflect the activity of an enzyme with its substrate *in vivo*. Further to this, it has been discussed in this thesis, as well as by Chandler *et al.*,[83] that MALDI-TOF-MS assays are intolerant to certain buffer conditions such as detergent, high salt concentrations and glycerol, all of which can help maintain protein conformation and activity. Finally, it was originally hypothesised that relative quantitation between the measured substrate and product rather than using a SIL would enable faster and cheaper development of assays for screening purposes. However, this work has highlighted that perhaps this may not be the most suitable approach for future assays. Characterising some enzyme kinetics, such as $K_{M,}$ that were dependent on substrate concentration became challenging with the relative substrate to product ratio method. In the presence of excess substrate, the quantitation of enzyme activity from product formation relative to the unmodified substrate was no longer representative of enzyme turnover, thus a narrower concentration window must be used. In addition, it was also observed that it was more challenging to achieve a good Z' value with this approach as the dynamic range between positive and negative controls was narrow. The use of an internal standard such as a SIL product derivative to quantitate enzyme activity would avoid both these problems. Therefore, it is unsurprising to observe that in the past decade this approach has been favoured by industrial companies, despite the extra cost. Taken together, this thesis work presents a positive and promising perspective of MALDI-TOF-MS as a readout for future enzymatic HTS assays, but also outlines some of its limitations that may reduce its applicability to certain targets or assay types.

Cellular assays often provide better *in vitro* models for drug discovery; thus, I explored the potential of MALDI-TOF-MS as a readout for cell based assays. This approach was inherently more difficult than an enzymatic product monitoring reaction

as the MS spectra is more complex and the biomolecules were typically unknown. Current literature surrounding this phenotyping approach varied significantly in their methodologies, therefore I performed rigorous method development to a fingerprinting approach of proteins in mammalian cells. Here, I demonstrated the compatibility of the optimised sample preparation method with MALDI-TOF-MS, as well as current automated liquid handling robotics. This protein fingerprinting approach was sensitive for phenotyping transient changes within mESC differentiation as well as compliant with robust and independent statistical analysis. This approach was then applied to an inflammatory model with the aim to develop a MALDI-TOF-MS cellular assay for identifying inhibitors of inflammation. Initial work identified a unique spectral phenotypes, or fingerprints, that corresponded to pro-inflammatory and resting monocytes. It was promising to observe the biological specificity that could be achieved with this approach as the pro-inflammatory spectral phenotype was induced specifically in response to bacterial ligands. It was also possible distinguish between IFN and NF-κB pro-inflammatory signalling inhibitors. A proof of concept screen revealed nilotinib as a hit compound with anti-inflammatory properties that was then validated by cellular biology and proteomic approaches. This study was promising and demonstrates the power of MALDI-TOF-MS to identify novel effects of compounds, which may in turn have the potential for drug repurposing.

However, this protein fingerprinting approach was not without limits. For the THP-1 assay, it wasn't possible to identify the differential features that influenced the pro-inflammatory phenotype, thus no target could be derived from this work. In addition, the poorer resolution of linear MALDI-TOF-MS resulted in protein features that drifted in *m/z* value due to base peak width. This variability increased with larger molecular weight biomolecules and may prove problematic for downstream analysis and confident peak assignment. Spectral alignment tools in combination with an internal

standard for normalisation could be useful to address this problem in future work. An interesting take on this work could be to focus on analysing different biomolecules such as metabolites, lipids and oligonucleotides directly from cells by MALDI-TOF-MS. These molecules tend to occupy the lower mass region; thus, it would be more favourable to use a reflectron mode where it is possible to perform MS/MS analysis and identify the differential features. There could also be potential to generate multiplexed assays, where multiple readouts could be monitored by utilising the properties of different matrices to identify different biomolecules from the same population or treatment.

In conclusion, the work in this thesis demonstrates the power of MALDI-TOF-MS as a future drug discovery screening tool. This technique is particularly applicable to the enzymatic assay screening field, where applications of MALDI-TOF-MS technology have grown year on year. A promising application that has arisen from this body of work could be MALDI-TOF-MS cell-based drug discovery assays. A cells phenotypic response or a particular biomolecule of interest could be rapidly screened in response to a treatment. This combined with the potential to identify multiple biomolecules and readouts from single assay could allow better drug characterisation at an early stage of the drug discovery process. When combined with complimentary mass spectrometry approaches, MALDI-TOF-MS phenotypic screening of a compounds effect in cell could reveal novel drug interactions as well as accelerate the lead optimisation process.

Bibliography

1. Münzenberg, G. Development of mass spectrometers from Thomson and Aston to present. *Int. J. Mass Spectrom.* **349–350**, 9–18 (2013).

2. The Nobel Prize in Physics 1989. *NobelPrize.org* https://www.nobelprize.org/prizes/physics/1989/summary/. (2020)

3. The Nobel Prize in Chemistry 2002. *NobelPrize.org* https://www.nobelprize.org/prizes/chemistry/2002/summary/. (2020)

4. Karas, M., Bachmann, D. & Hillenkamp, F. Influence of the wavelength in high-irradiance ultraviolet laser desorption mass spectrometry of organic molecules. *Anal. Chem.* ***57****,* 2935–2939 (1985).

5. Tanaka, K. *et al.* Protein and polymer analyses up to m/z 100 000 by laser ionization time-of-flight mass spectrometry. *Rapid Commun. Mass Sp.* **2**, 151–153 (1988).

6. Karas, M. & Hillenkamp, F. Laser desorption ionization of proteins with molecular masses exceeding 10,000 daltons. *Anal. Chem.* **60**, 2299–2301 (1988).

7. Karas, M. & Krüger, R. Ion Formation in MALDI: The Cluster Ionization Mechanism. *Chem. Rev.* **103**, 427–440 (2003).

8. Knochenmuss, R. MALDI mechanisms: wavelength and matrix dependence of the coupled photophysical and chemical dynamics model. *Analyst* **139**, 147–156 (2014).

9. Knochenmuss, R. Ion formation mechanisms in UV-MALDI. *Analyst* **131**, 966–986 (2006).

10. Karas, M., Glückmann, M. & Schäfer, J. Ionization in matrix-assisted laser desorption/ionization: singly charged molecular ions are the lucky survivors. *J. Mass. Spectrom.* **35**, 1–12 (20

11. Jaskolla, T. W. & Karas, M. Compelling evidence for Lucky Survivor and gas phase protonation: the unified MALDI analyte protonation mechanism. *J. Am. Soc. Mass Spectrom.* **22**, 976–988 (2011).

12. Beavis, R. C., Chaudhary, T. & Chait, B. T. α-Cyano-4-hydroxycinnamic acid as a matrix for matrix assisted laser desorption mass spectrometry. *Organic Mass Spectrometry* **27**, 156–158 (1992).

13. Chen, X., Carroll, J. A. & Beavis, R. C. Near-ultraviolet-induced matrix-assisted laser desorption/ionization as a function of wavelength. *J. Am. Soc. Mass. Spectrom.* **9**, 885–891 (1998).

14. Horneffer, V. *et al.* Is the incorporation of analytes into matrix crystals a prerequisite for matrix-assisted laser desorption/ionization mass spectrometry? A study of five positional isomers of dihydroxybenzoic acid. *Int. J. Mass. Spectrom.* **185–187**, 859–870 (1999).

15. Wiley, W. C. & McLaren, I. H. Time-of-Flight Mass Spectrometer with Improved Resolution. *Rev. Sci. Instrum.* **26**, 1150–1157 (1955).

16. Mamyrin, B. A., Karataev, V. I., Shmikk, D. V. & Zagulin, V. A. The mass-reflectron, a new nonmagnetic time-of-flight mass spectrometer with high resolution. *Soviet Journal of Experimental and Theoretical Physics* **37**, 45-48 (1973).

17. Medzihradszky, K. F. *et al.* The Characteristics of Peptide Collision-Induced Dissociation Using a High-Performance MALDI-TOF/TOF Tandem Mass Spectrometer. *Anal. Chem.* **72**, 552–558 (2000).

18. Pappin, D. J., Hojrup, P. & Bleasby, A. J. Rapid identification of proteins by peptide-mass fingerprinting. *Curr. Biol.* **3**, 327–332 (1993).

19. Sommerer, N., Centeno, D. & Rossignol, M. Peptide mass fingerprinting: identification of proteins by MALDI-TOF. *Methods Mol. Biol.* **355**, 219–234 (2007).

20. Welker, F. *et al.* Ancient proteins resolve the evolutionary history of Darwin's South American ungulates. *Nature* **522**, 81–84 (2015).

21. Caprioli, R. M., Farmer, T. B. & Gile, J. Molecular Imaging of Biological Samples: Localization of Peptides and Proteins Using MALDI-TOF MS. *Anal. Chem.* **69**, 4751–4760 (1997).

22. Croxatto, A., Prod'hom, G. & Greub, G. Applications of MALDI-TOF mass spectrometry in clinical diagnostic microbiology. *FEMS Microbiol. Rev.* **36**, 380–407 (2012).

23. Dole, M. *et al.* Molecular Beams of Macroions. *J. Chem. Phys.* **49**, 2240–2249 (1968).

24. Yamashita, M. & Fenn, J. B. Electrospray ion source. Another variation on the free-jet theme. *J. Phys. Chem.* **88**, 4451–4459 (1984).

25. Fenn, J. B., Mann, M., Meng, C. K., Wong, S. F. & Whitehouse, C. M. Electrospray ionization for mass spectrometry of large biomolecules. *Science* **246**, 64–71 (1989).

26. El-Aneed, A., Cohen, A. & Banoub, J. Mass Spectrometry, Review of the Basics: Electrospray, MALDI, and Commonly Used Mass Analyzers. *Appl. Spectrosc. Rev.* **44**, 210–230 (2009).

27. Taflin, D. C., Ward, T. L. & Davis, E. J. Electrified droplet fission and the Rayleigh limit. *Langmuir* **5**, 376–384 (1989).

28. Heck, A. J. R. & Heuvel, R. H. H. van den. Investigation of intact protein complexes by mass spectrometry. *Mass. Spectrom. Rev.* **23**, 368–389 (2004).

29. Ho, C. *et al.* Electrospray Ionisation Mass Spectrometry: Principles and Clinical Applications. *Clin. Biochem. Rev.* **24**, 3–12 (2003).

30. Banerjee, S. & Mazumdar, S. Electrospray Ionization Mass Spectrometry: A Technique to Access the Information beyond the Molecular Weight of the Analyte. *Int. J. Anal. Chem.* **2012,** 1-40 (2012)

31. Kingdon, K. H. A Method for the Neutralization of Electron Space Charge by Positive Ionization at Very Low Gas Pressures. *Phys. Rev.* **21**, 408–418 (1923).

32. Makarov, A. Electrostatic Axially Harmonic Orbital Trapping: A High-Performance Technique of Mass Analysis. *Anal. Chem.* **72**, 1156–1162 (2000).

33. Makarov, A. *et al.* Performance Evaluation of a Hybrid Linear Ion Trap/Orbitrap Mass Spectrometer. *Anal. Chem.* **78**, 2113–2120 (2006).

34. Gygi, S. P. & Aebersold, R. Mass spectrometry and proteomics. *Curr. Opin. Chem. Biol.* **4**, 489–494 (2000).

35. Aebersold, R. & Mann, M. Mass spectrometry-based proteomics. *Nature* **422**, 198–207 (2003).

36. Zhang, Y., Fonslow, B. R., Shan, B., Baek, M.-C. & Yates, J. R. Protein Analysis by Shotgun/Bottom-up Proteomics. *Chem. Rev.* **113**, 2343–2394 (2013).

37. Aslam, B., Basit, M., Nisar, M. A., Khurshid, M. & Rasool, M. H. Proteomics: Technologies and Their Applications. *J. Chromatogr. Sci.* **55**, 182–196 (2017).

38. Ong, S.-E. *et al.* Stable isotope labeling by amino acids in cell culture, SILAC, as a simple and accurate approach to expression proteomics. *Mol. Cell. Proteomics* **1**, 376–386 (2002).

39. Medzihradszky, K. F. In-solution digestion of proteins for mass spectrometry. *Meth. Enzymol.* **405**, 50–65 (2005).

40. Shevchenko, A., Tomas, H., Havlis, J., Olsen, J. V. & Mann, M. In-gel digestion for mass spectrometric characterization of proteins and proteomes. *Nat. Protoc.* **1**, 2856–2860 (2006).

41. Hughes, C. S. *et al.* Ultrasensitive proteome analysis using paramagnetic bead technology. *Mol. Syst. Biol.* **10**, 1–10 (2014).

42. Hughes, C. S. *et al.* Single-pot, solid-phase-enhanced sample preparation for proteomics experiments. *Nat. Protoc.* **14**, 68–85 (2019).

43. Zougman, A., Selby, P. J. & Banks, R. E. Suspension trapping (STrap) sample preparation method for bottom-up proteomics analysis. *Proteomics* **14**, 1006–1000 (2014).

44. Elinger, D., Gabashvili, A. & Levin, Y. Suspension Trapping (S-Trap) Is Compatible with Typical Protein Extraction Buffers and Detergents for Bottom-Up Proteomics. *J. Proteome Res.* **18**, 1441-1445 (2019)

45. Wiśniewski, J. R., Zougman, A., Nagaraj, N. & Mann, M. Universal sample preparation method for proteome analysis. *Nat. Methods* **6**, 359–362 (2009).

46. Ludwig, K. R., Schroll, M. M. & Hummon, A. B. Comparison of In-Solution, FASP, and S-Trap Based Digestion Methods for Bottom-Up Proteomic Studies. *J. Proteome Res.* **17**, 2480–2490 (2018).

47. Müller, T. & Winter, D. Systematic Evaluation of Protein Reduction and Alkylation Reveals Massive Unspecific Side Effects by Iodine-containing Reagents. *Mol. Cell. Proteomics* **16**, 1173–1187 (2017).

48. Batth, T. S. *et al.* Protein Aggregation Capture on Microparticles Enables Multipurpose Proteomics Sample Preparation. *Mol. Cell Proteomics* **18**, 1027–1035 (2019).

49. HaileMariam, M. *et al.* S-Trap, an Ultrafast Sample-Preparation Approach for Shotgun Proteomics. *J. Proteome Res.* **17**, 2917–2924 (2018).

50. Siepen, J. A., Keevil, E.-J., Knight, D. & Hubbard, S. J. Prediction of Missed Cleavage Sites in Tryptic Peptides Aids Protein Identification in Proteomics. *J Proteome Res.* **6**, 399–408 (2007).

51. Vaisar, T. & Urban, J. Probing Proline Effect in CID of Protonated Peptides. *J. Mass Spectrom.* **31**, 1185–1187 (1996).

52. Rietschel, B. *et al.* Elastase Digests. *Mol. Cell Proteomics* **8**, 1029–1043 (2009).

53. Doerr, A. DIA mass spectrometry. *Nat. Methods* **12**, 35–35 (2014).

54. Johnson, R. S., Martin, S. A. & Biemann, K. Collision-induced fragmentation of (M + H)+ ions of peptides. Side chain specific sequence ions. *Int. J. Mass Spectrom.* **86**, 137–154 (1988).

55. Mikesh, L. M. *et al.* The Utility of ETD Mass Spectrometry in Proteomic Analysis. *Biochim. Biophys. Acta* **1764**, 1811–1822 (2006).

56. Reilly, J. P. Ultraviolet photofragmentation of biomolecular ions. *Mass. Spectrom. Rev.* **28**, 425–447 (2009).

57. Cox, J. & Mann, M. MaxQuant enables high peptide identification rates, individualized p.p.b.-range mass accuracies and proteome-wide protein quantification. *Nat. Biotechnol.* **26**, 1367–1372 (2008).

58. Brosch, M., Yu, L., Hubbard, T. & Choudhary, J. Accurate and Sensitive Peptide Identification with Mascot Percolator. *J. Proteome Res.* **8**, 3176–3181 (2009).

59. Ma, B. *et al.* PEAKS: powerful software for peptide de novo sequencing by tandem mass spectrometry. *Rapid Commun. Mass Sp.***17**, 2337–2342 (2003).

60. Wichmann, C. *et al.* MaxQuant.Live Enables Global Targeting of More Than 25,000 Peptides. *Mol. Cell Proteomics* **18**, 982–994 (2019).

61. Ridgeway, M. E., Bleiholder, C., Mann, M. & Park, M. A. Trends in trapped ion mobility – Mass spectrometry instrumentation. *TRAC-Trend. Anal. Chem.* **116**, 324–331 (2019).

62. Meier, F. *et al.* Online parallel accumulation – serial fragmentation (PASEF) with a novel trapped ion mobility mass spectrometer. *Mol. Cell Proteomics* **15**, 2534-2545 (2018).

63. Meier, F. *et al.* Parallel accumulation – serial fragmentation combined with data-independent acquisition (diaPASEF): Bottom-up proteomics with near optimal ion usage. *bioRxiv* 656207 (2019).

64. Thompson, A. *et al.* Tandem mass tags: a novel quantification strategy for comparative analysis of complex protein mixtures by MS/MS. *Anal. Chem.* **75**, 1895–1904 (2003).

65. Hwang, T. J. *et al.* Failure of Investigational Drugs in Late-Stage Clinical Development and Publication of Trial Results. *JAMA Intern Med* **176**, 1826–1833 (2016).

66. Ozbal, C. C. *et al.* High throughput screening via mass spectrometry: a case study using acetylcholinesterase. *Assay Drug. Dev. Techn.* **2**, 373–381 (2004).

67. Hutchinson, S. E. *et al.* Enabling Lead Discovery for Histone Lysine Demethylases by High-Throughput RapidFire Mass Spectrometry. *J. Biomol. Screen.* **17**, 39–48 (2012).

68. Soulard, P. *et al.* Development of a high-throughput screening assay for stearoyl-CoA desaturase using rat liver microsomes, deuterium labeled stearoyl-CoA and mass spectrometry. *Anal. Chim. Acta* **627**, 105–111 (2008).

69. Highkin, M. K. *et al.* High-throughput screening assay for sphingosine kinase inhibitors in whole blood using RapidFire® mass spectrometry. *J. Biomol. Screen.* **16**, 272–277 (2011).

70. Forbes, C. D. *et al.* High-throughput mass spectrometry screening for inhibitors of phosphatidylserine decarboxylase. *J. Biomol. Screen.* **12**, 628–634 (2007).

71. Leveridge, M. *et al.* Demonstrating enhanced throughput of RapidFire mass spectrometry through multiplexing using the JmjD2d demethylase as a model system. *J. Biomol. Screen.* **19**, 278–286 (2014).

72. Bretschneider, T. *et al.* RapidFire BLAZE-Mode Is Boosting ESI-MS Toward High-Throughput-Screening. *SLAS Technol.* **4**, 386-393 (2019).

73. Zhang, H. Acoustic dispensing-mass spectrometry: the next high throughput bioanalytical platform for early drug discovery. *Bioanalysis* **9**, 1619–1621 (2017).

74. Gómez-Ríos, G. A. *et al.* Open Port Probe Sampling Interface for the Direct Coupling of Biocompatible Solid-Phase Microextraction to Atmospheric Pressure Ionization Mass Spectrometry. *Anal. Chem.* **89**, 3805–3809 (2017).

75. Sinclair, I. *et al.* Novel Acoustic Loading of a Mass Spectrometer: Toward Next-Generation High-Throughput MS Screening. *J. Lab. Autom.* **21**, 19–26 (2016).

76. Ellson, R. *et al.* Transfer of Low Nanoliter Volumes between Microplates Using Focused Acoustics—Automation Considerations. *JALA: Journal of the Association for Laboratory Automation* **8**, 29–34 (2003).

77. Roberts, K. *et al.* Implementation and Challenges of Direct Acoustic Dosing into Cell-Based Assays. *J. Lab. Autom.* **21**, 76–89 (2016).

78. Pagnotti, V. S., Chubatyi, N. D. & McEwen, C. N. Solvent Assisted Inlet Ionization: An Ultrasensitive New Liquid Introduction Ionization Method for Mass Spectrometry. *Anal. Chem.* **83**, 3981–3985 (2011).

79. Sinclair, I. *et al.* Acoustic Mist Ionization Platform for Direct and Contactless Ultrahigh-Throughput Mass Spectrometry Analysis of Liquid Samples. *Anal. Chem.* **91**, 3790–3794 (2019).

80. Trufelli, H., Palma, P., Famiglini, G. & Cappiello, A. An overview of matrix effects in liquid chromatography-mass spectrometry. *Mass Spectrom. Rev.* **30**, 491–509 (2011).

81. Sinclair, I., Davies, G. & Semple, H. Acoustic mist ionization mass spectrometry (AMI-MS) as a drug discovery platform. *Expert Opin. Drug. Discov.* **14**, 609–617 (2019).

82. Cornett, D. S. & Scholle, M. D. Advances in MALDI Mass Spectrometry within Drug Discovery. *SLAS Discov.* **22**, 1179–1181 (2017).

83. Chandler, J., Haslam, C., Hardy, N., Leveridge, M. & Marshall, P. A Systematic Investigation of the Best Buffers for Use in Screening by MALDI-Mass Spectrometry. *SLAS Discov.* **22**, 1262–1269 (2017).

84. Winter, M. *et al.* Automated MALDI Target Preparation Concept: Providing Ultra-High-Throughput Mass Spectrometry–Based Screening for Drug Discovery, Automated MALDI Target Preparation Concept: Providing Ultra-High-Throughput Mass Spectrometry–Based Screening for Drug Discovery. *SLAS Techol.* **24**, 209-211 (2018)

85. Greis, K. D. *et al.* MALDI-TOF MS as a Label-Free Approach to Rapid Inhibitor Screening. *J. Am. Soc. Mass Spectrom.* **17**, 815–822 (2006).

86. Ritorto, M. S. *et al.* Screening of DUB activity and specificity by MALDI-TOF mass spectrometry. *Nat. Commun.* **5**, 4763 (2014).

87. Komander, D. & Rape, M. The ubiquitin code. *Annu. Rev. Biochem.* **81**, 203–229 (2012).

88. Heideker, J. & Wertz, I. E. DUBs, the regulation of cell identity and disease. *Biochem. J.* **465**, 1–26 (2015).

89. Iphöfer, A. *et al.* Profiling ubiquitin linkage specificities of deubiquitinating enzymes with branched ubiquitin isopeptide probes. *ChemBioChem* **13**, 1416–1420 (2012).

90. McGouran, J. F., Gaertner, S. R., Altun, M., Kramer, H. B. & Kessler, B. M. Deubiquitinating enzyme specificity for ubiquitin chain topology profiled by di-ubiquitin activity probes. *Chem. Biol.* **20**, 1447–1455 (2013).

91. Hassiepen, U. *et al.* A sensitive fluorescence intensity assay for deubiquitinating proteases using ubiquitin-rhodamine110-glycine as substrate. *Anal. Biochem.* **371**, 201–207 (2007).

92. Cesare, V. D. *et al.* The MALDI-TOF E2/E3 Ligase Assay as Universal Tool for Drug Discovery in the Ubiquitin Pathway. *Cell Chem. Biol.* **25**, 1117-1127 (2018).

93. Heap, R. E., Gant, M. S., Lamoliatte, F., Peltier, J. & Trost, M. Mass spectrometry techniques for studying the ubiquitin system. *Biochem. Soc. T.* **45**, 1137–1148 (2017).

94. Kategaya, L. *et al.* USP7 small-molecule inhibitors interfere with ubiquitin binding. *Nature* **550**, 534–538 (2017).

95. Magiera, K. *et al.* Lithocholic Acid Hydroxyamide Destabilizes Cyclin D1 and Induces G0/G1 Arrest by Inhibiting Deubiquitinase USP2a. *Cell Chem. Biol*. **24**, 458-470 (2017).

96. Heap, R. E. *et al.* Identifying Inhibitors of Inflammation: A Novel High-Throughput MALDI-TOF Screening Assay for Salt-Inducible Kinases (SIKs). *SLAS Discov.* **22**, 1193–1202 (2017).

97. Beeman, K. *et al.* Integration of an In Situ MALDI-Based High-Throughput Screening Process: A Case Study with Receptor Tyrosine Kinase c-MET. *SLAS Discov.* **22**, 1203–1210 (2017).

98. Winter, M. *et al.* Establishing MALDI-TOF as Versatile Drug Discovery Readout to Dissect the PTP1B Enzymatic Reaction. *SLAS Discov.* **23**, 561–573 (2018).

99. Guitot, K. *et al.* A direct label-free MALDI-TOF mass spectrometry based assay for the characterization of inhibitors of protein lysine methyltransferases. *Anal. Bioanal. Chem.* **409**, 3767–3777 (2017).

100. Guitot, K. *et al.* Label-free measurement of histone lysine methyltransferases activity by matrix-assisted laser desorption/ionization time-of-flight mass spectrometry. *Anal. Biochem.* **456**, 25–31 (2014).

101. Hutchens, T. W. & Yip, T.-T. New desorption strategies for the mass spectrometric analysis of macromolecules. *Rapid Commun. Mass Sp.* **7**, 576–580 (1993).

102. Bounichou, M. *et al.* Self-assembled monolayer-assisted mass spectrometry. *J. Mater. Chem.* **19**, 8032–8039 (2009).

103. Mrksich, M. Mass spectrometry of self-assembled monolayers: a new tool for molecular surface science. *ACS Nano* **2**, 7–18 (2008).

104. Love, J. C., Estroff, L. A., Kriebel, J. K., Nuzzo, R. G. & Whitesides, G. M. Self-Assembled Monolayers of Thiolates on Metals as a Form of Nanotechnology. *Chem. Rev.* **105**, 1103–1170 (2005).

105. Gurard-Levin, Z. A., Scholle, M. D., Eisenberg, A. H. & Mrksich, M. High-throughput screening of small molecule libraries using SAMDI mass spectrometry. *ACS Comb. Sci.* **13**, 347–350 (2011).

106. Patel, K., Sherrill, J., Mrksich, M. & Scholle, M. D. Discovery of SIRT3 Inhibitors Using SAMDI Mass Spectrometry. *J. Biomol. Screen.* **20**, 842–848 (2015).

107. Szymczak, L. C., Huang, C.-F., Berns, E. J. & Mrksich, M. Combining SAMDI Mass Spectrometry and Peptide Arrays to Profile Phosphatase Activities. *Method. Enzymol.* **607**, 389–403 (2018).

108. Ban, L. *et al.* Discovery of glycosyltransferases using carbohydrate arrays and mass spectrometry. *Nat. Chem. Biol.* **8**, 769–773 (2012).

109. Gurard-Levin, Z. A., Kilian, K. A., Kim, J., Bähr, K. & Mrksich, M. Peptide arrays identify isoform-selective substrates for profiling endogenous lysine deacetylase activity. *ACS Chem. Biol.* **5**, 863–873 (2010).

110. VanderPorten, E. C., Scholle, M. D., Sherrill, J., Tran, J. C. & Liu, Y. Identification of Small-Molecule Noncovalent Binders Utilizing SAMDI Technology. *SLAS Discov.* **22**, 1211–1217 (2017).

111. Claydon, M. A., Davey, S. N., Edwards-Jones, V. & Gordon, D. B. The rapid identification of intact microorganisms using mass spectrometry. *Nat. Biotechnol.* **14**, 1584–1586 (1996).

112. Fenselau, C. & Demirev, P. A. Characterization of intact microorganisms by MALDI mass spectrometry. *Mass Spectrom. Rev.* **20**, 157–171 (2001).

113. Kliem, M. & Sauer, S. The essence on mass spectrometry based microbial diagnostics. *Curr. Opini. Microbiol.* **15**, 397–402 (2012).

114. Holland, R. D. *et al.* Rapid identification of intact whole bacteria based on spectral patterns using matrix-assisted laser desorption/ionization with time-of-flight mass spectrometry. *Rapid Commun. Mass Sp.* **10**, 1227–1232 (1996).

115. Wang, Z., Dunlop, K., Long, S. R. & Li, L. Mass Spectrometric Methods for Generation of Protein Mass Database Used for Bacterial Identification. *Anal. Chem.* **74**, 3174–3182 (2002).

116. Rahi, P., Prakash, O. & Shouche, Y. S. Matrix-Assisted Laser Desorption/Ionization Time-of-Flight Mass-Spectrometry (MALDI-TOF MS) Based Microbial Identifications: Challenges and Scopes for Microbial Ecologists. *Front. Microbiol.* **7**, 1-12 (2016).

117. Jarman, K. H. *et al.* An algorithm for automated bacterial identification using matrix-assisted laser desorption/ionization mass spectrometry. *Anal. Chem.* **72**, 1217–1223 (2000).

118. Gekenidis, M. T., Studer, P., Wüthrich, S., Brunisholz, R. & Drissner, D. Beyond the matrix-assisted laser desorption ionization (MALDI) biotyping workflow: in search of microorganism-specific tryptic peptides enabling discrimination of subspecies. *Appl. Environ. Microbiol.* **80**, 4234–4241 (2014).

119. Patel, R. MALDI-TOF MS for the Diagnosis of Infectious Diseases. *Clin. Chem.* **61**, 100–111 (2015).

120. Mutters, N. T. *et al.* Performance of Kiestra total laboratory automation combined with MS in clinical microbiology practice. *Ann. Lab. Med.* **34**, 111–117 (2014).

121. Vrioni, G. *et al.* MALDI-TOF mass spectrometry technology for detecting biomarkers of antimicrobial resistance: current achievements and future perspectives. *Ann. Transl. Med.* **6**, 1-14 (2018).

122. Burckhardt, I. & Zimmermann, S. Susceptibility Testing of Bacteria Using Maldi-Tof Mass Spectrometry. *Front. Microbiol.* **9**, 1-11 (2018).

123. Kostrzewa, M., Sparbier, K., Maier, T. & Schubert, S. MALDI-TOF MS: an upcoming tool for rapid detection of antibiotic resistance in microorganisms. *Proteom. Clin. Appl.* **7**, 767–778 (2013).

124. Serafim, V. *et al.* Classification of cancer cell lines using matrix-assisted laser desorption/ionization time-of-flight mass spectrometry and statistical analysis. *Int. J. Mol. Med.* **40**, 1096–1104 (2017).

125. Ouedraogo, R. *et al.* Whole-cell MALDI-TOF MS: A new tool to assess the multifaceted activation of macrophages. *J. Proteomics* **75**, 5523–5532 (2012).

126. Schwamb, S. *et al.* Monitoring CHO cell cultures: cell stress and early apoptosis assessment by mass spectrometry. *J. Biotechnol.* **168**, 452–461 (2013).

127. Petukhova, V. Z. *et al.* Whole Cell MALDI Fingerprinting Is a Robust Tool for Differential Profiling of Two-Component Mammalian Cell Mixtures. *J. Am. Soc. Mass Spectrom.* **30**, 344–354 (2019).

128. Portevin, D. *et al.* Quantitative whole-cell MALDI-TOF MS fingerprints distinguishes human monocyte sub-populations activated by distinct microbial ligands. *BMC Biotechnol.* **15**, 1-9 (2015).

129. Chen, X. *et al.* Ratiometric Mass Spectrometry for Cell Identification and Quantitation Using Intracellular “Dual-Biomarkers”. *Sci.Rep.* **7**, 1-10 (2017).

130. Stübiger, G. *et al.* MALDI-MS Protein Profiling of Chemoresistance in Extracellular Vesicles of Cancer Cells. *Anal. Chem.* **90**, 13178–13182 (2018).

131. Fuchs, B. & Schiller, J. MALDI-TOF MS analysis of lipids from cells, tissues and body fluids. *Subcell. Biochem.* **49**, 541–565 (2008).

132. Reddy, J. K. & Sambasiva Rao, M. Lipid Metabolism and Liver Inflammation. II. Fatty liver disease and fatty acid oxidation. *Am. J. Physiol-Gastr. L.* **290**, 852–858 (2006).

133. Goldberg, I. J., Trent, C. M. & Schulze, P. C. Lipid Metabolism and Toxicity in the Heart. *Cell Metab.* **15**, 805–812 (2012).

134. Holčapek, M. *et al.* Lipidomic analysis of plasma, erythrocytes and lipoprotein fractions of cardiovascular disease patients using UHPLC/MS, MALDI-MS and multivariate data analysis. *J. Chromatogr. B* **990**, 52–63 (2015).

135. Neumann, E. K., Comi, T. J., Rubakhin, S. S. & Sweedler, J. V. Lipid Heterogeneity between Astrocytes and Neurons Revealed by Single-Cell MALDI-MS Combined with Immunocytochemical Classification. *Angew. Chem. Int. Edit.* **58**, 5910–5914 (2019).

136. Neumann, E., K., Ellis, J. F., Triplett, A. E., Rubakhin, S. S. & Sweedler J V. Lipid Analysis of 30 000 Individual Rodent Cerebellar Cells Using High-Resolution Mass Spectrometry. *Anal. Chem.* **91**, 7871-7878 (2019)

137. Weigt, D. *et al.* Mechanistic MALDI-TOF Cell-Based Assay for the Discovery of Potent and Specific Fatty Acid Synthase Inhibitors. *Cell Chem. Biol.* (2019). **26**, 1322-1331

138. Weigt, D., Sammour, D. A., Ulrich, T., Munteanu, B. & Hopf, C. Automated analysis of lipid drug-response markers by combined fast and high-resolution whole cell MALDI mass spectrometry biotyping. *Sci. Rep.* **8**, 1-9 (2018).

139. Mills, C. D., Kincaid, K., Alt, J. M., Heilman, M. J. & Hill, A. M. M-1/M-2 macrophages and the Th1/Th2 paradigm. *J. Immunol.* **164**, 6166–6173 (2000).

140. Martinez, F. O. & Gordon, S. The M1 and M2 paradigm of macrophage activation: time for reassessment. *F1000Prime Rep* **6**, 1-13 (2014).

141. Gordon, S. Alternative activation of macrophages. *Nat. Rev. Immunol.* **3**, 23–35 (2003).

142. Delavary, B. M., van der Veer, W. M., van Egmond, M., Niessen, F. B. & Beelen, R. H. J. Macrophages in skin injury and repair. *Immunobiology* **216**, 753–762 (2011).

143. Mantovani, A., Biswas, S. K., Galdiero, M. R., Sica, A. & Locati, M. Macrophage plasticity and polarization in tissue repair and remodelling. *J. Pathol.* **229**, 176–185 (2013).

144. Rőszer, T. Understanding the Mysterious M2 Macrophage through Activation Markers and Effector Mechanisms. *Mediat. Inflamm.* **2015**, 1-16 (2015).

145. Mantovani, A. *et al.* The chemokine system in diverse forms of macrophage activation and polarization. *Trends Immunol.* **25**, 677–686 (2004).

146. Nonnenmacher, Y. & Hiller, K. Biochemistry of proinflammatory macrophage activation. *Cell. Mol. Life Sci.* **75**, 2093–2109 (2018).

147. Aderem, A. & Underhill, D. M. Mechanisms of phagocytosis in macrophages. *Annu. Rev. Immunol.* **17**, 593–623 (1999).

148. Blum, J. S., Wearsch, P. A. & Cresswell, P. Pathways of Antigen Processing. *Annu. Rev. Immunol.* **31**, 443–473 (2013).

149. Tang, D., Kang, R., Coyne, C. B., Zeh, H. J. & Lotze, M. T. PAMPs and DAMPs: Signals that Spur Autophagy and Immunity. *Immunol. Rev.* **249**, 158–175 (2012).

150. Yamamoto, M. & Takeda, K. Current views of toll-like receptor signaling pathways. *Gastroenterol Res Pract* **2010**, 240365 (2010).

151. Mogensen, T. H. Pathogen Recognition and Inflammatory Signaling in Innate Immune Defenses. *Clin. Microbiol. Rev.* **22**, 240–273 (2009).

152. Takeuchi, O. *et al.* Cutting edge: role of Toll-like receptor 1 in mediating immune response to microbial lipoproteins. *J. Immunol.* **169**, 10–14 (2002).

153. Schaefer, L. Complexity of danger: the diverse nature of damage-associated molecular patterns. *J. Biol. Chem.* **289**, 35237–35245 (2014).

154. Headland, S. E. & Norling, L. V. The resolution of inflammation: Principles and challenges. *Semin. Immunol.* **27**, 149–160 (2015).

155. Serhan, C. N. & Savill, J. Resolution of inflammation: the beginning programs the end. *Nat. Immunol.* **6**, 1191–1197 (2005).

156. McNelis, J. C. & Olefsky, J. M. Macrophages, Immunity, and Metabolic Disease. *Immunity* **41**, 36–48 (2014).

157. Gordon, S. & Plüddemann, A. Tissue macrophages: heterogeneity and functions. *BMC Biol.* **15**, 1-18 (2017).

158. Austyn, J. M. & Gordon, S. F4/80, a monoclonal antibody directed specifically against the mouse macrophage. *Eur. J. Immunol.* **11**, 805–815 (1981).

159. Hooper, L. V. & Macpherson, A. J. Immune adaptations that maintain homeostasis with the intestinal microbiota. *Nat. Rev. Immunol.* **10**, 159–169 (2010).

160. Bauer, H., Paronetto, F., Burns, W. A. & Einheber, A. The Enhancing Effect of the Microbial Flora on Macrophage Function and the Immune Response: A Study in Germfree Mice. *J.Exp. Med.* **123**, 1013–1024 (1966).

161. Joseph, B. & Venero, J. L. A brief overview of multitalented microglia. *Methods Mol. Biol.* **1041**, 3–8 (2013).

162. Prinz, M. & Priller, J. Microglia and brain macrophages in the molecular age: from origin to neuropsychiatric disease. *Nat. Rev. Neurosci.* **15**, 300–312 (2014).

163. Hall, C. J. *et al.* Repositioning drugs for inflammatory disease – fishing for new anti-inflammatory agents. *Dis. Model. Mech.* **7**, 1069–1081 (2014).

164. Cassetta, L. & Pollard, J. W. Targeting macrophages: therapeutic approaches in cancer. *Nat. Rev. Drug Discov.* **17**, 887–904 (2018).

165. Mantovani, A., Marchesi, F., Malesci, A., Laghi, L. & Allavena, P. Tumour-associated macrophages as treatment targets in oncology. *Nat. Rev. Clin. Oncol.* **14**, 399–416 (2017).

166. De Palma, M. & Lewis, C. E. Cancer: Macrophages limit chemotherapy. *Nature* **472**, 303–304 (2011).

167. Cassetta, L. & Pollard, J. W. Targeting macrophages: therapeutic approaches in cancer. *Nat.Rev. Drug Discov.* **17**, 887–904 (2018).

168. Okazawa, H. *et al.* Negative regulation of phagocytosis in macrophages by the CD47-SHPS-1 system. *J. Immunol.* **174**, 2004–2011 (2005).

169. Chao, M. P. *et al.* Anti-CD47 antibody synergizes with rituximab to promote phagocytosis and eradicate non-Hodgkin lymphoma. *Cell* **142**, 699–713 (2010).

170. Gilroy, D. W., Lawrence, T., Perretti, M. & Rossi, A. G. Inflammatory Resolution: new opportunities for drug discovery. *Nat. Rev. Drug Discov.* **3**, 401–416 (2004).

171. Hansen, E. *et al.* A versatile high throughput screening system for the simultaneous identification of anti-inflammatory and neuroprotective compounds. *J. Alzheimers Dis.* **19**, 451–464 (2010).

172. Baig, M. S. *et al.* Repurposing Thioridazine (TDZ) as an anti-inflammatory agent. *Sci. Rep.* **8**, 1–10 (2018).

173. de Anda-Jáuregui, G., Guo, K., McGregor, B. A. & Hur, J. Exploration of the Anti-Inflammatory Drug Space Through Network Pharmacology: Applications for Drug Repurposing. *Front. Physiol.* **9**, (2018).

174. Tyanova, S., Temu, T., Cox, J. The MaxQuant computational platform for mass spectrometry-based shotgun proteomics. *Nat. Protoc.* **11**, 2301-2319 (2016)

175. Pickup, J. C. Inflammation and activated innate immunity in the pathogenesis of type 2 diabetes. *Diabetes Care* **27**, 813–823 (2004).

176. O'Shea, J. J., Ma, A. & Lipsky, P. Cytokines and autoimmunity. *Nat. Rev. Immunol.* **2**, 37–45 (2002).

177. Sun, B. & Karin, M. Obesity, inflammation, and liver cancer. *J. Hepatol.* **56**, 704–713 (2012).

178. Liu, Y.-C., Zou, X.-B., Chai, Y.-F. & Yao, Y.-M. Macrophage Polarization in Inflammatory Diseases. *Int. J. Biol. Sci.* **10**, 520–529 (2014).

179. Saraiva, M. & O'Garra, A. The regulation of IL-10 production by immune cells. *Nat. Rev. Immunol.* **10**, 170–181 (2010).

180. Marlow, G. J., van Gent, D. & Ferguson, L. R. Why interleukin-10 supplementation does not work in Crohn's disease patients. *World J. Gastroentero.* **19**, 3931–3941 (2013).

181. Li, M.-C. & He, S.-H. IL-10 and its related cytokines for treatment of inflammatory bowel disease. *World J. Gastroenterol*. **10**, 620–625 (2004).

182. DiMasi, J. A., Feldman, L., Seckler, A. & Wilson, A. Trends in risks associated with new drug development: success rates for investigational drugs. *Clin. Pharmacol. Ther.* **87**, 272–277 (2010).

183. Fleming, B. D. & Mosser, D. M. Regulatory macrophages: setting the threshold for therapy. *Eur. J. Immunol.* **41**, 2498–2502 (2011).

184. Clark, K. *et al.* Phosphorylation of CRTC3 by the salt-inducible kinases controls the interconversion of classically activated and regulatory macrophages. *Proc. Natl. Acad. Sci. U.S.A.* **109**, 16986–91 (2012).

185. Darling, N. J., Toth, R., Arthur, J. S. C. & Clark, K. Inhibition of SIK2 and SIK3 during differentiation enhances the anti-inflammatory phenotype of macrophages. *Biochem. J.* **474**, 521–537 (2017).

186. MacKenzie, K. F. *et al.* PGE_2 induces macrophage IL-10 production and a regulatory-like phenotype via a protein kinase A-SIK-CRTC3 pathway. *J. Immunol.* **190**, 565–577 (2013).

187. Patel, K. *et al.* The LKB1-salt-inducible kinase pathway functions as a key gluconeogenic suppressor in the liver. *Nat. Commun.* **5**, 4535 (2014).

188. Katoh, Y. *et al.* Salt-inducible kinase (SIK) isoforms: their involvement in steroidogenesis and adipogenesis. *Mol. Cell. Endocrinol.* **217**, 109–112 (2004).

189. Luan, B. *et al.* CREB pathway links PGE2 signaling with macrophage polarization. *Proc. Natl. Acad. Sci. U.S.A.* **112**, 15642–15647 (2015).

190. Sundberg, T. B. *et al.* Small-molecule screening identifies inhibition of salt-inducible kinases as a therapeutic strategy to enhance immunoregulatory functions of dendritic cells. *Proc. Natl. Acad. Sci. U.S.A.* **111**, 12468–12473 (2014).

191. Ozanne, J., Prescott, A. R. & Clark, K. The clinically approved drugs dasatinib and bosutinib induce anti-inflammatory macrophages by inhibiting the salt-inducible kinases. *Biochem. J.* **465**, 271–279 (2015).

192. Lombardi, M. S., Gilliéron, C., Dietrich, D. & Gabay, C. SIK inhibition in human myeloid cells modulates TLR and IL-1R signaling and induces an anti-inflammatory phenotype. *J. Leukoc. Biol.* **99**, 711–721 (2016).

193. Ubersax, J. A. & Ferrell, J. E. Mechanisms of specificity in protein phosphorylation. *Nat. Rev. Mol. Cell Biol.* **8**, 530–541 (2007).

194. Okochi, M. *et al.* Constitutive phosphorylation of the Parkinson's disease associated alpha-synuclein. *J. Biol. Chem.* **275**, 390–397 (2000).

195. Sternberger, N. H., Sternberger, L. A. & Ulrich, J. Aberrant neurofilament phosphorylation in Alzheimer disease. *Proc. Natl. Acad. Sci. U.S.A.* **82**, 4274–4276 (1985).

196. Viatour, P., Merville, M.-P., Bours, V. & Chariot, A. Phosphorylation of NF-κB and IκB proteins: implications in cancer and inflammation. *Trends Biochem. Sci.* **30**, 43–52 (2005).

197. Cohen, P. The role of protein phosphorylation in human health and disease. The Sir Hans Krebs Medal Lecture. *Eur. J. Biochem.* **268**, 5001–5010 (2001).

198. Cohen, P. Protein kinases--the major drug targets of the twenty-first century? *Nat. Rev. Drug Discov.* **1**, 309–315 (2002).

199. Ahsen, O. von & Bömer, U. High-Throughput Screening for Kinase Inhibitors. *ChemBioChem* **6**, 481–490 (2005).

200. Mortier, J. *et al.* NF-κB inducing kinase (NIK) inhibitors: Identification of new scaffolds using virtual screening. *Bioorg. Med. Chem. Lett.* **20**, 4515–4520 (2010).

201. Fukunaga, R. & Hunter, T. MNK1, a new MAP kinase-activated protein kinase, isolated by a novel expression screening method for identifying protein kinase substrates. *EMBO J.* **16**, 1921–1933 (1997).

202. Zhang, Q. *et al.* Discovery of EGFR Selective 4,6-Disubstituted Pyrimidines from a Combinatorial Kinase-Directed Heterocycle Library. *J. Am. Chem. Soc.* **128**, 2182–2183 (2006).

203. Anastassiadis, T., Deacon, S. W., Devarajan, K., Ma, H. & Peterson, J. R. Comprehensive assay of kinase catalytic activity reveals features of kinase inhibitor selectivity. *Nat. Biotechnol.* **29**, 1039–1045 (2011).

204. Taub, M. Salt Inducible Kinase Signaling Networks: Implications for Acute Kidney Injury and Therapeutic Potential. *Int. J. Mol. Sci.* **20**, 1-19 (2019).

205. Koo, S.-H. *et al.* The CREB coactivator TORC2 is a key regulator of fasting glucose metabolism. *Nature* **437**, 1109–1111 (2005).

206. Henriksson, E. *et al.* SIK2 regulates CRTCs, HDAC4 and glucose uptake in adipocytes. *J. Cell. Sci.* **128**, 472–486 (2015).

207. Sun, X., Gao, L., Chien, H.-Y., Li, W.-C. & Zhao, J. The regulation and function of the NUAK family. *J. Mol. Endocrinol.* **51**, 15-22 (2013).

208. Krause, E., Wenschuh, H. & Jungblut, P. R. The Dominance of Arginine-Containing Peptides in MALDI-Derived Tryptic Mass Fingerprints of Proteins. *Anal. Chem.* **71**, 4160–4165 (1999).

209. Annan, R. S. & Carr, S. A. Phosphopeptide analysis by matrix-assisted laser desorption time-of-flight mass spectrometry. *Anal. Chem.* **68**, 3413–3421 (1996).

210. Spengler, B., Kirsch, D., Kaufmann, R. & Cotter, R. J. Metastable decay of peptides and proteins in matrix-assisted laser-desorption mass spectrometry. *Rapid Commun. Mass Sp.* **5**, 198–202 (1991).

211. Hollemeyer, K., Heinzle, E. & Tholey, A. Identification of oxidized methionine residues in peptides containing two methionine residues by derivatization and matrix-assisted laser desorption/ionization mass spectrometry. *Proteomics* **2**, 1524–1531 (2002).

212. Charter, N. W., Kauffman, L., Singh, R. & Eglen, R. M. A generic, homogenous method for measuring kinase and inhibitor activity via adenosine 5'-diphosphate accumulation. *J. Biomol. Screen.* **11**, 390–399 (2006).

213. Johnson, K. A. & Goody, R. S. The Original Michaelis Constant: Translation of the 1913 Michaelis-Menten Paper. *Biochemistry* **50**, 8264–8269 (2011).

214. Tamaoki, T. *et al.* Staurosporine, a potent inhibitor of phospholipid/Ca++dependent protein kinase. *Biochem. Biophy. Res. Co.* **135**, 397–402 (1986).

215. Morrison, J. F. Kinetics of the reversible inhibition of enzyme-catalysed reactions by tight-binding inhibitors. *BBA-Enzymology* **185**, 269–286 (1969).

216. Zhang, J.-H., Chung, T. D. Y. & Oldenburg, K. R. A Simple Statistical Parameter for Use in Evaluation and Validation of High Throughput Screening Assays. *J. Biomol. Screen.* **4**, 67–73 (1999).

217. Birmingham, A. *et al.* Statistical Methods for Analysis of High-Throughput RNA Interference Screens. *Nat. Methods* **6**, 569–575 (2009).

218. Wein, M. N., Foretz, M., Fisher, D. E., Xavier, R. J. & Kronenberg, H. M. Salt-Inducible Kinases: Physiology, Regulation by cAMP, and Therapeutic Potential. *Trends Endocrin. Met.* **29**, 723–735 (2018).

219. Mousset, C. M. *et al.* Comprehensive Phenotyping of T Cells Using Flow Cytometry. *Cytom. Part A* **95**, 647–654 (2019).

220. Barlogie, B. *et al.* Flow Cytometry in Clinical Cancer Research. *Cancer. Res.* **43**, 3982–3997 (1983).

221. Suslov, O. N., Kukekov, V. G., Ignatova, T. N. & Steindler, D. A. Neural stem cell heterogeneity demonstrated by molecular phenotyping of clonal neurospheres. *Proc. Natl. Acad. Sci. U.S.A.* **99**, 14506–14511 (2002).

222. Oughton, J. A. & Kerkvliet, Immune Cell Phenotyping Using Flow Cytometry. *Curr. Protoc. Toxicol.* **66**, 1-34 (2015).

223. Yu, Y.-R. A. *et al.* A Protocol for the Comprehensive Flow Cytometric Analysis of Immune Cells in Normal and Inflamed Murine Non-Lymphoid Tissues. *PLoS One* **11**, 1-23 (2016).

224. Suresh, S. *et al.* Connections between single-cell biomechanics and human disease states: gastrointestinal cancer and malaria. *Acta Biomater.* **1**, 15–30 (2005).

225. Di Carlo, D. A mechanical biomarker of cell state in medicine. *J. Lab. Autom.* **17**, 32–42 (2012).

226. Otto, O. *et al.* Real-time deformability cytometry: on-the-fly cell mechanical phenotyping. *Nat. Methods* **12**, 199–202 (2015).

227. Gossett, D. R. *et al.* Hydrodynamic stretching of single cells for large population mechanical phenotyping. *Proc. Natl. Acad. Sci. U.S.A.* **109**, 7630–7635 (2012).

228. Ornatsky, O., Baranov, V. I., Bandura, D. R., Tanner, S. D. & Dick, J. Multiple cellular antigen detection by ICP-MS. *J. Immunol. Methods* **308**, 68–76 (2006).

229. Kay, A. W., Strauss-Albee, D. M. & Blish, C. A. Application of Mass Cytometry (CyTOF) for Functional and Phenotypic Analysis of Natural Killer Cells. *Method. Mol. Biol.* **1441**, 13–26 (2016).

230. Holzlechner, M. *et al.* In Situ Characterization of Tissue-Resident Immune Cells by MALDI Mass Spectrometry Imaging. *J. Proteome Res.* **16**, 65–76 (2017).

231. Hanrieder, J., Wicher, G., Bergquist, J., Andersson, M. & Fex-Svenningsen, Å. MALDI mass spectrometry based molecular phenotyping of CNS glial cells for prediction in mammalian brain tissue. *Anal. Bioanal. Chem.* **401**, 135–147 (2011).

232. Fenselau, C. & Demirev, P. A. Characterization of intact microorganisms by MALDI mass spectrometry. *Mass Spectrom. Rev.* **20**, 157–171 (2001).

233. Wang, Z., Dunlop, K., Long, S. R. & Li, L. Mass Spectrometric Methods for Generation of Protein Mass Database Used for Bacterial Identification. *Anal. Chem.* **74**, 3174–3182 (2002).

234. Williams, T. L., Andrzejewski, D., Lay, J. O. & Musser, S. M. Experimental factors affecting the quality and reproducibility of MALDI TOF mass spectra obtained from whole bacteria cells. *J. Am. Soc. Mass Spectrom.* **14**, 342–351 (2003).

235. Wunschel, S. C. *et al.* Bacterial analysis by MALDI-TOF mass spectrometry: An inter-laboratory comparison. *J. Am. Soc. Mass Spectrom.* **16**, 456–462 (2005).

236. Alatoom, A. A., Cunningham, S. A., Ihde, S. M., Mandrekar, J. & Patel, R. Comparison of Direct Colony Method versus Extraction Method for Identification of Gram-Positive Cocci by Use of Bruker Biotyper Matrix-Assisted Laser Desorption Ionization–Time of Flight Mass Spectrometry. *J. Clin. Microbiol.* **49**, 2868–2873 (2011).

237. Toh-Boyo, G. M., Wulff, S. S. & Basile, F. Comparison of sample preparation methods and evaluation of intra- and intersample reproducibility in bacteria MALDI-MS profiling. *Anal. Chem.* **84**, 9971–9980 (2012).

238. Bizzini, A., Durussel, C., Bille, J., Greub, G. & Prod'hom, G. Performance of Matrix-Assisted Laser Desorption Ionization-Time of Flight Mass Spectrometry for Identification of Bacterial Strains Routinely Isolated in a Clinical Microbiology Laboratory. *J. Clin. Microbiol.* **48**, 1549–1554 (2010).

239. Vaňhara, P. *et al.* Intact Cell Mass Spectrometry as a Quality Control Tool for Revealing Minute Phenotypic Changes of Cultured Human Embryonic Stem Cells: Mass Spectrometry Quality Control of Cell Cultures. *Stem Cell Transl. Med.* **7**, 109–114 (2018).

240. Ouedraogo, R. *et al.* Global Analysis of Circulating Immune Cells by Matrix-Assisted Laser Desorption Ionization Time-of-Flight Mass Spectrometry. *PLoS One* **5**, 1-9 (2010).

241. Heap, R. E., Segarra-Fas, A., Blain, A. P., Findlay, G. M. & Trost, M. Profiling embryonic stem cell differentiation by MALDI TOF mass spectrometry: development of a reproducible and robust sample preparation workflow. *Analyst* **144***,* 6371-6381 (2019)

242. Munteanu, B., von Reitzenstein, C., Hänsch, G. M., Meyer, B. & Hopf, C. Sensitive, robust and automated protein analysis of cell differentiation and of primary human blood cells by intact cell MALDI mass spectrometry biotyping. *Anal. Bioanal. Chem.* **404**, 2277–2286 (2012).

243. Vargha, M., Takáts, Z., Konopka, A. & Nakatsu, C. H. Optimization of MALDI-TOF MS for strain level differentiation of Arthrobacter isolates. *J. Microbiol. Methods* **66**, 399–409 (2006).

244. AlMasoud, N., Xu, Y., Nicolaou, N. & Goodacre, R. Optimization of matrix assisted desorption/ionization time of flight mass spectrometry (MALDI-TOF-MS) for the characterization of Bacillus and Brevibacillus species. *Anal. Chim. Acta* **840**, 49–57 (2014).

245. Angelini, R. *et al.* Cardiolipin fingerprinting of leukocytes by MALDI-TOF/MS as a screening tool for Barth syndrome. *J. Lipid Res.* **56**, 1787–1794 (2015).

246. Eriksson, C., Masaki, N., Yao, I., Hayasaka, T. & Setou, M. MALDI Imaging Mass Spectrometry-A Mini Review of Methods and Recent Developments. *Mass Spectrom. (Tokyo)* **2**, 1-6 (2013).

247. Agar, N. Y. R., Yang, H. W., Carroll, R. S., Black, P. M. & Agar, J. N. Matrix solution fixation: histology-compatible tissue preparation for MALDI mass spectrometry imaging. *Anal. Chem.* **79**, 7416–7423 (2007).

248. Pouton, C. W. & Haynes, J. M. Embryonic stem cells as a source of models for drug discovery. *Nat. Rev. Drug Discov.* **6**, 605–616 (2007).

249. Yang, Y.-H. K., Ogando, C. R., Wang See, C., Chang, T.-Y. & Barabino, G. A. Changes in phenotype and differentiation potential of human mesenchymal stem cells aging in vitro. *Stem Cell Res. Ther.* **9**, 1-14 (2018).

250. Ying, Q.-L. *et al.* The ground state of embryonic stem cell self-renewal. *Nature* **453**, 519–523 (2008).

251. Silva, J. *et al.* Promotion of Reprogramming to Ground State Pluripotency by Signal Inhibition. *PLoS Biol.* **6**, 2253-2247 (2008).

252. Wisztorski, M., Franck, J., Salzet, M. & Fournier, I. MALDI direct analysis and imaging of frozen versus FFPE tissues: what strategy for which sample? *Methods Mol. Biol.* **656**, 303–322 (2010).

253. Allwood, D. A., Dreyfus, R. W., Perera, I. K. & Dyer, P. E. UV Optical Absorption of Matrices Used for Matrix-assisted Laser Desorption/Ionization. *Rapid Commun. Mass Spectrom.* **10**, 1575–1578 (1996).

254. Robinson, K. N., Steven, R. T. & Bunch, J. Matrix Optical Absorption in UV-MALDI MS. *J. Am. Soc. Mass Spectrom.* **29**, 501–511 (2018).

255. Huang, Y., Liu, Y., Zheng, C. & Shen, C. Investigation of Cross-Contamination and Misidentification of 278 Widely Used Tumor Cell Lines. *PLoS One* **12**, 1-16 (2017).

256. Michelini, E., Cevenini, L., Mezzanotte, L., Coppa, A. & Roda, A. Cell-based assays: fuelling drug discovery. *Anal. Bioanal. Chem.* **398**, 227–238 (2010).

257. Butcher, E. C. Can cell systems biology rescue drug discovery? *Nat. Rev. Drug Discov.* **4**, 461–467 (2005).

258. An, W. F. & Tolliday, N. Cell-Based Assays for High-Throughput Screening. *Mol. Biotechnol.* **45**, 180–186 (2010).

259. Kunapuli, P. *et al.* Identification of small molecule antagonists of the human mas-related gene-X1 receptor. *Anal. Biochem.* **351**, 50–61 (2006).

260. Zeng, C. *et al.* Functional assays to define agonists and antagonists of the sigma-2 receptor. *Anal. Biochem.* **448**, 68–74 (2014).

261. Han, S. *et al.* Identification of coumarin derivatives as a novel class of allosteric MEK1 inhibitors. *Bioorg. Med. Chem. Lett.* **15**, 5467–5473 (2005).

262. Gerets, H. H. J., Dhalluin, S. & Atienzar, F. A. Multiplexing cell viability assays. *Methods Mol. Biol.* **740**, 91–101 (2011).

263. Liu, Y., Beyer, A. & Aebersold, R. On the Dependency of Cellular Protein Levels on mRNA Abundance. *Cell* **165**, 535–550 (2016).

264. Durick, K. & Negulescu, P. Cellular biosensors for drug discovery. *Biosens. Bioelectron.* **16**, 587–592 (2001).

265. Hanson, G. T. & Hanson, B. J. Fluorescent probes for cellular assays. *Comb. Chem. High T. Scr.* **11**, 505–513 (2008).

266. Minor, L. K. Label-free cell-based functional assays. *Comb. Chem. High T. Scr.* **11**, 573–580 (2008).

267. Palucka, A. K. & Coussens, L. M. The Basis of OncoImmunology. *Cell* **164**, 1233–1247 (2016).

268. Fink, M. P. & Warren, H. S. Strategies to improve drug development for sepsis. *Nat. Rev. Drug Discov.* **13**, 741–758 (2014).

269. Kozlov, S. V. Development of a cell-based assay to quantify the inflammatory potential of test substances and screen compound libraries for anti-cancer drug candidates in a high-throughput format. *Methods Mol. Biol.* **512**, 159–167 (2009).

270. Meijer, K., Vonk, R. J., Priebe, M. G. & Roelofsen, H. Cell-based screening assay for anti-inflammatory activity of bioactive compounds. *Food Chem.* **166**, 158–164 (2015).

271. d'Alençon, C. A. *et al.* A high-throughput chemically induced inflammation assay in zebrafish. *BMC Biol.* **8**, 1-16 (2010).

272. Kelly, C., Jefferies, C. & Cryan, S.-A. Targeted liposomal drug delivery to monocytes and macrophages. *J Drug Deliv.* **2011**, 1-11 (2011).

273. Parameswaran, N. & Patial, S. Tumor Necrosis Factor-α Signaling in Macrophages. *Crit. Rev. Eukar. Gene* **20**, 87–103 (2010).

274. Wajant, H., Pfizenmaier, K. & Scheurich, P. Tumor necrosis factor signaling. *Cell Death Differ.* **10**, 45–65 (2003).

275. Clark, I. A. How TNF was recognized as a key mechanism of disease. *Cytokine Growth F. R.* **18**, 335–343 (2007).

276. Maini, R. N., Elliott, M. J., Brennan, F. M. & Feldmann, M. Beneficial effects of tumour necrosis factor-alpha (TNF-alpha) blockade in rheumatoid arthritis (RA). *Clin. Exp. Immunol.* **101**, 207–212 (1995).

277. van der Poll, T., van de Veerdonk, F. L., Scicluna, B. P. & Netea, M. G. The immunopathology of sepsis and potential therapeutic targets. *Nat. Rev. Immunol.* **17**, 407–420 (2017).

278. Vassalli, P. The pathophysiology of tumor necrosis factors. *Annu. Rev. Immunol.* **10**, 411–452 (1992).

279. Adegbola, S. O., Sahnan, K., Warusavitarne, J., Hart, A. & Tozer, P. Anti-TNF Therapy in Crohn's Disease. *Int. J. Mol. Sci.* **19**, 1-21 (2018).

280. Lv, S. *et al.* Anti-TNF-α therapy for patients with sepsis: a systematic meta-analysis. *Int. J. Clin. Pract.* **68**, 520–528 (2014).

281. Faustman, D. & Davis, M. TNF receptor 2 pathway: drug target for autoimmune diseases. *Nat. Rev. Drug Discov.* **9**, 482–493 (2010).

282. Palladino, M. A., Bahjat, F. R., Theodorakis, E. A. & Moldawer, L. L. Anti-TNF-α therapies: the next generation. *Nat. Rev. Drug Discov.* **2**, 736–746 (2003).

283. Pauls, E. *et al.* Essential role for IKKβ in production of type 1 interferons by plasmacytoid dendritic cells. *J. Biol. Chem.* **287**, 19216–19228 (2012).

284. Steegmaier, M. *et al.* BI 2536, a Potent and Selective Inhibitor of Polo-like Kinase 1, Inhibits Tumor Growth In Vivo. *Curr. Biol.* **17**, 316–322 (2007).

285. Reddy, M. C. *et al.* C-Phycocyanin, a selective cyclooxygenase-2 inhibitor, induces apoptosis in lipopolysaccharide-stimulated RAW 264.7 macrophages. *Biochem. Biophys. Res. Co.* **304**, 385–392 (2003).

286. Zhou, X. M. *et al.* Non-steroidal anti-inflammatory drugs induce apoptosis in gastric cancer cells through up-regulation of bax and bak. *Carcinogenesis* **22**, 1393–1397 (2001).

287. Kantarjian, H. M. *et al.* Nilotinib is effective in patients with chronic myeloid leukemia in chronic phase after imatinib resistance or intolerance: 24-month follow-up results. *Blood* **117**, 1141–1145 (2011).

288. Ciuffa, R. *et al.* Contribution of Mass Spectrometry-Based Proteomics to the Understanding of TNF-α Signaling. *J. Proteome Res.* **16**, 14–33 (2017).

289. Andreakos, E. *et al.* Distinct pathways of LPS-induced NF-κB activation and cytokine production in human myeloid and nonmyeloid cells defined by selective utilization of MyD88 and Mal/TIRAP. *Blood* **103**, 2229–2237 (2004).

290. Håversen, L., Ohlsson, B. G., Hahn-Zoric, M., Hanson, L. A. & Mattsby-Baltzer, I. Lactoferrin down-regulates the LPS-induced cytokine production in monocytic cells via NF-kappa B. *Cell. Immunol.* **220**, 83–95 (2002).

291. Leister, K. P. *et al.* Two High Throughput Screen Assays for Measurement of TNF-α in THP-1 Cells. *Curr. Chem. Genomics* **5**, 21–29 (2011).

292. Singh, U., Tabibian, J., Venugopal, S. K., Devaraj, S. & Jialal, I. Development of an In Vitro Screening Assay to Test the Antiinflammatory Properties of Dietary Supplements and Pharmacologic Agents. *Clin. Chem.* **51**, 2252–2256 (2005).

293. Kannan, L., Rath, N. C., Liyanage, R. & Lay, J. O. Identification and Characterization of Thymosin β-4 in Chicken Macrophages Using Whole Cell MALDI-TOF. *Ann. N.Y. Acad. Sci.* **1112**, 425–434 (2007).

294. Crockford, D., Turjman, N., Allan, C. & Angel, J. Thymosin beta4: structure, function, and biological properties supporting current and future clinical applications. *Ann. N.Y. Acad. Sci.* **1194**, 179–189 (2010).

295. Young, J. D. *et al.* Thymosin beta 4 sulfoxide is an anti-inflammatory agent generated by monocytes in the presence of glucocorticoids. *Nat. Med.* **5**, 1424–1427 (1999).

296. Kawai, T. & Akira, S. Signaling to NF-kappaB by Toll-like receptors. *Trends Mol. Med.* **13**, 460–469 (2007).

297. Jiang, Z., Mak, T. W., Sen, G. & Li, X. Toll-like receptor 3-mediated activation of NF-kappaB and IRF3 diverges at Toll-IL-1 receptor domain-containing adapter inducing IFN-beta. *Proc. Natl. Acad. Sci. U.S.A.* **101**, 3533–3538 (2004).

298. Dzamko, N. *et al.* The IkappaB kinase family phosphorylates the Parkinson's disease kinase LRRK2 at Ser935 and Ser910 during Toll-like receptor signaling. *PLoS One* **7**, 1-15 (2012).

299. Hu, J. *et al.* Polo-like kinase 1 (PLK1) is involved in toll-like receptor (TLR)-mediated TNF-α production in monocytic THP-1 cells. *PLoS ONE* **8**, 1-8 (2013).

300. Vertii, A. *et al.* The Centrosome Undergoes Plk1-Independent Interphase Maturation during Inflammation and Mediates Cytokine Release. *Dev. Cell* **37**, 377–386 (2016).

301. Bixby, D. & Talpaz, M. Mechanisms of resistance to tyrosine kinase inhibitors in chronic myeloid leukemia and recent therapeutic strategies to overcome resistance. *Hematol-Am. Soc. Hemat.* **1**, 461–476 (2009).

302. Akashi, N. *et al.* Comparative suppressive effects of tyrosine kinase inhibitors imatinib and nilotinib in models of autoimmune arthritis. *Mod. Rheumatol.* **21**, 267–275 (2011).

303. Guo, K. *et al.* Treatment Effects of the Second-Generation Tyrosine Kinase Inhibitor Dasatinib on Autoimmune Arthritis. *Front. Immunol.* **9**, 1-12 (2019).

304. Manley, P. W. *et al.* Structural resemblances and comparisons of the relative pharmacological properties of imatinib and nilotinib. *Bioorgan. Med. Chem.* **18**, 6977–6986 (2010).

305. Gleixner, K. V. *et al.* Polo-like Kinase 1 (Plk1) as a Novel Drug Target in Chronic Myeloid Leukemia: Overriding Imatinib Resistance with the Plk1 Inhibitor BI 2536. *Cancer Res.* **70**, 1513–1523 (2010).

306. Cushing, L. *et al.* IRAK4 kinase activity controls Toll-like receptor-induced inflammation through the transcription factor IRF5 in primary human monocytes. *J. Biol. Chem.* **292**, 18689–18698 (2017).

307. Baud, V. *et al.* Signaling by proinflammatory cytokines: oligomerization of TRAF2 and TRAF6 is sufficient for JNK and IKK activation and target gene induction via an amino-terminal effector domain. *Gene. Dev.* **13**, 1297–1308 (1999).

308. Vollmer, S. *et al.* The mechanism of activation of IRAK1 and IRAK4 by interleukin-1 and Toll-like receptor agonists. *Biochem. J.* **474**, 2027–2038 (2017).

309. Webb, D. R. Animal models of human disease: inflammation. *Biochem. Pharmacol.* **87**, 121–130 (2014).

310. van der Weyden, L., White, J. K., Adams, D. J. & Logan, D. W. The mouse genetics toolkit: revealing function and mechanism. *Genome Biol.* **12**, 1-11 (2011).

311. Blanchard, F. & Chipoy, C. Histone deacetylase inhibitors: new drugs for the treatment of inflammatory diseases? *Drug Discov. Today* **10**, 197–204 (2005).

312. Zhang, F., Wen, Y. & Guo, X. CRISPR/Cas9 for genome editing: progress, implications and challenges. *Hum. Mol. Genet.* **23**, 40-46 (2014).

313. Davis, M. J. *et al.* Macrophage M1/M2 Polarization Dynamically Adapts to Changes in Cytokine Microenvironments in Cryptococcus neoformans Infection. *mBio* **4**, 1-10 (2013).

314. Chamberlain, L. M., Godek, M. L., Gonzalez-Juarrero, M. & Grainger, D. W. Phenotypic non-equivalence of murine (monocyte-) macrophage cells in biomaterial and inflammatory models. *J. Biomed. Mater. Res. A* **88**, 858–871 (2009).

315. Taciak, B. *et al.* Evaluation of phenotypic and functional stability of RAW 264.7 cell line through serial passages. *PLOS One* **13**, 1-13 (2018).

316. Andreu, N. *et al.* Primary macrophages and J774 cells respond differently to infection with *Mycobacterium tuberculosis*. *Sci. Rep.* **7**, 1-12 (2017).

317. ten Hagen, T. L., van Vianen, W. & Bakker-Woudenberg, I. A. Isolation and characterization of murine Kupffer cells and splenic macrophages. *J. Immunol. Methods* **193**, 81–91 (1996).

318. Zhang, X., Goncalves, R. & Mosser, D. M. The isolation and characterization of murine macrophages. *Curr. Protoc. Immunol.* ***111,*** 14.1.1-14.1.16 (2008).

319. Tushinski, R. J. *et al.* Survival of mononuclear phagocytes depends on a lineage-specific growth factor that the differentiated cells selectively destroy. *Cell* **28**, 71–81 (1982).

320. Guilbert, L. J. & Stanley, E. R. The interaction of 125I-colony-stimulating factor-1 with bone marrow-derived macrophages. *J. Biol. Chem.* **261**, 4024–4032 (1986).

321. Shi, Y. *et al.* Granulocyte-macrophage colony-stimulating factor (GM-CSF) and T-cell responses: what we do and don't know. *Cell Res.* **16**, 126–133 (2006).

322. Laar, L. van de, Coffer, P. J. & Woltman, A. M. Regulation of dendritic cell development by GM-CSF: molecular control and implications for immune homeostasis and therapy. *Blood* **119**, 3383–3393 (2012).

323. Austin, P. E., McCulloch, E. A. & Till, J. E. Characterization of the factor in L-cell conditioned medium capable of stimulating colony formation by mouse marrow cells in culture. *J. Cell. Physiol.* **77**, 121–133 (1971).

324. Englen, M. D., Valdez, Y. E., Lehnert, N. M. & Lehnert, B. E. Granulocyte/macrophage colony-stimulating factor is expressed and secreted in cultures of murine L929 cells. *J. Immunol. Methods* **184**, 281–283 (1995).

325. Boltz-Nitulescu, G. *et al.* Differentiation of Rat Bone Marrow Cells Into Macrophages Under the Influence of Mouse L929 Cell Supernatant. *J. Leukocyte Biol.* **41**, 83–91 (1987).

326. Assouvie, A., Daley-Bauer, L. P. & Rousselet, G. Growing Murine Bone Marrow-Derived Macrophages. *Methods Mol. Biol.* **1784**, 29–33 (2018).

327. Weischenfeldt, J. & Porse, B. Bone Marrow-Derived Macrophages (BMM): Isolation and Applications. *Cold Spring Harb. Protoc.* **3**, 1-6 (2008).

328. Marim, F. M., Silveira, T. N., Jr, D. S. L. & Zamboni, D. S. A Method for Generation of Bone Marrow-Derived Macrophages from Cryopreserved Mouse Bone Marrow Cells. *PLOS One* **5**, 1-8 (2010).

329. Lee, C. M. & Hu, J. Cell density during differentiation can alter the phenotype of bone marrow-derived macrophages. *Cell Biosci.* **3**, 1-5 (2013).

330. Fleit, H. B. & Rabinovitch, M. Interferon induction in marrow-derived macrophages: Regulation by L cell conditioned medium. *J. Cell. Physiol.* **108**, 347–352 (1981).

331. Milhaud, P. G., Compagnon, B., Bienvenüe, A. & Philippot, J. R. Interferon production of L929 and HeLa cells enhanced by polyriboinosinic acid-polyribocytidylic acid pH-sensitive liposomes. *Bioconjugate Chem.* **3**, 402–407 (1992).

332. Stuart, P. M., Zlotnik, A. & Woodward, J. G. Induction of class I and class II MHC antigen expression on murine bone marrow-derived macrophages by IL-4 (B cell stimulatory factor 1). *J. Immunol.* **140**, 1542–1547 (1988).

333. Modolell, M., Corraliza, I. M., Link, F., Soler, G. & Eichmann, K. Reciprocal regulation of the nitric oxide synthase/arginase balance in mouse bone marrow-derived macrophages by TH 1 and TH 2 cytokines. *Eur. J. Immunol.* **25**, 1101–1104 (1995).

334. Cooper, P. H., Mayer, P. & Baggiolini, M. Stimulation of phagocytosis in bone marrow-derived mouse macrophages by bacterial lipopolysaccharide: correlation with biochemical and functional parameters. *J. Immunol.* **133**, 913–922 (1984).

335. Francke, A., Herold, J., Weinert, S., Strasser, R. H. & Braun-Dullaeus, R. C. Generation of Mature Murine Monocytes from Heterogeneous Bone Marrow and Description of Their Properties. *J. Histochem. Cytochem.* **59**, 813–825 (2011).

336. Mosher, D. F. Physiology of Fibronectin. *Annu. Rev. Med.* **35**, 561–575 (1984).

337. Goldberg, B. & Green, H. An Analysis of Collagen Secretion by Established Mouse Fibroblast Lines. *J. Cell Biol.* **22**, 227–258 (1964).

338. Schwanhäusser, B. *et al.* Global quantification of mammalian gene expression control. *Nature* **473**, 337–342 (2011).

339. Lieschke, G. J. & Burgess, A. W. Granulocyte Colony-Stimulating Factor and Granulocyte-Macrophage Colony-Stimulating Factor. *N. Engl. J. Med.* **327**, 99–106 (1992).

340. Calandra, T. & Roger, T. Macrophage migration inhibitory factor: a regulator of innate immunity. *Nat. Rev. Immunol.* **3**, 791–800 (2003).

341. Hashimoto, S., Yamada, M., Motoyoshi, K. & Akagawa, K. S. Enhancement of Macrophage Colony-Stimulating Factor–Induced Growth and Differentiation of Human Monocytes by Interleukin-10. *Blood* **89**, 315–321 (1997).

342. Lukic, A. *et al.* GM-CSF– and M-CSF–primed macrophages present similar resolving but distinct inflammatory lipid mediator signatures. *FASEB J.* **31**, 4370–4381 (2017).

343. Zecha, J. *et al.* TMT Labeling for the Masses: A Robust and Cost-efficient, In-solution Labeling Approach. *Mol. Cell Proteomics* **18**, 1468–1478 (2019).

344. Olsen, J. V. *et al.* Higher-energy C-trap dissociation for peptide modification analysis. *Nat. Methods* **4**, 709–712 (2007).

345. Ting, L., Rad, R., Gygi, S. P. & Haas, W. MS3 eliminates ratio distortion in isobaric multiplexed quantitative proteomics. *Nat. Methods* **8**, 937–940 (2011).

346. Bantscheff, M. *et al.* Robust and sensitive iTRAQ quantification on an LTQ Orbitrap mass spectrometer. *Mol. Cell Proteomics* **7**, 1702–1713 (2008).

347. Ow, S. Y. *et al.* iTRAQ underestimation in simple and complex mixtures: 'the good, the bad and the ugly'. *J. Proteome Res.* **8**, 5347–5355 (2009).

348. Karp, N. A. *et al.* Addressing accuracy and precision issues in iTRAQ quantitation. *Mol. Cell Proteomics* **9**, 1885–1897 (2010).

349. Paulo, J. A., O'Connell, J. D. & Gygi, S. P. A Triple Knockout (TKO) Proteomics Standard for Diagnosing Ion Interference in Isobaric Labeling Experiments. *J. Am. Soc. Mass Spectrom.* **27**, 1620–1625 (2016).

350. Christensen, J. E., Andreasen, S. Ø., Christensen, J. P. & Thomsen, A. R. CD11b expression as a marker to distinguish between recently activated effector CD8+ T cells and memory cells. *Int. Immunol.* **13**, 593–600 (2001).

351. Collin, M., McGovern, N. & Haniffa, M. Human dendritic cell subsets. *Immunology* **140**, 22–30 (2013).

352. Lin, H.-H. *et al.* The macrophage F4/80 receptor is required for the induction of antigen-specific efferent regulatory T cells in peripheral tolerance. *J. Exp. Med.* **201**, 1615–1625 (2005).

353. Aulner, N. *et al.* High Content Analysis of Primary Macrophages Hosting Proliferating Leishmania Amastigotes: Application to Anti-leishmanial Drug Discovery. *PLOS Neglect. Trop. D.* **7**, 1-11 (2013).

354. Lamotte, S., Aulner, N., Späth, G. F. & Prina, E. Discovery of novel hit compounds with broad activity against visceral and cutaneous Leishmania species by comparative phenotypic screening. *Sci. Rep.* **9**, 1-11 (2019).

355. Mescher, A. L. Macrophages and fibroblasts during inflammation and tissue repair in models of organ regeneration. *Regeneration* **4**, 39–53 (2017).

356. Smith, R. S., Smith, T. J., Blieden, T. M. & Phipps, R. P. Fibroblasts as sentinel cells. Synthesis of chemokines and regulation of inflammation. *Am. J. Pathol.* **151**, 317–322 (1997).

357. Donato, R. Intracellular and extracellular roles of S100 proteins. *Microsc. Res. Techniq.* **60**, 540–551 (2003).

358. Ryckman, C., Vandal, K., Rouleau, P., Talbot, M. & Tessier, P. A. Proinflammatory activities of S100: proteins S100A8, S100A9, and S100A8/A9 induce neutrophil chemotaxis and adhesion. *J. Immunol.* **170**, 3233–3242 (2003).

359. Chen, Z. *et al.* CRL4B DCAF11 E3 ligase targets p21 for degradation to control cell cycle progression in human osteosarcoma cells. *Sci. Rep.* **7**, 1–12 (2017).